Southeast Offshore Storage Resource Assessment (SOSRA)

Federal Agency:	U.S. Department of Energy/NETL
Federal Number:	DE-FE0026086
Project Title:	Southeast Offshore Storage Resource Assessment
Co-Principal Investigators:	Kenneth Nemeth, Executive Director nemeth@sseb.org; 770-242-7712 Kimberly Sams-Gray, Managing Director gray@sseb.org; 770-242-7712
Report Type:	Final Progress Report
Reporting Period Start Date: Reporting Period End Date:	October 1, 2015 September 30, 2019
Principal Authors:	Kimberly Gray, Gerald Hill, Patricia Berry, SSEB / HILL Nino Ripepi, VA Tech Jack Pashin, Oklahoma State University James Knapp, Oklahoma State University Denise Hills, Geological Survey of Alabama David Riestenberg, Advanced Resources International
Report Issue Date:	December 2019
Submitting Organization:	Southern States Energy Board 6325 Amherst Court Peachtree Corners, Georgia 30092 Phone: (770) 242-7712 Fax: (770) 242-0421 SSEB Website: www.sseb.org
Signature of Official:	

Disclaimer

"This report was prepared as an account of work sponsored by an agency of the United States Government. Neither the United States Government nor any agency thereof, nor any of their employees, makes any warranty, express or implied, or assumes any legal liability or responsibility for the accuracy, completeness, or usefulness of any information, apparatus, product, or process disclosed, or represents that its use would not infringe privately owned rights. Reference herein to any specific commercial product, process, or service by trade name, trademark, manufacturer, or otherwise does not necessarily constitute or imply its endorsement, recommendation, or favoring by the United States Government or any agency thereof. The views and opinions of authors expressed herein do not necessarily state or reflect those of the United States Government or any agency thereof."

Abstract

Subsurface geologic storage of CO_2 can play a major role in offsetting greenhouse gas emissions in a manner that is safe, economical, and acceptable to the public. Due to legal advantages and potential vast resource capacity, offshore storage offers an attractive alternative to onshore storage. Indeed, the success of the Sleipner project in the North Sea demonstrates the technical feasibility of offshore storage as not only a viable option, but as an early opportunity for commercial deployment (e.g., Arts et al., 2009).

Although the storage capacity of offshore reservoirs is expected to be vast, no comprehensive assessment of the offshore storage resource in the southeastern United States had been performed. In a preliminary analysis of a 10,000 mi^2 area of offshore Alabama and the western Florida Panhandle, Hills and Pashin (2010) suggested that about 170 Gt of CO_2 could be stored in Miocene sandstone and that at least 30 Gt could be stored in deeper Cretaceous formations.

A task force convened by the Southern States Energy Board (SSEB) and the Interstate Oil and Gas Compact Commission (IOGCC) found that no assessment had been made of the offshore storage resource potential in the shelf areas of the Atlantic seaboard and the eastern Gulf of Mexico in the southeastern US (SSEB, 2013). Considering that the U.S. Environmental Protection Agency estimates that about 40% of anthropogenic CO_2 emissions in the US are generated in the southeast, the lack of an offshore CO_2 assessment constitutes a major gap in understanding of the regional storage resource.

In order to address this significant gap in knowledge of the regional storage resources and geologic capacity the Southern States Energy Board (SSEB) led a coalition of southern universities and technical experts to assess prospective geologic storage resources for carbon dioxide (CO_2) in the State and Federal waters of three planning areas: The Mid-Atlantic; The South Atlantic; and The eastern Gulf of Mexico. The Southeast Offshore Storage Resource Assessment (SOSRA) project developed a high-level approximation of the amount of CO_2 that might be stored utilizing key geologic and environmental factors which influence the storage potential. The research included significant advances in knowledge and technology that will facilitate assessment and quantification of offshore CO_2 storage resources in the SOSRA region and provide a pathway toward commercialization.

Topical reports produced (links available in the Appendix):

- Scoping and Protocol Development for Best Practices
- Modeling Based MVA Recommendations
- Infrastructure Development Recommendations
- Target Development Recommendations
- SOSRA Prospective Storage Resource Assessment Results

Table of Contents

Executive Summary

The Southern States Energy Board (SSEB) led a coalition of southern universities and technical experts to assess prospective geologic storage resources for carbon dioxide (CO_2) in the State and Federal waters of three planning areas: The Mid-Atlantic; The South Atlantic; and The eastern Gulf of Mexico. The Southeast Offshore Storage Resource Assessment (SOSRA) project team developed a high-level approximation of the amount of CO_2 that might be stored utilizing key geologic and environmental factors which influence the storage potential. The research includes significant advances in knowledge and technology that will facilitate assessment and quantification of offshore CO_2 storage resources in the SOSRA region and provide a pathway toward commercialization.

A diverse suite of data analysis techniques were used to ensure that a high quality assessment was performed and storage capacity was predicted to within ±30 percent. Utilizing existing geologic and geophysical data such as seismic reflection surveys, geophysical well logs, and supporting reservoir data (i.e., pressure, temperature, etc.), the size and geology of the prospective storage resources, including areal extent, thickness, and physical properties such as porosity and permeability, were defined. The research allowed for the following objectives to be met over a phased approach:

- Provide an overview of the basic geologic framework of the SOSRA region, identify potential storage units, and define the key planning areas.
- Provide a robust characterization of offshore CO_2 storage opportunities, as well as conduct a volumetric analysis that is consistent with established procedures employed by the National Energy Technology Laboratory (NETL) for CO_2 assessment.
- Provide limited modeling of offshore CO_2 storage to identify well and reservoir configurations that are capable of meeting the goal of 30 megatonnes or greater storage in key focus areas.
- Development of scoping and protocol for best practices to advance the state of knowledge by identifying paths to deployment and applicable technologies that improve the effectiveness while reducing the cost of storage operations.

The SOSRA project also included a robust knowledge sharing and technology transfer initiative to ensure that the products of this effort were disseminated widely and available to industrial, academic, governmental, and public stakeholders.

The final report is divided into four sections. The first section primarily reflects the efforts of SSEB, Gerald Hill PhD Inc, and Crescent Resource Innovation. The following three sections reflect the work completed by each project planning area. This format was chosen in order to provide a more cohesive flow from Task 2: Geologic Overview through to Task 5: Geologic Characterization and Volumetric Calculations.

Experimental Methods / Approach

The project team completed multiple tasks which contributed to the development of a high-level approximation of the amount of CO_2 that might be stored utilizing key geologic and environmental factors that influence the storage potential.

Methods included mapping of the geologic characteristics of key formations in the study area, evaluation of potential carbon storage resources, and identification and simulation of CO_2 injection in target development areas.

The physical and geological properties of the candidate carbon storage formations, including formation geometries, porosity, and permeability, were evaluated to ensure that the criteria for safe and permanent storage were met.

A broad range of maps, such as structure contour, isopach, and isochron maps were developed based on the stratigraphic markers, fault planes, and bed cutoffs. Porosity and permeability information was gridded and contoured. These mapping products were used to determine parameters for the Prospective Storage Resource Assessment and volumetric calculations. A quantitative estimate of carbon dioxide storage resource was calculated for each SOSRA study area. The volumetric approach developed by DOE in Appendix B of The United States 2012 Carbon Utilization and Storage Atlas for saline formations and oil and gas reservoirs was the primary methodology for storage resource estimation. Storage parameters such as total area, net thickness and average porosity, were used in conjunction with statistically derived efficiency factors to calculate an effective storage resource volume.

Basic numerical reservoir simulations were performed to predict CO_2 plume extent over various time frames. The modeling identified the well and reservoir configurations that can meet the goal of 30 megatonne or greater storage in key focus areas. Multiple well and reservoir configurations, including vertical wells, directional wells, single-zone storage, and stacked storage, informed the modeling. In some areas multiple models were run to determine the most likely well type and configuration. The detailed simulations investigated the storage capabilities under a variety of injection scenarios, as well as assessed geochemical interactions among rock, brine, and CO_2. Utilizing the results from the assessment the team has developed recommendations for the commercial deployment of offshore carbon storage operations in the target development areas.

Results and Discussion

Schedule/Milestone Status

Southern States Energy Board; Gerald Hill PhD Inc; Crescent Resource Innovation

Task 1.0: Project Management and Planning

Subtask 1.1 – Overall Project Management, Planning, and Communication

SSEB monitored and tracked the project's technical and financial progress. SSEB coordinated and reviewed all deliverables from sub-recipients and submitted them to DOE/NETL. SSEB evaluated the progress of each task through frequent communication with the lead sub-

recipients. SSEB provided financial management of the overall project to include issuing sub-recipient contracts, budget negotiations and tracking, and monitoring federal cost and cost share for SSEB and the project team. SSEB enforced reporting requirements to meet DOE requests and assisted subgrant holders in compliance with the requests.

A comprehensive communications plan was developed upon award to ensure proper communication of the project's status and risks with DOE/NETL, the project team, and appropriate stakeholders. SSEB provided regular briefings to DOE/NETL and attended the Kickoff Meeting, annual program review meetings, and provided a final project briefing to report project status. To support and foster knowledge sharing and interaction within the project team, SSEB hosted several conference calls and annual in-person team meetings. During these meetings, key stakeholders participated in an advisory capacity on behalf of their respective states and affiliations.

Subtask 1.2 – Project Management Plan

The SOSRA project was managed in accordance with the current and approved Project Management Plan (PMP). The PMP is a living document that outlined the project organization and structure, PMP implementation and coordination strategy, and potential risks to the project. It also provided a resource loaded schedule and Gantt chart, work breakdown structure, funding and costing profiles, milestone log, success criteria and decision points and the current Statement of Project Objectives (SOPO).

The initial PMP was prepared and submitted to NETL on October 14, 2015 and revised on June 30, 2017 and March 28, 2018.

Subtask 1.3 – Planning Area Managers' Technical and Financial Project Coordination

Planning Area Managers provided technical and financial coordination for their respective teams. A third tier of "Planning Area Partners" was assembled to provide technical expertise and advice to the Planning Area Managers. Members of the project team provided regular briefings to DOE and attended the Kickoff Meeting, annual program review meetings, and provided a final project briefing to report project status. The presentation file(s) were submitted to NETL/DOE as deliverables under Subtask 1.1 and the links can be found in the Appendix.

Task 6.0: Best Practices

Subtask 6.1 - BPM Scoping and Protocol Development

In the original DOE funding opportunity announcement (DOE 2015), one goal of the Carbon Storage Program was to "*Develop Best Practice Manuals for monitoring, verification, accounting (MVA), and assessment; site screening, selection, and initial characterization; public outreach; well management activities; and risk analysis and simulation*" by producing information that would be useful for inclusion in DOE Best Practices Manuals.

During a SOSRA project review meeting with DOE/NETL on March 7-8, 2017, it was noted that there was no universal best practices initiative among DOE's current offshore projects. It was decided that SSEB would focus on best practices for CO_2 infrastructure development in support of offshore CO_2 storage (including storage with utilization) in the Gulf of Mexico.

SOSRA Deliverable 6.1.a., *Scoping and Protocol Development for Best Practices*, was drafted to provide a frame of reference for developing best practices (consistent standards and

operational characteristics) for CO_2 collection, injection, and storage, and in outlining the basis for a legal and regulatory framework for offshore CO_2 storage, including storage with utilization.

Subtask 6.2 - BPM Development and Drafting

Activities in Subtask 6.2 build upon work completed for SOSRA Subtask 6.1 and the deliverable 6.1.a *"Scoping and Protocol Development for Best Practices"*. Key elements from the earlier report were retained in the updated deliverable 6.2.a "Leading Practices Development Framework" (link in the Appendix). The Scoping and Protocol document was discussed during a March 2019 project review meeting. Project team members noted that no CO_2 storage projects exist in U.S. waters and, therefore, it would be premature to contemplate best practices for the offshore. Two working groups were set up to determine how existing onshore best practices could be used to inform future offshore CO_2 infrastructure projects.

Input from the two working groups has been used to prepare a "Development Framework" (link in the Appendix) that will serve as a handoff from the SOSRA Project to the SECARB Offshore Gulf of Mexico (GoM) Project DE-FE0031557. The SECARB Offshore GoM Project, also being led by SSEB, will build upon work done in SOSRA, with a specific focus on the eastern Gulf of Mexico.

Activities completed by the SOSRA working groups included:

- Conducting best practices reviews for Characterization, Risk and Monitoring
- Organizing offshore CO_2 infrastructure into six categories for purposes of review
- Selecting onshore examples for an *Inventory of Available Practices* applicable to the six infrastructure categories
- Down-selecting from examples of available onshore practices to form a *Matrix of Leading Practices* for the offshore.

Recommendations for continuation within the SECARB Offshore GoM Project include:

- Continue to review onshore best practices and expand the *Matrix of Leading Practices*
- Work with international (North Sea) experts with offshore CO_2 infrastructure experience to refine the *Matrix of Leading Practices*
- Work with oil & gas experts with Gulf of Mexico experience to refine the *Matrix of Leading Practices* with respect to available industry practices that may be applicable to CO_2 infrastructure.

Task 7.0: NatCarb and Atlas

Subtask 7.1 – National Carbon Sequestration Database and Geographic Information System (NatCarb)

Storage resource data for the SOSRA planning areas was provided to DOE/NETL for inclusion in the National Carbon Sequestration Database and Geographic Information System (NatCarb). SSEB lead this effort in cooperation with DOE/NETL, and the SOSRA Planning Area Managers.

Storage resource data for the three SOSRA planning areas was submitted to EDX in the prescribed geodatabase format for inclusion in the NatCarb database.

Subtask 7.2 – United States Carbon Utilization and Storage Atlas (Atlas)

The project team was required to provide project-specific information, if requested, to be included in the "United States Carbon Utilization and Storage Atlas." No specific requests were made by DOE, as the Atlas was not revised during the project timeframe. The storage resource data submitted for NatCarb is available for use if needed in any future Atlas updates.

Task 8.0: Outreach

Subtask 8.1 – Public Outreach

Throughout the four-year project performance period the SOSRA team successfully completed eighty-seven outreach, knowledge sharing, and technology transfer activities. These activities incorporated the development and dissemination of outreach materials, databases, contributions to data reporting agencies including the NatCarb database and Atlas, and recommendation reports on key topics related to the commercial deployment of offshore carbon storage operations.

Topical reports produced:

- Scoping and Protocol Development for Best Practices
- Modeling Based MVA Recommendations
- Infrastructure Development Recommendations
- Target Development Recommendations
- SOSRA Prospective Storage Resource Assessment Results

Links to all topical reports & presentations can be found in the Appendix.

Meetings with presentations:

1. September 2015, Special Projects: Carbon Management Program (SOSRA Project Overview); SSEB Executive Committee Meeting, White Sulphur Springs, West Virginia
2. October 2015, The Future of Work in the American South (SOSRA Project Overview); SSEB Associate Members Meeting, St. Louis, Missouri
3. June 2017, Southeast Offshore Storage Resource Assessment (SOSRA); 2nd International Workshop on Offshore CO_2 Geologic Storage, Beaumont, Texas
4. August 2017, Southeast Offshore Storage Resource Assessment (SOSRA); NETL Carbon Capture, Utilization, Storage, and Oil & Gas Technologies Review Meeting, Pittsburgh, Pennsylvania
5. May 2018, Fast Tracking Infrastructure Development for Future Offshore CO_2 Storage; 3rd Annual International Offshore Storage Workshop, Oslo, Norway
6. August 2018, Southeast Offshore Storage Resource Assessment (SOSRA); NETL Carbon Capture, Utilization, Storage, and Oil & Gas Technologies Review Meeting, Pittsburgh, Pennsylvania

Subtask 8.2 - Knowledge Sharing and Technology Transfer

The project team promoted information exchange and knowledge sharing through various avenues, including the Regional Carbon Sequestration Partnerships' working groups, the SOSRA advisory partners, direct briefings and conferences, conference calls, emails, website links, electronic newsletters and press releases, and social media. Presentation PowerPoints, papers and proceedings are available on OSTI.

These tasks increased the visibility of the Carbon Storage Program to SSEB's carbon management industrial partners, member governors and state legislators, private industry,

policymakers, regulators, and federal and state officials, emphasizing the safety and technology readiness of offshore carbon storage operations.

The project team enhanced outreach and education through the development of a project website. The website incorporated the project goals, methods, and accomplishments. The website is hosted by the South Carolina Geological Survey and has the added benefit of being able to continue after the project has completed and become a part of the S.C. Department of Natural Resources' growing resource database.

The web resources that were developed to disseminate information to stakeholders about the project included narratives of the project's goals and progress using the StoryMap format, and data visualization and analysis tools. Stakeholders can use the tools to extract information that is relevant to their discipline and spatial interests. The tools were developed using different environments including web mapping APIs (e.g. Mapbox, Leaflet, ArcGIS JavaScript API) and the GIS server infrastructure established at the South Carolina Department of Natural Resources. The tools were built so that other offshore resource assessment datasets can be integrated, providing a larger context of offshore resources for interested parties.

A "*Summary Report of Knowledge Sharing and Technology Transfer Activities*" (link in the Appendix) was developed and includes a comprehensive list outlining all formal outreach and knowledge sharing activities.

Eastern Gulf of Mexico

Task 2.0: Geologic Overview

Subtask 2.1 - Main Geologic Provinces

The eastern Gulf of Mexico (EGOM) focus area spans the continental shelf from Mississippi to the Florida Keys (Fig. 2.1). The offshore limit of the study area follows the West Florida Escarpment and the Early Cretaceous Reef Trend from the western end of the Florida Keys to where the reef trend intersects Louisiana State Waters. The bulk of the study area is in the Eastern Gulf of Mexico Planning Area of the Bureau of Ocean Energy Management (BOEM). However, the northwestern part of the study area, which includes the outer continental shelf offshore of Alabama and Mississippi, is within the BOEM Central Gulf of Mexico Planning Area.

The EGOM focus area contains two subprovinces, which are the DeSoto Canyon Salt Basin, which is in the northwestern part of the region, and the West Florida Shelf, which is a giant carbonate platform that includes the Middle Ground Arch, Tampa Embayment, Sarasota Arch, and the South Florida Basin (Buffler and Sawyer, 1985; Dobson and Buffler, 1997).

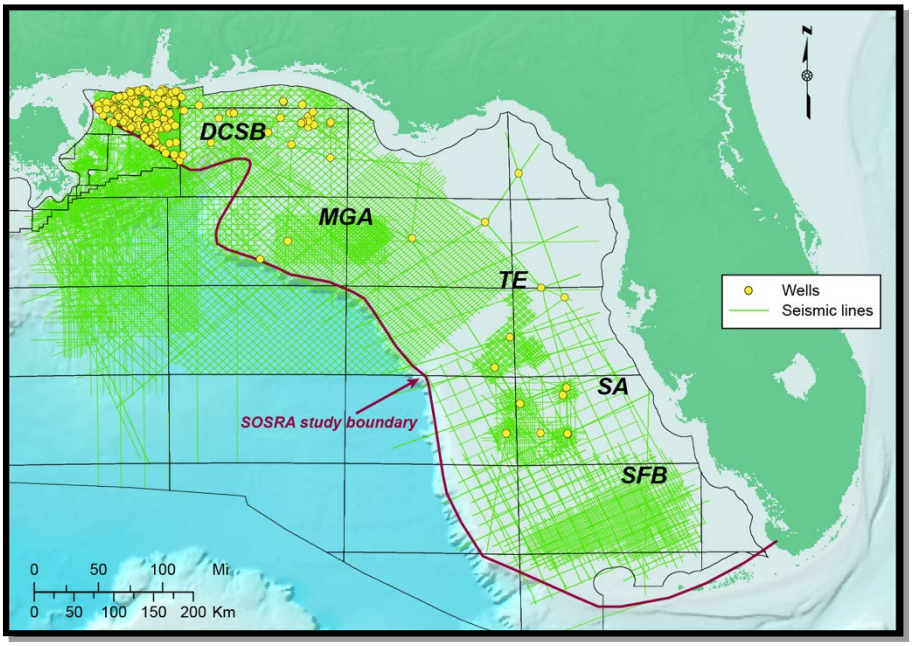

Fig. 2.1. Map of the Eastern Gulf of Mexico showing extent of focus area and available well and seismic control. Green lines are publicly available reflection seismic profiles. Well control shown in yellow (note dense well control in northwestern part of focus area).

The sedimentary succession in this focus area is generally 6-12 km thick and overlies a Paleozoic-Early Jurassic basement complex containing Triassic rift basins and large continental margin volcanic wedges.

In the DeSoto Canyon Salt Basin, a major post-rift unconformity is overlain by the Jurassic Louann Salt. Jurassic and Early Cretaceous strata above the salt contain a variety of extensional structures, including salt rollers, diapirs, and giant salt pillows (Figs. 2.2-2.4). In the western part of the salt basin, a broad continental shelf succession lacking significant faults is developed above the Jurassic section. Indeed, Upper Cretaceous and younger strata are gently

deformed and were deposited mainly on a stable continental shelf. Mesozoic strata include a complex array of carbonate and siliciclastic rock types (MacRae and Watkins, 1996; Petty, 1997, 1999; Pashin et al., 2016). Petroleum exploration, however, has proven technically challenging in the region, and the greatest success has been found in the ultra-deep (>6 km) Jurassic and shallow (~1 km) Miocene natural gas reservoirs of the Mobile area (Mancini et al., 1985; Story, 1998; Handford and Baria, 2003; Pashin et al., 2016).

The West Florida Shelf is dominated by Mesozoic carbonate rocks and has been a site of limited hydrocarbon exploration (Pollastro et al., 2001) (Fig. 2.1). The West Florida Shelf is about 500 km wide and is characterized by a broad expanse with water shallower than 80 m (Figs. 2.5, 2.6). Seaward of this expanse, the shelf steepens, with the upper continental slope intersecting the Cretaceous Reef Trend in about 1.5 km of water. The continental slope steepens abruptly at the west edge of the reef trend, forming the West Florida

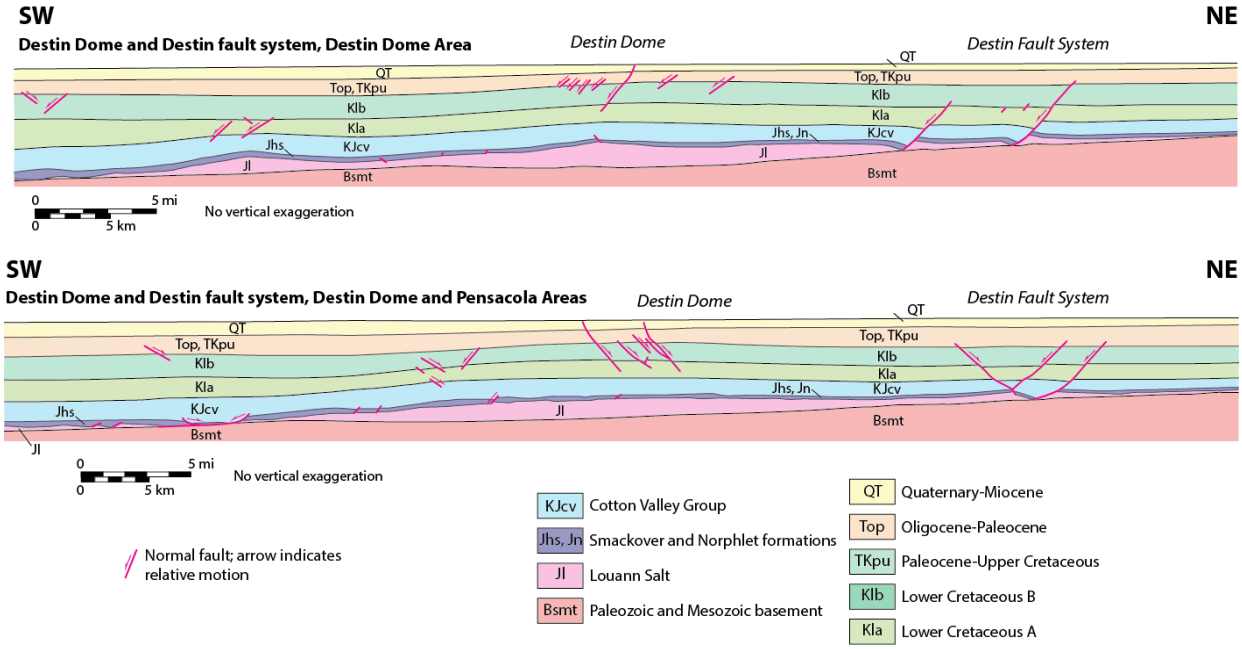

Figure 2.2. Structural cross sections of the Destin fault system and Destin Dome, northeastern Desoto Canyon Salt Basin, eastern Gulf of Mexico focus area. Interpretations based on depth-converted public domain seismic profiles (after Pashin et al., 2016).

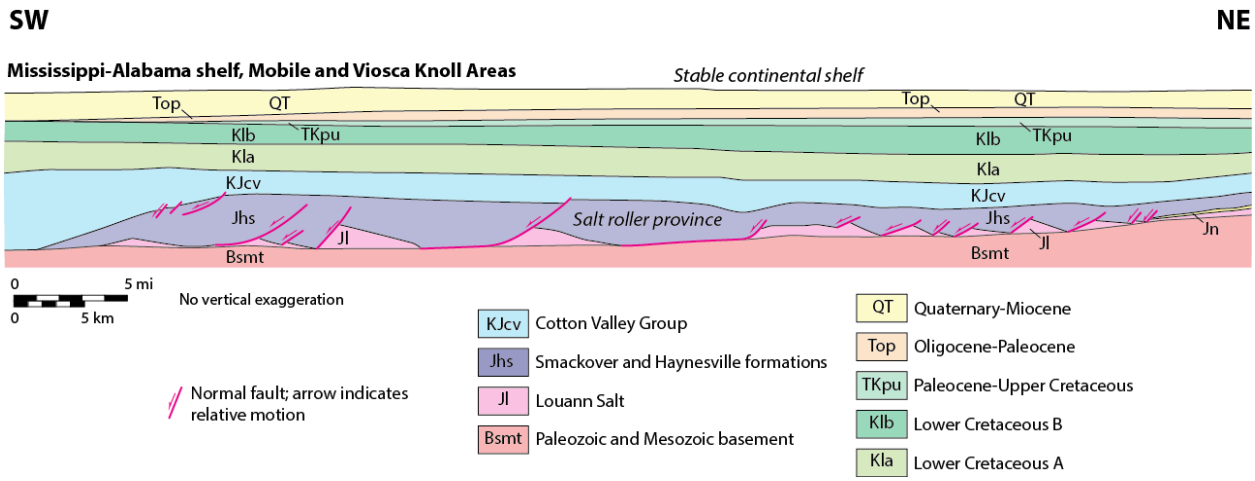

Figure 2.3. Structural cross section of the Mississippi-Alabama continental shelf showing salt rollers and associated extensional structures in the western DeSoto Canyon Salt Basin. Interpretation based on depth-converted public domain seismic profile (after Pashin et al., 2016).

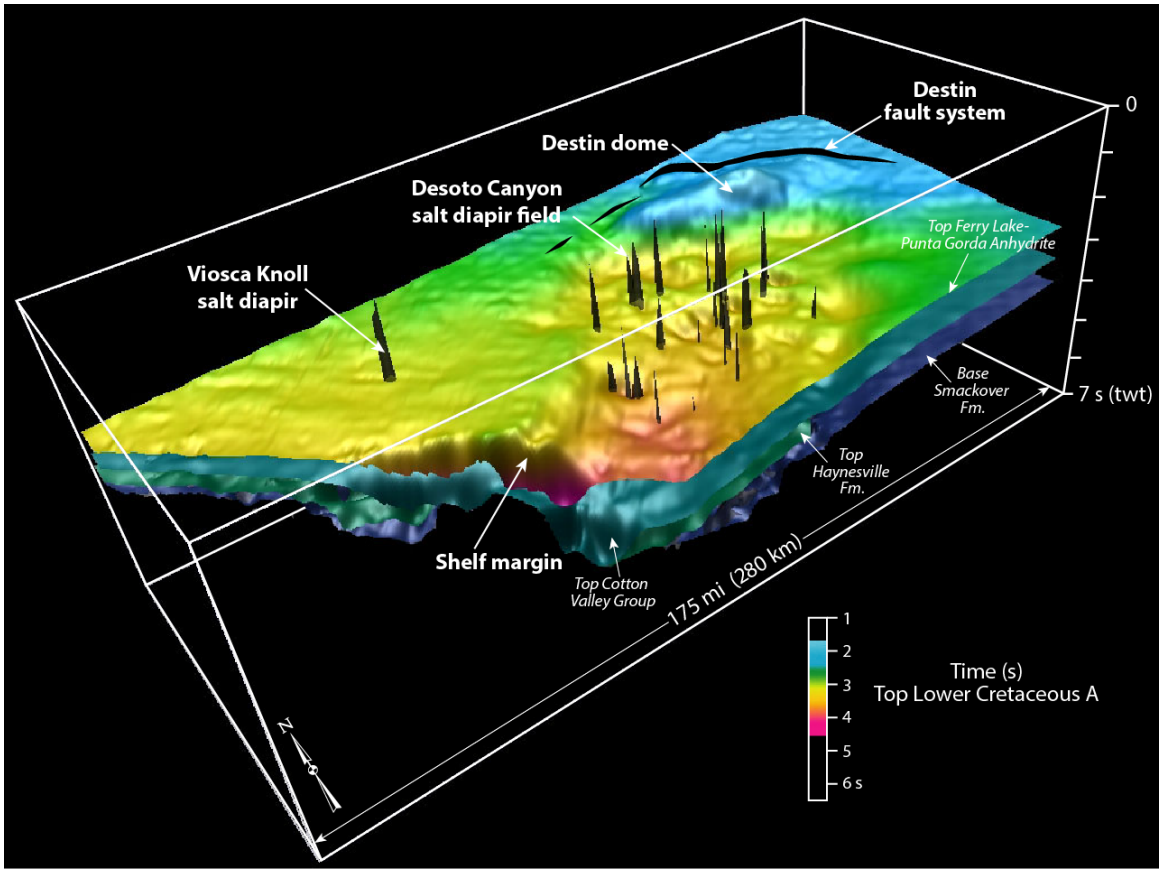

Figure 2.4. Three-dimensional visualization of geologic structure in the DeSoto Canyon Salt Basin of the Mississippi-Alabama-Florida shelf (after Pashin et al., 2016). Upper surface is the Ferry Lake-Punta Gorda Anhydrite. Visualization based on grids generated from public domain seismic profiles.

Escarpment. This escarpment is onlapped by sediment of the continental rise at water depths beyond 3 km.

Jurassic salt is thin or absent along much of the West Florida Shelf, and so post-rift siliciclastic and carbonate strata tend to rest directly on crystalline basement (Fig. 6). Weakly divergent seismic reflections within the Cretaceous carbonate platform section, which is composed principally of limestone, dolomite, and anhydrite can be traced across the shelf to the slope break (Charbonneau, 2018). The Lower Cretaceous Reef Trend and the West Florida Escarpment form a distinctive curvilinear feature that extends from the Florida Keys to the northwest corner of the EGOM focus area (Fig. 1).

Above the Cretaceous carbonate platform is a thick Upper Cretaceous-Quaternary section containing numerous clinoform seismic reflections (Roberts and Erickson, 2009; Charbonneau, 2018) (Fig. 6). A major downlap surface is developed at the top of the carbonate platform succession, and the distally steepened slope of the modern shelf is subparallel to the clinoform reflections. Hence, the modern slope break east of the reef trend is the product of a long history of seaward progradation, and the shallow shelf nearshore represents a progradational wedge top. Interestingly, the seaward limit of the progradational wedge just reaches the Lower Cretaceous reef trend with little sediment having spilled over the escarpment.

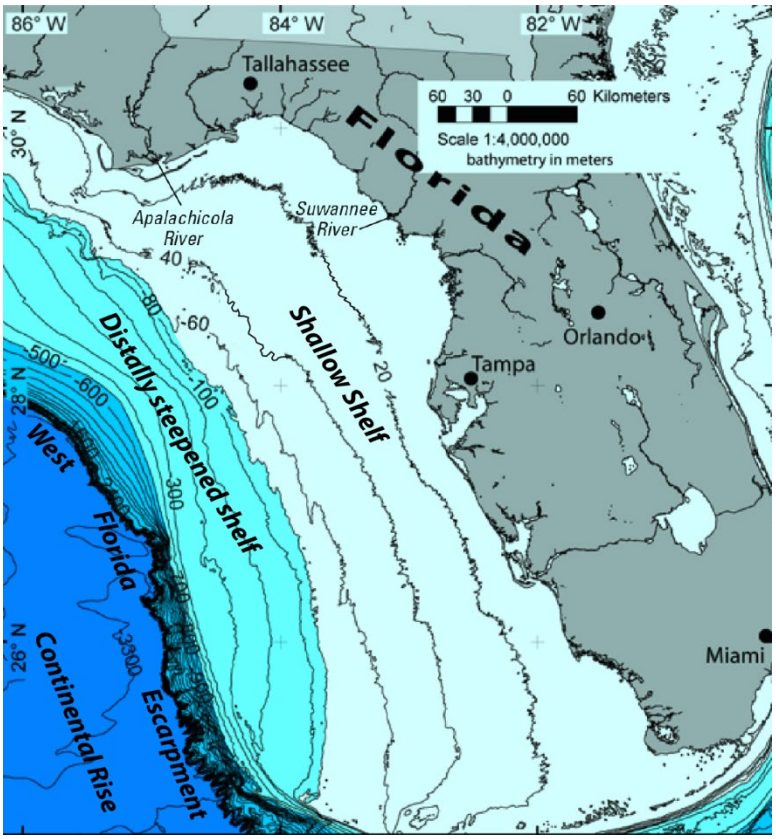

Figure 2.5. Bathymetric map of the West Florida Shelf showing location of shallow shelf, distally steepened shelf, and West Florida Escarpment (source: U.S. Geological Survey).

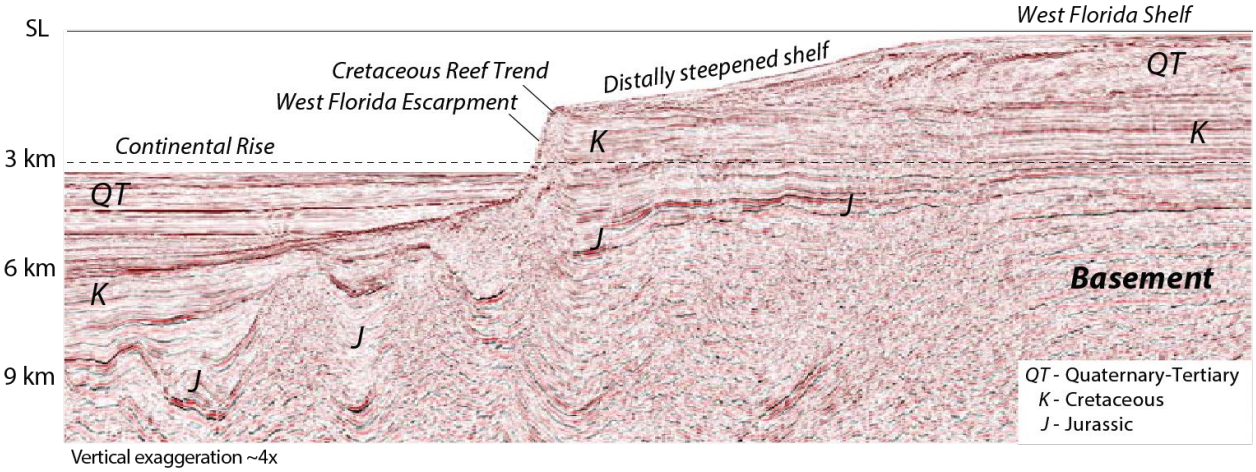

Figure 2.6. Seismic reflection profile of the West Florida Shelf and continental rise, Eastern Gulf of Mexico (modified from Roberts and Erickson, 2009).

Subtask 2.2 - Potential Storage Units; Subtask 2.3 – Planning Areas

A variety of potential storage units have been identified in the EGOM focus area, which include a variety sandstone and carbonate formations. In addition, some key shale and evaporite reservoir seals have been identified that can help ensure safe, permanent storage in the target formations. Offshore formations in the study area are thought to be geopressured at depths below 4 km, and so this study focuses on shallower strata. Importantly, the DeSoto Canyon Salt Basin and the West Florida Shelf each have a different portfolio of potential storage units and reservoir seals.

Most proven petroleum reservoirs in the DeSoto Canyon Salt Basin are too deep (> 6 km) to facilitate economically viable CO_2 storage or enhanced hydrocarbon recovery operations. However, porous intervals have been identified in shallower carbonate and siliciclastic strata of Cretaceous age (Petty, 1997, 1999; Chandra, 2018) (Fig. 2.7). Some of the shallow Miocene sand units are thought to have major storage potential (Hills and Pashin, 2010), and additional capacity may exist in Paleocene sandstone. The floor of the CO_2 storage target zone is a carbonate-evaporite section that includes the Ferry Lake Anhydrite, which is a proven reservoir seal onshore (Eaves, 1976; Esposito et al., 2008). The Paluxy Formation, which was proven as a storage unit during the SECARB Phase III Anthropogenic Test (Koperna et al., 2012), contains sandstone at a depth of about 2 km and is sealed by the basal mudstone and carbonate of the overlying Washita-Fredericksburg interval (Folaranmi, 2015; Pashin et al., 2016).

The main rock types identified in the geophysical well logs are sandstone, shale, limestone, anhydrite, chalk and clay. Cross sections are intended to establish reservoir geometry, seal location and geometry, and stratigraphic architecture. Two cross-sections from the DeSoto Canyon Salt Basin that were made where well spacing is closest are presented and discussed herein (Plates 1, 2). Plate 1 is a strike cross-section traversing the Mobile Area, whereas Plate 2 is a dip cross section traversing the Mobile and Viosca Knoll Areas. The cross-sections include Cretaceous strata shallower than 4 km (12,000 ft) and include strata from the Lower Cretaceous Ferry Lake Anhydrite through the Paleogene mudstone section.

Owing to its low density porosity and high resistivity, the Ferry Lake Anhydrite was the most readily recognized stratigraphic marker in the section and was commonly used as an initial datum for correlating well logs. The Ferry Lake Anhydrite is about 125-200 m (400-600 ft) thick in the study area is composed of interbedded anhydrite (6-20 m; 20-60 ft), limestone (6-30 m; 20-100 ft), and shale (3-6 m; 10-20 ft). The anhydrite beds are discontinuous in cross-section A-A' (Plate 1). The Ferry Lake Anhydrite is overlain by the Mooringsport Formation, which is about 250-425 m (125-1,400 ft) thick and is composed primarily of limestone (>90%) with some thin (<10%) intervals of shale; mudlog descriptions and porosity logs suggest that some tight sandstone units are present in the Viosca Knoll Area.

The Paluxy Formation overlies the Mooringsport Formation and is composed of interbedded sandstone, limestone and shale in the Mobile Area (Plates 1, 2). The Paluxy is 125-550 m (400 to 1,800 ft) thick (Fig. 2.8). Thickness is generally greater than 335 m (1100 ft) in the Mobile and Viosca Knoll Areas and decreases to 12 m (400 ft) in the northwestern Destin Dome Area. Thickness variation in the Paluxy Formation owes mainly to intertonguing with Mooringsport carbonate (Plate 2). Thickness of the Paluxy increases to about 550 m (1,800 ft) in the salt withdrawal synclines around Destin Dome and thins to about 125 m (400 ft) in the crestal region of the dome. The Paluxy becomes richer in limestone southwestward into the Viosca Knoll Area (Plate 2). Within the Paluxy there are more than 12 regional sandstone units; they range in thickness from about 7-43 m (20 to 140 ft).

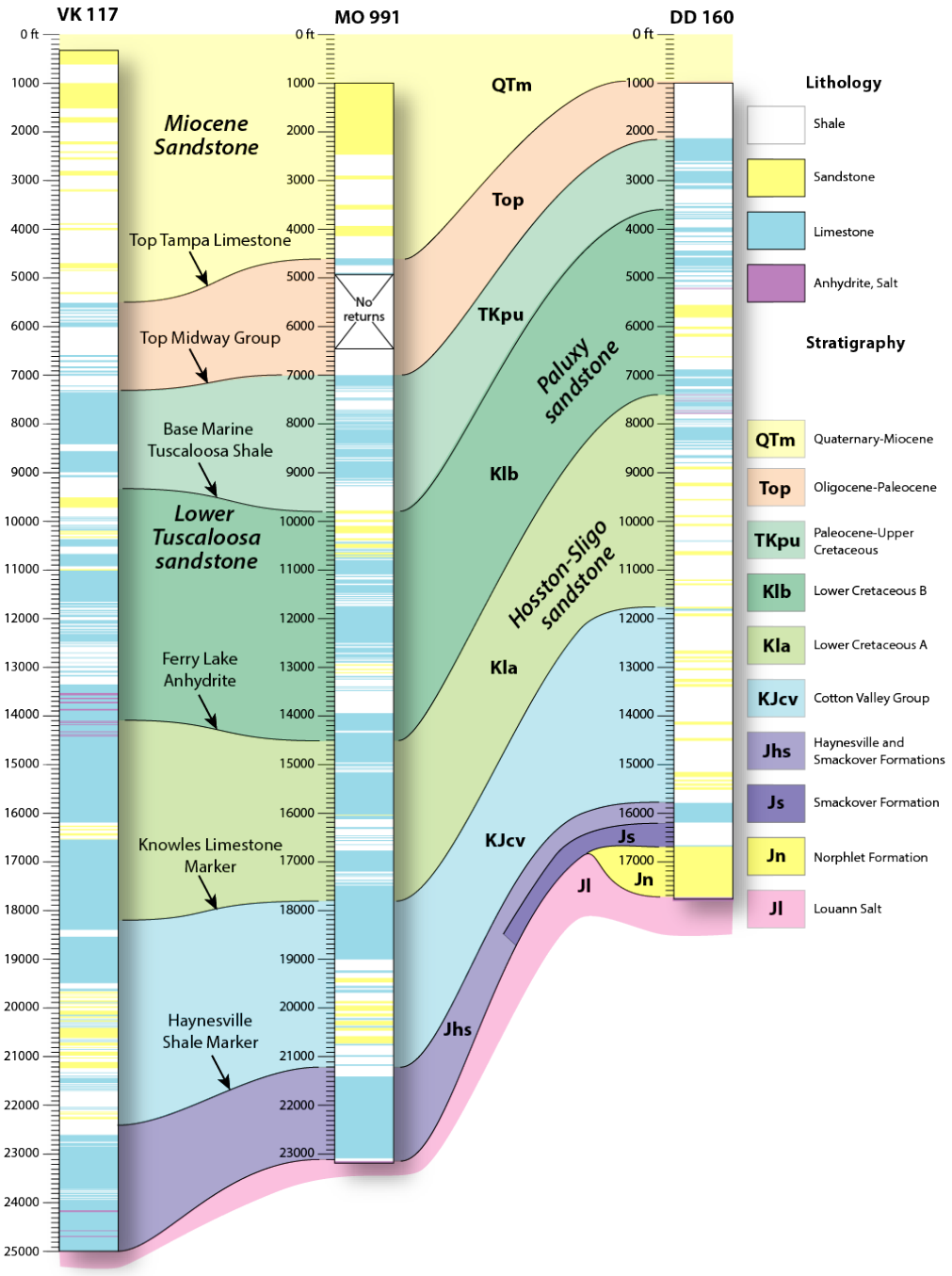

Figure 2.7. Generalized lithologic columns identifying potential sandstone saline formations in the DeSoto Canyon Salt Basin (after Pashin et al., 2016). Shaded intervals between columns are major stratigraphic units that have been mapped regional using publicly available seismic reflection data.

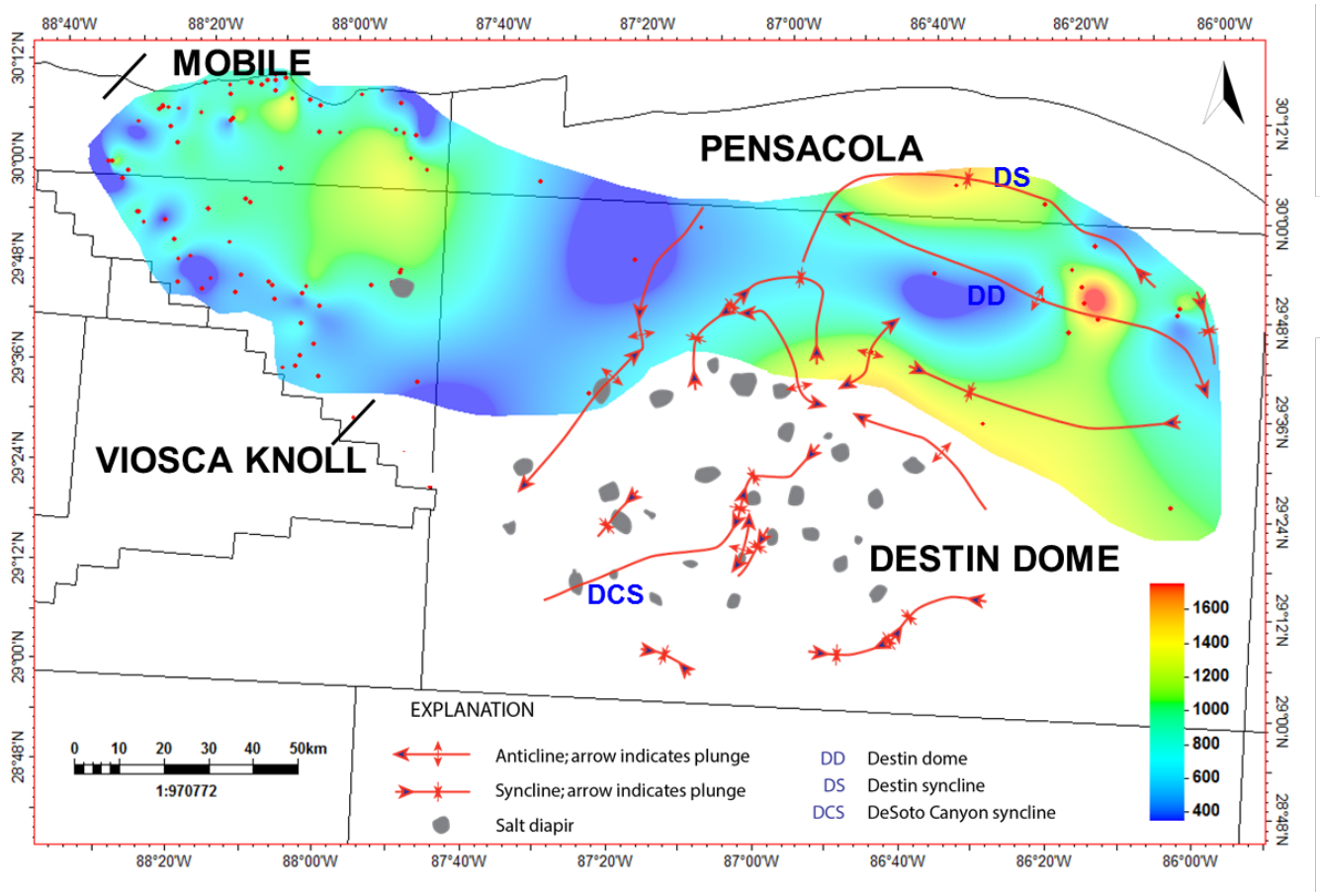

Figure 2.8. Isochore map of the Paluxy Formation in the DeSoto Canyon Salt Basin.

The lower part of the Paluxy Formation is rich in mud and contains multiple single-storey sandstone lenses. The thickness of these sandstone lenses ranges from about 3-21 m (10-70 ft). The SP, GR, density and resistivity log curves are variable and include blocky and Christmas tree signatures. Blocky SP, GR and high resistivity signatures indicate little variation in grain size and porosity, whereas Christmas tree signatures typically reflect fining-upward trends with porosity also decreasing upward. These variations result in significant stratigraphic heterogeneity.

The upper Paluxy is dominated by sandstone bodies that tend to thicken upward in section. These sandstone units are thicker than 15 m (50 ft) and more widespread laterally than the lower sandstone units and possess variable log signatures. These sandstone units are interbedded with fewer shale as compared to the lower Paluxy. This complex multi-storey stacking is observed in all drilled wells and is indicative of the depositional heterogeneity. Porosity in the Paluxy Formation commonly exceeds 20%. Geophysical logs from well G02486 in the Destin Dome Area show a typical Paluxy sandstone unit (Fig. 2.9). The sandstone is about 24 m (80 ft) thick and has porosity ranging between 12 and 26%; average porosity is about 21.5%.

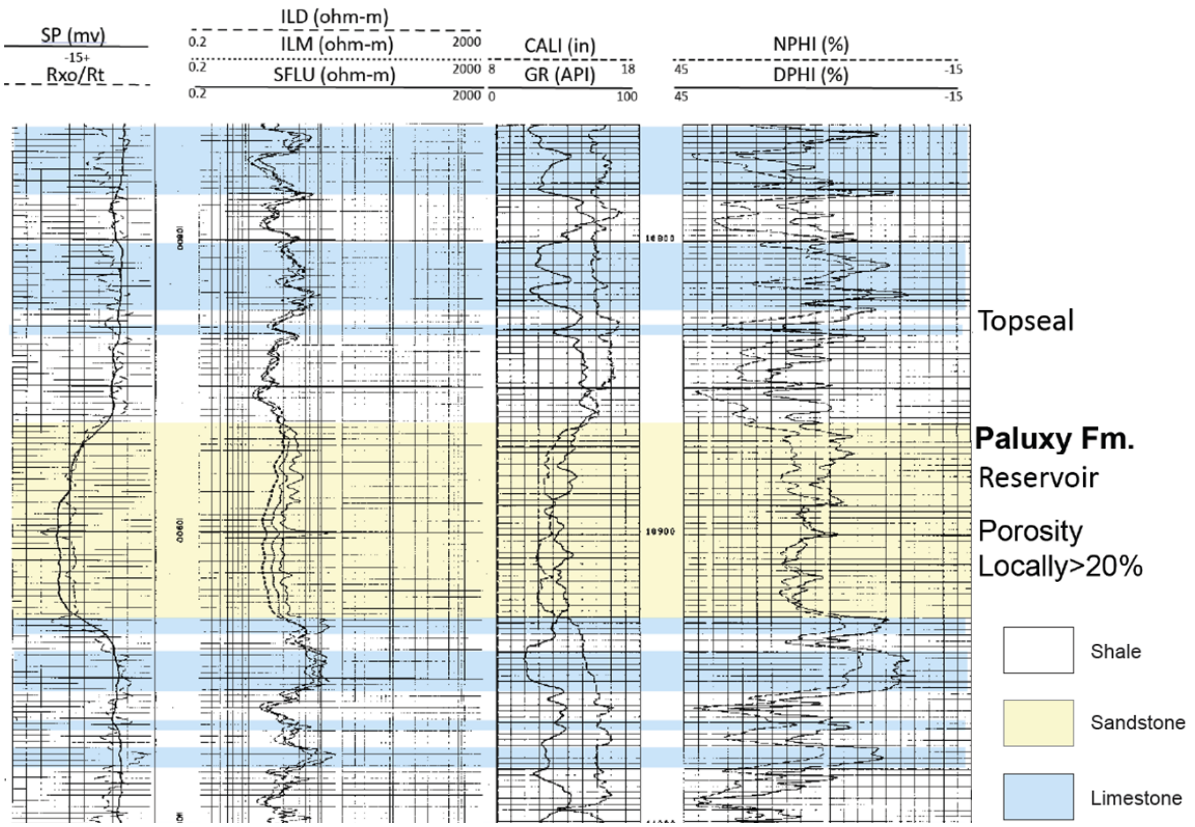

Figure 2.9. Interpretation of geophysical well logs of the Paluxy Formation in well GO2486, Destin Dome Area.

The Paluxy Formation is overlain by the Washita-Fredericksburg interval, which has a total thickness of about 350-1,000 m (1,200 to 3,200 ft). An isochore map indicates that the thickest Washita-Fredericksburg sections are in the Mobile and Viosca Knoll areas (Fig. 2.10). The lower part of the Washita-Fredericksburg interval is composed principally of limestone with numerous interbeds of shale and sandstone and gradationally becomes shale rich in the upper section (Plates 1, 2). This limestone-dominated section ranges in thickness from 300-600 m (1,000 to 2,000 ft) (Fig. 2.11). The percentage of limestone in the Washita-Fredericksburg section increases southward (Plate 2), and porosity of the limestone generally ranges between 0 and 4%. Sandstone bodies in the southern part of the Viosca Knoll Area are thin and discontinuous and typically have porosity less than 8%. The upper Washita-Fredericksburg section is rich in mudstone and contains numerous discontinuous sandstone bodies (Plates 1, 2). Few of these sandstone units have porosity greater than 15%, and those that do are in the upper part of the Washita-Fredericksburg interval at the approximate level of the Dantzler sand (Chasteen, 1983). A major sandstone unit is developed in the strike cross-section (Plate 1). The SP logs typically have a blocky signature for this Washita-Fredericksburg sandstone unit. Geophysical logs from the Mobile Area show a typical reservoir sandstone unit from the upper Washita-Fredericksburg interval (Fig. 2.12). The sandstone is about 27m (90 ft) in thickness and has porosity between 21 and 26% with an average porosity of about 23%.

Farther offshore (wells MO 991 and VK 117), the Cretaceous section is dominated by carbonate (Fig. 2.7). However, the sandstone of the Lower Tuscaloosa Group, which was proven as a storage target in the SECARB Plant Daniel and Cranfield tests (e.g., Koperna et al., 2009;

Hovorka et al., 2013), is widespread and is sealed by the Marine Shale of the Tuscaloosa Group. The lower Tuscaloosa Group sharply overlies the Washita-Fredericksburg interval. The thickness of the lower Tuscaloosa is generally between 60-120 m (200-400 ft) (Fig. 2.13). It thins rapidly to 24-446 m (80-150 ft) in the area of the Destin Dome Anticline. The Massive sand, which forms the base of the Lower Tuscaloosa, ranges from 67-90 m (220-300 ft) in thickness throughout the study area except in the crestal region of Destin Dome where it is only about 12 m (40 ft) thick (Petty, 1997). The SP and GR curves tend to be blocky and thus reflect generally uniform grain size and porosity in vertical section.

Porosity of lower Tuscaloosa sandstone is typically between 18 and 22%. A well log from the Pensacola Area shows a sandstone section with a gross thickness of 45 m (150 ft) (Fig. 2.14). This sandstone has porosity ranging between 18 and 28% with an average porosity of about 22%. A distinct positive SP deflection marks the base of the Marine Tuscaloosa shale, which is about 60-90 m (200-300 ft) thick throughout the study area and is a regional seal for petroleum reservoirs the lower Tuscaloosa Group (Mancini et al., 1987; Petty, 1997) (Fig. 2.7; Plates 1 and 2). The upper Tuscaloosa Group and Eutaw Formation contain little sandstone and are thus difficult to identify in the DeSoto Canyon Salt Basin. Accordingly, upper Tuscaloosa and Eutaw strata have been mapped with the Marine Tuscaloosa shale as a matter of practicality.

The Eutaw Formation is overlain by the thick chalk of the Selma Group. The Selma Group is about 335-442 m (1,100-1,450 ft) thick (Plate 1) in the Mobile and Viosca Knoll Areas and can be easily correlated throughout the basin due to its consistent resistivity signature. An isochore map of the Marine-Upper Tuscaloosa Group and Selma Group combined shows that the thickness varies between 180 and 700 m (600-2300 ft) (Fig. 2.15). Thickness is generally greater than 450 m (1500 ft) in the Mobile and Viosca Knoll Areas and decreases to about 600 ft in the eastern Destin Dome Area.

The Selma Group is overlain by 450-700 m (1,500- 2,300 ft) of strata that are assigned to the Paleogene-age Midway, Wilcox, and Claiborne Groups (Pashin et al., 2016). This interval is dominated by mudstone, and several sandstone units are included that are beyond the scope of this study. Shallower strata include the Oligocene-Miocene-age Tampa Limestone and the Miocene Pensacola Clay, the latter of which contains significant natural gas reservoirs and additional potential CO_2 sinks that are outside the scope of this thesis research (Hills and Pashin, 2010).

Numerous Paleogene-Miocene sandstone units occur in the northwestern part of the salt basin and, as previously mentioned, are productive nearshore. A preliminary assessment of the Miocene sandstone units (Hills and Pashin, 2010) suggests that the gas reservoirs are too small to accommodate sustained large-scale CO_2 storage operations, but major capacity may exist in the saline formations, which contain the bulk of the sandstone in the Miocene Series. Mudstone seals are clearly developed above natural gas accumulations, which image as bright spots in seismic profiles, but the geometry and extent of these seals is incompletely understood.

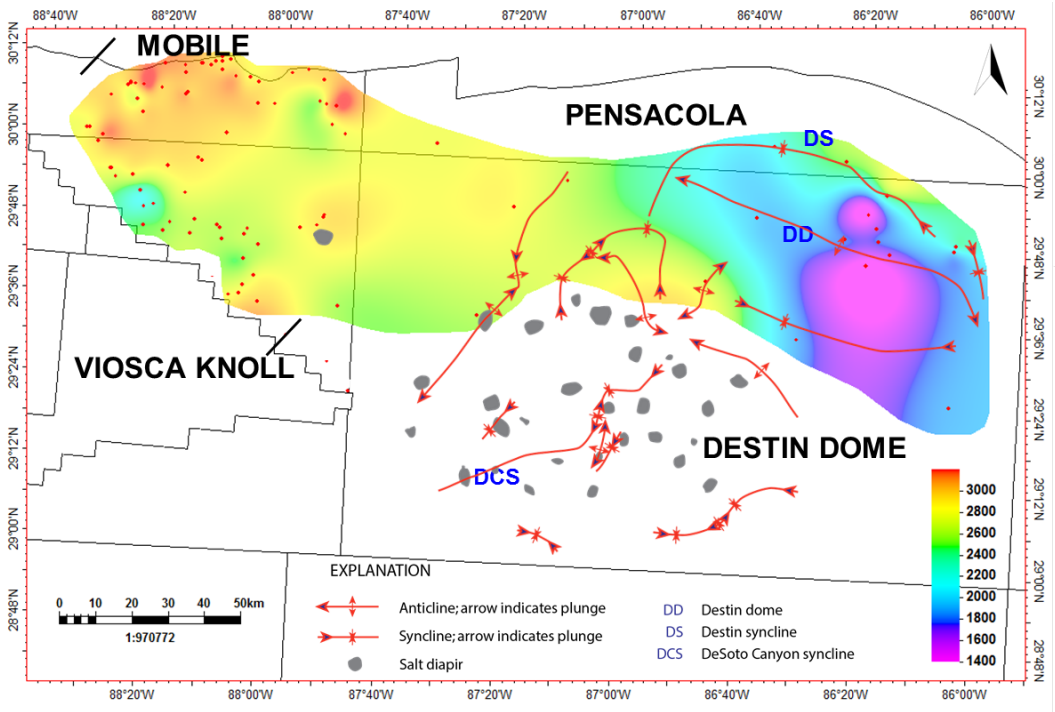

Figure.2.10. Isochore map of the Washita-Fredericksburg interval.

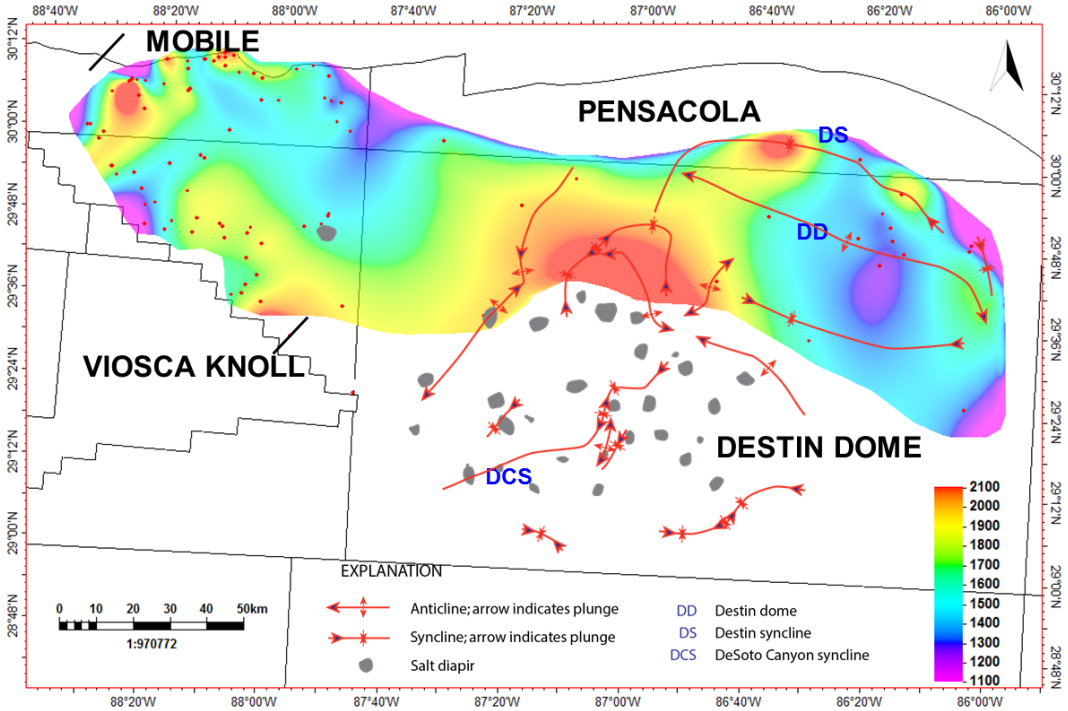

Figure 2.11. Isochore map of the basal limestone of the Washita-Fredericksburg interval.

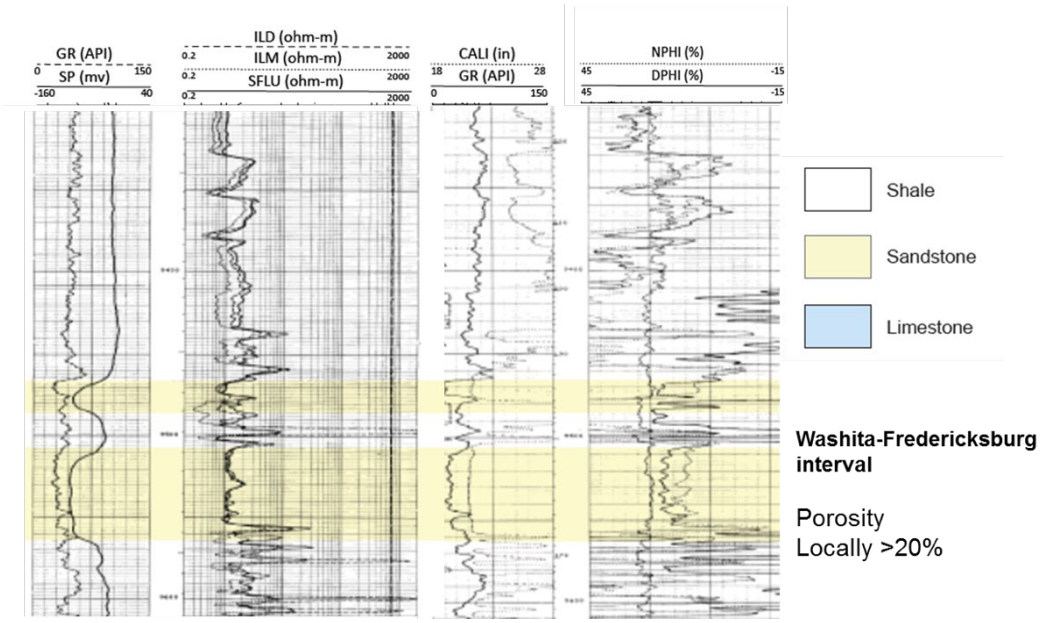

Figure 2.12. Interpretation of geophysical well logs of the Washita-Fredericksburg interval in the Mobile Area.

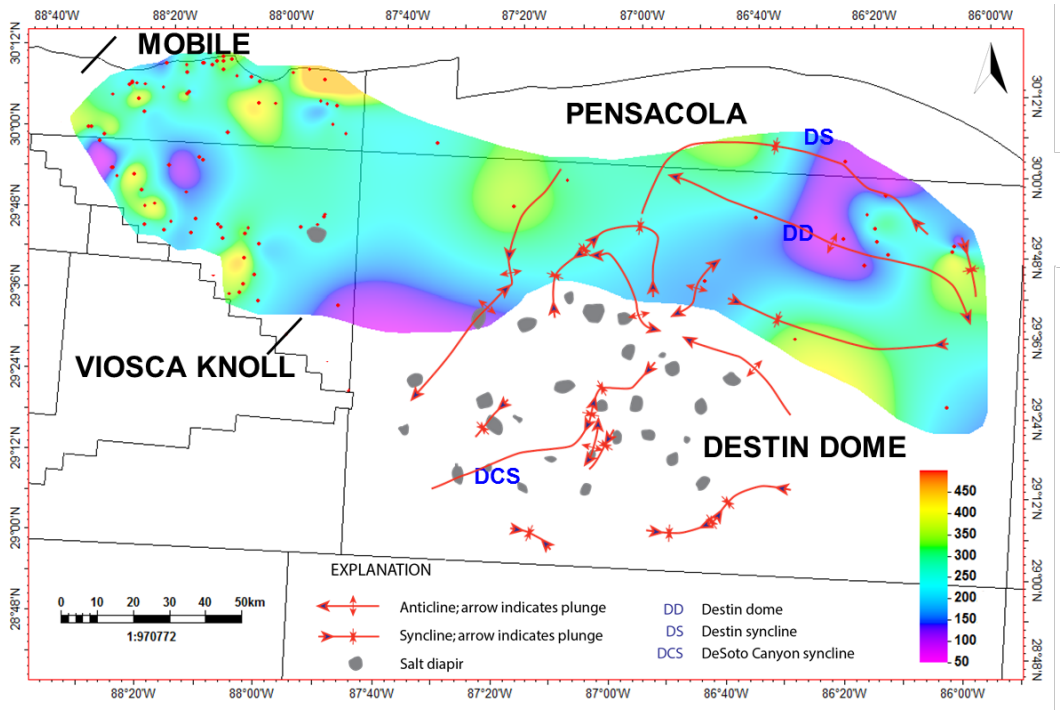

Figure 2.13. Isochore map of the lower Tuscaloosa Group.

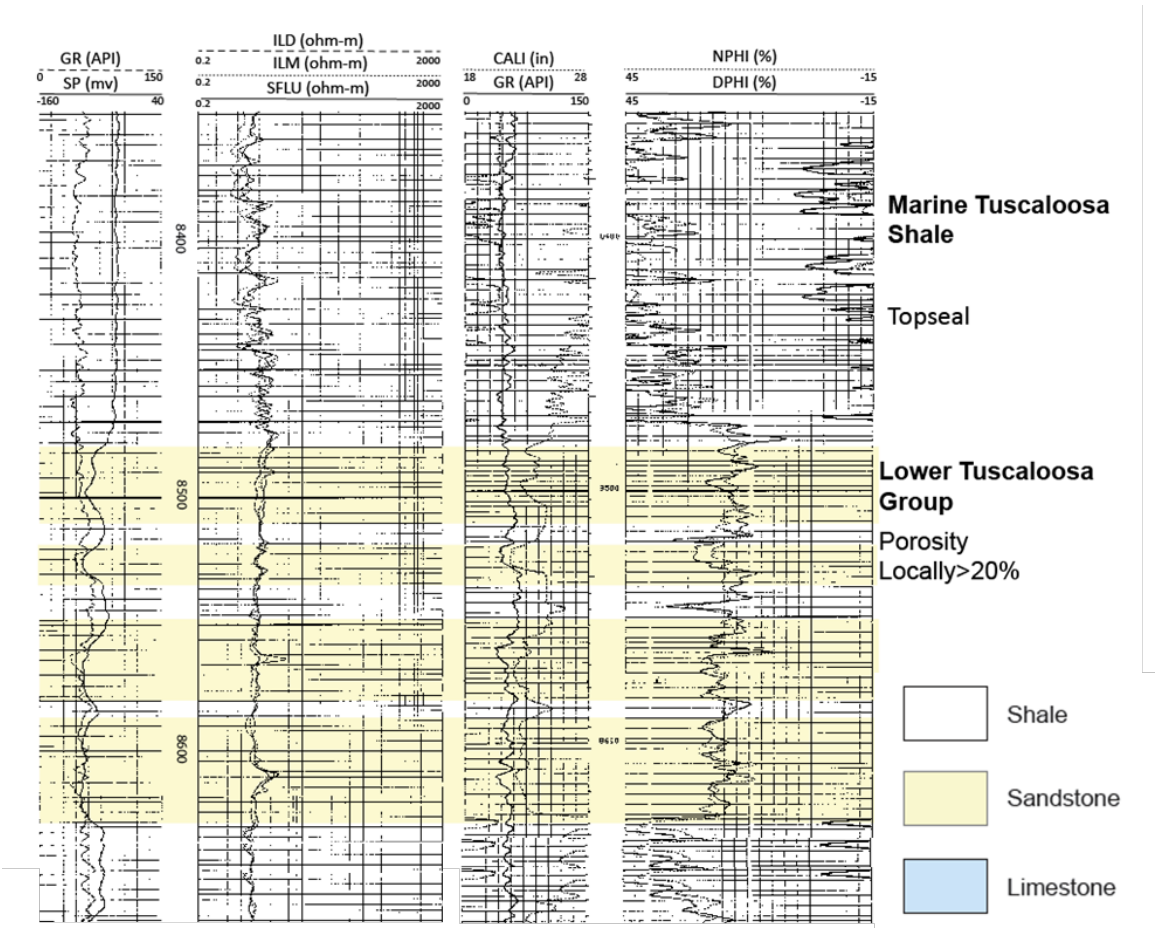

Figure 2.14. Interpretation of geophysical well logs of the lower Tuscaloosa Group in the Mobile Area.

In the DeSoto Salt Basin, Cenozoic strata of Paleocene-Eocene age are subdivided into the Midway, Wilcox, Claiborne, and Jackson Groups. Paleocene and Eocene strata form a cyclic succession of coastal-plain and shallow-marine siliciclastic, lignite, and marl (Mancini and Tew, 1991). Above the Jackson Group is a section of Oligocene and Miocene strata. Oligocene strata include shallow-marine carbonate and siliciclastic rocks, and Miocene strata of the Pensacola Clay contain mainly poorly consolidated clay and sand, which appear to include fluvial, deltaic, and shelf deposits (Smith, 1991; Bascle et al, 2001). The lower part of the Midway Group contains thick shale units with significant sealing capacity. The Wilcox Group contains numerous thick and permeable sandstone units. Ample data are available in the Mobile and Viosca Knoll Areas, as well as in scattered wells throughout the Destin Dome and Pensacola Areas.

Based on a recent assessment of the onshore South Florida Basin that was performed by the U.S. Geological Survey (Roberts-Ashby et al., 2015), the principal reservoirs favorable for CO_2 storage are in the Lower Cretaceous carbonate-evaporite successions and in the lower part of the Paleogene section. Four assessment units were defined in the Cretaceous-Paleogene section in the offshore part of the West Florida Shelf and are in order of stratigraphic succession (1) the Punta Gorda assessment unit, (2) the Gordon Pass assessment unit, (3) the Panther Camp assessment unit, and (4) the Cedar Keys assessment unit (Fig. 2.16, Plates 3, 4).

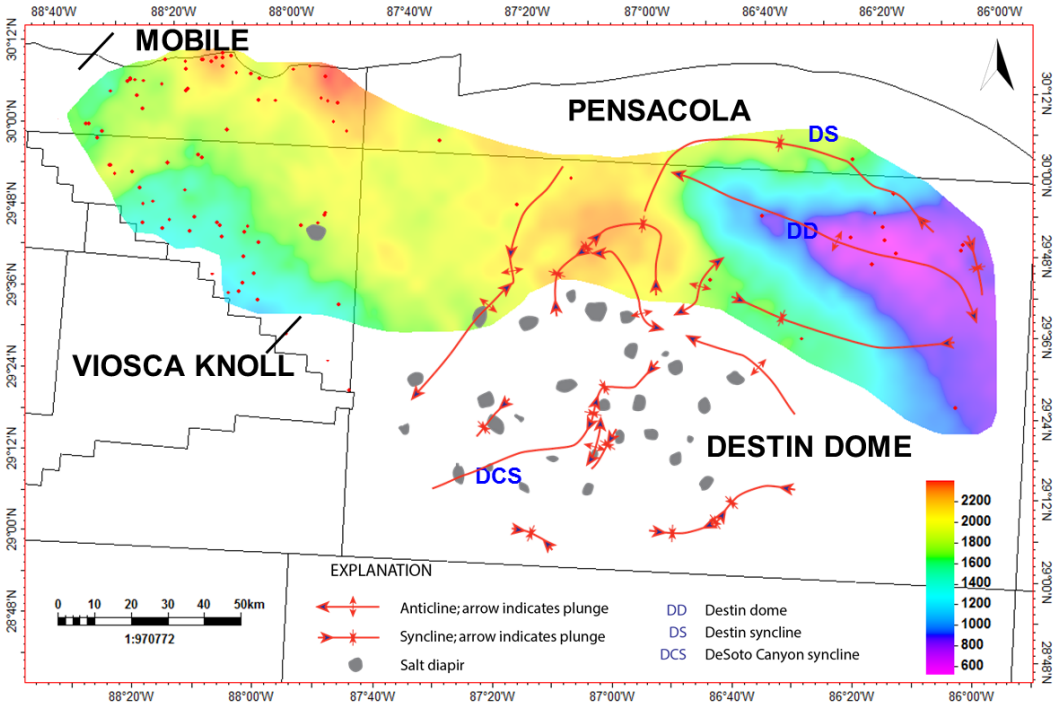

Figure 2.15. Combined isochore map of the Marine shale of the Tuscaloosa Group and the chalk of the Selma Group.

The Punta Gorda assessment unit consists of the Lehigh Acres Formation and the Punta Gorda Anhydrite (Fig.2.16; Plates 3, 4). The Lehigh Acres Formation is composed primarily of limestone and dolomite intercalated with some thin anhydrite beds. Porous dolomite intervals in the Lehigh Acres have net thickness of about 52 m (170 ft), while those in the Able Member are about 50 m (160 ft) thick. The upper part of the assessment unit is the Punta Gorda Anhydrite, which is a regionally continuous marker interval that is 60-120 m (200-400 ft) thick.

The Gordon Pass assessment unit includes the Marco Junction Formation, the Lake Trafford Formation, and the Gordon Pass Formation (Figs. 2.17, 2.18; Plates 3, 4). Dolomite is abundant in these formations, particularly on the Sarasota Arch, and limestone predominates in the Tampa Embayment. The Marco Junction Formation generally contains 24-36 m (80-120 ft) of porous dolomite with interbedded anhydrite. The Lake Trafford Formation generally contains 24-30 m (80-100 ft) of porous dolomite with interbedded limestone and anhydrite. Towards the northwest end of the study area, the Lake Trafford Formation is composed principally of limestone (Plates 3, 4). The Gordon Pass is a regionally continuous anhydrite marker that is up to 107 m (350 ft) thick and contains interbeds of dolomite and limestone.

The Panther Camp assessment unit consists of the Dollar Bay Formation (Big Cypress Group) and the Panther Camp Anhydrite (Figs. 2.16, 2.19; Plates 3, 4). The lower Dollar Bay is dominantly tight limestone that thickens with depth and distance from the Sarasota Arch and ranges from 40-170 m (130-550 ft) thick. The upper Dollar Bay contains several thick intervals 6-12 m(20-40 ft) of dolomite interbedded with lenses of anhydrite. Overlying the Dollar Bay Formation is a regionally continuous section of Panther Camp Anhydrite, which ranges in thickness from 20-67 m (65-220 ft).

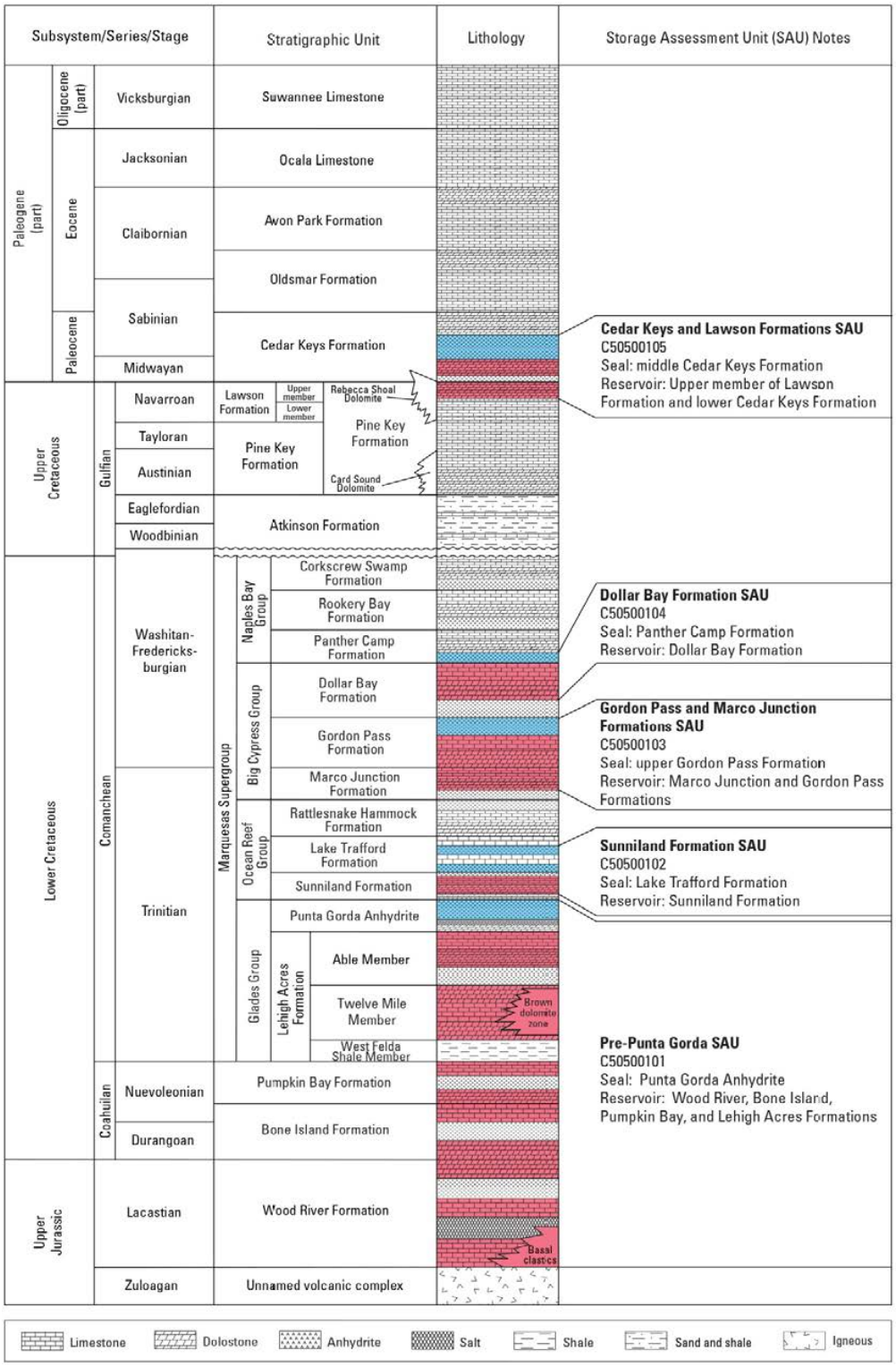

Figure 2.16. Stratigraphic column showing prospective storage targets and reservoir seals in onshore southern Florida (after Roberts-Ashby et al., 2015).

Between the Panther Camp and Cedar Keys assessment units are the Naples Bay Group and the Atkinson Formation (Fig. 2.16). The Naples Bay Group consists of the Rookery Bay Formation and the Corkscrew Swamp Formation. The Rookery Bay Formation is a tight limestone unit that thins towards the West Florida Escarpment and the crest of the Sarasota Arch (Plates 3, 4). Near the edge of the Tampa Embayment, the limestone thickens to a maximum of 223 m (730 ft). Near the West Florida Escarpment, the limestone of the Rookery Bay Formation passes into dolomite towards a structural high near the shelf margin. The Corkscrew Swamp Formation contains dolomite interbedded with anhydrite. Although there is abundant dolomite, this formation was not considered as a reservoir assessment unit because the anhydrite layers are thin, as is the overlying shale of the Atkinson Formation. The Atkinson Formation is dominantly a marine shale unit that is correlated with the Marine shale of the Tuscaloosa Group (Applin and Applin, 1967). The Atkinson Formation marks the base of the Upper Cretaceous section, and the base of the formation is thought to be a regional disconformity (Buffler, 1980). The Atkinson Formation is no more than 15 m (50 ft) thick in the study area.

The Cedar Keys assessment unit includes the Upper Cretaceous Pine Key and Lawson Formations, as well as the lower part of the Cedar Keys Formation (Fig. 2.20, Plates 3, 4). This is the thickest and shallowest assessment unit considered in this area. At the base of the Pine Key Formation is a section of Upper Cretaceous chalk. Above the chalk is thick, porous limestone that is about 305 m (1,000 ft) thick and thins toward the southwest (Plates 3, 4). Above the Pine Key is the Lawson Formation, which is composed of porous dolomite; the Lawson was logged only in two wells. The upper member of the Lawson onshore is coarse crystalline dolostone containing nodular and lensoid gypsum and anhydrite (Roberts-Ashby et al., 2015). The overlying Cedar Keys Formation is of Paleocene age and contains porous dolomite interbedded with anhydrite; the interval is not logged in most wells. The anhydrite beds in the Cedar Keys Formation appear to be continuous in the proximal shelf, where the Upper Cretaceous-Paleocene section is thickest, but are absent in the west and southwest part of the study area. Net thickness of the anhydrite beds is 40-46 m (130-150 ft).

The Tertiary-Quaternary section above the Cedar Keys assessment unit consists primarily of limestone and shale. Stratigraphic nomenclature varies significantly from the Florida Panhandle to the South Florida Basin (Southeastern Geological Society, 1986), and little is known about how offshore shelf stratigraphy relates to onshore stratigraphy because of a lack of well control. However, in onshore areas, Eocene through early Miocene strata constitute the Floridian aquifer system, which is a world-class aquifer resource. Saline formations with storage capacity may exist offshore in equivalent strata. The Miocene section contains potential aquifers and argillaceous confining units in the Pensacola Clay and the Hawthorn Group, which form the bulk of the prograding sediment wedge on the on the West Florida Shelf.

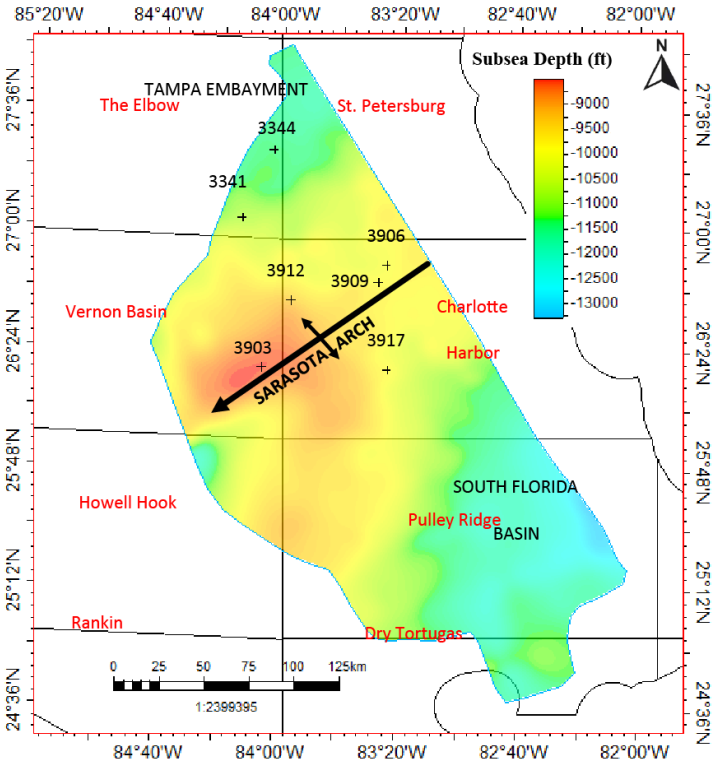

Figure 2.17. Subsea structure map of the top of the Punta Gorda Formation.

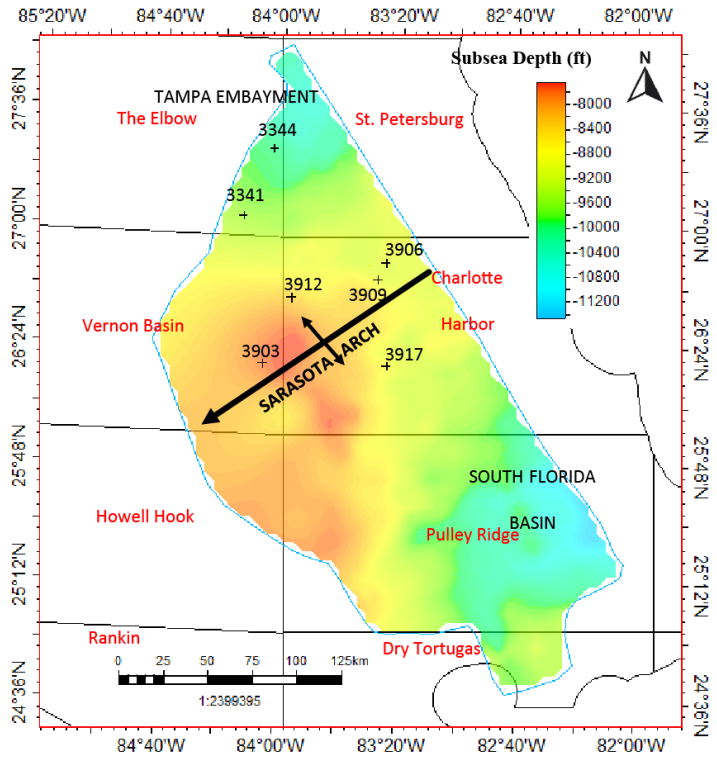

Figure 2.18. Subsea structure map of the top of the Gordon Pass Formation.

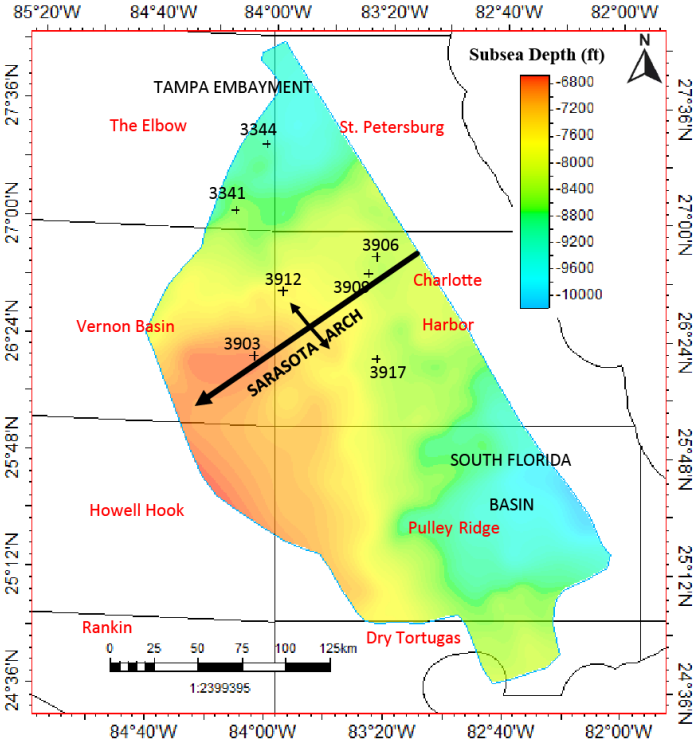

Figure 2.19. Subsea structure map of the top of the Panther Camp Formation.

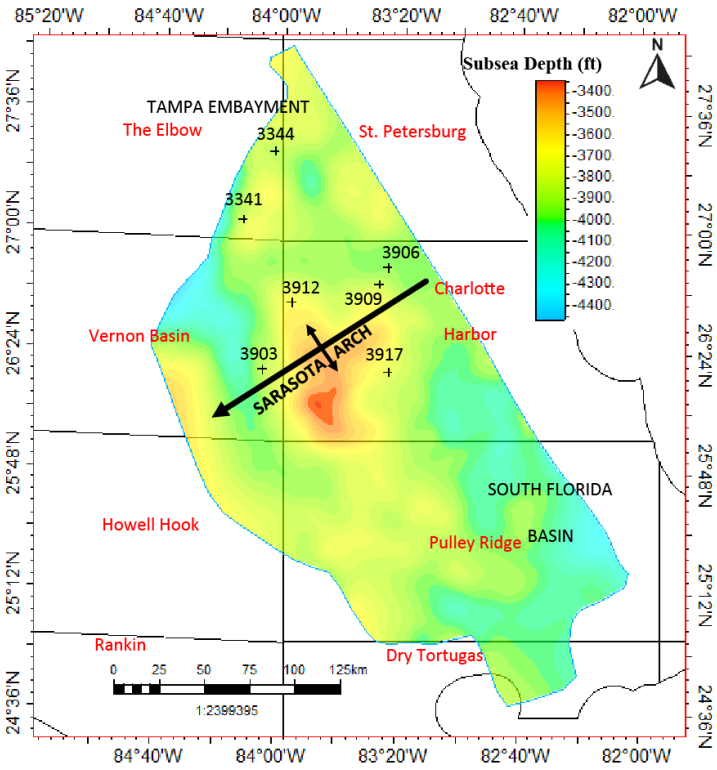

Figure 20. Subsea structure map of the top of the Cedar Keys Formation.

Task 3.0: Data Collection

Subtask 3.1 - Seismic Databases

A broad range of data are available for assessment of storage capacity in the EGOM focus area (Fig. 2.1), including seismic reflection surveys, geophysical well logs, and a broad range of other supporting data. Seismic reflection data in the region include numerous 2D and 3D surveys, and most 2D surveys are now more than 25 years old and are thus available to the public through BOEM. The EGOM project team has worked extensively with the data from the DeSoto Canyon Salt Basin, which are of high quality, providing clear imaging from the surface to the top of Jurassic salt or crystalline basement. Seismic surveys of similar vintage and quality are available from the West Florida Shelf. In all, 1,038 seismic reflection profiles are available from the study area. All publicly available seismic data were acquired and loaded into Kingdom 2D/3D Pak and Petrel. These data consist primarily of processed 2D SEG-Y images that offer exceptional imaging quality, showing stratal geometry clearly from the surface into crystalline basement.

Data coverage in most areas is dense enough to facilitate stratigraphic and balanced structural modeling, as well as advanced 3D visualization of geologic structure (Pashin et al., in press). The only significant gaps in coverage are in Tampa Bay and on parts of the Sarasota Arch (Fig. 2.1), In these areas, data are still sufficient to facilitate a useful understanding of geologic architecture and basic reservoir volumetrics.

Subtask 3.2 - Well Logs

Well data include seismic velocity surveys, mud logs, and geophysical well logs. More than 1,100 wells have been drilled in the study area, and the vast majority of these wells are in the Mobile and Viosca Knoll areas (Fig. 2.1). Digital checkshot (seismic velocity) data are available from 71 wells, and numerous paper records are available for other wells (Fig. 3.1). These facilitate velocity-depth control and conversion of seismic profiles from the time domain to the depth domain. Analysis of the velocity data indicates a high degree of consistency throughout the region, and so the profiles can be depth-converted with confidence. Velocity data were loaded into the Kingdom system, and most interpretive work was completed in the depth domain.

All offshore wells in the region have been logged, and the logs are available to the public in raster form. Raster images of 3,470 logs from 403 wells were acquired from BOEM and have been incorporated into the Kingdom, Petrel, and Petra projects. Well logs are diverse and include sample logs, resistivity logs, gamma ray logs, neutron-density logs, sonic logs, and dipmeter logs. Most wells penetrating Cretaceous or deeper strata were designed with multiple casing strings and were thus logged in multiple runs. This resulted in a wealth of fluid and temperature data.

Sample logs are available from most wells penetrating Cretaceous and older strata and provide vital lithologic control that helps with identification of reservoirs and seals and constrains interpretations of porosity. Sonic, resistivity, gamma ray, and porosity logs are available from most of these wells and provide the primary control for identifying and characterizing stratigraphic units and quantifying reservoir volumetrics (Figs. 3.2-3.6) Sonic logs are of further utility for developing synthetic seismograms, which help develop well-seismic ties.

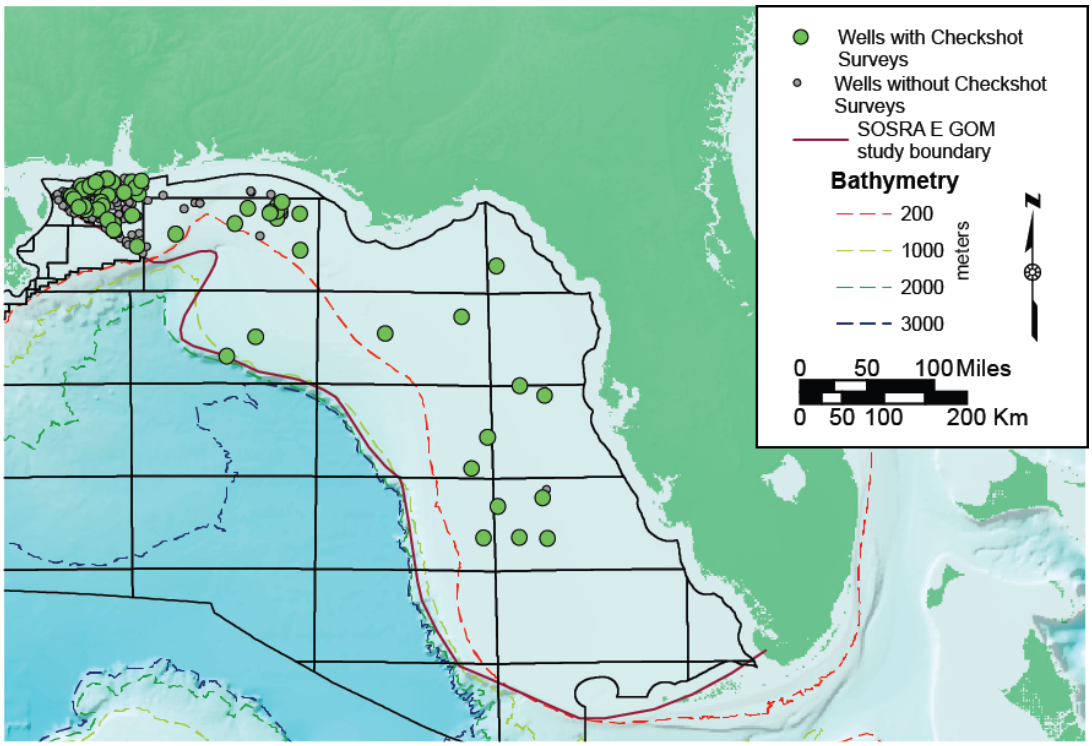

Figure 3.1. Map of the Eastern Gulf of Mexico showing locations of wells with checkshot (seismic velocity) surveys.

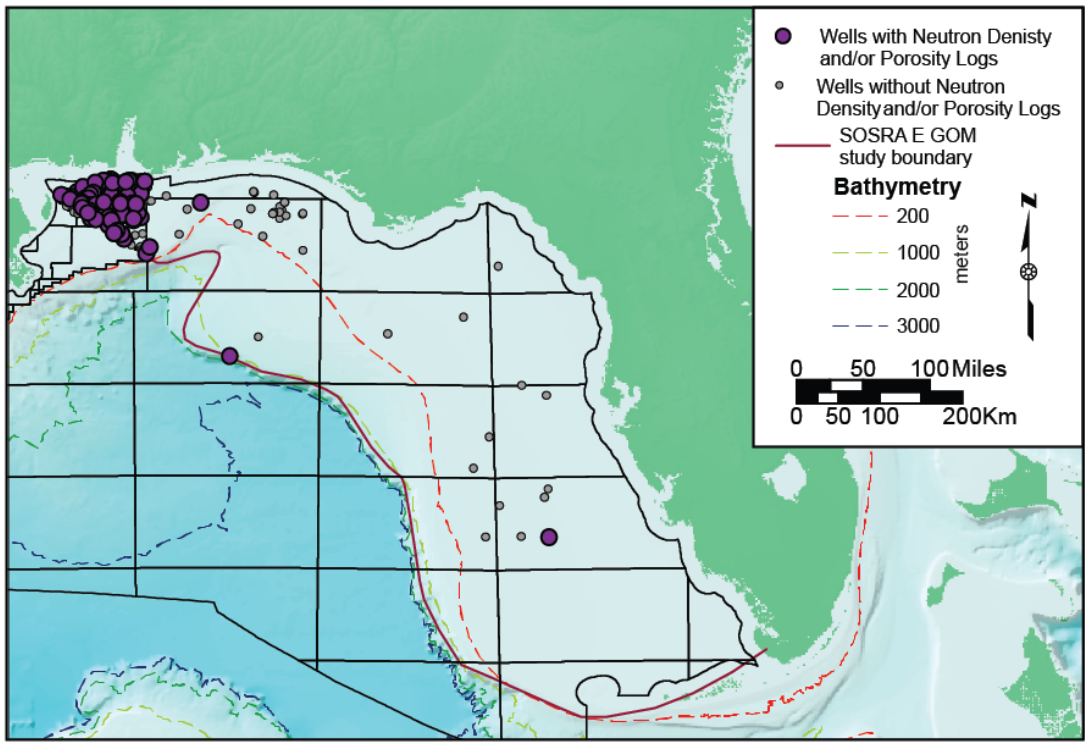

Figure 3.2. Map of the Eastern Gulf of Mexico showing locations of wells with sonic logs.

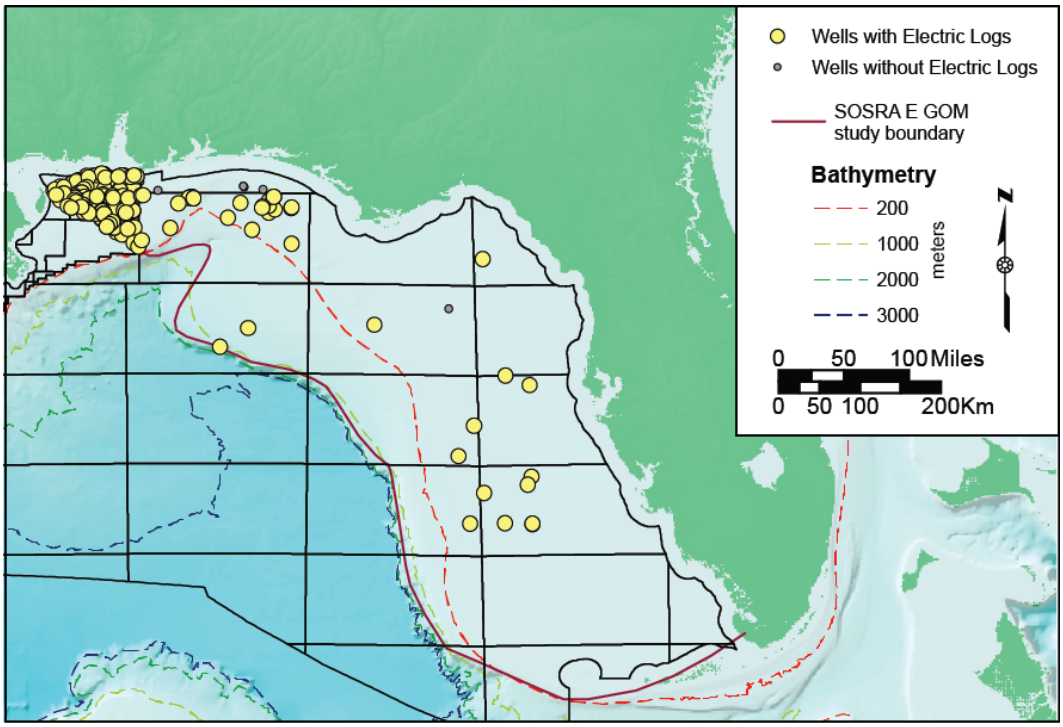

Figure 3.3. Map of the Eastern Gulf of Mexico showing locations of wells with electric logs, which are primarily induction logs run with shallow (10-inch) and deep (90-inch) electrode spacings.

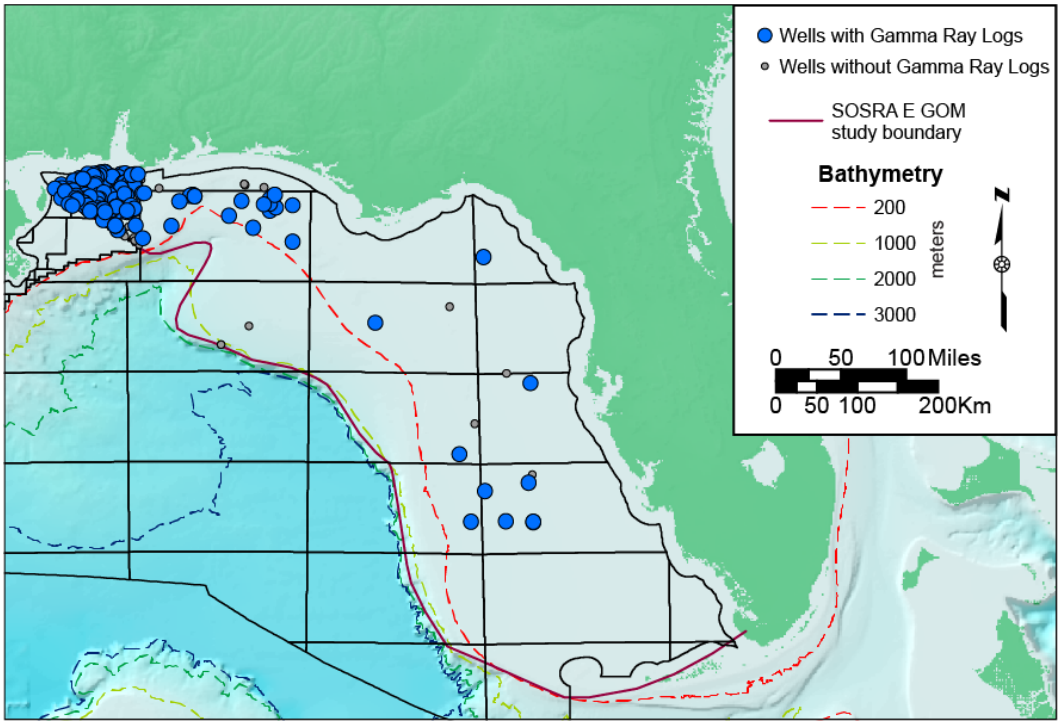

Figure 3.4. Map of the Eastern Gulf of Mexico showing locations of wells with gamma ray logs.

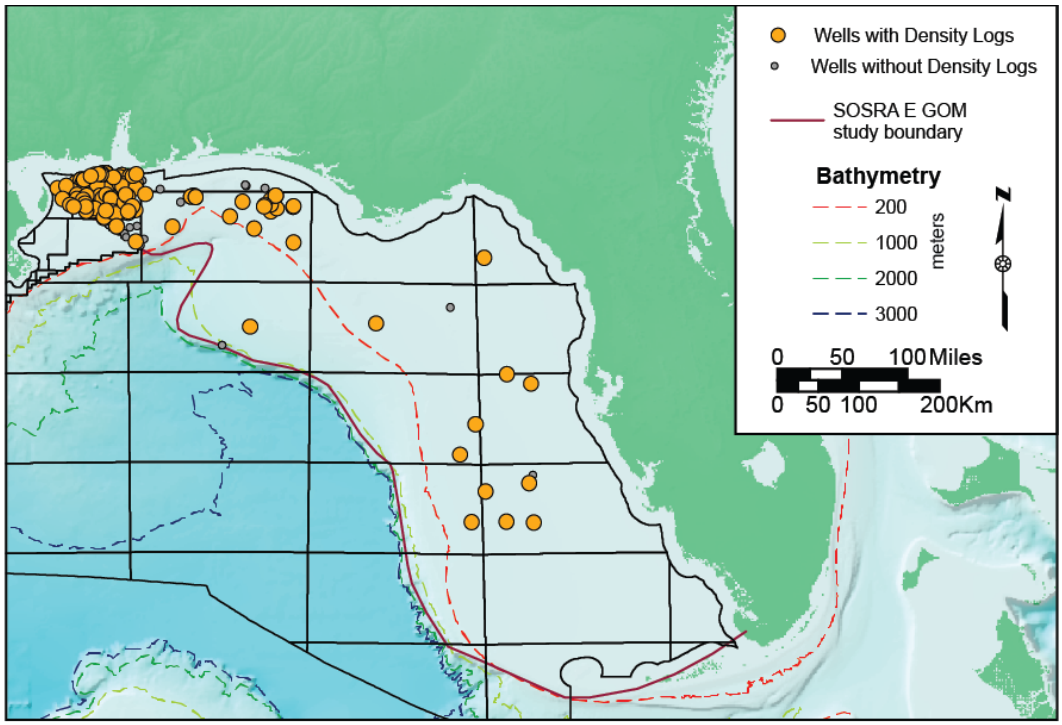

Figure 3.5. Map of the Eastern Gulf of Mexico showing locations of wells with density logs.

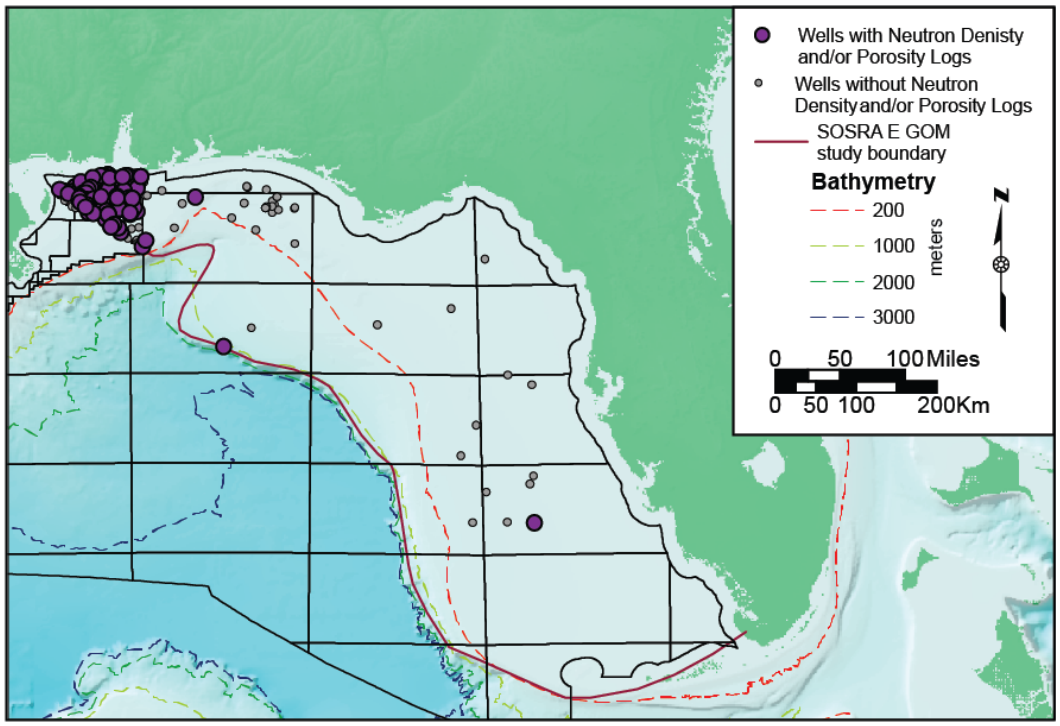

Figure 3.6. Map of the Eastern Gulf of Mexico showing locations of wells with neutron logs.

Geographic coverage of well data is variable in the study area. In the Mobile and Viosca Knoll Areas, data are abundant and facilitate extremely detailed assessment of storage capacity (Figs. 3.1-3.6). Data are relatively sparse on the West Florida Shelf, which remains a significant exploration frontier. These wells were drilled mainly in the 1970s, and so many were not logged with modern density and neutron porosity tools, and neutron logs are available for only one well. Nevertheless, the logs that are available in these areas have robust supporting data suites which facilitate identification of reservoirs and seals, identification of geologic trends, and the log suite is adequate for characterizing reservoir volumetrics.

Subtask 3.3 - Additional Data

Additional supporting data are available for many wells, including biostratigraphic reports, which aid in the identification and correlation of stratigraphic units. A broad range of GIS data are available through BOEM and the U.S. Geological Survey, including bathymetric surveys, geographic grids, lease maps, well location databases, and infrastructural databases. All essential GIS data have been acquired and loaded into the Kingdom, Petrel, and Petra projects.

Task 4.0: Data Analysis

This program requires the integration of diverse forms of geologic data. Key data elements are GIS layers, well data, and geophysical data, particularly seismic reflection surveys. The first step of this research was to identify and acquire the relevant GIS resources, well data, and seismic data in the study area, and these data were summarized in a Comprehensive Project Database. GIS layers were loaded into Kingdom 2D/3D Pak, which is the main software package used to organize and analyze project data. Seismic reflection data were then loaded, and quality control measures were then employed to ensure consistency of navigation and reflection data. Well data were then loaded, and rock types and stratigraphic units were interpreted based on mud logs and geophysical well logs. The log data have been instrumental for identifying candidate sinks and reservoir seals. Velocity surveys were then used to tie seismic and well data, and synthetic seismograms are being developed to verify the seismic responses of key stratigraphic markers. Once stratigraphic markers were identified, then seismic interpretation commenced at the regional level.

Subtask 4.1 - Quality Assessment

A broad range of data are available for assessment of storage capacity in the EGOM focus area (Figs. 2.1, 3.1-3.6), including seismic reflection surveys, geophysical well logs, and a broad range of other supporting data. Seismic reflection data in the region include numerous 2D and 3D surveys, and most 2D surveys are now more than 25 years old and are thus available to the public through BOEM. The EGOM project team has worked extensively with the data from the DeSoto Canyon Salt Basin, which are of high quality, providing clear imaging from the surface to the top of Jurassic salt or crystalline basement. Seismic surveys of similar vintage and quality are available from the West Florida Shelf. In all, 1,038 seismic reflection profiles are available from the study area. All publicly available seismic data have been acquired and loaded into Kingdom 2D/3D Pak and Petrel. These data consist primarily of processed 2D SEG-Y images that offer exceptional imaging quality, showing stratal geometry clearly from the surface into crystalline basement.

Well data include seismic velocity surveys, mud logs, and geophysical well logs. More than 1,100 wells have been drilled in the study area, and the vast majority of these wells are in the

Mobile and Viosca Knoll areas (Fig. 2.1). These facilitate velocity-depth control and conversion of seismic profiles from the time domain to the depth domain. Analysis of the velocity data indicates a high degree of consistency throughout the region, and so the profiles can be depth-converted with confidence. Velocity data have been loaded into the Kingdom system, and most interpretive work is now proceeding in the depth domain.

All offshore wells in the region have been logged, and the logs are available to the public in raster form. Raster images of 3,470 logs from 403 wells have been acquired from BOEM and have been incorporated into the Kingdom project (Figs. 3.1-3.6). Well logs are diverse and include sample logs, resistivity logs, gamma ray logs, neutron-density logs, sonic logs, and dipmeter logs. Most wells penetrating Cretaceous or deeper strata were designed with multiple casing strings and were thus logged in multiple runs. This resulted in a wealth of fluid and temperature data.

Sample logs are available from most wells penetrating Cretaceous and older strata and provide vital lithologic control that helps with identification of reservoirs and seals and constrains interpretations of porosity. Sonic, resistivity, gamma ray, and porosity logs are available from most of these wells and provide the primary control for identifying and characterizing stratigraphic units and quantifying reservoir volumetrics. Sonic logs are of further utility for developing synthetic seismograms, which help develop well-seismic ties.

Subtask 4.2 - Coverage Assessment

Geographic coverage of well data is variable in the study area and has been discussed by Pashin et al. (2017). In the Mobile and Viosca Knoll Areas, data are abundant and facilitate extremely detailed assessment of storage capacity. Data are relatively sparse on the West Florida Shelf, which remains a significant exploration frontier. These wells were drilled mainly in the 1970s, and so many were not logged with modern density and neutron porosity tools. Nevertheless, the logs that are available in these areas have robust supporting data suites that are helpful for assessing reservoir quality.

Seismic data coverage in most areas is dense enough to facilitate stratigraphic and balanced structural modeling, as well as advanced 3D visualization of geologic structure (Pashin et al., 2016b). The only significant gaps in coverage are in Tampa Bay and on parts of the Sarasota Arch (Fig. 2.1). In these areas, data are still sufficient to facilitate a useful understanding of geologic architecture and basic reservoir volumetrics.

The quality and coverage of seismic and well data in the eastern Gulf of Mexico is more than adequate to make a detailed assessment of geology and reservoir volumetrics. Multifold 2-D seismic profiles were shot in a dense grid that facilitates detailed subsurface mapping, quantitative stratigraphic and structural analysis, and delineation of candidate CO_2 sinks and reservoir seals at the regional scale. In many areas, such as the DeSoto Canyon Salt Basin, these data are sufficient for prospect generation and the development of CO_2 storage pilots and projects.

Wells are abundant in the Mobile and Viosca Knoll Areas, which have a history of major offshore exploration production operations, whereas well coverage is sparse in the West Florida Shelf. Where coverage is sparse, the geophysical log data are adequate to develop well-seismic ties and to identify and characterize potential CO_2 sinks and seals. Some of these wells pre-date modern porosity log suites, but the density and sonic logs do facilitate analysis of reservoir volumetrics. Combined with the dense grid of seismic coverage, the data are sufficient for

delineation of trends and projection into areas with only seismic data, such as the South Florida Basin.

In conclusion, the project team felt that the data quality and coverage in the eastern Gulf of Mexico are robust and facilitate detailed assessment of offshore geology and quantification of CO_2 storage potential. Accordingly, the project team recommended moving forward with this research at the appropriate milestone.

Subtask 4.3 - Well-Seismic Ties

Digital checkshot (seismic velocity) data are available from 71 wells, and numerous paper records are available for other wells (Fig. 4.1). Analysis of the checkshot data indicates that the velocity field is very stable throughout the DeSoto Canyon Salt Basin, which contains a mix of carbonate and siliciclastic strata. Velocity-depth relationships differ in the West Florida shelf, which is dominated by carbonates with seismic velocity. Basic seismic-well ties based on checkshot surveys have proven to be quite robust, with the seafloor and well imaged seismic events occurring at the depths expected from comparison of checkshot and lithologic data. Synthetic seismograms, moreover, are proving useful for substantiating the seismic signature of key stratigraphic markers and for identifying imaging anomalies related to changes of frequency and phase in the different seismic surveys used in this research.

Subtask 4.4 - Seismic Interpretation

Major stratigraphic reflections can be traced readily throughout the study area, and the Ferry Lake-Punta Gorda anhydrite marker is indispensable for tying the stratigraphy of the West Florida Shelf with that of the DeSoto Canyon Salt Basin.

An important challenge for this research is tying reservoir sandstone and carbonate intervals to the seismic profiles and constraining the areal extent of these intervals. Major seismic events are more closely associated with seals than with the target reservoirs, and so mapping reservoir facies requires careful evaluation of well data and interpretation of seismic data. In many areas, the amplitude of a major reflectors appears to correlate with the thickness and extent of the major reservoir seals, which helps constrain regions where storage may be viable. Porous reservoir intervals are readily identified in geophysical well logs, but the seismic signature of these intervals is indistinct. Accordingly, analyzing and understanding geospatial trends in reservoir quality is essential for mapping reservoir extent on the basis of seismic datasets.

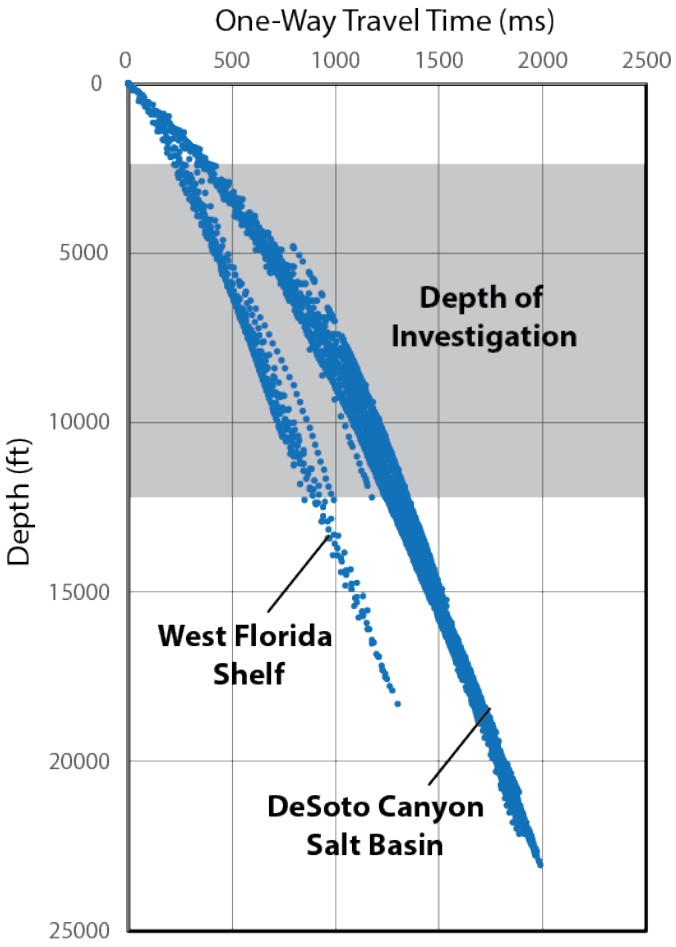

Figure 4.1. Traveltime-depth plot based on 71 checkshot records showing difference in seismic velocity field in the DeSoto Canyon Salt Basin and the West Florida Shelf.

Task 5.0: Geologic Characterization and Volumetric Calculations

Subtask 5.1 - Reservoir Characterization; Subtask 5.2 – Mapping

DeSoto Canyon Salt Basin

The net sandstone isolith map of Paluxy Formation demonstrates the variability of sandstone distribution in the study area (Fig. 5.1). Net sand thickness generally ranges from 30-110 m (100-350 ft) across most of the study area but is as thin as 15 m (50 ft) in the central part of the basin and in the western part of the crestal region of Destin Dome. The thickness increases to 113 m (370 ft) in the salt withdrawal synclines on the flanks of Destin Dome.

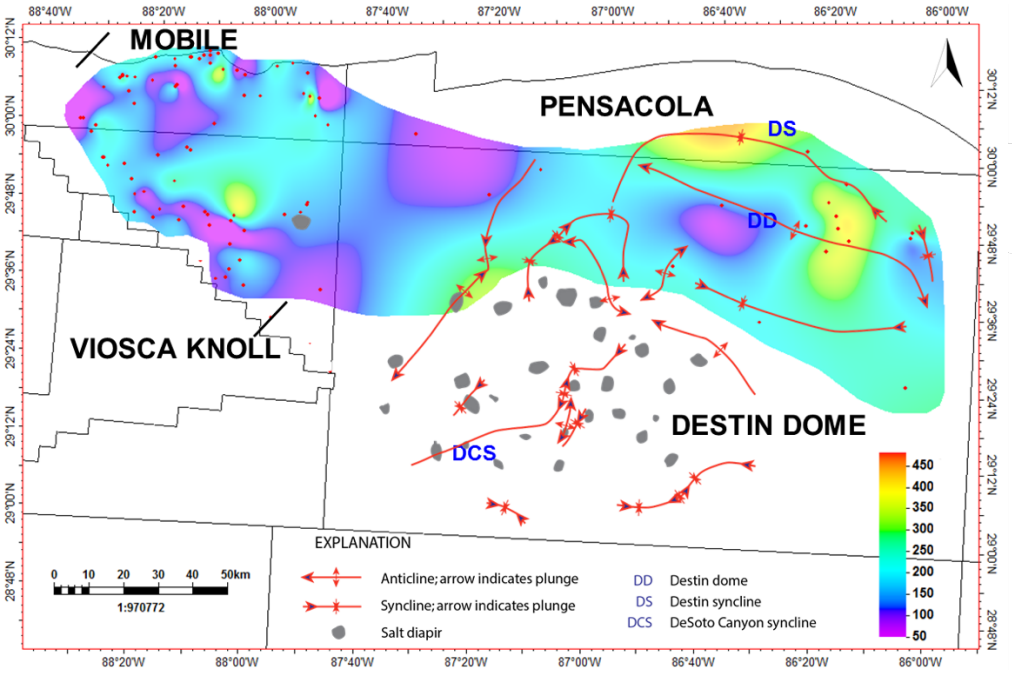

Figure 5.1. Net sandstone isolith map of the Paluxy Formation.

The Washita-Fredericksburg net sandstone isolith map shows that the distribution of qualified sandstone is limited (Fig. 5.2). Some sandstone is present in the Mobile and Viosca Knoll Areas with thickness varying from 0-36 m (0-120 ft) with the thickest accumulations along two northwest-southeast and north-south trending axes. Some reservoir quality sandstone with thickness generally ranging from 6-24 m (20-80 ft) is present in the salt withdrawal synclines on the flanks of Destin Dome.

The lower Tuscaloosa net sandstone isolith map (Fig. 5.3) shows that the sandstone unit is thickest in the Mobile, western Pensacola and Viosca Knoll Areas, with thickness ranging from 30-90 m (100-300 ft). The sandstone, however, is very thin (< 30 m; 100 ft) in the southern and eastern part of the basin in the Destin Dome Area and is thinner than 9 m (30 ft) in the crestal region of the Destin Dome Anticline.

Figure 5.4 is the average porosity map for qualified sandstone in the Paluxy Formation. The map shows that sandstone in the eastern part of the basin (Destin Dome and Pensacola Areas) in places has elevated porosity ranging from 20 to 24%. These high porosity values for the thin sandstone units in this area may be an artifact of sparse well control. On the other hand, sandstone in the western part of the basin (Mobile and Viosca Knoll Areas) generally has lower porosity (15-18%).

Since reservoir quality sandstone units in the Washita-Fredericksburg interval are limited to a very small area of the basin, including the Mobile and Viosca Knoll Areas and the northwestern part of the Destin Syncline, the porosity map highlights only this region. The average porosity values vary between 15 and 23% (Fig. 5.5).

The Massive sand of the lower Tuscaloosa Group, on the other hand, has higher average porosity than the Paluxy Formation and the Washita-Fredericksburg interval (Fig. 5.6).

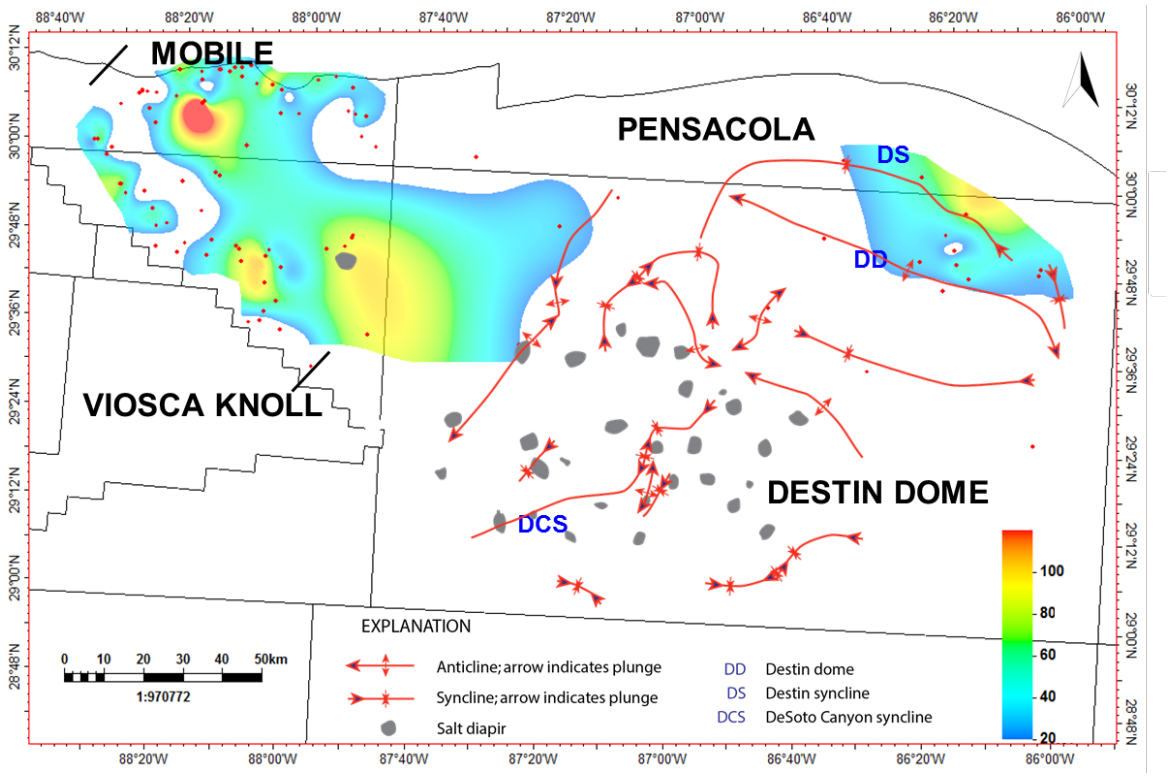

Figure 5.2. Net sandstone isolith map of the Washita-Fredericksburg interval.

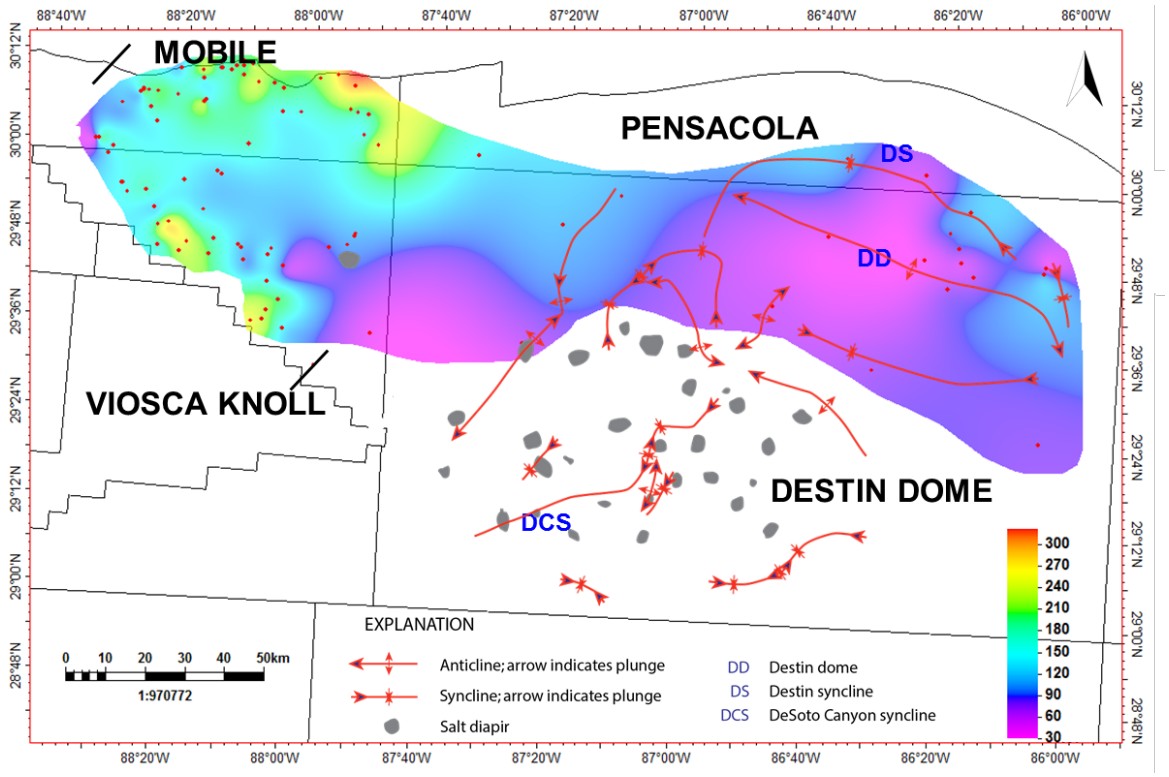

Figure 5.3. Net sandstone isolith map of the lower Tuscaloosa Group.

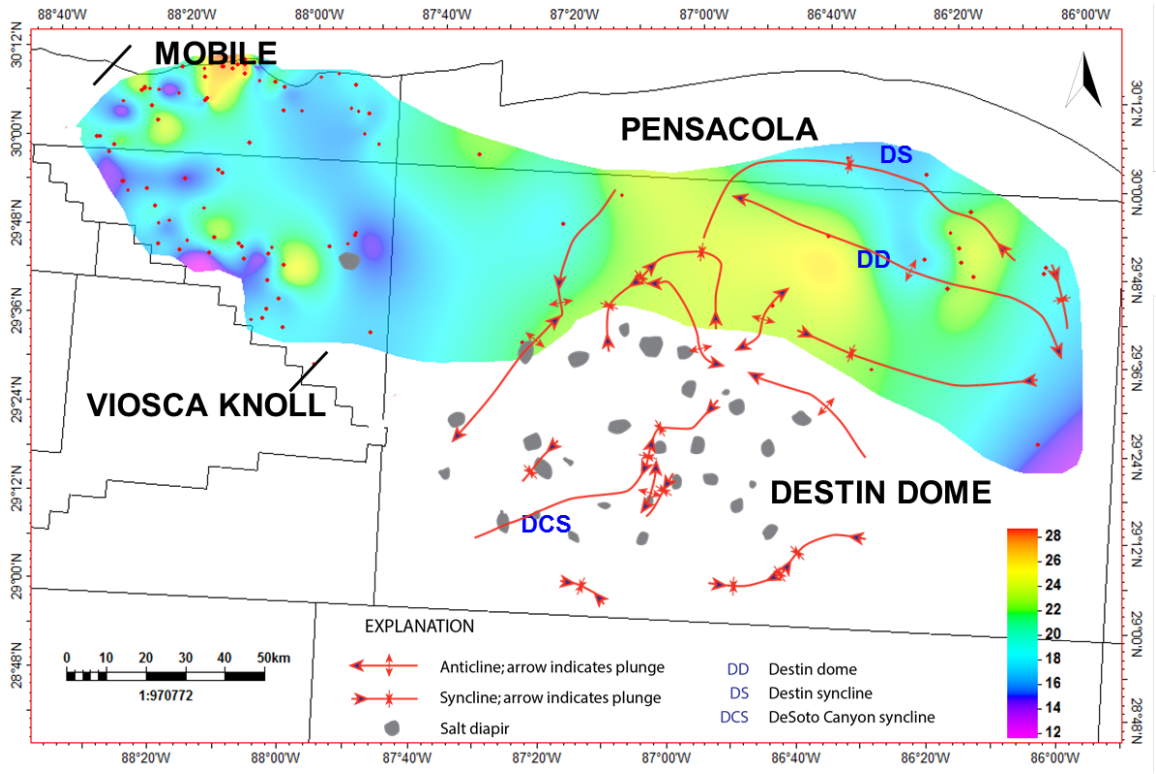

Figure 5.4. Average porosity of qualified sandstone in the Paluxy Formation.

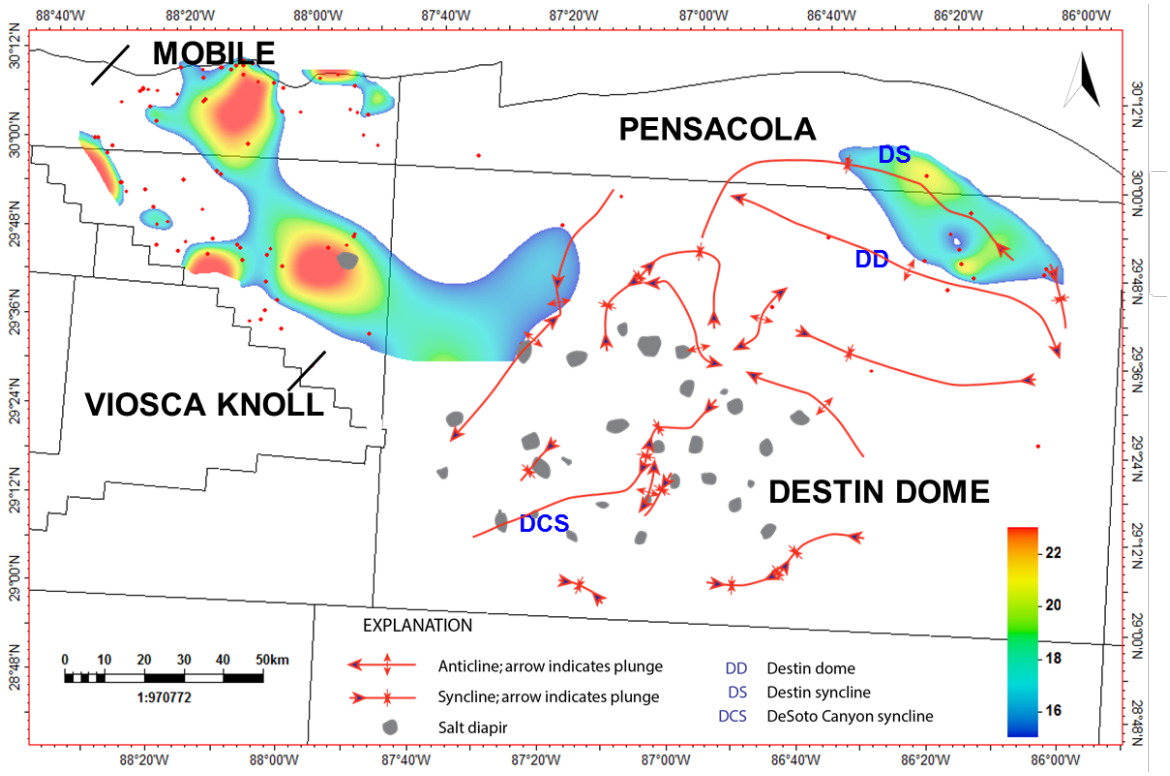

Figure 5.5. Average porosity of qualified sandstone in the Washita-Fredericksburg interval.

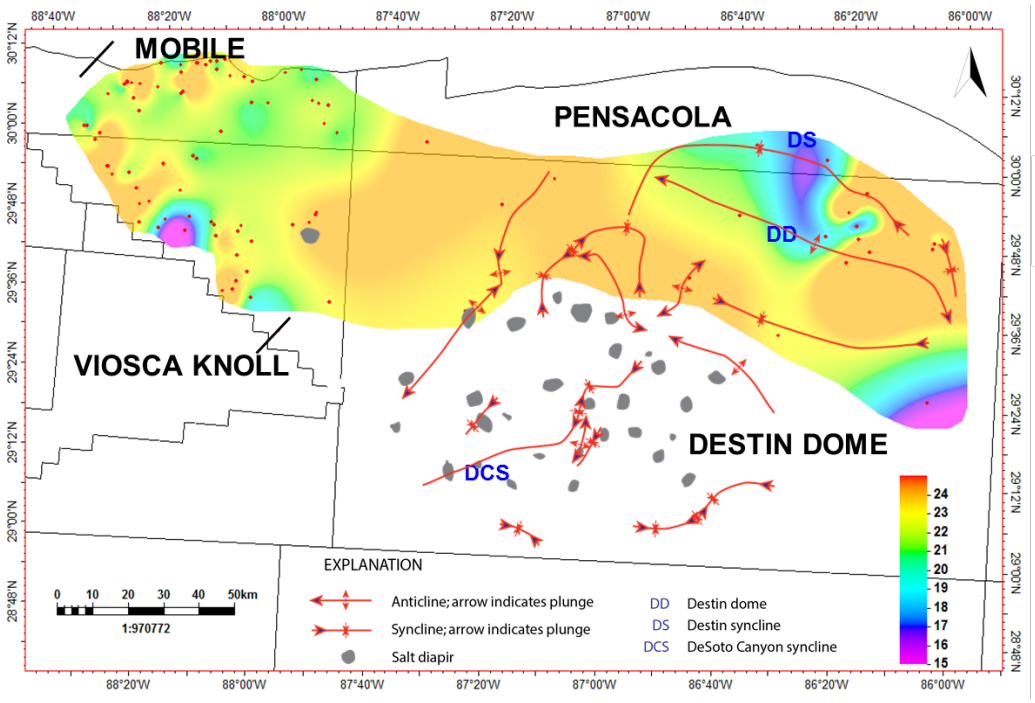

Figure 5.6. Average porosity of qualified sandstone in the lower Tuscaloosa Group.

Average porosity of the lower Tuscaloosa generally varies from 20-25% in the Mobile and Viosca Knoll Areas. Porosity averages about 24% in the eastern part of the basin and is locally lower than 15%.

Table 1 shows the variation of porosity values in all qualified Cretaceous reservoirs based on geophysical log analysis. Note that these values only represent sandstone meeting the qualification criteria, which are minimum porosity of 15% and thickness exceeding 6 m (20 ft). Since the range of the data and standard deviation are low, mean and median porosity values are close and reflect a normal population distribution. Of the three reservoirs evaluated, the lower Tuscaloosa Group has the highest mean porosity, which is estimated to be 22.5%.

A lack of routine core analysis data means that the permeability of Cretaceous sandstone in the study area is unknown. However, onshore core data from these formations reveal basic porosity-permeability relationships in the formations being considered as storage targets (Pashin et al., 2008; Folaranmi, 2015). Figure 5.7 shows a scatterplot of porosity vs. permeability in Cretaceous sandstone (Pashin et al., 2008). Permeability values range from 125 to more than 5,000 mD and follow a log-normal distribution. The geometric mean values are 236, 184, and 269 mD in the Paluxy Formation, Washita-Fredericksburg interval, and the lower Tuscaloosa Group, respectively.

Due to varying stratigraphy and stratigraphic nomenclature, age-equivalent Paleocene-Miocene units were mapped together (e.g., Alabama Claiborne Group and Florida Avon Park Formation were unified as the middle Eocene undifferentiated). For isochore maps, net sand isolith maps, and storage resource calculations, these were further consolidated into two units for study. These units are a Paleocene-mid Eocene interval and an upper Eocene-Miocene interval.

Table 1. Porosity statistics for Cretaceous reservoirs in DeSoto Canyon Salt Basin.

Stratigraphic Unit	Minimum	Maximum	Mean	Median	Standard Deviation
Lower Tuscaloosa Group	16.0	26.0	22.5	22.7	1.9
Washita-Fredericksburg interval	15.0	23.0	18.2	18.5	2.3
Paluxy formation	15.0	28.0	19.9	20.1	2.4

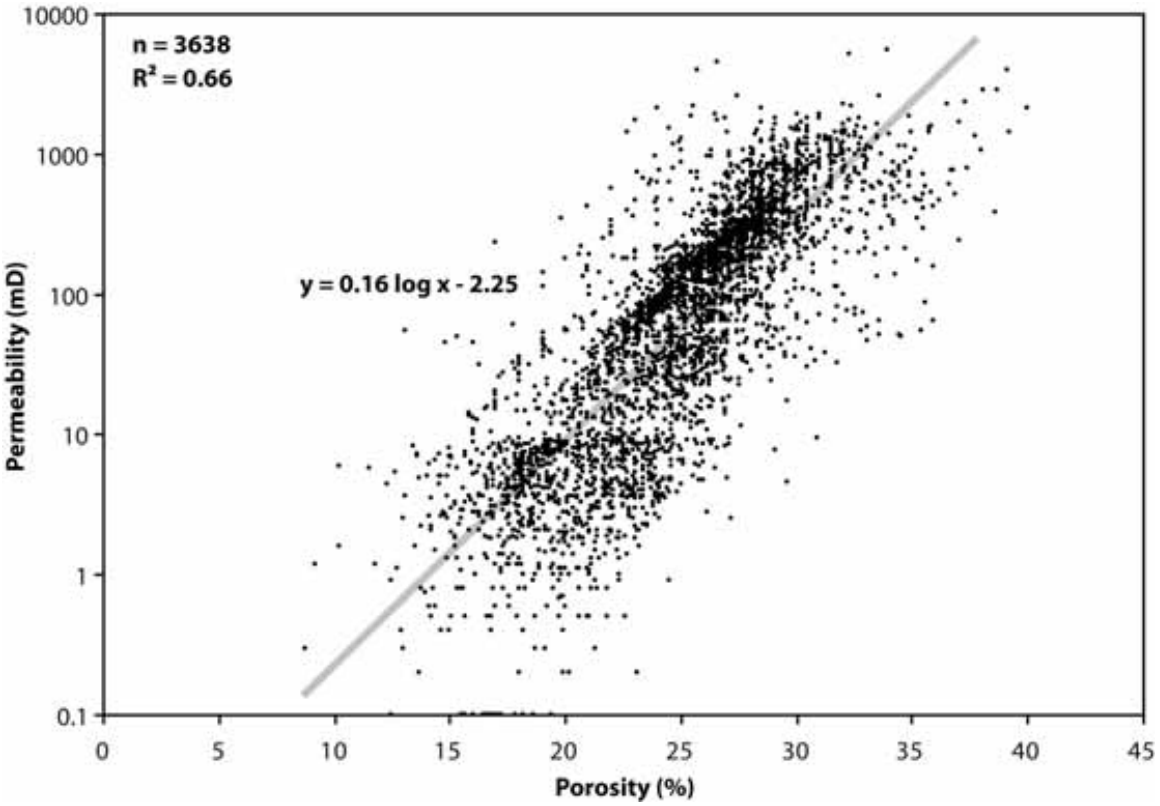

Figure 5.7. Cross-plot of porosity and permeability data from core analyses of Cretaceous sandstone in southwestern Alabama (modified from Pashin et al., 2008).

Isochore maps show that the total thickness of the Cenozoic section is greatest in DeSoto Canyon Salt Basin, specifically in the Mobile, and Viosca Knoll Areas (Fig. 5.8), with the majority of the section above the Middle Eocene (Fig. 5.9). In the DeSoto Canyon Salt Basin, the Cenozoic section generally thins to the east, with significant thinning over Destin Dome. The Cenozoic section also thins in the area of the Florida Middle Ground Arch (Fig. 5.8). The upper Eocene-Miocene units are all shallower than 760 m (2500 ft) below sea level on the crest of

Destin Dome and in large portions of the Middle Ground Arch. Farther south in the Tampa Embayment, the Cenozoic section thickens.

Net qualified reservoir thickness in the Cenozoic section (Figs. 5.10-5.13) is more variable than gross interval thickness, and suggests complex relationships among sandstone, shale, and carbonate facies. Qualified sand in the upper Eocene-Miocene interval is thickest in the Viosca Knoll Area. The high variability of net reservoir thickness suggests complex relationships between reservoir sand bodies, that cannot be resolved at the regional scale; understanding the interconnectedness of the sand bodies would require additional data control for more detailed mapping. An estimate of minimum sealing strata thickness was mapped and follows a similar trend as isochore thickness, with the thickest seals in the Viosca Knoll and southwestern Destin Dome Areas.

Porosity data from 751 core analyses (conventional and sidewall) of potential Cenozoic reservoirs were available for 42 wells, and all but one of those wells are in the Mobile and Viosca Knoll areas. Porosity in the Mobile-Viosca Knoll areas is variable and generally increases to the northwest (Fig. 5.14). The one Destin Dome well with core analysis data is the eastern part of the area and was not included in the map.

Sarasota Arch

The axial trace of the Sarasota Arch trends northeast-southwest, plunges toward the West Florida Escarpment, and was likely formed by differential subsidence since the Late Jurassic (Foote, 1985, Martin and Case, 1975) (Figs 5.15, 5.16, Plate 3). Foote (1985) indicated that the Sarasota Arch was active during the Cretaceous. Differential uplift of the Sarasota Arch relative to the Tampa Embayment and the South Florida Basin resulted in the thinning of strata across the arch. Structure maps of the Punta Gorda, Gordon Pass, and Panther Camp Formations show only minor changes in the structure of the Sarasota Arch (Figs. 5.17-5.19). All three maps show the width of the arch to be approximately 210 km wide and shows the locations of the Tampa Embayment and the South Florida Basin. In all three maps, a domal structure, which is the highest part of the arch in the study area, is present in the area of well OCSG-3903. In contrast, deposition during the Cedar Keys time indicates that the arch is muted relative to the other intervals mapped and that a domal structure is northeast of the domal structure in the older beds. Nearly all wells within this project are located near the axial trace of the Sarasota Arch, except OCSG-3341 and OCSG-3344 which are located on the northern limb near the Tampa Embayment.

Figure 5.15 is a strike-oriented seismic line that shows the simplicity of the structure on the shelf, with subparallel reflectors defining the broad, open structure of the Sarasota Arch. Figure 5.16 is a dip line traversing the shelf and showing the shelf margin and upper part of the West Florida Escarpment. The Lower Cretaceous section is dominated by subparallel reflections, and clinoform elements are developed near the shelf margin. The structure of the Sarasota Arch is observed in the NE-central portion of the seismic survey (Fig. 5.15). Additionally, the clinoform strata at the shelf margin are slightly elevated relative to the adjacent shelf strata. This figure also shows that the Cedar Keys assessment unit forms a

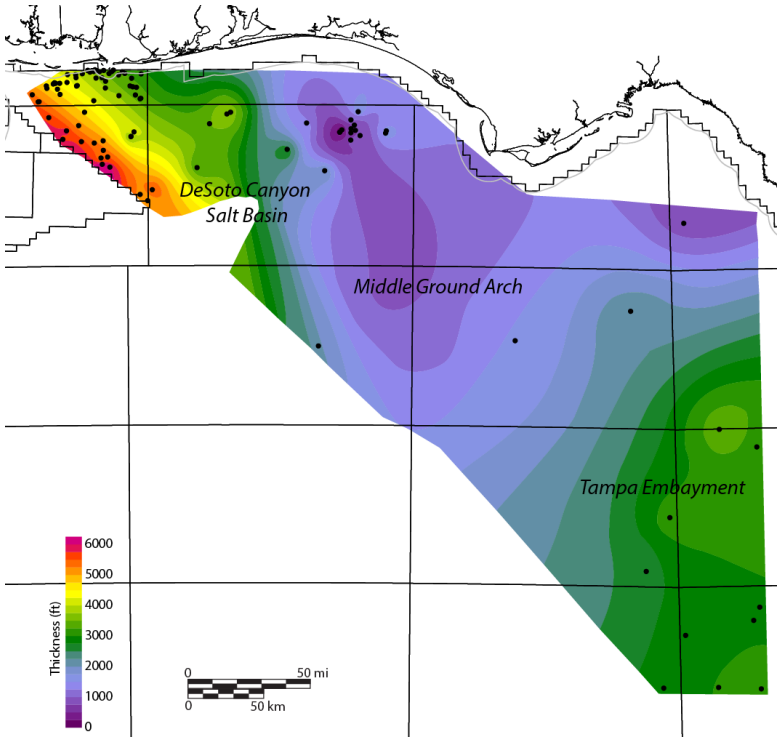

Figure 5.8. Isochore map showing thickness of the Cenozoic section beyond a depth of 762 m (2,500 ft) in the DeSoto Canyon Salt Basin, Middle Ground Arch, and Tampa Embayment.

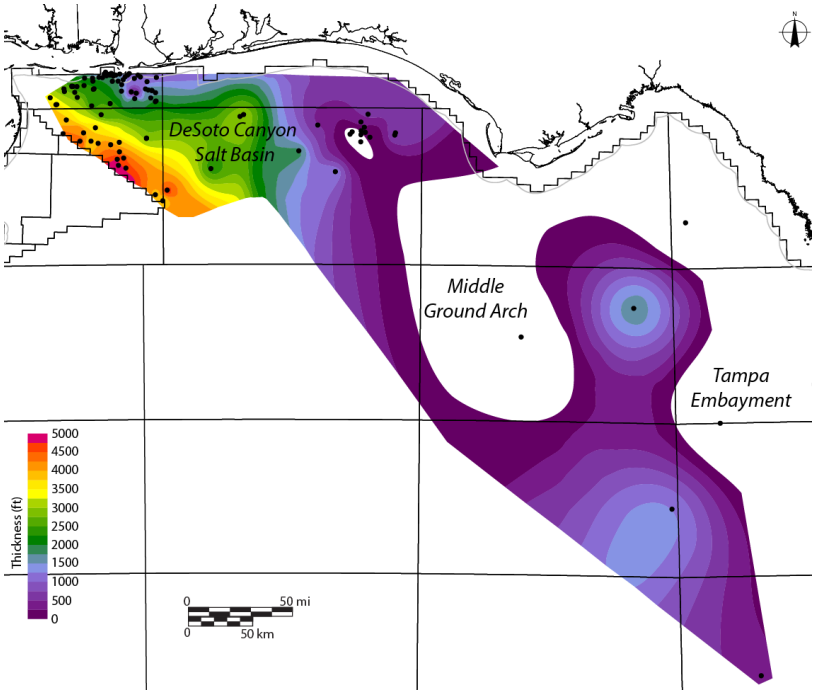

Figure 5.9. Isochore map showing thickness of the upper Eocene-Miocene section beyond a depth of 762 m (2,500 ft) in the DeSoto Canyon Salt Basin, Middle Ground Arch, and Tampa Embayment.

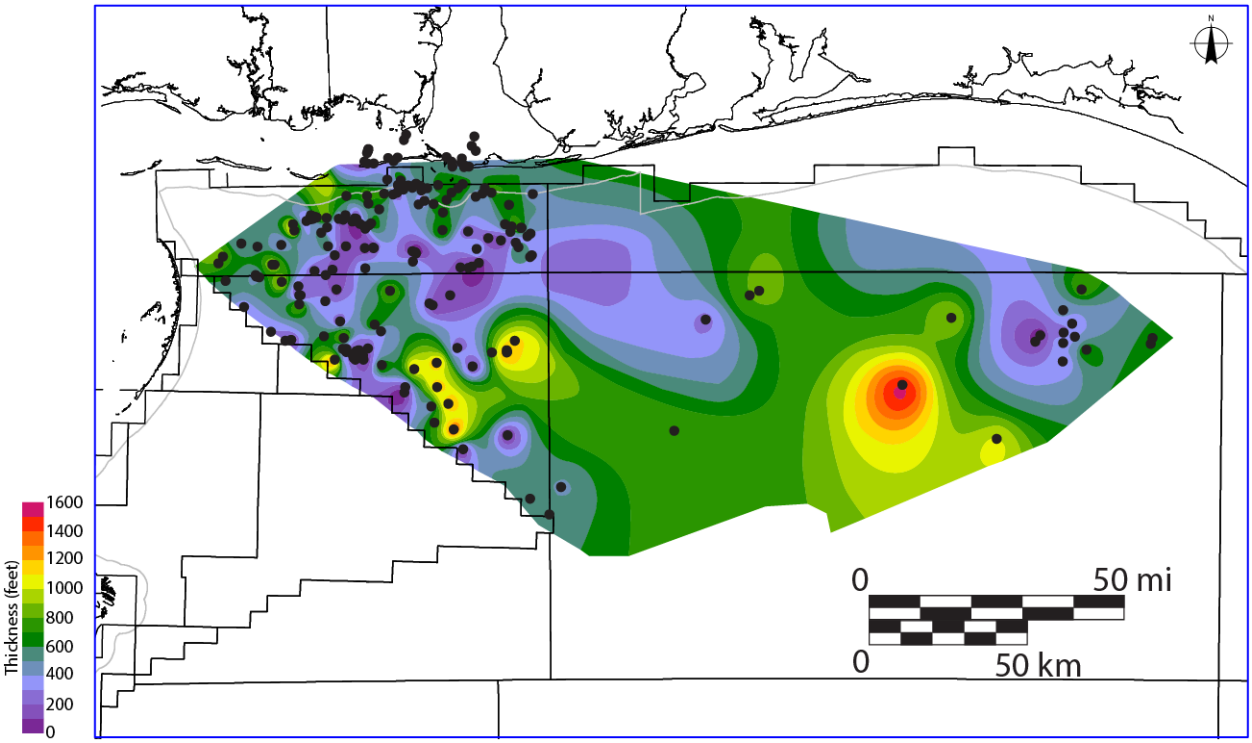

Figure 5.10. Net sand isolith map of the Cenozoic section in the DeSoto Canyon Salt Basin.

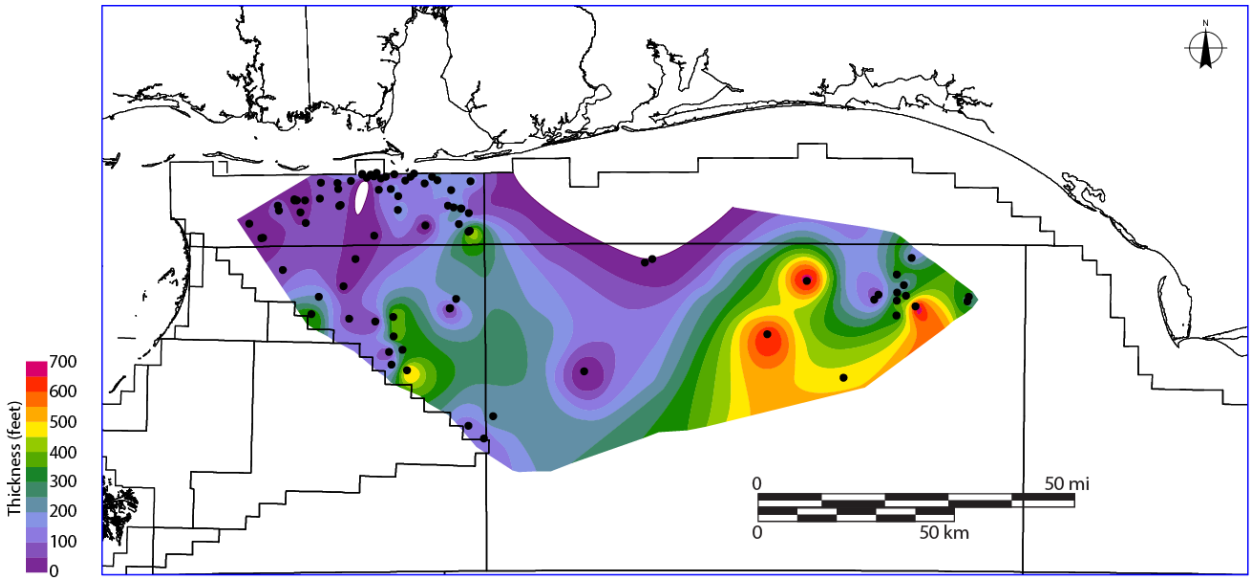

Figure 5.11. Net sand isolith map of the Paleocene-mid Eocene section in the DeSoto Canyon Salt Basin.

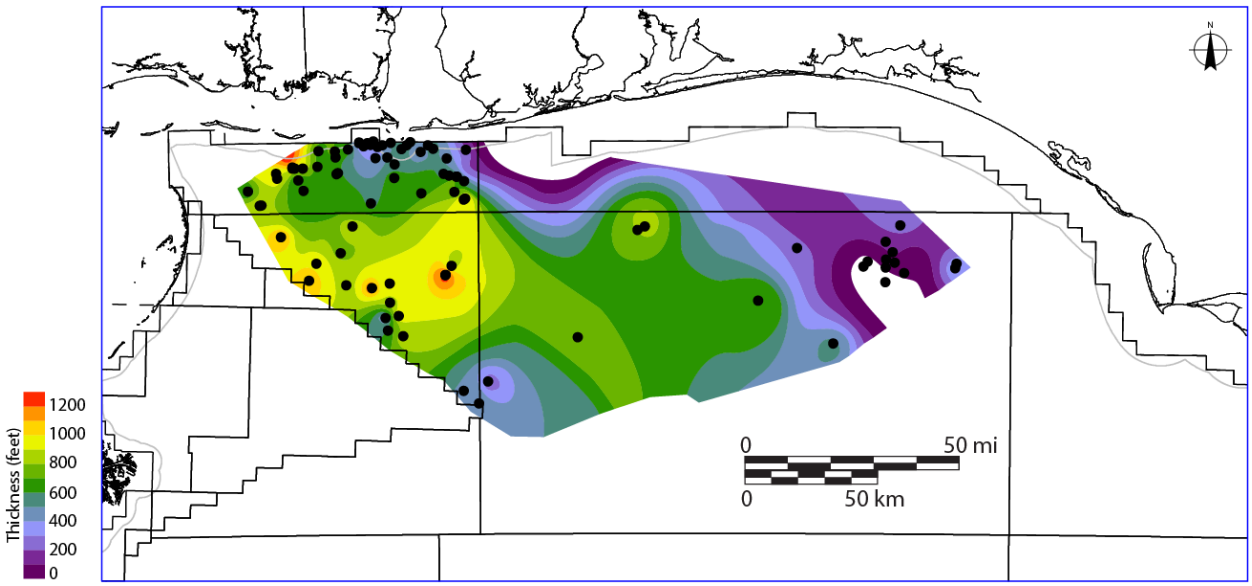

Figure 5.12. Net sand isolith map of the upper Eocene-Miocene section in the DeSoto Canyon Salt Basin.

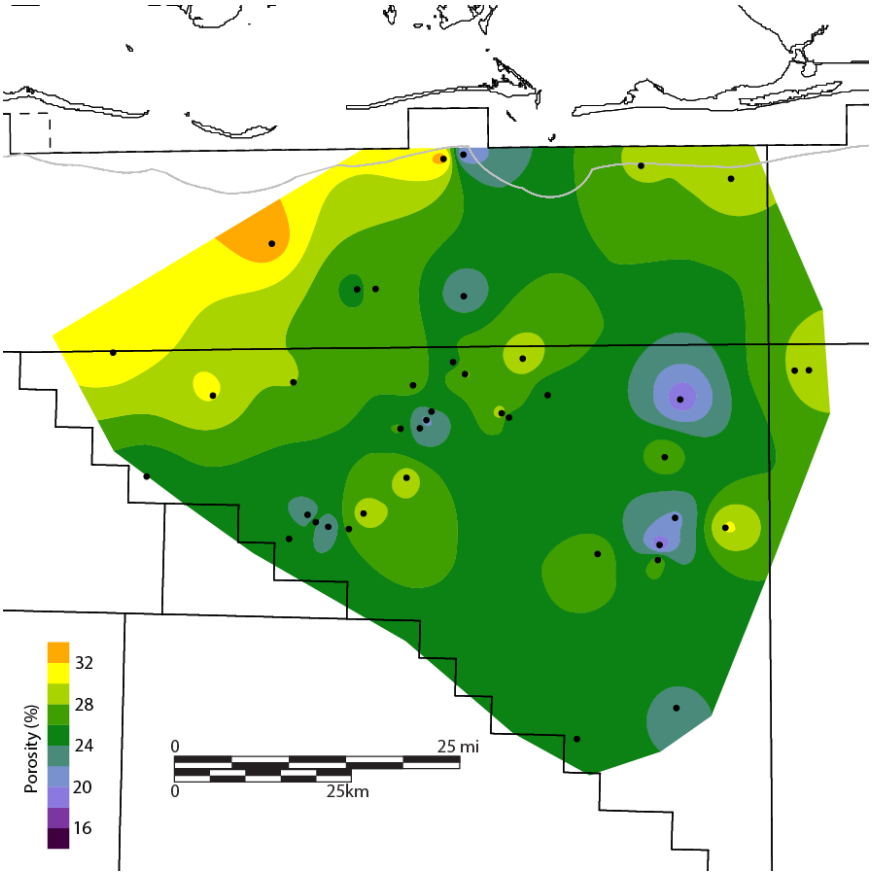

Figure 5.13. Net sand isolith map of the upper Eocene-Miocene section in the western DeSoto Canyon Salt Basin.

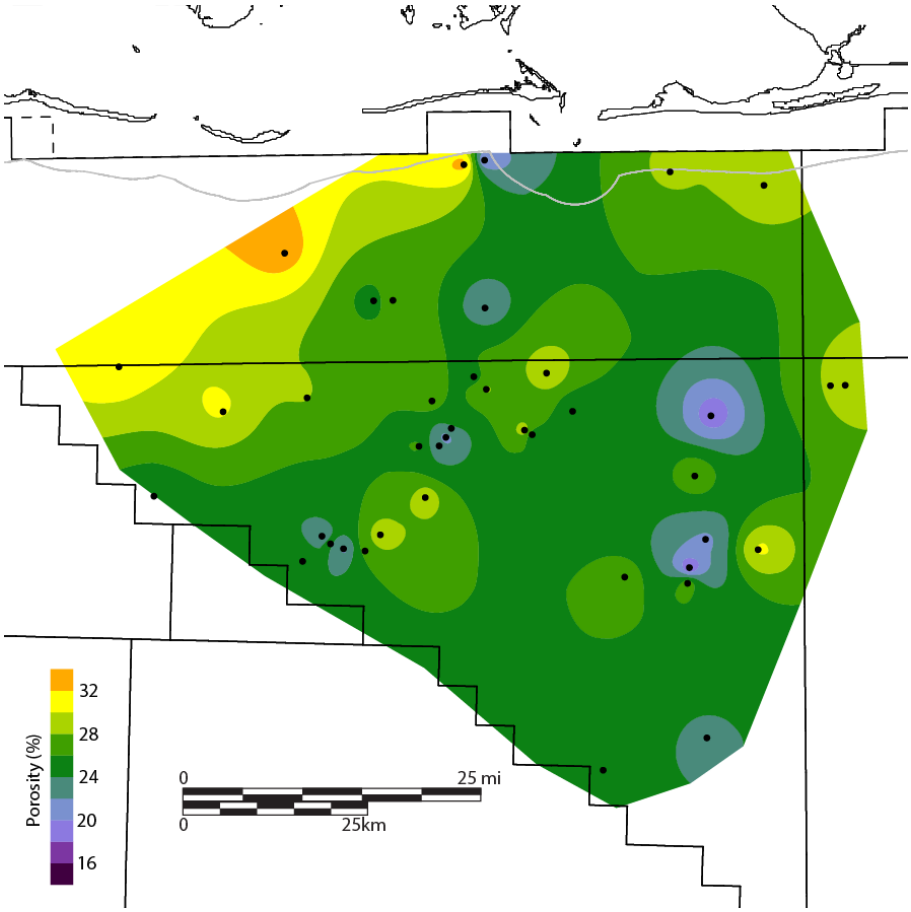

Figure 5.14. Map of average sand porosity in the Cenozoic section in the western DeSoto Canyon Salt Basin.

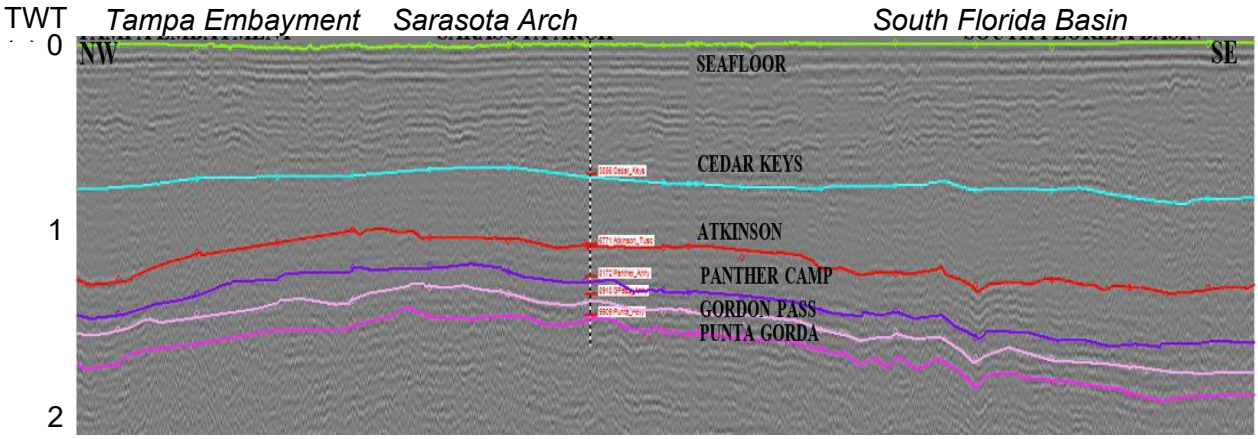

Figure 5.15. Strike seismic profile 4-108a showing regional structure of the West Florida Shelf.

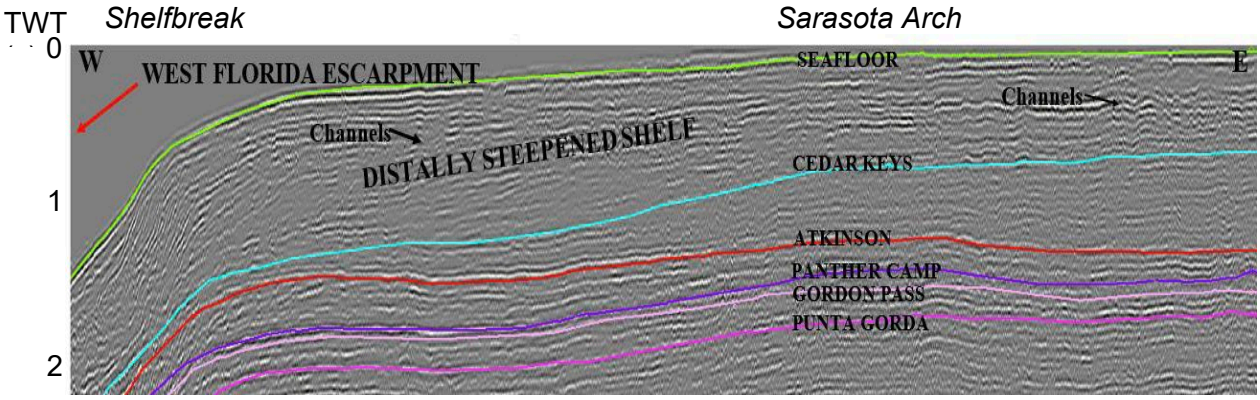

Figure 5.16. Dip seismic profile 4-101 showing stratal geometry and structure of the West Florida Shelf.

southwestward thinning wedge of sediment that marks the initiation of a major westward progradation from the peninsula and establishment of the distally steepened shelf that persists today. Tertiary strata (post-Cedar Keys) are channelform in the proximal part of the profile and clinoform in the distal part. Unfortunately, some of seismic lines do not adequately image the Lower Cretaceous section because of noise related to channeling and paleokarst in the post-Cedar Keys section. Primary strike lines trending SE-NW were relatively flat with only subtle changes in structure of the Sarasota Arch (Fig. 5.15). In contrast, the dip lines depict the distally steepened shelf towards the West Florida Escarpment (Fig. 5.16).

Porous strata within the Punta Gorda, Gordon Pass, and Panther camp assessment units are all dolomite, whereas the upper Cretaceous-Paleocene Cedar Keys assessment unit includes porous limestone in addition to porous dolomite. Qualified reservoir (porosity >15%, thickness >6 m; 20 ft) in the Punta Gorda assessment unit is the dolomite of the Lehigh Acres Formation within the Glades Group. Qualified reservoir in the Gordon Pass assessment unit is dolomite of the Marco Junction Formation in the Big Cyprus Group. Porous dolomite of the Dollar Bay Formation constitutes the reservoir for the Panther Camp assessment unit of the Naples Bay Group. The Cretaceous-Paleocene Cedar Keys assessment unit includes dolomite reservoirs in the Cedar Keys and Lawson Formations and the porous limestone reservoir in the Upper Pine Key Formation.

The highest average porosity in the Punta Gorda assessment unit approaches 25% at well OCSG-3912 (Fig. 5.17). Figure 5.17 establishes the typical reservoir to seal relationship found throughout the study with thick sections of porous dolomite capped by regionally continuous anhydrite. Reservoir quality dolomite of the Lehigh Acres Formation is overlain by the thick Punta Gorda anhydrite topseal. The formation is largely unqualified in the Tampa Embayment and South Florida Basin. Porosity is primarily developed on the northern flank of the Sarasota Arch (Fig. 5.18), and the net thickness map trend (Fig. 5.19) suggests that the paleostructure may be slightly different from modern structure. Where there is porous dolomite in the Punta Gorda assessment unit, the average net interval thickness is 87 m (287 ft), and porosity is principally developed on the northwestern limb of the Sarasota Arch (Figs. 5.19, 5.19). A maximum net thickness of about 120 m (400 ft) is in the northern flank of the arch, and the dolomitic interval thickens southwest toward the shelf margin (Fig. 5.19). Net porous dolomite is absent in the Tampa Embayment where minimal reservoir is

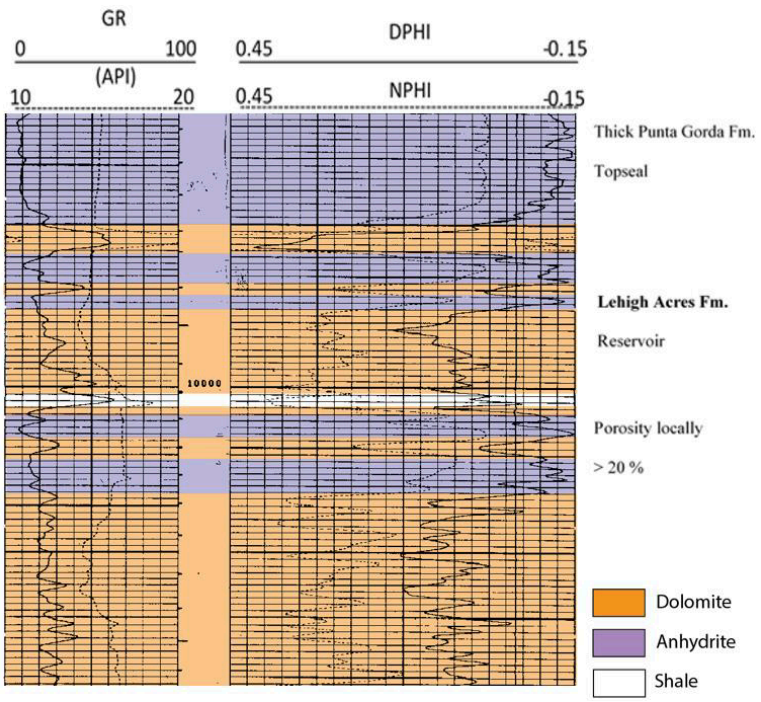

Figure 5.17. Interpretation of geophysical logs from well OCSG-3912 in the Lehigh Acres dolomite reservoir.

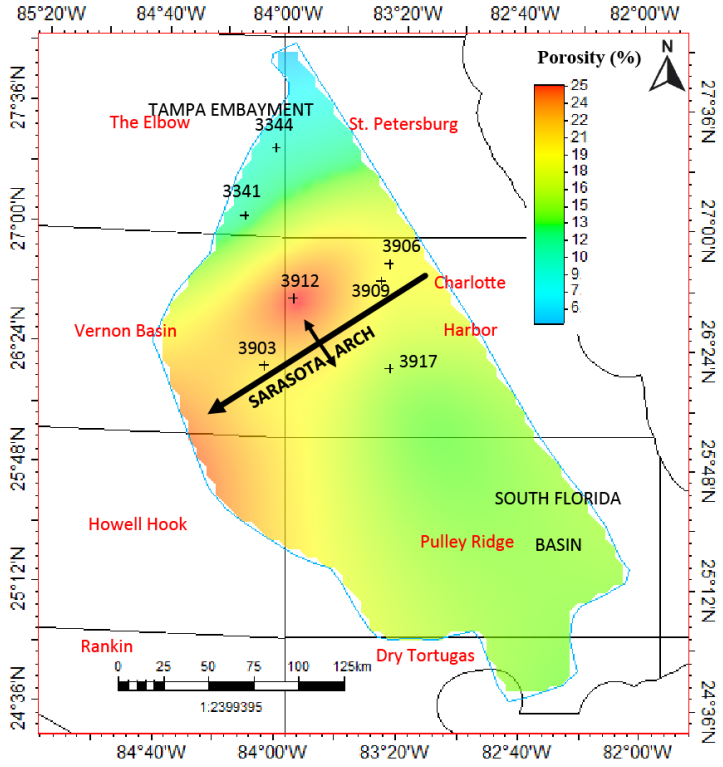

Figure 5.18. Porosity map of the Lehigh Acres Formation in the Punta Gorda assessment unit.

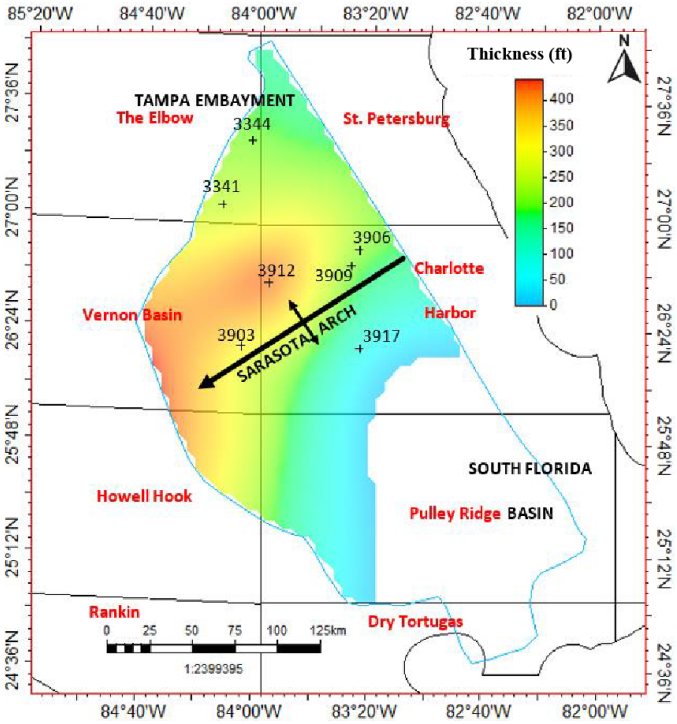

Figure 5.19. Net porous dolomite isolith map of the Able and Twelve Mile Members of the Lehigh Acres Formation in the Punta Gorda assessment unit.

observed in well OCSG-3917 (Fig. 5.19). The average total porosity of the Lehigh Acres Formation is about 18.5%. Reservoir-quality dolomite is also developed in the Marco Junction Formation of the Gordon Pass assessment unit as seen in log analysis of well OCSG-3903 (Table 2; Fig. 5.20). Alternating sections of reservoir quality dolomite (>15% porosity) and sealing anhydrite of the Gordon Pass punctuate this section. However, the Sunniland Formation at the base of the storage unit is not a target for sequestration, as the porosity values did not meet the criteria for a minimum 15% porosity cutoff. Porosity is highest near the shelf margin close to well OCSG-3903, and on the northern flank of the Sarasota Arch (Fig. 5.20). The average net thickness of reservoir containing greater than 15 percent porosity within the assessment unit is around 40 m (130 ft) and is located in the Marco Junction and Lake Trafford Formations. Due to limited well control, any significant increases in net thickness of reservoir are apparent when analyzing the net porous dolomite isolith map (Fig. 5.21). Net thickness of porous reservoir increases from 30 m (100 ft) on the eastern portion of the study area, to 120 m (395 ft) in well OCSG-3903 and is greatest near the shelf margin (Fig. 5.22). The average total porosity of the Marco Junction and Lake Trafford Formations ranges from 19.7% in well OCSG-3906 to 20.6% in wells OCSG-3344 and OCSG-3903 (Fig. 5.23; Table 2).

The Dollar Bay Formation within the Panther Camp assessment unit is composed of thick dolomite reservoirs separated by thin anhydrite beds and capped by the Panther Camp anhydrite topseal. The basal limestone of the Dollar Bay varies in thickness from 40 m (130 ft) on top of the Sarasota Arch to more than 165 m (550 ft) in the adjacent basins. This unit is not a target interval for storage and does not meet the minimum 15% porosity cutoff for this study. Increases in porosity/thickness trends are similar to those in the Gordon Pass assessment unit towards the shelf margin (Figs. 5.24, 5.25).

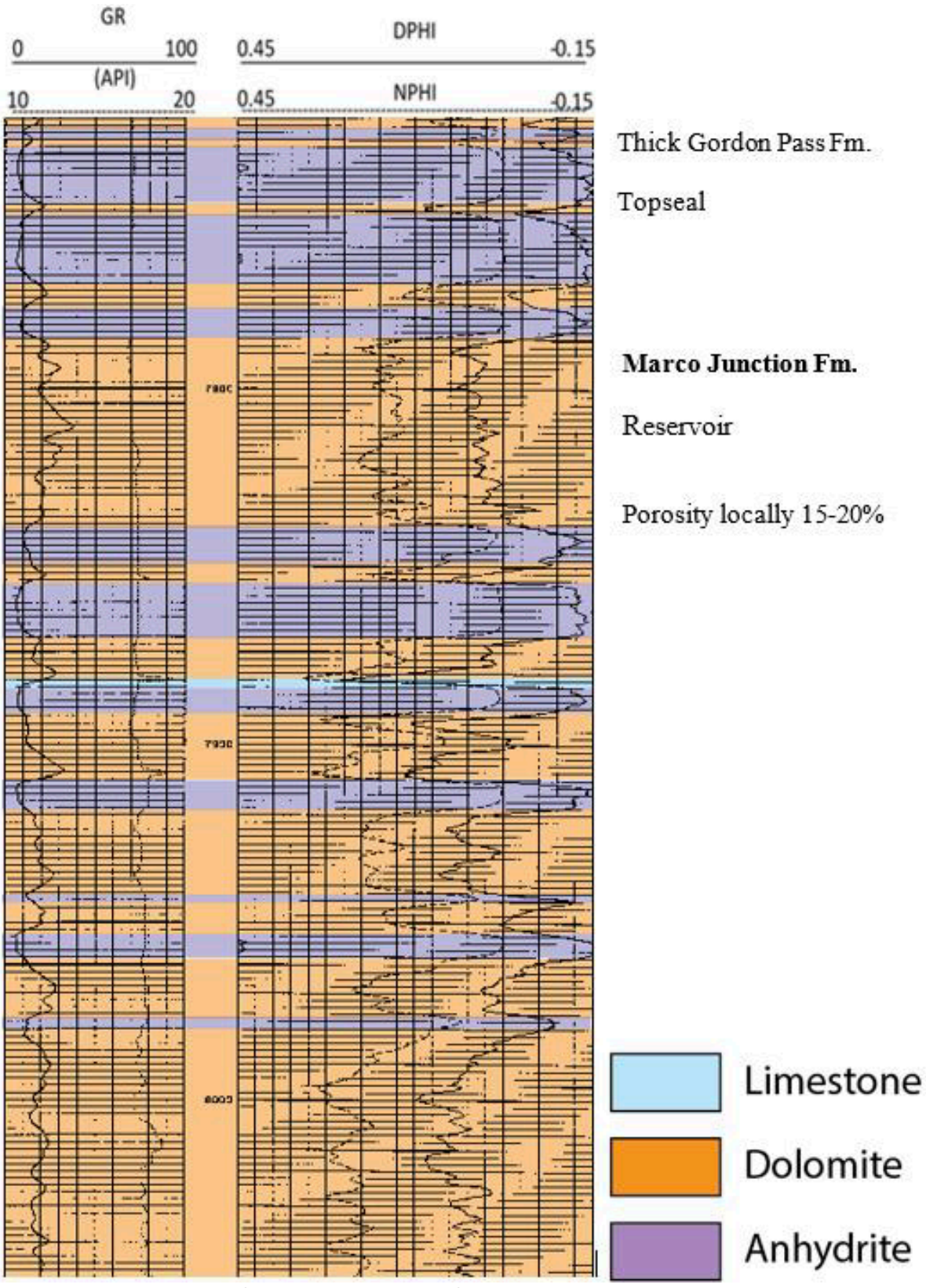

Figure 5.20. Interpretation of geophysical well logs from well OCSG-3903 in the Marco Junction dolomite reservoir.

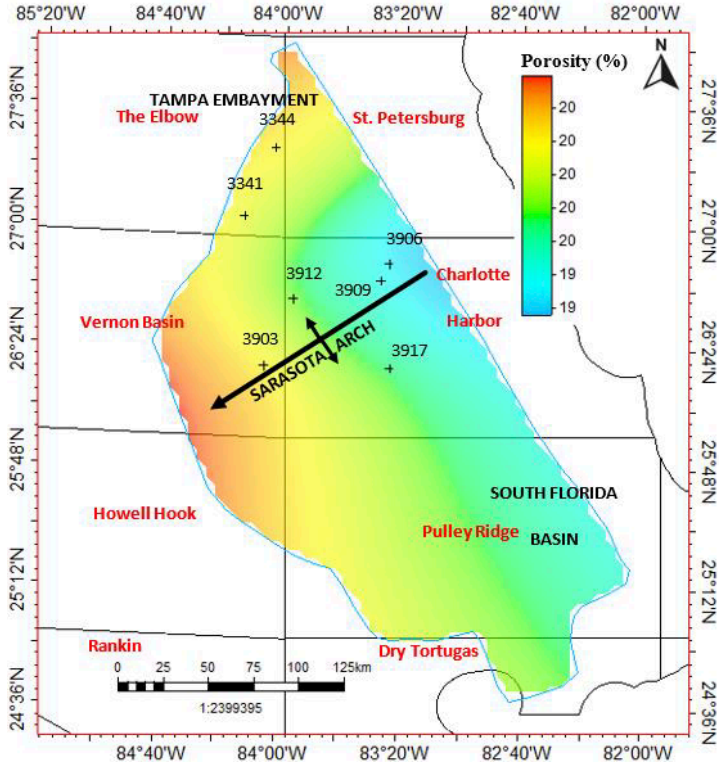

Figure 5.21. Average porosity map of the Marco Junction and Lake Trafford Formations in the Gordon Pass assessment unit.

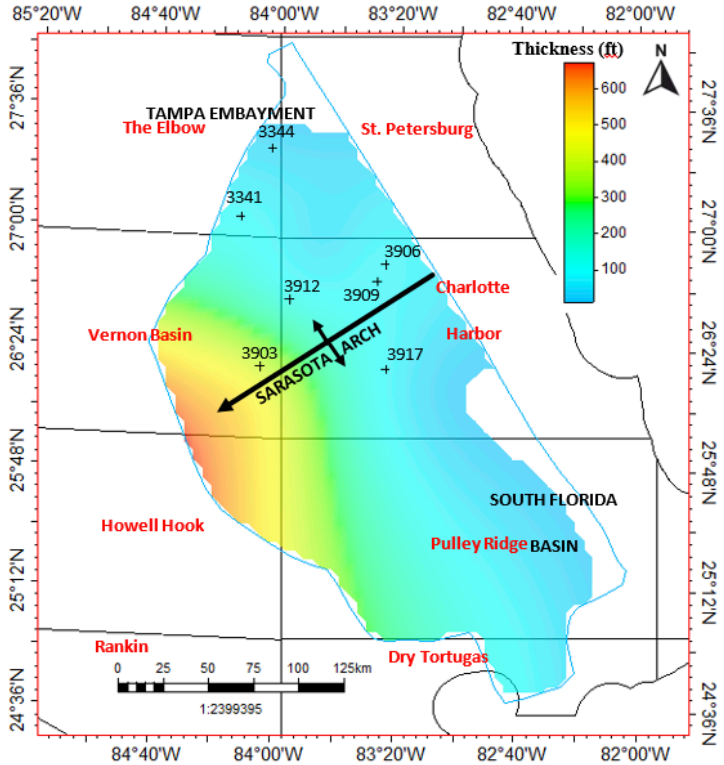

Figure 5.22. Net porous dolomite isolith map of the Marco Junction and Lake Trafford Formations in the Gordon Pass assessment unit.

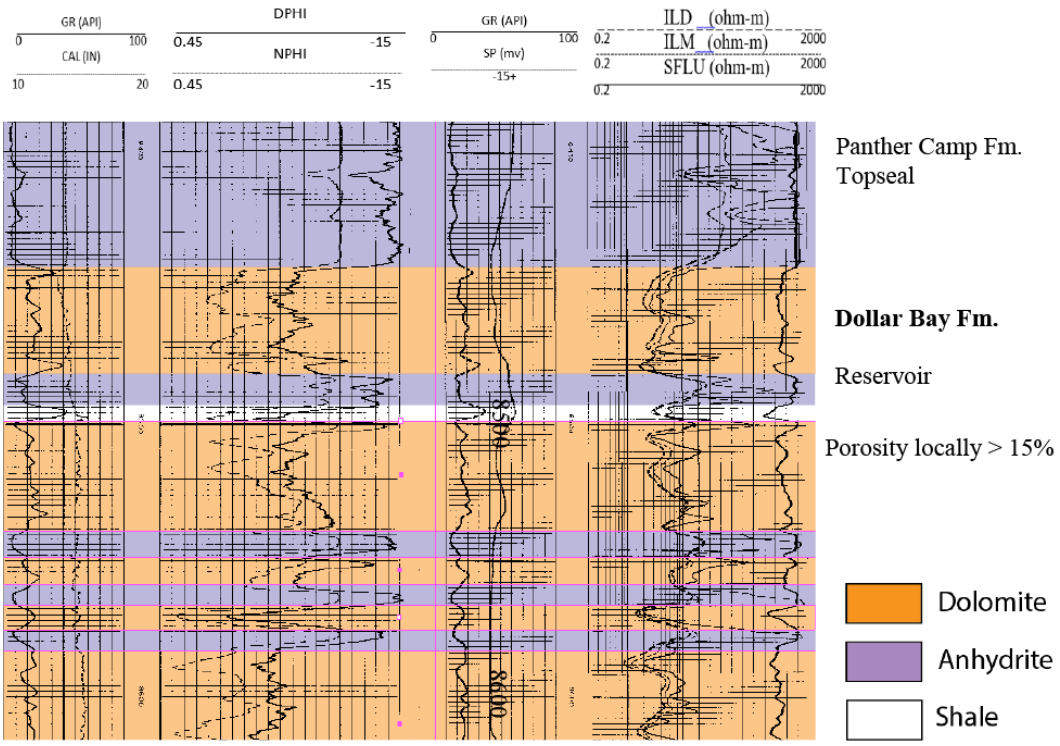

Figure 5.23. Interpretation of geophysical logs from well OCSG-3903 in the Marco Junction dolomite reservoir.

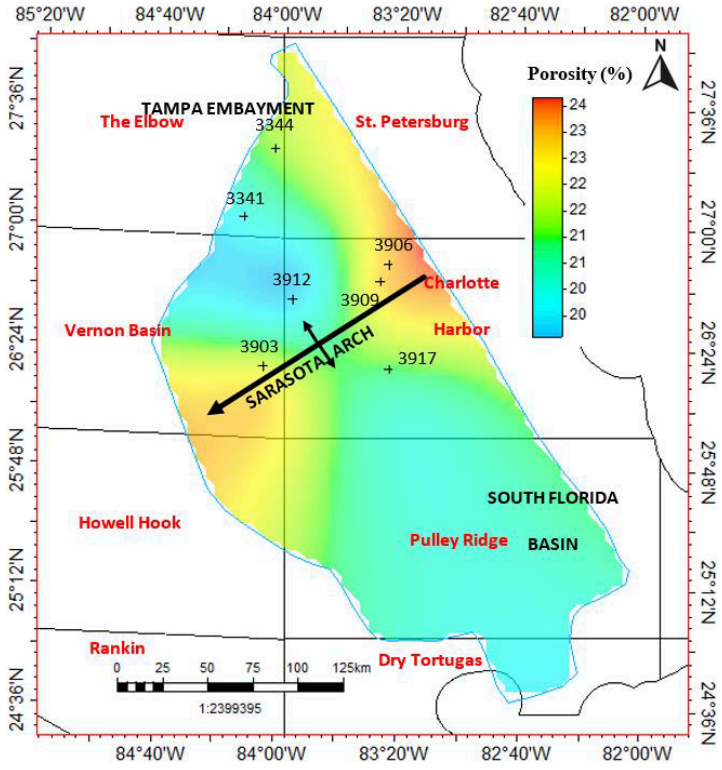

Figure 5.24. Average porosity map of the Dollar Bay Formation in the Panther Camp assessment unit.

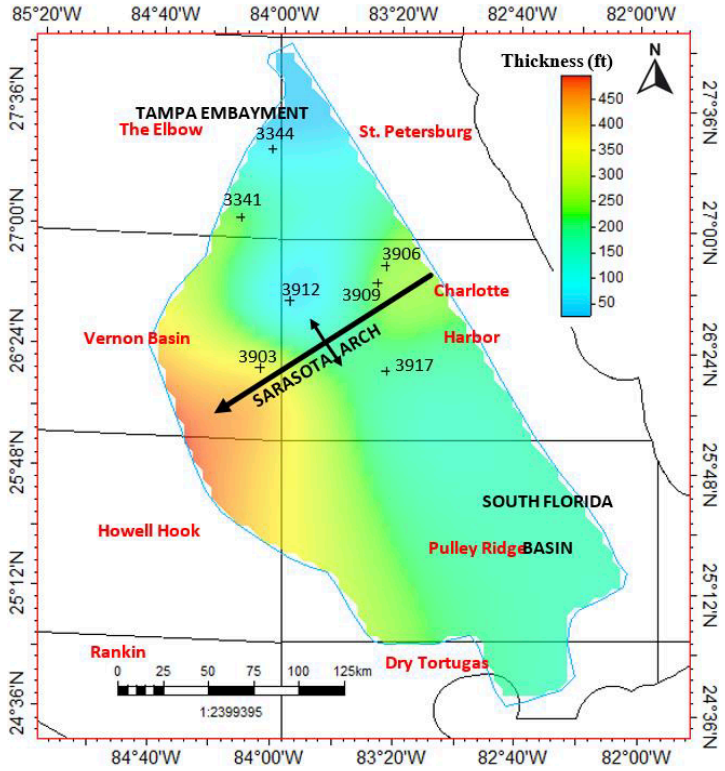

Figure 5.25. Net porous dolomite isolith map of the Dollar Bay Formation in the Panther Camp assessment unit.

Table 2. Average total porosity of qualified dolomite in the West Florida Shelf.

	Well						
Assessment Unit	**OCSG 3341**	**OCSG 3344**	**OCSG 3903**	**OCSG 3906**	**OCSG 3917**	**OCSG 3909**	**OCSG 3912**
Cedar Keys	N/A	N/A	N/A	26.6	23.7	26.7	N/A
Panther Camp	20.4	21.8	22.4	23.4	21.4	23.3	19.8
Gordon Pass	20.5	20.6	20.6	19.7	20.1	19.8	20.2
Punta Gorda	<15	<15	21	19.6	17.7	19.5	25.6

Porosity is highest near wells OCSG-3906 and OCSG-3909 close to the crest of the Sarasota Arch (Fig. 5.24). The net porous thickness of qualified Dollar Bay reservoir ranges from 20-107 m (65-350 ft). The proportion and thickness of dolomite in the Dollar Bay Formation tends to increase toward the crest of the Sarasota Arch and the shelf margin (Fig. 5.25; Plate 1). The average total porosity of the Dollar Bay Formation ranges from 19.8% in well OCSG-3912, to 23.4% in well OCSG-3906 (Table 2).

The Upper Cretaceous Pine Key and Lawson formations and the Paleocene Cedar Keys formation constitute the youngest assessment unit evaluated in this area. The rocks in these formations contain much higher porosity (up to 30%) than those in the older assessment units (Fig. 5.26). In well OCSG-3917, dolomite reservoir of the Lower Cedar Keys Formation is

located at a depth of around 1,220 m (4,000 ft) and is overlain by the Middle Cedar Keys anhydrite seal.

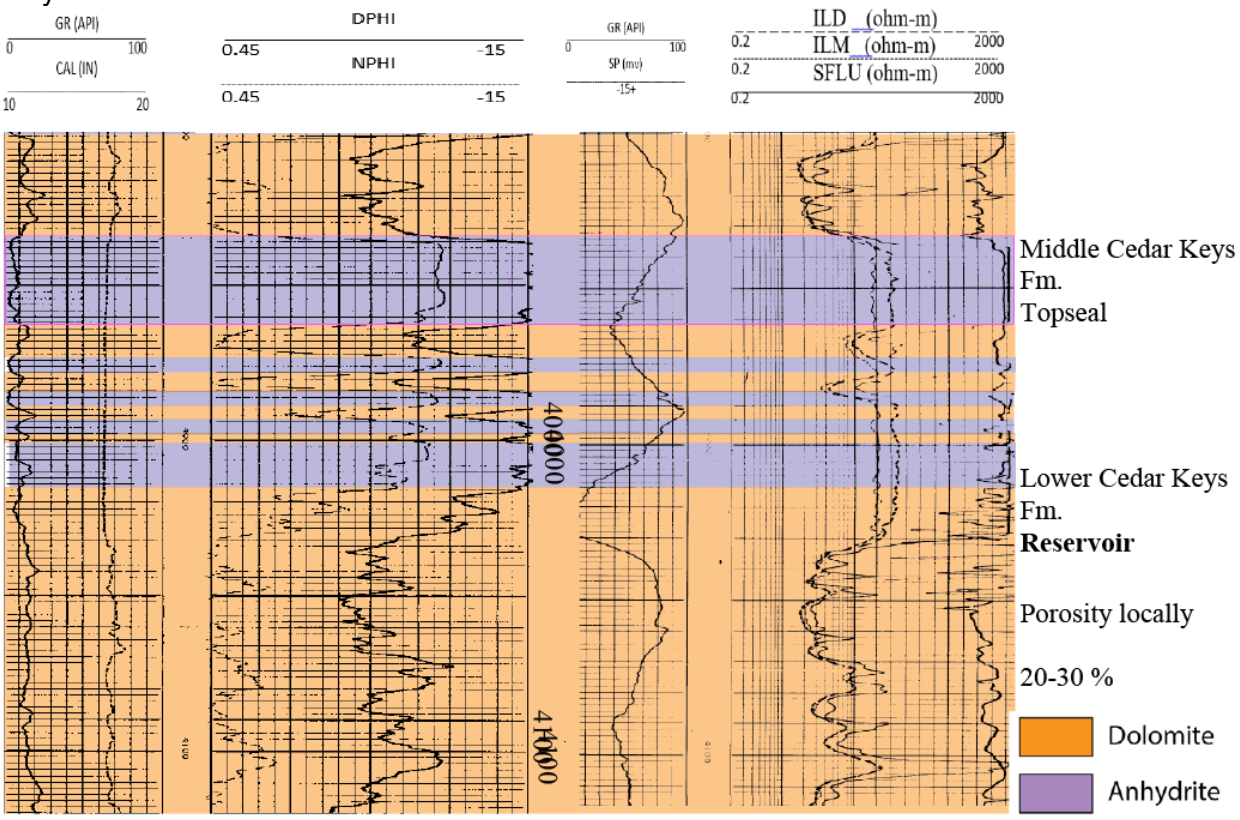

Fig. 5.26. Interpretation of geophysical well logs from well OCSG-3917 in the lower Cedar Keys dolomite reservoir.

As stated previously, the basal part of the Pine Key Formation contains a thick section of chalk, which tends to have very low permeability and is thus not included in this assessment. Porosity decreases towards the Tampa Embayment and South Florida Basin areas and is highest on the northern flank of the Sarasota Arch near the shelf margin at well OCSG-3903, and near the crest at wells OCSG-3909 and OCSG-3906 (Fig. 5.27). The proportion and thickness of reservoir increases towards the eastern portion of the study area to over 600 m (2,000 ft) near the crest of the Sarasota Arch near wells OCSG-3909 and OCSG-3906 (Fig. 5.28). Due to the westward progradation from the peninsula and southwestward thinning wedge of sediment, the same increases in thickness near the shelf margin in older reservoirs is not observed in the Cedar Keys assessment unit. The Cedar Keys assessment unit has the highest net thickness of porous carbonate, with an average thickness of around 610 m (2,000 ft) of qualified limestone and dolomite (Plates 3, 4).

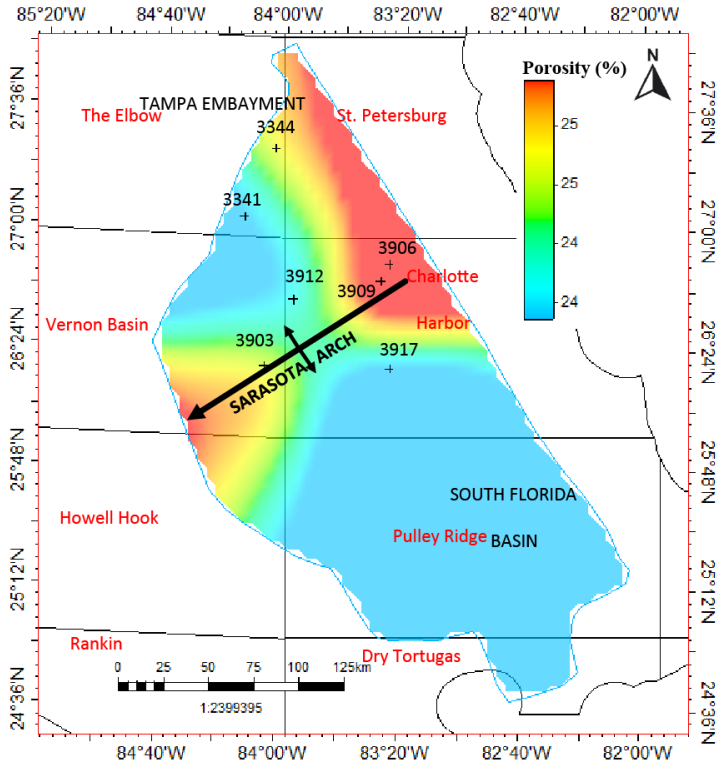

Figure 5.27. Map of average porosity in the Pine Key and Lawson Formations.

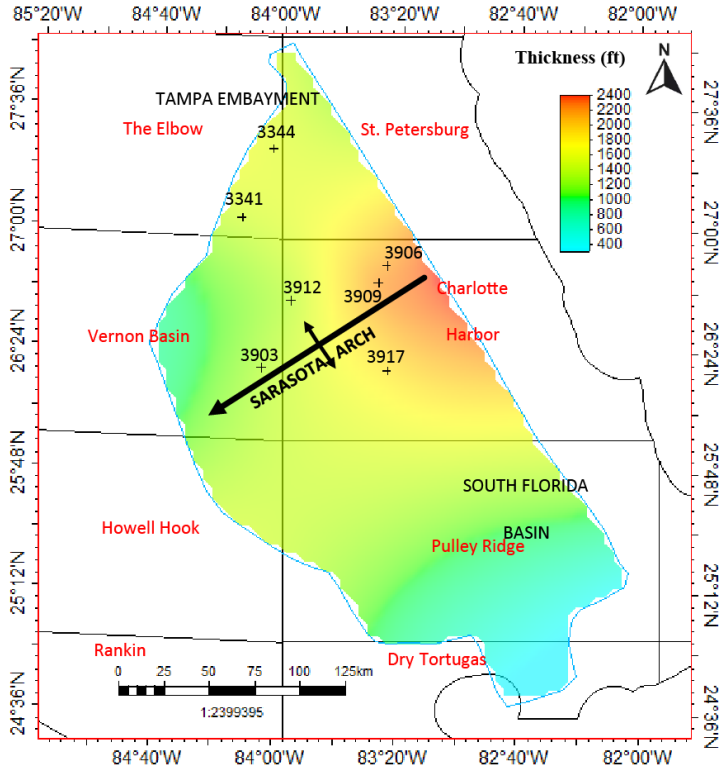

Figure 5.28. Net porous dolomite isolith map of the Pine Key and Lawson Formations.

Subtask 5.3 - CO_2 Storage Resource

DeSoto Canyon Salt Basin

Reservoirs under a normal hydrostatic gradient and normal geothermal gradient reach the critical point at a depth of about 756 m (2,480 ft), and therefore all zones being considered in the current study of offshore are expected to store CO_2 in a supercritical state (Fig. 5.29). Pressure and temperature at average reservoir depth for the eastern part of the Gulf of Mexico Basin were determined using the pressure-depth and temperature-depth plots by Pashin et al. (2008) and have been listed in Table 2. A PVT chart for CO_2 under hydrostatic and lithostatic pressure conditions (Bachu, 2003) shows the range of CO_2 density for the selected reservoirs (Fig. 5.30). The CO_2 density has been estimated at 790, 760 and 720 kg/m^3 for the Paluxy Formation, Washita-Fredericksburg interval and the lower Tuscaloosa Group, respectively.

Table 3 summarizes the reservoir properties used to calculate the CO_2 storage resource of the Paluxy Formation, Washita-Fredericksburg interval, and the Lower Tuscaloosa Group. Net sandstone thickness in the lower Tuscaloosa Group averages about half of that in the Paluxy Formation.

A storage resource estimate using efficiency factors where volumetric variables are well constrained and efficiency factors can be based on displacement terms is shown in Table 4. The P_{50} CO_2 storage capacity estimated using this method for Paluxy, Washita-Fredericksburg, and lower Tuscaloosa sandstone are 17.13, 1.06 and 9.76 Gt, respectively. Table 5 shows average storage capacity in million tonnes (Mt) per unit area (km^2, mi^2, and 9-mi^2 offshore blocks).

Maps showing the storage capacity per unit area (tonnes/km^2) for the Paluxy Formation, the Washita-Fredericksburg interval and the lower Tuscaloosa Group, and the total capacity of the three target units were drawn and are shown in Figures 5.31-5.34. Figure 5.31 shows that the Paluxy Formation has storage capacity exceeding 2 Mt/km^2 in the withdrawal synclines around the Destin Dome. Capacity is highly variable in the Mobile and Viosca Knoll Areas, where capacity ranges from 0 to 1.8 Mt/km^2. Storage capacity in the Washita-Fredericksburg interval is concentrated largely in the Mobile and Viosca Knoll Areas. The highest capacity is observed along a northwest-southeast trending axis. These values ranges from 0.1 to 0.8 Mt/km^2 (Fig. 5.32).

Storage capacity in the lower Tuscaloosa Group also is concentrated along the shore in the Mobile Area and near the shelf margin of the Viosca Knoll Areas with about 85% of the storage capacity being in this area (Fig. 5.33). Figure 5.34 is a total storage capacity map combining all three intervals. Average storage capacity is 2.1 Mt/km^2. This map indicates that sandstone is concentrated near the shoreline in the Mobile Area in the withdrawal synclines flanking Destin Dome. While the sandstone concentration appears to be significantly less in the central part of the basin northeast to the Desoto Canyon Diapir Province in the Destin Dome and Pensacola Areas, a lack of well control limits their detailed assessment.

Two areas of interest (AOIs) were defined to assess the Cenozoic storage resource in the DeSoto Canyon Salt Basin: (1) the Destin Dome AOI and (2) the Mobile-Viosca Knoll AOI (Figs. 5.35-5.37). The Destin Dome AOI has an average storage resource (P_{50}) of just over 5 Mt/km^2 and a maximum storage resource 10 Mt CO_2/km^2 (Fig. 5.35). The average storage resource per unit area in the Mobile-Viosca Knoll AOI is 6 Mt CO_2/km^2 for the entire

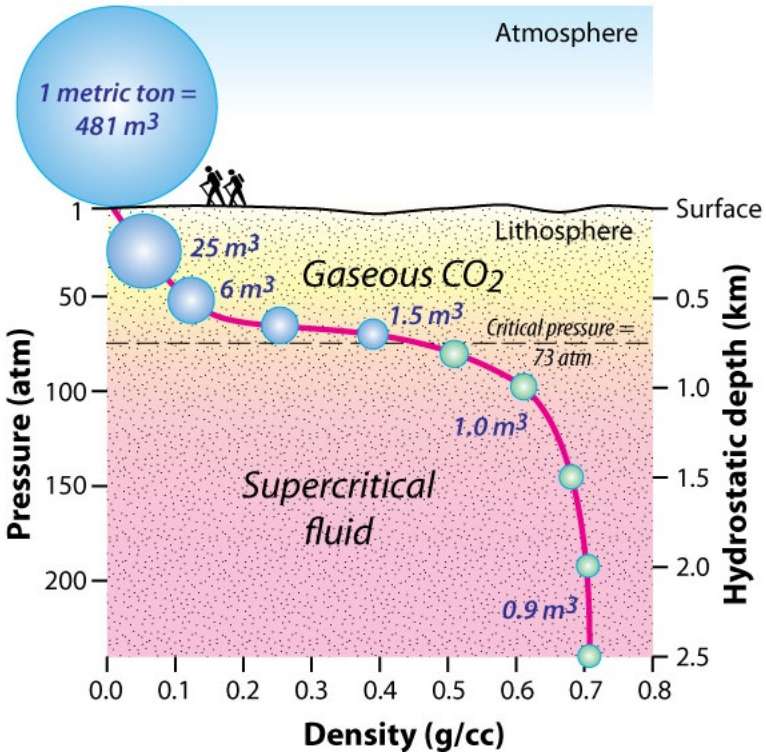

Figure 5.29. Relationships among CO_2 density, pore pressure, and equivalent hydrostatic depth.

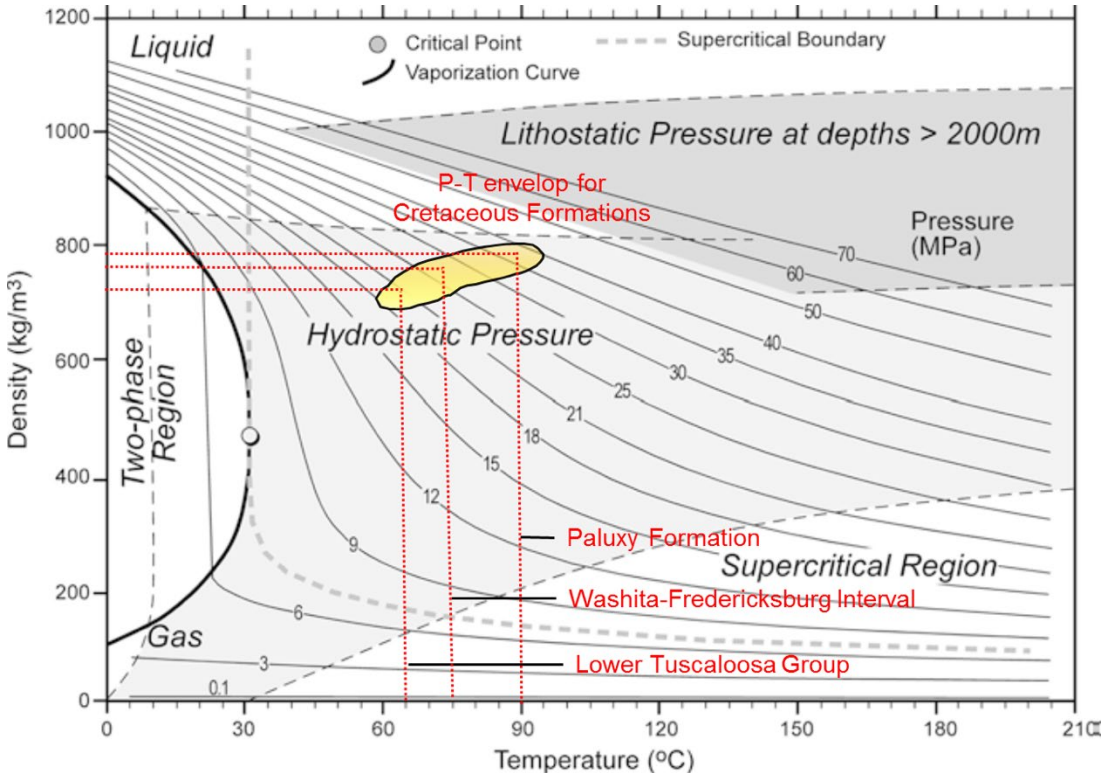

Figure 5.30. Variation of CO_2 density as a function of temperature and pressure (modified from Bachu, 2003). Yellow area marks pressure-temperature conditions in the DeSoto Canyon Salt Basin.

Table 3. Reservoir properties in the Paluxy Formation, Washita-Fredericksburg interval and lower Tuscaloosa Group.

Reservoir Parameters	Paluxy	Washita-Fredericksburg	Lower Tuscaloosa
Reservoir Area (m^2)	13466500000	13466500000	13466500000
Average Sandstone Thickness (ft)	190.0	25.5	104.6
Average Reservoir Porosity (%)	19.9	9.5	22.5
Average Reservoir Depth (ft)	10000	8500	7000
Average Reservoir Temperature (^oC)	90	80	65
Average Reservoir Pressure (MPa)	37	28	21
CO_2 Density at Reservoir Depth (kg/m^3)	790	760	720
Reservoir Capacity at 100% CO_2 Saturation (Gt)	122.4	7.5	69.7

Table 4. CO_2 storage capacity of the Paluxy Formation, Washita-Fredericksburg interval and lower Tuscaloosa Group using the efficiency factors for displacement terms in Goodman et al. (2011).

Categories	Paluxy	Washita-Fredericksburg	Lower Tuscaloosa
Reservoir Capacity at 100% CO_2 Saturation (Gt)	122.4	7.5	69.7
Efficiency Factor (P_{10}) %	7.40	7.40	7.40
Efficiency Factor (P_{50}) %	14.00	14.00	14.00
Efficiency Factor (P_{90}) %	24.00	24.00	24.00
Reservoir CO_2 Storage Capacity (P_{10}) (Gt)	9.06	0.56	5.16
Reservoir CO_2 Storage Capacity (P_{50}) (Gt)	17.13	1.06	9.76
Reservoir CO_2 Storage Capacity (P_{90}) (Gt)	29.37	1.81	16.73

Table 5. P_{50} storage capacity per unit area in the Paluxy Formation, Washita-Fredericksburg interval and lower Tuscaloosa Group. *G stands for the volume of the CO_2 storage resource.*

Categories	Paluxy	Washita-Fredericksburg	Lower Tuscaloosa
G (P_{50}/km^2) (Mt)	1.27	0.08	0.72
G (P_{50}/mi^2) (Mt)	3.30	0.20	1.88
G (P_{50}/9 mi^2 offshore block) (Mt)	29.66	1.83	16.89

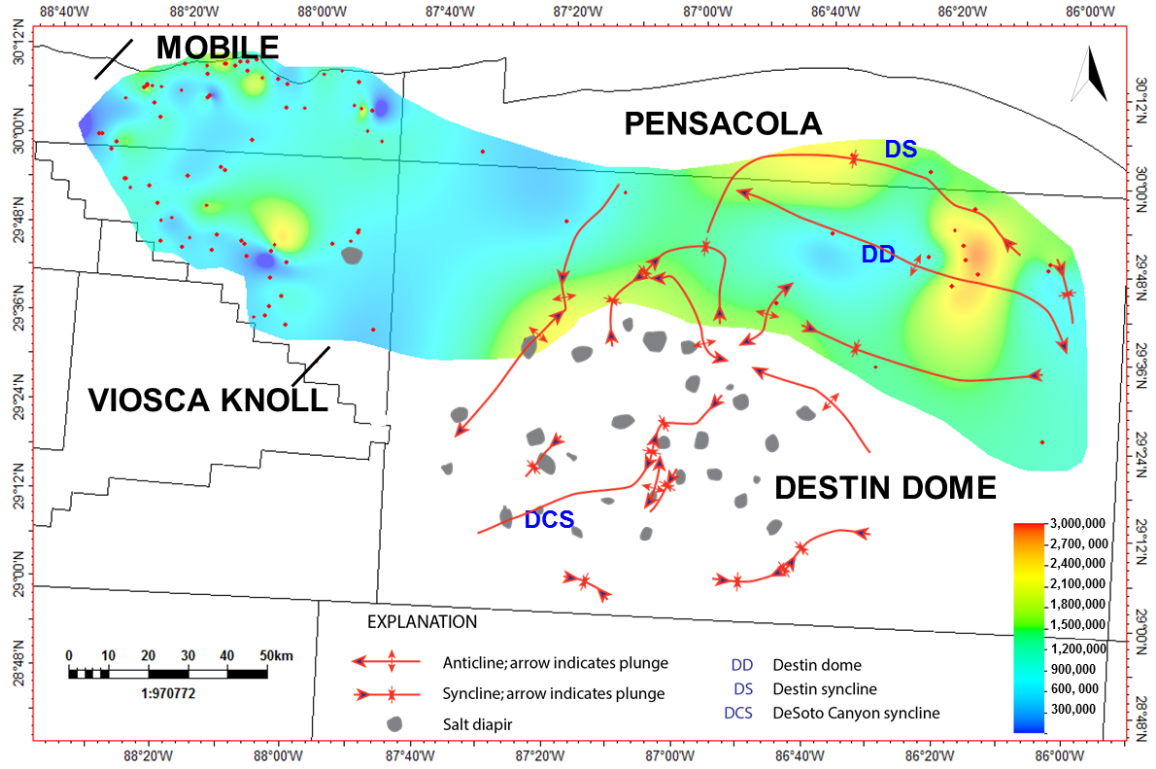

Figure 5.31. Storage resource map of the Paluxy Formation in the DeSoto Canyon Salt Basin.

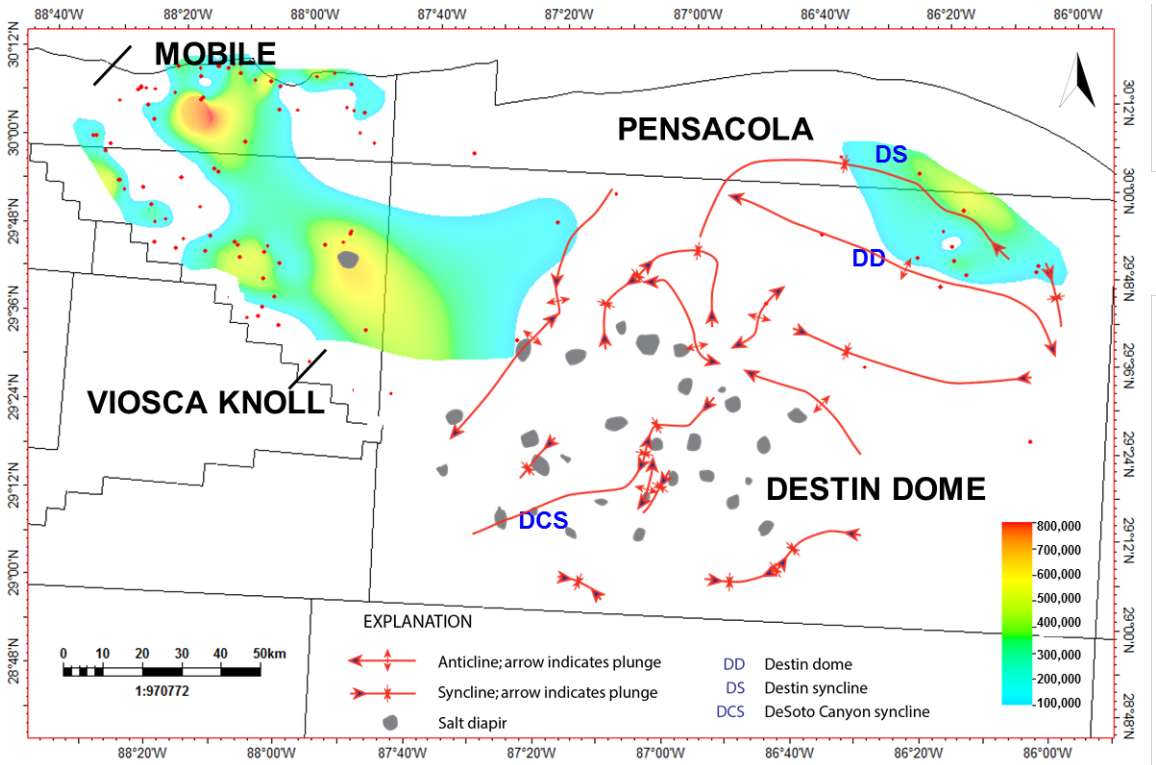

Figure 5.32. Storage resource map of the Washita-Fredericksburg interval in the DeSoto Canyon Salt Basin.

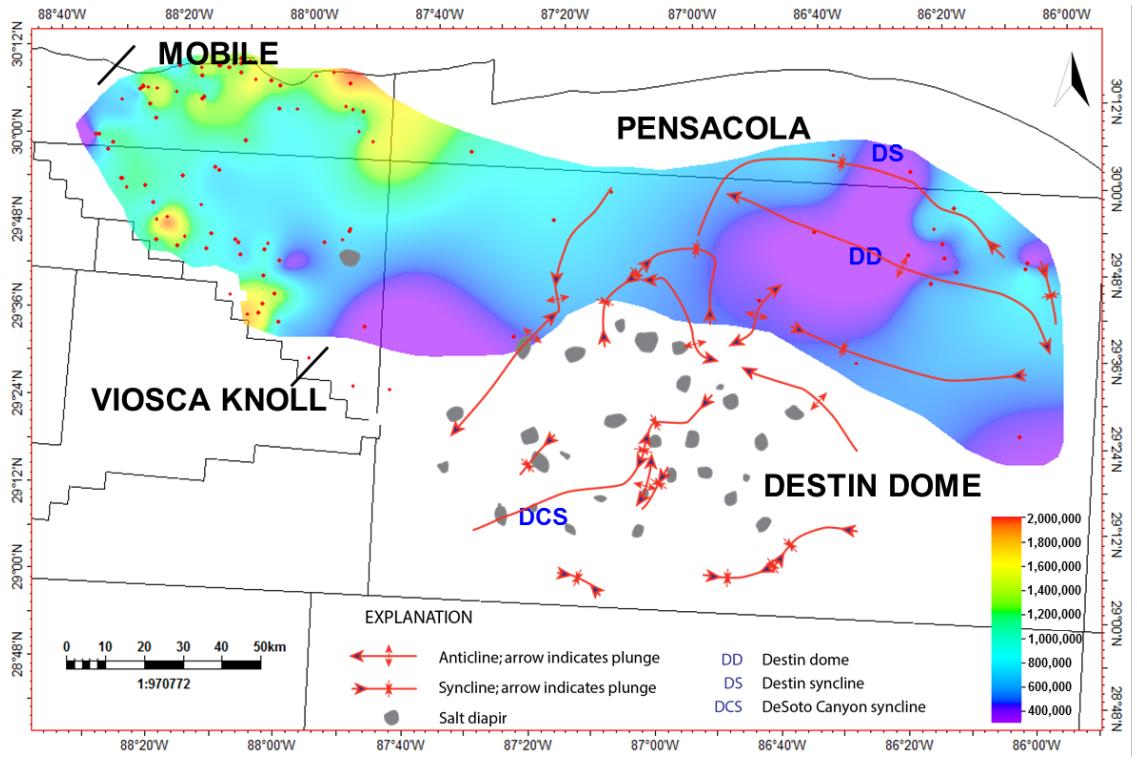

Figure 5.33. Storage resource map of the lower Tuscaloosa Group in the DeSoto Canyon Salt Basin.

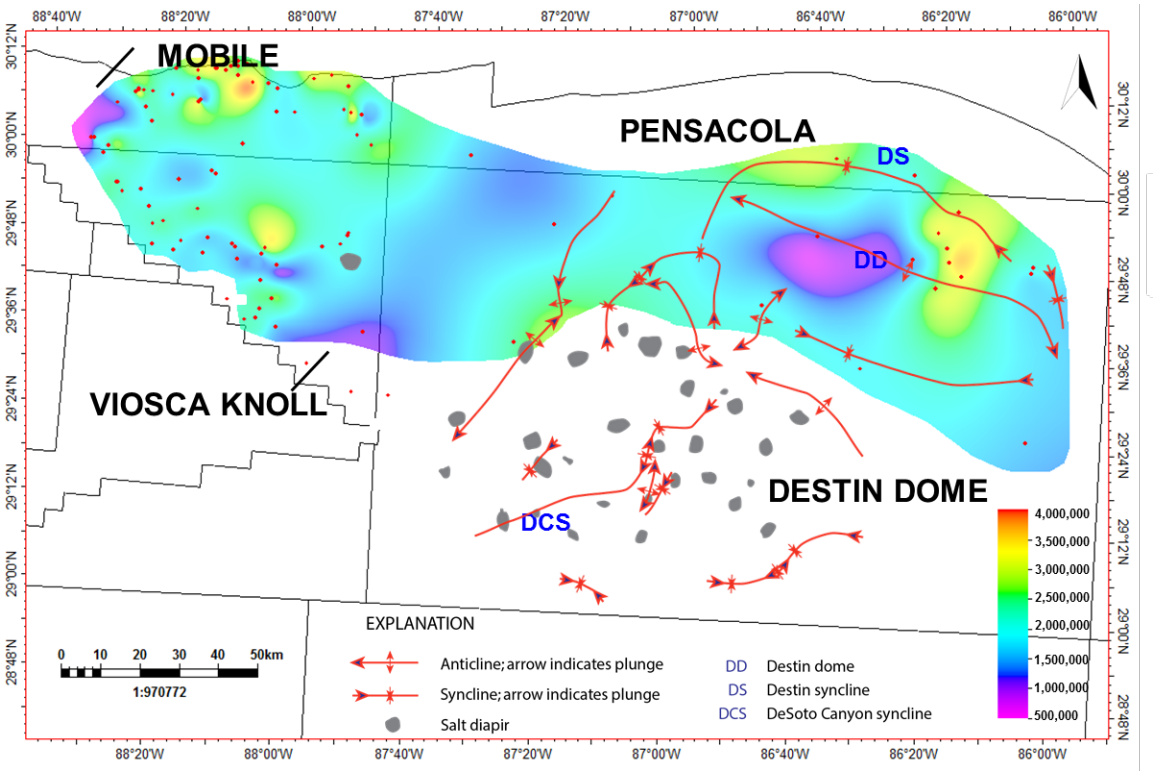

Figure 5.34. Cumulative storage capacity in Cretaceous saline formations in the DeSoto Canyon Salt Basin.

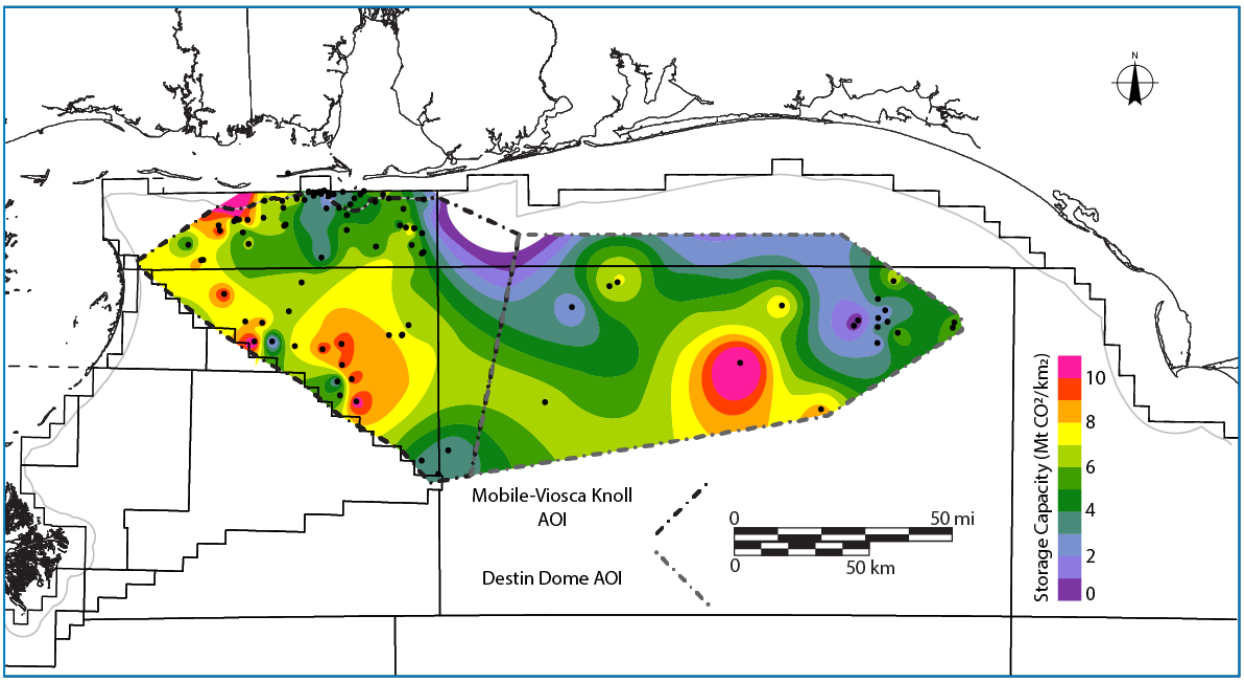

Figure 5.35. Total estimated CO_2 storage resource in Cenozoic strata in the DeSoto Canyon Salt Basin.

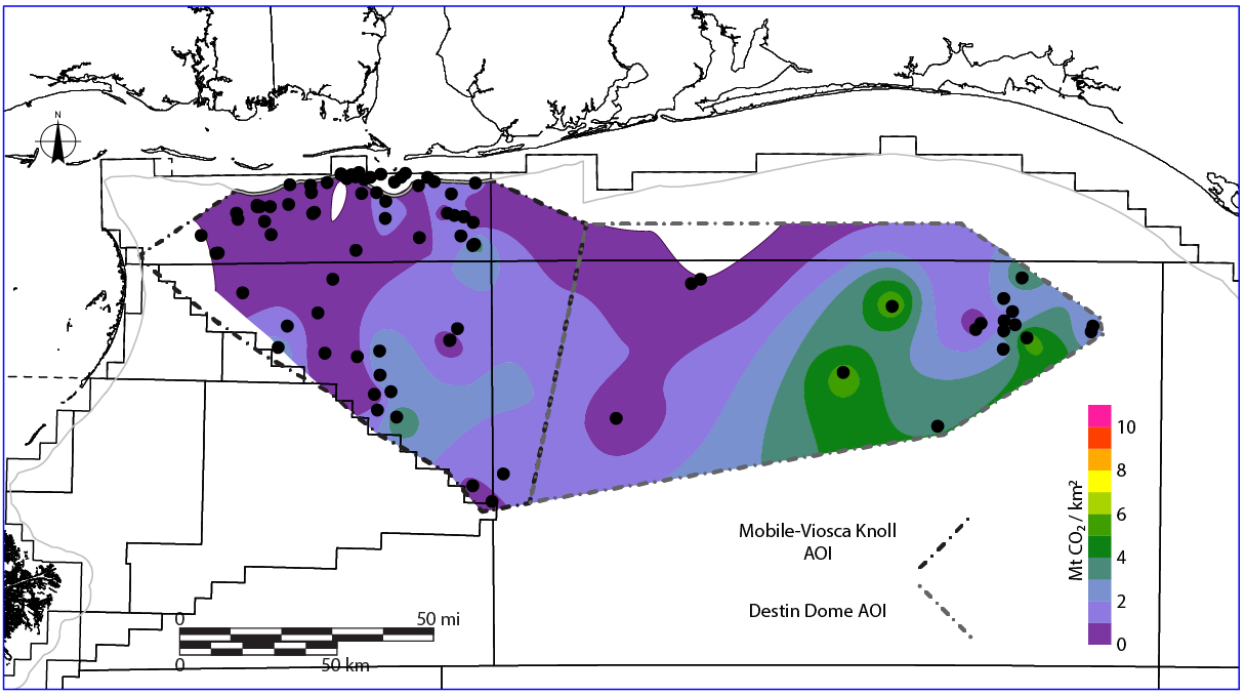

Figure 5.36. Total estimated CO_2 storage resource in Paleocene-mid Eocene strata in the DeSoto Canyon Salt Basin.

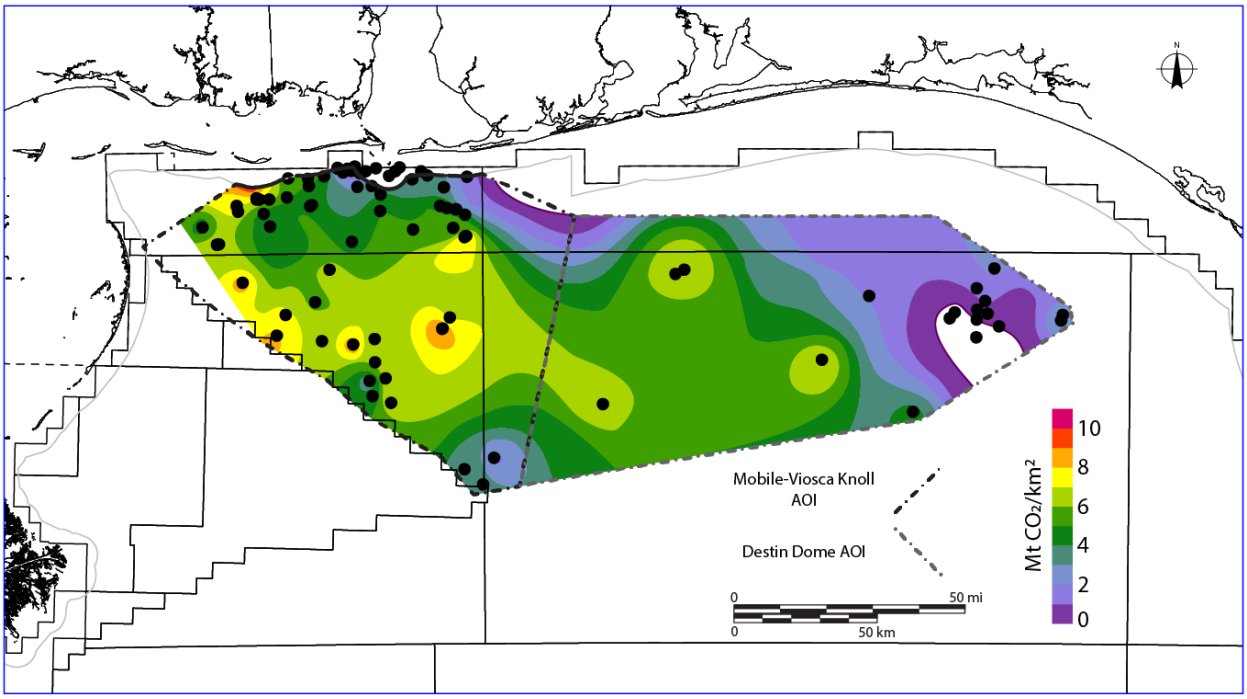

Figure 5.37. Total estimated CO_2 storage resource in upper Eocene-Miocene strata in the DeSoto Canyon Salt Basin.

Cenozoic section, with some locations capable of storing up to 10 Mt CO_2/km^2. Most of this resource is in the Paleocene-mid Eocene assessment units. The total P_{50} storage resource in the Destin Dome AOI is estimated to be 99 Gt and in the Viosca Knoll AOI is 133 Gt (Table 6). The greatest potential within the Mobile-Viosca Knoll AOI is within the younger Eocene-Miocene units, with an estimated P_{50} storage resource of 46 Gt.

Estimated minimum seal thickness (-750 m, or -2,500 ft subsea depth to top of Middle Eocene) (Fig. 5.38) varies from 0 m at the crest of Destin Dome to more than 1,200 m (4,000 ft) in the Viosca Knoll Area near the Cretaceous shelfbreak. This makes the Cenozoic strata in the eastern portion of the Destin Dome AOI less attractive for CO_2 storage than the western half of the Destin Dome AOI and Mobile-Viosca Knoll AOI. Taking into account seal thickness, reservoir thickness, and existing infrastructure, the most favorable areas to store CO_2 in the Cenozoic section would be in the Mobile, Viosca Knoll, and northwestern Destin Dome Areas.

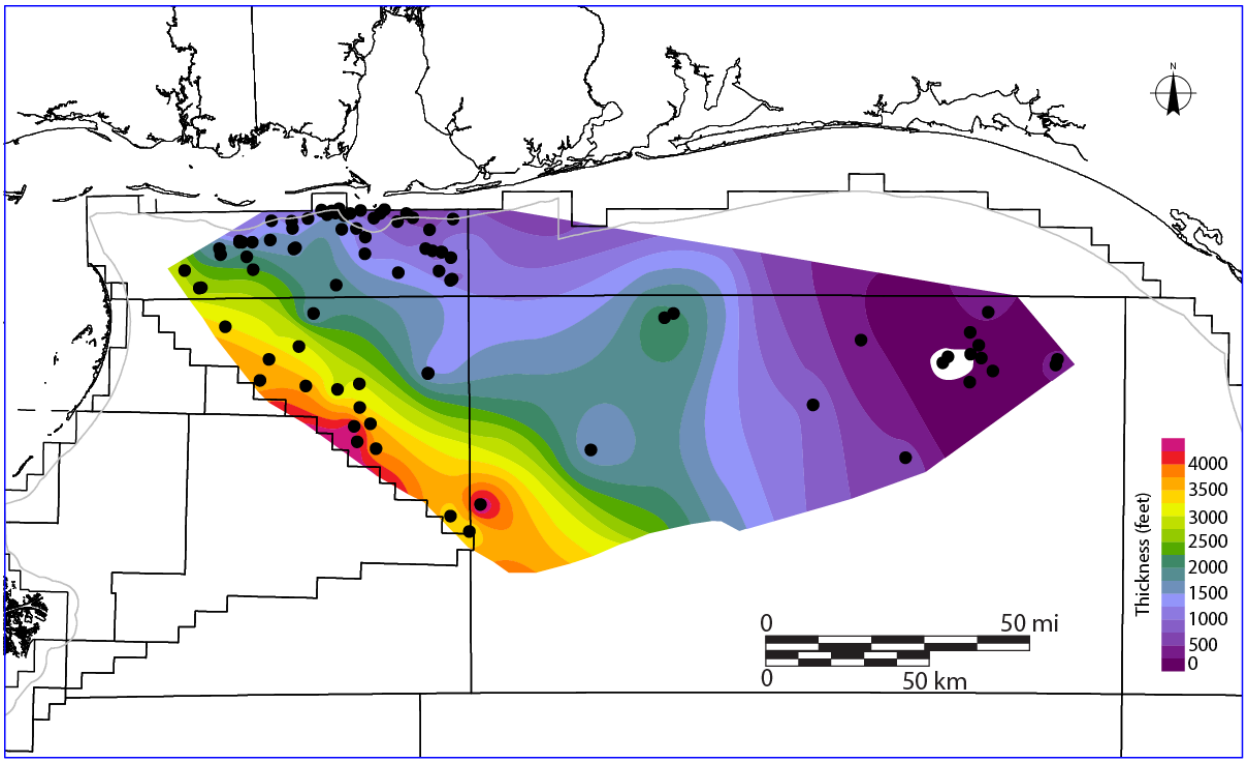

Figure 5.38. Net thickness of sealing mud and carbonate in mid Eocene-Miocene strata in the DeSoto Canyon Salt Basin.

Table 6. Summary of the CO_2 storage resource in Cenozoic strata of the DeSoto Canyon Salt Basin.

		Mobile-Viosca Knoll AOI	Destin Dome AOI	Total
All Cenozoic strata	P10	29	34	63
	P50	56	64	120
	P90	95	110	205
Paleocene-mid Eocene strata	P10	5	12	17
	P50	10	22	32
	P90	17	38	55
upper Eocene-Miocene strata	P10	24	22	46
	P50	46	42	88
	P90	78	72	151

Sarasota Arch

The primary reservoirs described in the area of the Sarasota Arch are dolomitic. CO_2 density values used for volumetric calculations were determined as a function of temperature and pressure, and values range from 700 to 800 kg/m^3 (Fig. 5.39). The calculated storage resource for each assessment unit is summarized in Tables 7-9 and Figures 59-62.

The Lehigh Acres Formation within the Punta Gorda assessment unit is a potential storage target for CO_2 and contains reservoir quality dolomite at depths of around 3,200 m (10,500 ft). The best potential target for storage is in the area surrounding well OCSG-3912 due to increased porosity identified during log analysis, with a P_{50} storage resource of around 5 Mt/km^2 (Fig. 5.40; Table 8). There is no projected storage potential in the southeastern portion because the net thickness of reservoir was less than 20 feet in well OCSG-3917, and may be absent in the South Florida Basin.

Within the Gordon Pass assessment unit, dolomite of the Marco Junction and Lake Trafford Formations has the highest storage potential near well OCSG-3903, which coincides with the highest point on the subsea structure map (Figs. 2.18, 5.41; Plate 2). The P_{50} storage potential of this assessment unit decreases from around 4 Mt/km^2 near well OCSG-3903, to an average of about 1-2 Mt/km^2 near the surrounding wells.

Similarly, the Dollar Bay Formation within the Panther Camp assessment unit contains its highest P_{50} storage capacity values near well OCSG-3903 with a local average of 4 Mt/km^2, and is also the structural high for this assessment interval (Figs. 2.19, 5.42; Plate 2).

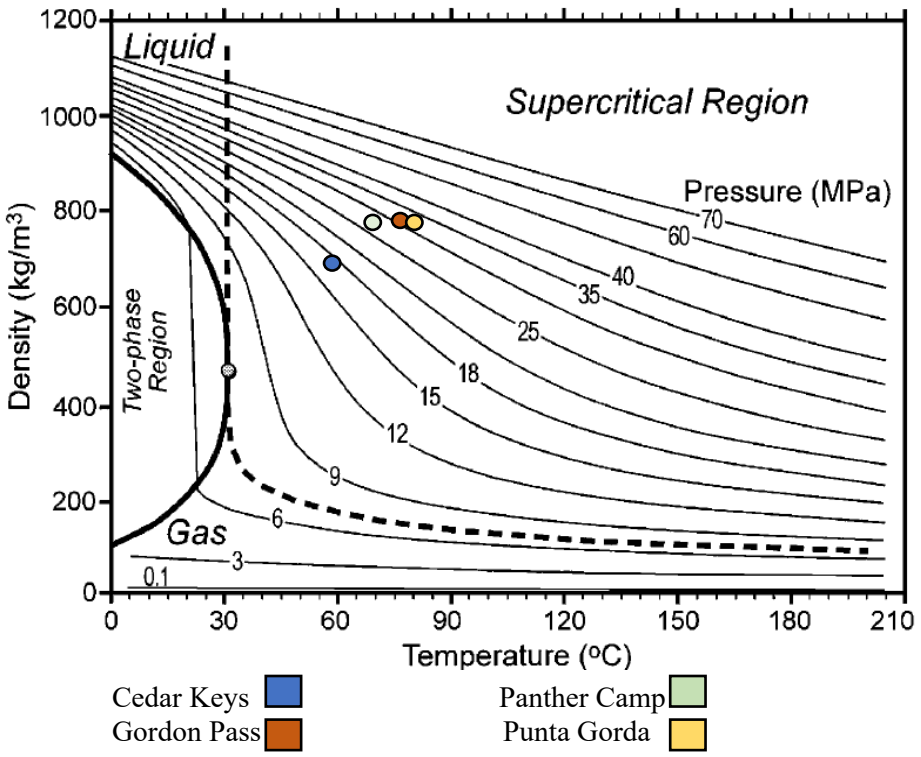

Figure 5.39. Variation of CO_2 density as a function of temperature and pressure (modified from Bachu, 2003). Data points mark pressure-temperature conditions in the Sarasota Arch.

Table 7. Estimated P_{10} storage resource in the Sarasota Arch region.

Assessment Unit	Thickness (m)	Mean Porosity	Density (kg/m^3)	P_{10} Efficiency	Storage Resource (Gt)
Upper Cedar Keys	305	0.237	700	0.16	366
Lower Cedar Keys	107	0.237	700	0.10	80
Panther Camp	67	0.214	790	0.16	82
Gordon Pass	55	0.203	800	0.16	64
Punta Gorda	67	0.171	800	0.16	66
Total	**600**				**658**

Table 8. Estimated P_{50} storage resource in the Sarasota Arch region.

Assessment Unit	Thickness (m)	Mean Porosity	Density (kg/m^3)	P_{50} Efficiency	Storage Resource (Gt)
Upper Cedar Keys	305	0.237	700	0.210	480
Lower Cedar Keys	107	0.237	700	0.150	121
Panther Camp	67	0.214	790	0.210	107
Gordon Pass	55	0.203	800	0.210	85
Punta Gorda	67	0.171	800	0.210	87
Total	**600**				**879**

Table 9. Estimated P_{90} storage resource in the Sarasota Arch region.

Assessment Unit	Thickness (m)	Mean Porosity	Density (kg/m^3)	P_{90} Efficiency	Estimated Storage Resource (Gt)
Upper Cedar Keys	305	0.237	700	0.210	594
Lower Cedar Keys	107	0.237	700	0.150	169
Panther Camp	67	0.214	790	0.210	133
Gordon Pass	55	0.203	800	0.210	105
Punta Gorda	67	0.171	800	0.210	107
TOTAL	**600**				**1108**

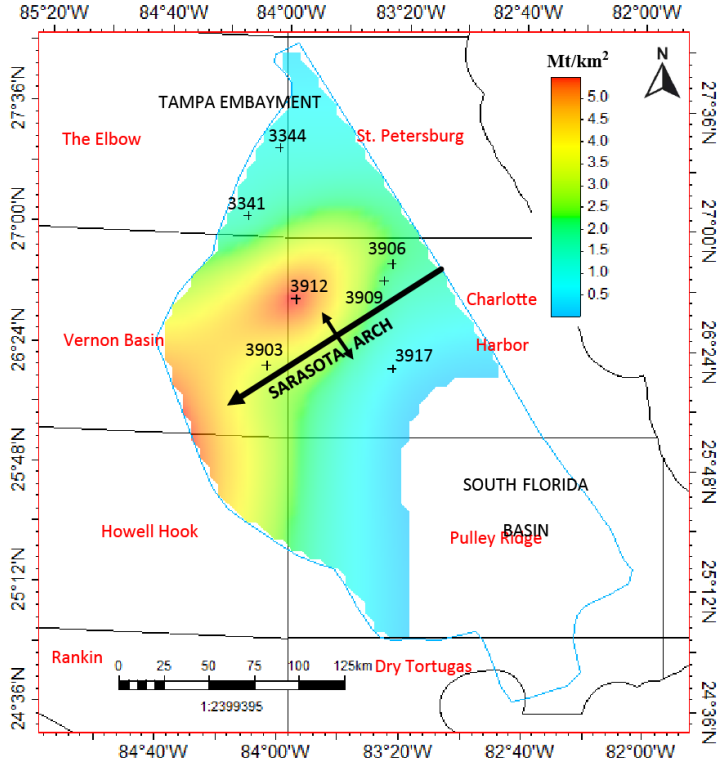

Figure 5.40. Estimated CO_2 storage resource in the Punta Gorda assessment unit.

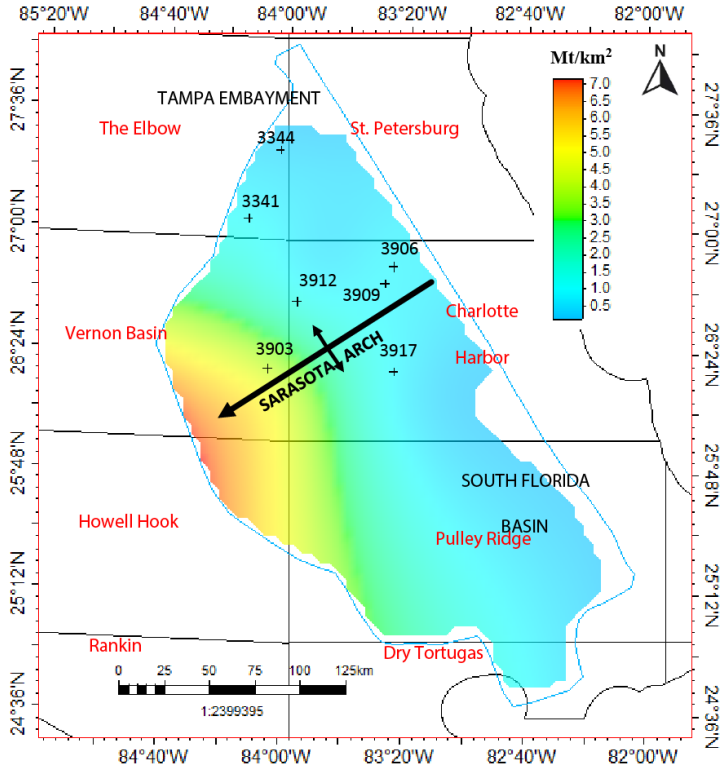

Figure 5.41. Estimated CO_2 storage resource in the Gordon Pass assessment unit.

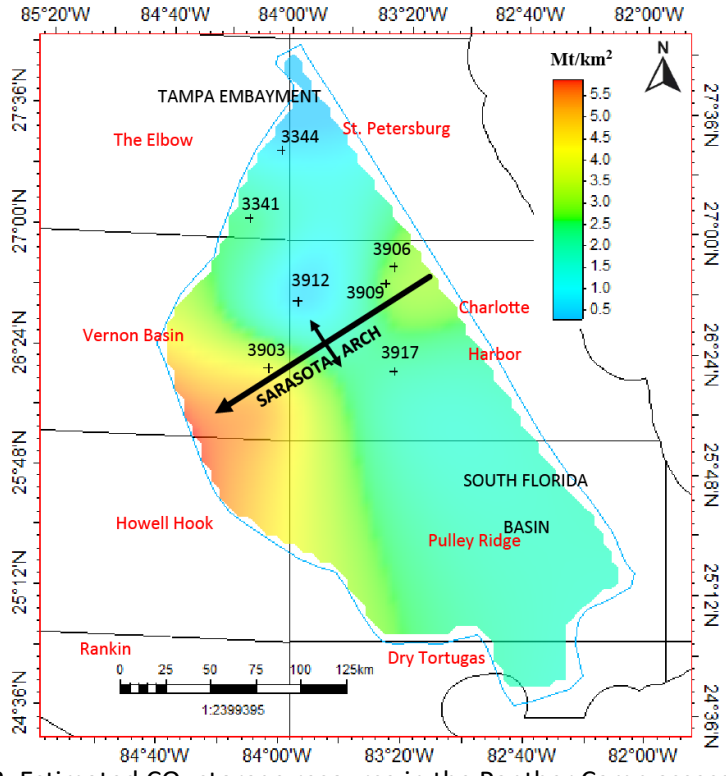

Figure 5.42. Estimated CO_2 storage resource in the Panther Camp assessment unit.

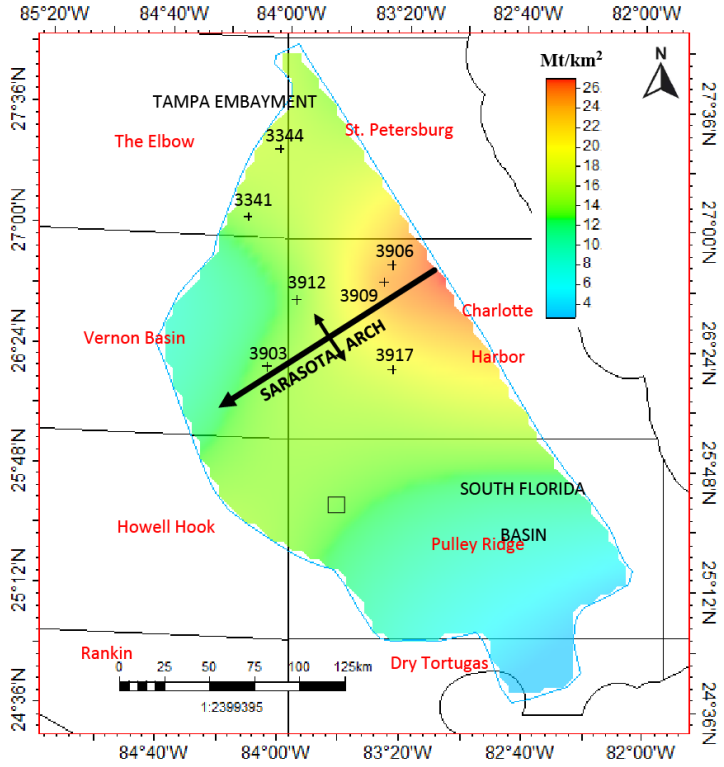

Figure 5.43. Estimated CO_2 storage resource in the Cedar Keys assessment unit.

In contrast to the other potential reservoirs, the thick limestone and dolomite within the Cedar Keys assessment unit project a much larger storage resource. The limestone in the upper portion of the Pine Key Formation contributes P_{50} storage potential of about 480 Gt, while the dolomite of the Lawson and Lower Cedar Keys Formation are estimated to contain around 120 Gt of P_{50} storage potential (Table 8). Storage potential in the area of wells OCSG-3906, and 3909 have P_{50} values near 23 Mt/km^2 (Fig. 5.43).

Subtask 5.4 - Identification of Target Development Areas

DeSoto Canyon Salt Basin

Stratigraphic analysis indicates that the Paluxy Formation is a net thickening- and coarsening-upward succession composed of interbedded sandstone, limestone and shale. The Paluxy Formation is considered a net progradational package of fluvial, coastal and shallow marine sandstone beds interbedded with shale (Mancini and Puckett, 2002). The variability observed in the SP log signatures from blocky to Christmas-tree is consistent with a range of possible depositional environments ranging from a bedload-dominated fluvial systems to coastal deposits. The Paluxy Formation becomes richer in limestone towards the Viosca Knoll Area as seen in the dip cross-section (Plate 2) where it is in facies relationship with the carbonate platform deposits landward of the Lower Cretaceous reef trend (Pashin et al., 2008).

Qualified sandstone in the Paluxy Formation generally has net thickness greater than 60 m (200 ft) on the stable shelf in the Mobile and Pensacola Areas and in the withdrawal synclines flanking Destin Dome (Fig. 5.1). The concentration of sand in the withdrawal synclines around Destin Dome indicates that deposition of the Paluxy Formation was contemporaneous with salt movement and diversion of sand around the early uplift, which Pashin et al. (2016) referred to

Ancestral Destin Dome. While sandstone units in the Paluxy Formation generally exhibit reservoir quality porosity, sandstone thickness and internal heterogeneity that are extremely variable, reflecting the complexity of the depositional systems (Plates 1, 2; Figs. 5.1, 5.4). Petrologic analysis of Paluxy fluvial and interfluvial deposits onshore in southwest Alabama indicates depositional and diagenetic processes associated with reservoir architecture and paleosol development to be major causes of reservoir heterogeneity in the Paluxy Formation (Folaranmi, 2015); however, it remains unclear precisely how depositional and diagenetic processes in offshore areas, which may include coastal deposits, relate to those onshore.

The net sandstone isolith map in Figure 5.2 indicates that reservoir-quality sandstone units in the Washita-Fredericksburg interval are localized and tend to be restricted to the stratigraphic level of the Dantzler sand (Plates 1, 2; Figs. 2.8, 5.2). The geophysical log signatures for individual units are predominantly fining-upward to blocky (Fig. 2.9) and, the map patterns suggest that deposition occurred in a bedload-dominated fluvial systems (Fig. 5.2). The most significant accumulation of Washita-Fredericksburg sandstone occurs in a southeast-tending belt suggestive of a fluvial axis along which sediment was transported toward the diapir province of the DeSoto Canyon Syncline. While Washita-Fredericksburg sandstone lacks regional continuity, it provides significant storage objectives locally and may be particularly attractive where it occurs in tandem with Paluxy and lower Tuscaloosa objectives. This lack of highly porous in the Washita-Fredericksburg interval contrasts with the observations made onshore (Pashin et al., 2008), where Washita-Fredericksburg is a sand-rich interval and appears to be part of a braidplain. The linear trends offshore suggest formation of major transitive fluvial axes on a coastal plain. The braidplain was likely tributary to these axes. This transition, along with the presence of a thick basal limestone, indicates diminishing sediment supply and transition from continental to coastal and marine environments (Mancini and Puckett, 2002).

The Massive sand of the lower Tuscaloosa Group has been interpreted as stacked beach-barrier and inlet deposits in southwestern Alabama and southeastern Mississippi (Mancini et al., 1987; Petrusak et al., 2009). The dominant blocky geophysical log signature of the Massive sand has been interpreted as the product of aggradational sedimentation, whereas fining upward in the upper part of the sandstone is thought to indicate backstepping associated with marine transgression (Mancini and Puckett, 2005). Onshore cores in southeastern Mississippi contain marine fossils, and the basal disconformity at the base of the Massive sand is interpreted as the product of extensive marine reworking and ravinement formation (Pashin et al., 2008).

The isochore map of the lower Tuscaloosa Group in Fig. 2.13 shows that the reservoir quality sandstone is over 60 m (200 ft) thick on the stable shelf in the Mobile, western Pensacola and Viosca Knoll Areas. It thins out towards the south of the basin (<30 m; 100 ft) and in the Destin Dome Area. This thinning of the Massive sand of the lower Tuscaloosa Group has been attributed to the growth of the Destin Dome anticline and distance from the sediment source (Petty, 1995). Structural restorations indicate that the main Destin Dome structure grew mainly during and after Tuscaloosa-Midway deposition (Pashin et al., 2016). The net sandstone isolith map of the lower Tuscaloosa Group indicates that large parts of the Mobile and Viosca Knoll Areas contain qualified sandstone with net thickness >45 m (150 ft) that provide attractive locations for offshore CO_2 storage. The lower Tuscaloosa Group also has the highest average porosity of the sandstone units evaluated and is the shallowest of all the three potential CO_2 storage target, which make it a primary storage objective particularly close to shore in the Mobile Area.

The main geological risk for CO_2 storage is arguably seal integrity (Damen et al., 2006). By definition, a prospective geological sink must not only have adequate porosity and permeability to store large volumes of carbon dioxide but should also be overlain by at least one regionally extensive sealing stratum. All proposed Cretaceous reservoirs are below several sealing stratigraphic units, including the nonporous basal carbonate of the Washita-Fredericksburg interval, the Marine Tuscaloosa shale, chalk of the Selma Group, and the Porters Creek Clay of the Midway Group. Careful examination of the well logs showed that while the upper part of the Washita-Fredericksburg interval contains some reservoir quality sandstone beds, there is very little sandstone in the basal Washita-Fredericksburg limestone unit, which is 300-600 m (1,000 to 2,000 ft) thick across the basin. Density porosity is effectively zero, and so the limestone section serves as the primary topseal above the Paluxy sandstone units. The Marine Tuscaloosa shale, which is interpreted as a condensed section (Mancini et al., 1987), immediately overlies the lower Tuscaloosa Group and is uniformly thick (60-90 m; 200-300 ft) throughout the study area. The Marine shale is regionally extensive and is considered the primary seal for onshore petroleum accumulations in the lower Tuscaloosa Group (Mancini et al., 1987), which is the largest oil producer in Mississippi. The presence of multiple sealing layers in the Tuscaloosa-Midway section, including the Marine shale, the chalk of the Selma Group, and the Paleocene mudstone units, also helps minimize the risk of leakage.

The DeSoto Canyon Salt Basin exhibits significant structural complexity in the Cretaceous section. The basin contains multiple anticlines cored by salt pillows, crestal faults atop the pillow-cored anticlines, and the peripheral faults of the Destin fault system, and the DeSoto Canyon diapir field (Pashin et al., 2016). Growth of the peripheral faults was mainly during Early Cretaceous time. While the faults are not mappable by seismic data in the Upper Cretaceous Formations, several seismic lines demonstrate that the tip regions of the faults extend into the Upper Cretaceous section (Pashin et al., 2016). Accordingly, caution is required when considering CO_2 sinks in proximity to the Destin fault system. In addition, crestal faults above salt pillows also pose risk, and so the crestal regions of the salt pillows may not be viable storage targets and may pose risk for plume migration along the anticlinal flanks near these structures.

The evaluated area is about 13,466 km^2 (~5,200 mi^2) and the estimated P_{50} storage capacity for this area is about 17, 1, and 10 Gt for Paluxy, Washita-Fredericksburg and lower Tuscaloosa assessment units, respectively. The combined storage capacity of the Cretaceous targets therefore is about 28 Gt in the DeSoto Canyon Salt Basin. The numbers obtained from this evaluation support the preliminary estimates made by Hills and Pashin (2010) that offshore Cretaceous formations in the study area can store more than 30 Gt of CO_2.

Volumetric analysis indicates that the Paluxy Formation, lower Tuscaloosa Group, and Cenozoic sand units are the main reservoir units that have Gt-class CO_2 storage capacity and potentially high injectivity. Together, these three intervals account for nearly all of the assessed Cretaceous storage capacity in the basin (Figs. 5.31-5.34). The Washita-Fredericksburg interval has relatively low storage potential (P_{50} = 1 Gt), but where qualified sandstone is present, it can be a viable storage objective and would be an attractive component of a stacked storage strategy.

While the Paluxy Formation has a greater net storage resource than the lower Tuscaloosa Group, care must be taken to recognize the lateral heterogeneity and discontinuity of individual sandstone units. However, this proved not to be an obstacle for injection into the Paluxy Formation during the SECARB Anthropogenic Test (Koperna et al., 2012). Stratigraphic cross-sections reveal complex vertical stacking of lensoid sandstone units in the Paluxy Formation

and the Washita-Fredericksburg interval (Plates 1, 2). The Massive sand of the lower Tuscaloosa Group, on the other hand, appears to be continuous across large parts of the salt basin and is especially thick in the Mobile Area closest to the modern coast.

Net sandstone thickness and porosity maps (Figs. 5.1-5.6) highlight the variability of reservoir quality and can help with selection of the most suitable injection locations in the study area. The Paluxy Formation has an extremely variable reservoir distribution with most of the capacity concentrated in the northeastern Destin Dome and eastern Pensacola Areas (Fig. 5.31). Some of this storage capacity is in the Destin syncline. This area includes the peripheral faults of the Destin fault system and therefore may pose a risk to reservoir and seal integrity. The reservoirs in the Washita-Fredericksburg interval and the lower Tuscaloosa Group are concentrated in the stable shelf in the Mobile and Viosca Knoll Areas. The structure in this area is very simple, save for one major salt diapir (Figs. 2.4, 5.32, 5.33).

On the basis of the location of the reservoir units, the vertical stacking of individual sandstone bodies, the structural framework of the region, and available well control, the Mobile and Viosca Knoll Areas appear to provide the most suitable locations for CO_2 injection into Cretaceous rocks in the DeSoto Canyon Salt Basin. The combined storage resource in this region ranges from 2 to 4 Mt/km^2 and averages about 2.9 Mt/km^2, which is significantly higher than the average storage capacity of all the Cretaceous sandstone units (2.1 Mt/km^2) in the vicinity of Destin Dome. The combined storage resource for an offshore block in this area is between 47 and 93 Mt with an average of about 69 Mt.

These storage resource numbers are encouraging. According to the U.S. GHG inventory (https://ghgdata.epa.gov/ghgp/main.do), the 2016 greenhouse gas emissions from few key power plants close to shore, such as Plant Barry in Alabama, Plant Daniel in Mississippi, and Plant Crist in Florida were 7.5 Mt, 5.2 Mt and 3.1 Mt, respectively. Plants Barry and Daniel have been used in pilot CO_2 storage programs led by the Southeastern Regional Carbon Sequestration Partnership (SECARB) and have successfully demonstrated CO_2 sequestration in the offshore Cretaceous reservoirs (Koperna et al., 2009, 2012). The combined emissions from Plants Barry, Daniel, and Crist are about 15.8 Mt with an average for the three plants of 5.3 Mt/year. Considering this as average annual emissions from a major coal-fired power plant, each offshore block (9.0 mi^2; 23.3 km^2) in the Mobile and Viosca Knoll Areas is capable of sequestering annual emissions from 13 such power plants.

Leakage risks from CO_2 storage can occur through manmade pathways (e.g., wells) or natural pathways (e.g., faults, fractures). Presence of multiple sealing beds of regional extent above the lower Tuscaloosa Group helps minimize risk, and the shale and tight limestone beds within the main sandstone-bearing intervals can serve as baffles and barriers to cross-formational flow. In addition, porous sandstone units above the target injection zone may act as buffers that can trap fugitive CO_2 before it reaches the major reservoir seals. Pressure data and regional geochemical data (Meng et al., 2018) indicate that the reservoirs in the study area are normally pressured. However, geomechanical studies will be helpful for identifying and mitigating any potential risks related to reservoir and seal integrity.

While thick sealing intervals help minimize the risk of CO_2 migrating out of the storage complex, the biggest challenge for CO_2 storage, especially in the Paluxy Formation, will be managing stratigraphic heterogeneity, especially in areas with sparse well control. Offsetting existing wells will be an effective strategy to maximize the probability of contacting thick and porous sandstone bodies. The SECARB Phase III Anthropogenic test has established the feasibility of large-scale CO_2 sequestration in the Paluxy Formation in Alabama (Koperna et al., 2012). A

small-scale test conducted at Plant Daniel in southeast Mississippi evaluated the lower Tuscaloosa Group (Koperna et al., 2009; Petrusak et al., 2009), and a large-scale SECARB Phase III test was performed at the Cranfield Field in Mississippi (Hovorka et al., 2013). These tests have stressed the importance of high-resolution reservoir characterization and simulation for accurate long-term CO_2 plume prediction for commercial-scale storage. A variety of CO_2 monitoring, verification and accounting (MVA) strategies were used in these tests that provide vital information on plume extent, plume geometry, pressure footprint, and confinement of CO_2 in the reservoir zone. Numerous wells in the Mobile Area reach total depth in ultra-deep Jurassic gas reservoirs of the Norphlet Formation. Cretaceous strata are typically behind the long string of well casing. Dry holes, however, are typically not cased and thus pose the greatest risk of cross-formational flow. Understanding wellbore-related risks is important, because offshore CO_2 storage wells may make use of existing infrastructure and offset older exploratory and production wells.

Fig. 5.44 illustrates a conceptual model of the storage complex including the reservoirs, baffles, barriers and seals that defines the container where CO_2 can be stored in the Cretaceous System. It also depicts injection through single-zone, multi-zone, and directional wells following the model of Pashin et al. (2008). Single-zone wells are well suited for areas where only one sandstone interval, such as the Massive sand of the lower Tuscaloosa Group, is prospective. A stacked storage strategy employing wells completed in multiple sandstone units helps limit the overall geographic and pressure footprint of the plume. Directional wells, by contrast, maximize reservoir contact, injection rate, and storage efficiency.

Sarasota Arch

Abundant anhydrite, dolomite, and limestone beds indicate that the West Florida Platform formed in an arid, tropical to sub-tropical climate, and the major carbonate-anhydrite successions appear to record relative changes of sea level in the platform interior. Changes of sea level and uplift of the Sarasota Arch apparently led to the increase of evaporation reflux on the arch where the development of circulation-restricting barriers led to the formation of shelf wide evaporative lagoons (Adams and Rhodes, 1960; Hardie, 1987; Morse et al., 2007). This caused increases in the salinity of brine, which became dense enough to displace connate water and seep downward through the lagoon floor where magnesium replaced part of the calcium to recrystallize as porous dolomite. The proposed depositional model indicates that the West Florida Platform was primarily deposited in a restricted rimmed platform margin where there are hypersaline conditions favorable for dolomitization and evaporite deposition (Fig. 5.45).

A previous study of chalky limestone and micrite in the Gordon Pass Formation interpreted the depositional environment as distal back reef (Winston, 1976). Onshore investigation of the Panther Camp assessment unit suggests that the Dollar Bay Formation was deposited during both sea level regressions and transgressions, and is largely composed of carbonates and evaporites deposited in a marine tidal flat-lagoonal setting, and in an open

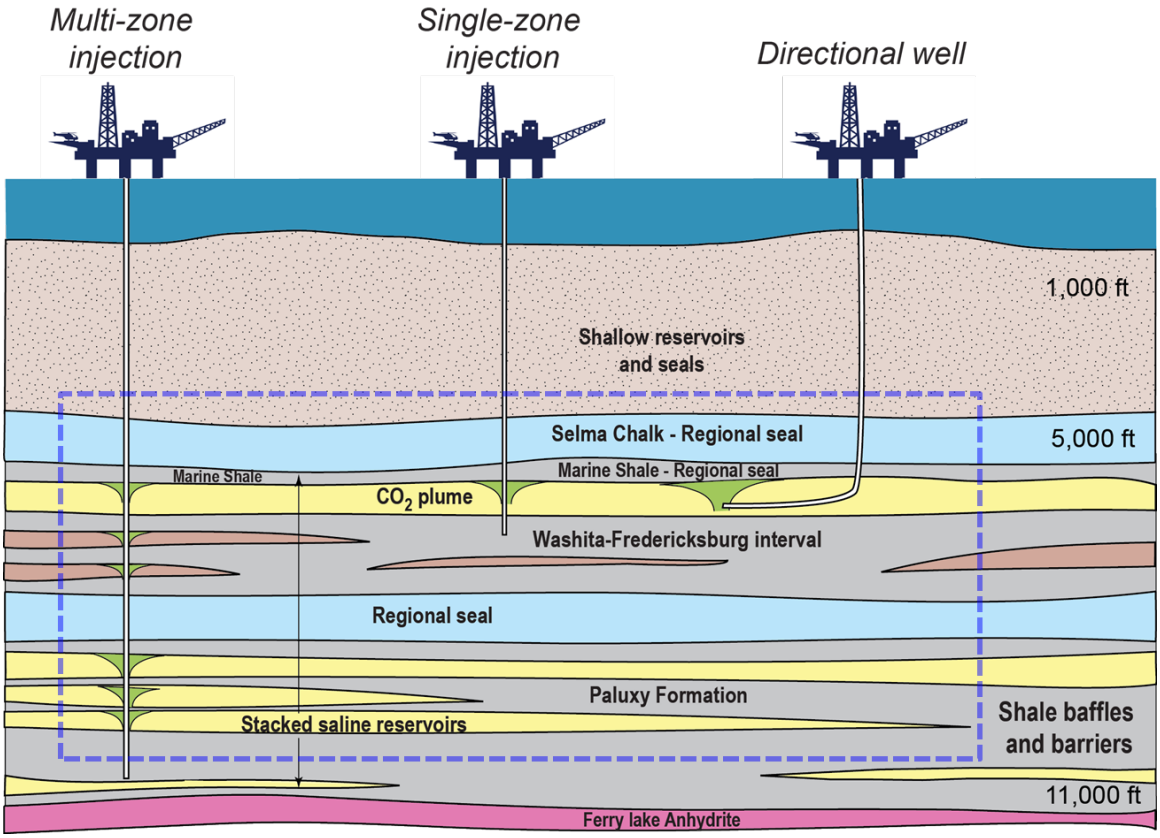

Figure 5.44. Conceptual model of a geological CO_2 storage complex in the targeted reservoirs over the stable shelf in the Mobile and Viosca Knoll Areas.

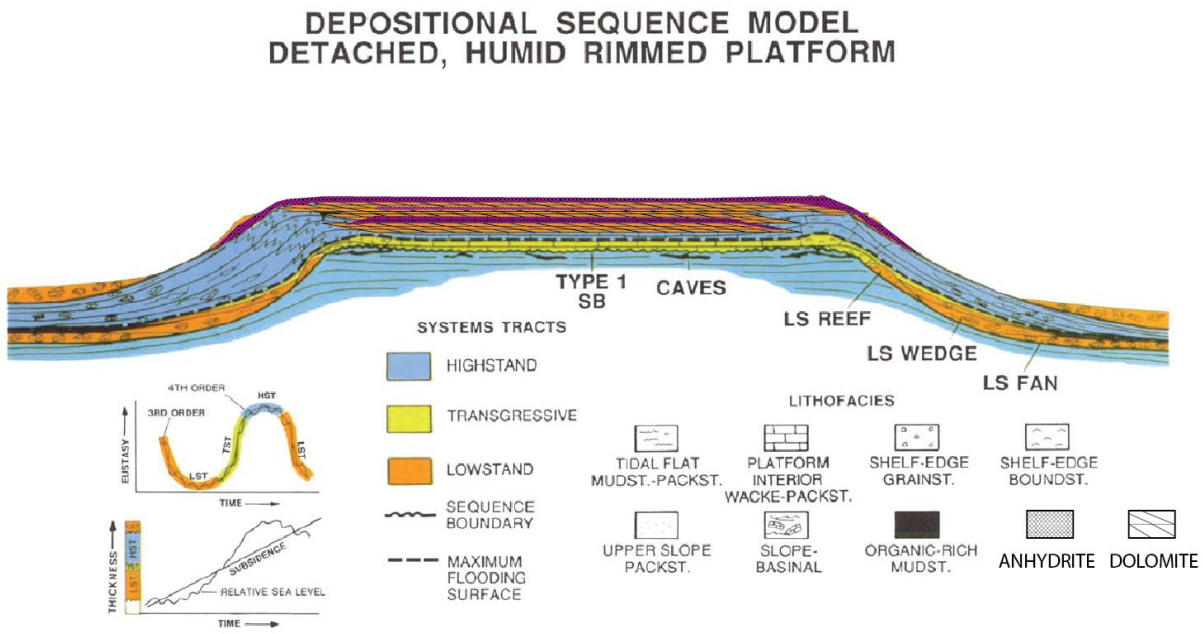

Figure 5.45. Evaporitic carbonate platform model representative of the West Florida Shelf and Sarasota Arch (modified from Handford and Loucks, 1993).

marine subtidal platform (Mitchell-Tapping, 1990, Pollastro, 2001). The Cedar Keys Formation in onshore areas is thought to have been deposited in a tidal flat environment during the Paleocene, and possibly continuing into the Eocene (Pollastro, 2001), and more open marine facies may be present in the West Florida Shelf.

As stated previously, porous dolomite is thickest in the crestal region of the Sarasota Arch, and the proportion of limestone increases in the adjacent basins (Tampa Embayment and South Florida Basin) (Plates 3, 4). Cross-section A-A' shows that all of the Lower Cretaceous assessment units in the study area thin from the Tampa Embayment onto the Sarasota Arch, indicating that the arch grew during deposition. Sediment deposited on the Sarasota Arch is prone to dolomitization and diagenetically enhanced porosity development due to the evaporation reflux and circulation restricting barriers in the platform margin (Adams and Rhodes, 1960). This is true for the complete Lower Cretaceous section and for the Lawson Formation.

Identification of the storage resource in each assessment unit was achieved by using the defined reservoir properties during well log analysis and seismic interpretation, and leveraging them with CO_2 density values and storage efficiency factors for each assessment unit to generate the storage resource maps and perform the volumetric calculations. Previously discussed storage resource maps of the Punta Gorda, Gordon Pass, and Panther Camp assessment units average 2.5 Mt/km^2, while the Cedar Keys assessment unit averages 15 Mt/km^2. Higher storage potential exists in targeted locations, and indeed reinforces the hypothesis that each offshore block holds the capacity to store annual greenhouse gas emissions from multiple coal-fired power plants in peninsular Florida. Caution should be taken due to the fact that the volumetric calculations include the entire study area, and it is likely because of limited well control that many of the reservoirs do not extend into the Tampa Embayment or South Florida Basin.

The qualified reservoirs within the Lehigh acres Formation of the Punta Gorda assessment unit are almost entirely porous dolomite. The storage resource map indicates that the best storage location occurs near well OCSG-3912 with 5 Mt/km^2 of storage potential, or 116 Mt per offshore block in the surrounding area. The limestone units within the Punta Gorda assessment interval are generally nonporous and thus do not meet the minimum 15% porosity requirement for qualification. Comparisons between the strike cross section, subsea structure maps, and porosity maps reveal trends of reservoir heterogeneity. Two wells located in the Elbow Area, which is at the southeast end of the Tampa Embayment, contain mainly nonporous limestone in the Lehigh Acres Formation (Plate 3). In general, the reservoirs of the Lehigh Acres formation provide an attractive target for CO_2 sequestration on the Sarasota Arch, where porous dolomite predominates.

Potential storage objectives in the Gordon Pass assessment unit are similar to those in the Punta Gorda assessment unit. The qualified reservoirs are in porous dolomite of the Gordon Pass and Marco Junction Formations. The storage resource map indicates that the best storage location is near well OCSG-3903 with 5 Mt/km^2, or 116 Mt per offshore block of storage potential near the shelf margin. The two northernmost wells, OCSG-3344, and OCSG-3341, which are in the Tampa Embayment, are the only wells penetrating the Gordon Pass assessment unit that are dominated by nonporous limestone.

The distribution of porous dolomite in the Dollar Bay Formation of the Panther Camp assessment unit again shows that the Sarasota Arch played an important role in dolomitization

and porosity development. The best storage locations are located near wells OCSG-3903 and OCSG-3906 with 4 Mt/km^2 or 93 Mt of storage potential per offshore block. The Dollar Bay reservoir in the Panther Camp assessment unit has similar net thickness to the Lehigh Acres reservoir within the Punta Gorda assessment unit, yet the P_{50} CO_2 storage resource is much larger at about 107 Gt and is attributed primarily to the high porosity and continuity of the reservoir in the study area (Table 4; Plates 3, 4).

The youngest reservoirs assessed in the Sarasota Arch region are the limestone reservoirs of the Pine Key Formation and the dolomitic reservoirs of the Lawson and Cedar Keys Formations. The best storage locations are located near wells OCSG-3909 and OCSG-3906 with greater than 22 Mt/km^2 of storage potential, or 512 Mt per offshore block. This area is the most prospective target location for subsurface CO_2 storage attributed to reservoir thickness, high porosity, shallow depth, and identified overlying seals. The porous limestone unit in the Pine Key Formation is about 110 m (350 ft) thick across the study area, and only the upper Pine Key is considered a target interval. It is important to note that limestone, like that in the Pine Key assessment unit, has a lower P_{50} displacement efficiency factor than dolomite (Goodman, 2011; Table 8). Storage of CO_2 in the Pine Key Formation should be considered since the storage resource approaches 120 Gt; however, the overlying Lawson and lower Cedar Keys porous dolomite units may provide even more attractive targets for CO_2 storage. Together, the dolomite reservoirs of the Upper Cretaceous Lawson Formation and the Paleocene Cedar Keys Formation have net thickness greater than 300 m (1,000 ft) and account for more than half of the total estimated storage resource in the study area (~480 Gt.) (Table 4, Fig. 5.9). With mean porosity of about 24 percent, there is value in further analysis of the Cedar Keys assessment unit. However, the chalky nature of many Cretaceous and Cenozoic limestone units may limit permeability and, hence, injectivity.

All of the impermeable sealing strata identified as caprocks for the saline formations in the study area are anhydrite, and nonporous limestone and Atkinson shale may provide additional sealing capacity. As discussed previously in the stratigraphic framework section, there is an abundance of both thick anhydrite beds, and stacked layers of laterally continuous anhydrite interbedded with the dolomite. Many of the thin anhydrite layers (< 3 m; 10 ft) can be correlated across the study area (Plates 3, 4). Furthermore, the thick and laterally continuous anhydrite beds at the top of the Punta Gorda, Gordon Pass, and Panther Camp assessment units are considered low-risk seals.

The Cedar Keys assessment unit does follow some trends similar to those in the other assessment units. The stacked anhydrite beds have net thickness between 40-46 m (130-150 ft), yet this stratigraphic section was not logged in most wells. The lateral extent of the Cedar Keys anhydrite beds is not known due to sparse well control in the study area. The anhydrite layers appear to be absent in the Tampa Embayment at wells OCSG-3341, 3344, and also at well OCSG-3903. This suggests that the best possibilities for early injection would be in the crestal region of the Sarasota Arch where the presence of widespread is confirmed. Unfortunately, the thick anhydrite seals onshore do not extend throughout the assessment unit. Generally, the anhydrite beds in the Cedar Keys Formation are about 3 m (10 ft) thick and are thus much thinner than those in the other assessment units. For purposes of analyzing risks of potential commercial CO_2 sequestration, the Cedar Keys assessment unit is considered higher risk than the other assessment units until further studies can be completed in order to assess the lateral extent of confining units.

Subtask 5.5 – CO_2 Storage Capacity

The P_{50} storage resource characterized by this study is about 28 Gt in Cretaceous sandstone of the DeSoto Canyon Salt Basin, 879 Gt in Cretaceous carbonate of the Sarasota Arch, and 120 Gt in Cenozoic sand of the DeSoto Canyon Area. Thus the total storage resource in the EGOM region is estimated to be 1,027 Gt. According to Goodman et al. (2011), CO_2 storage capacity represents the geologic storage potential when "current economic and regulatory considerations are included." Economic considerations include the cost of separation, capture, transport to the storage site, injection, and well maintenance, and these factors are beyond the scope of this investigation. In terms of regulatory climate, there is a strong case for offshore CO_2 storage because of common ownership of the reservoirs and the apparent applicability of the 45Q tax credit. Accordingly, the EGOM team considers the storage capacity to approach the volume of the storage resource until there is more information regarding the regulatory logistics and economic viability of offshore storage operations. Regardless, it is clear that ample multi-gigatonne-class storage capacity exists in the DeSoto Canyon Salt Basin and the Sarasota Arch to store most if not all anthropogenic CO_2 emissions originating near the coastal regions of Mississippi, Alabama, and Florida.

Task 8.0: Outreach

Subtask 8.1 – Public Outreach

Links to all presentations & posters can be found in the Appendix

Meetings with presentations:

1. November 2015, Southeastern Offshore Storage Resource Assessment – Eastern Gulf of Mexico; kickoff meeting at the National Energy Technology Laboratory, Pittsburgh, Pennsylvania
2. March 2016, Southeast Offshore Storage Resource Assessment (SOSRA) Eastern Gulf of Mexico; 11th Annual SECARB Stakeholder's Meeting, Atlanta, Georgia
3. May 2016, Feasibility of Alabama's Gulf Coast for Offshore CO_2 Geologic Storage and Enhanced Oil Recovery; Fifth Annual Continuing Education Conference of the Alabama Board of Licensure for Professional Geologists, Birmingham, Alabama.
4. June 2016, SOSRA: Opportunities in the Eastern Gulf of Mexico for CO_2 Storage; American Association of Petroleum Geologists Annual Conference and Exposition, Calgary, Alberta
5. August 2016, Southeastern Offshore Storage Resource Assessment – Eastern Gulf of Mexico; NETL Carbon Capture, Utilization, Storage, and Oil & Gas Technologies Review Meeting, Pittsburgh, PA
6. September 2016, Evolution of Giant Salt Pillows, Eastern Gulf of Mexico: Implications for Exploration and CO_2 storage; Geological Society of America Annual Meeting, Denver, Colorado
7. September 2016, Investigation the Eastern Gulf of Mexico for Potential Geologic Storage of CO_2; Geological Society of America Annual Meeting, Denver, Colorado
8. October 2016, Petroleum Exploration and Development Frontiers in Southwest Alabama; Alabama Oil and Gas Seminar, Tuscaloosa, Alabama

9. October 2016, Southeast Offshore Storage Resource Assessment for CO_2 Sequestration: The Role of the Gulf of Mexico; Southeastern Environmental Conference, Orange Beach, Alabama
10. December 2016, Mesozoic of the Gulf Rim and Beyond: New Progress in Science and Exploration of the Gulf of Mexico Basin: 35th Gulf Coast Section SEPM Perkins-Rosen Research Conference, Houston, Texas
11. March 2017, Southeastern Offshore Storage Resource Assessment – Eastern Gulf of Mexico; 12th Annual SECARB Stakeholders Meeting, Atlanta, Georgia.
12. April 2017, Offshore CO_2 Storage; US-Taiwan International CCS Conference, Taipei, Taiwan
13. June 2017, Establishing CO_2 Utilization, Storage and Pipeline Systems for Oil Fields in Shallow and Deep Waters of the Gulf of Mexico; International Workshop on Offshore Geologic CO_2 Storage, sponsored by University of Texas, Bureau of Economic Geology, Beaumont, Texas
14. July 2017, Offshore CO_2 Storage Potential of the Eastern Gulf of Mexico; Carbon Management Technology Conference, Houston, Texas
15. September 2017, Assessing CO_2 Storage Potential in the Eastern Gulf of Mexico Continental Shelf; Colloquium at the Boone Pickens School of Geology, Oklahoma State University, Stillwater, Oklahoma
16. March 2018, Southeastern Offshore Storage Resource Assessment – Eastern Gulf of Mexico; 13th Annual SECARB Stakeholders Meeting, Atlanta, Georgia.
17. August 2018, Southeast Offshore Storage Resource Assessment (SOSRA); NETL Carbon Capture, Utilization, Storage, and Oil & Gas Technologies Review Meeting, Pittsburgh, Pennsylvania
18. November 2018, Geological and Geomechanical Characteristics of the Potential CO_2 Storage Reservoirs, Eastern Gulf of Mexico; Geological Society of America Annual Meeting, Indianapolis, Indiana.
19. February 2019, Southeast Offshore Storage Resource Assessment (SOSRA); GOMCarb & SECARB Offshore Joint Partnership Meeting, Beaumont, Texas.
20. March 2019, Southeastern Offshore Storage Resource Assessment – Eastern Gulf of Mexico; 14th Annual SECARB Stakeholders Meeting, Atlanta, Georgia.

<u>Poster presentations:</u>

1. April 2016, Geologic framework and CO_2 storage potential of the eastern Gulf of Mexico Continental Shelf; International Workshop on Offshore Geologic CO_2 Storage, Austin, Texas
2. April 2017, DeSoto Canyon Salt Basin Geology & Petroleum Systems; American Association of Petroleum Geologists Annual Conference and Exposition, Houston, Texas
3. April 2017, Offshore CO_2 Storage Resource Assessment; US-Taiwan International CCS Conference, Taipei, Taiwan
4. June 2017, DeSoto Canyon Salt Basin Geology & Sequestration Potential; International Workshop on Offshore Geologic CO_2 Storage, Beaumont, Texas.

5. June 2017, CO_2 Storage Potential of the MAFLA Shelf, Eastern Gulf of Mexico; International Workshop on Offshore Geologic CO_2 Storage, Beaumont, Texas
6. October 2017, SOSRA Eastern Gulf of Mexico Update; Geological Society of America Annual Meeting, Seattle, Washington
7. October 2017, In-situ stress in the DeSoto Canyon Salt Basin, Eastern Gulf of Mexico; Geological Society of America Annual Meeting, Seattle, Washington
8. October 2017, Geological characterization and CO_2 Storage Potential of Cretaceous sandstone on the eastern Gulf of Mexico continental shelf; Geological Society of America Annual Meeting, Seattle, Washington
9. May 2018, Geomechanical characteristics of the DeSoto Canyon Salt Basin, eastern Gulf of Mexico; American Association of Petroleum Geologists Annual Conference and Exposition, Salt Lake City, Utah

Subtask 8.2 - Knowledge Sharing and Technology Transfer

Links to all publications & abstracts can be found in the Appendix

Publications:

1. Jingyao Meng, Chandra, Avinash, Pashin, J. C., Spears, Justin, Xue, Liang, and Sholanke, Seyi, in review, Structural framework and fault analysis in the east-central Gulf of Mexico: Implications for offshore storage of carbon dioxide: Journal of Structural Geology.
2. Jingyao Meng, Pashin, J. C., and Nygaard, Runar, in press, Geomechanical characteristics of the potential sinks and seals in the DeSoto Canyon Salt Basin, eastern Gulf of Mexico: Environmental Geosciences
3. Jingyao Meng, Pashin, J. C., Nygaard, Runar, and Chandra, Avinash, 2018, Analysis of the stress field in the DeSoto Canyon Salt Basin for ensuring safe offshore carbon storage: International Journal of Greenhouse Gas Control, v. 79, p. 279-288.
4. Pashin, J. C., Chandra, Avinash, Charbonneau, Paul, Meng Jingyao, Hills, D. J., and Redden, M. R., 2017, Offshore CO_2 storage potential of the eastern Gulf of Mexico: Houston, American Institute of Chemical Engineers: Carbon Management Technology Conference Proceedings, contribution P489770, 20 p.
5. Pashin, J. C., Guohai Jin, and Hills, D. J., 2016, Mesozoic petroleum systems and structure in the Mobile, Pensacola, Destin Dome, and Viosca Knoll Areas of the MAFLA Shelf, in Lowery, C., Snedden, J. W., and Blum, M. D., eds., Mesozoic of the Gulf Rim and Beyond: New Progress in Science and Exploration of the Gulf of Mexico Basin: GCSSEPM Perkins-Rosen Special Publication, p. 416-449.

Abstracts:

1. Pashin, J. C., Guohai Jin, Hills, D. J., and Meng Jingyao, 2016, Evolution of giant salt pillows in the Destin Dome Area, eastern Gulf of Mexico: Implications for petroleum exploration and geologic CO_2 storage: Geological Society of America Abstracts with Programs, v. 48, no. 7, doi: 10.1130/abs/2016AM-283732.
2. Hills, D. J., Pashin, J. C., and Redden, M. R., 2016, Southeast Offshore Storage Resource Assessment: Opportunities in the eastern Gulf of Mexico for CO_2 storage:

American Association of Petroleum Geologists Annual Convention and Exhibition Program, unpaginated CD-ROM.

3. Hills, D. J., Pashin, J. C., and Redden, M. R., 2016, Investigating the eastern Gulf of Mexico for potential geologic storage of CO_2: Geological Society of America Abstracts with Programs, v. 48, no. 7, doi: 10.1130/abs/2016AM-280642.
4. Pashin, J. C., Hills, D. J., Chandra, Avinash, Charboneau, Paul, Guohai Jin, McIntyre-Redden, M. R., and Meng Jingyao, 2017, CO_2 storage potential of the MAFLA shelf, eastern Gulf of Mexico: Beaumont, Texas, Texas Bureau of Economic Geology, 2nd International Workshop on Offshore CO_2 Storage Proceedings, unpaginated.
5. Pashin, J. C., Hills, D. J., Chandra, Avinash, Charboneau, Paul, Guohai Jin, McIntyre-Redden, M. R., and Meng Jingyao, 2017, Offshore CO_2 storage potential of the MAFLA continental shelf, eastern Gulf of Mexico: Houston, Texas, American Institute of Chemical Engineers, Carbon Management Technology Conference Program, p. 40-41.
6. Pashin, J. C., Guohai Jin, Hills, D. J., and Meng Jinyao, 2017, Jurassic Gravitational Shelf Spreading in the western DeSoto Canyon Salt Basin, Mobile, Viosca Knoll and Destin Dome Areas, East-Central Gulf of Mexico: American Association of Petroleum Geologists Annual Convention and Exhibition Program, unpaginated CD-ROM.
7. Meng Jingyao, Pashin, J. C., and Chandra, A., 2017, In-situ stress in the DeSoto Canyon Salt Basin, Eastern Gulf of Mexico: Geological Society of America Abstracts with Programs, v. 49, no. 6, doi: 10.1130/abs/2017AM-297935.
8. Chandra, A., Pashin, J. C., and Meng Jingyao, 2017, Geological characterization of Cretaceous sandstone on the eastern Gulf of Mexico continental shelf: CO_2 sequestration potential of Cretaceous Formations: Geological Society of America Abstracts with Programs, v. 49, no. 6, doi: 10.1130/abs/2017AM-298296.
9. Pashin, J. C., Achang, M., Chandra, A., Folaranmi, A., T., Martin, S., Meng Jingyao, Wethington, C., Urban, S., Riestenberg, D., Koperna, G., Redden-McIntyre, M. R., Hills, D. H., and Esposito, R. A., 2018, The Paluxy Formation in the east-central Gulf of Mexico Basin: Geology of an ultra-giant anthropogenic CO_2 sink: American Association of Petroleum Geologists Annual Convention and Exposition Program, unpaginated CD-ROM.
10. Meng Jingyao, Pashin, J. C., and Chandra, Avinash, 2018, Geomechanical characteristics of the DeSoto Canyon Salt Basin, eastern Gulf of Mexico: American Association of Petroleum Geologists Annual Convention and Exposition Program, unpaginated CD-ROM.
11. Meng Jingyao, Pashin, J. C., Nygaard, Runar, and Chandra, Avinash, 2018, Geological and geomechanical characteristics of the potential CO_2 storage reservoirs, eastern Gulf of Mexico: Geological Society of America Abstracts with Programs, v. 50, no. 6, doi: 10.1130/abs/2018AM-320167.
12. Hills, D. J., Koster, J., and Pashin, J. C., 2018, Seismic reflection data interpretation to support project ECO2S, Kemper County, MS: American Association of Petroleum Geologists Annual Convention and Exposition Program, unpaginated CD-ROM.
13. Jingyao Meng, Pashin, J. C., Nygaard, Runar, and Chandra, Avinash, 2019, Fault and seal analysis in the DeSoto Canyon Salt Basin: Implications for offshore CO_2 storage: American Association of Petroleum Geologists Annual Convention and Exposition Program, unpaginated CD-ROM

Task 9.0: Closeout and Reporting

Subtask 9.1 – Modeling-based MVA Recommendations

Offshore CO_2-EOR amenable depleted oilfields and saline reservoirs contain large quantities of pore space available for CO_2 storage. Both CO_2-EOR amenable fields and saline reservoirs present different monitoring challenges because they occupy different levels of field development and geological conditions within the reservoir. Here, the feasibility of each monitoring technology category is assessed, and a suite of technologies is recommended in both cases. For CO_2-EOR storage fields, primarily well based monitoring technologies should be employed because of a large number of preexisting wells and the effect of residual hydrocarbon saturation negating the use of seismic imaging. In contrast, surveillance technologies from all monitoring categories should be utilized in saline storage reservoirs that include 3D/4D seismic, gravimetry, shallow based sonar imaging, and well based monitoring technologies. Ultimately, these recommendations suggest potential technologies for demonstrating containment, conformance, and environmental monitoring at an offshore CCS site. A deliverable detailing the work that informed these conclusions is provided in Deliverable 9.1.a and the link can be found in the Appendix.

Subtask 9.2 – Infrastructure Development Recommendations

With conventional oil production winding down from many of the existing platforms in the Gulf of Mexico, there is a window of opportunity to take advantage of the infrastructure already in place and re-work it for CO_2-EOR and CO_2 storage. Support by from the Federal Government, with industry commitment, could allow pipelines and CO_2 recycling centers to be constructed in optimal locations in the Gulf of Mexico. This could give existing platforms, close to abandonment, renewed purpose with CO_2-EOR injections. Research and modeling have shown that there are still plays to be made in these fields. Upwards of 1.89 billion barrels of oil are potentially accessible by the conceptual CO_2 pipelines described in this report (link in the Appendix). The next step is taking advantage of the existing infrastructure, making offshore CO_2-EOR cost efficient and effective.

Subtask 9.3 – Target Development Recommendations

The storage resource numbers from the eastern Gulf of Mexico are encouraging. According to the U.S. GHG inventory (https://ghgdata.epa.gov/ghgp/main.do), the 2016 greenhouse gas emissions from few key power plants close to shore, such as Plant Barry in Alabama, Plant Daniel in Mississippi, and Plant Crist in Florida were 7.5 Mt, 5.2 Mt and 3.1 Mt, respectively. Plants Barry and Daniel have been used in pilot CO_2 storage programs led by the Southeastern Regional Carbon Sequestration Partnership (SECARB) and have successfully demonstrated CO_2 sequestration in the onshore Cretaceous reservoirs (Koperna et al., 2009, 2012). The combined emissions from Plants Barry, Daniel, and Crist are about 15.8 Mt with an average for the three plants of 5.3 Mt/year. Considering this as average annual emissions from a major coal-fired power plant, an average offshore block (9.0 mi^2; 23.3 km^2) in the Mobile and Viosca Knoll Areas is capable of sequestering annual emissions from 13 such power plants. The link to the full report can be found in the Appendix.

References Cited

Adams, J. E., and Rhodes, M .L. 1960, Dolomitization by Seepage Refluxion: AAPG Bulletin, v. 44, p. 1912-1920.

Applin, P. L., and Applin, E. R., 1967, The Gulf Series in the subsurface in northern Florida and southern Georgia: U.S. Geological Survey Professional Paper 524-G, 34 p.

Bachu, S., 2003, Screening and ranking of sedimentary basins for sequestration of CO2 in geological media in response to climate change: Environmental Geology, v. 44, p. 277-289.

Bascle, B.J., Nixon, L.D., and Ross, K.M., 2001, Atlas of Gulf of Mexico gas and oil sands as of January 1, 1999: U.S. Department of the Interior, Minerals Management Service, Gulf of Mexico OCS Regional Office, Office of Resource Evaluation, OCS Report, MMS 2001–086, 342 p.

Buffler, R. T., 1980, Structure and early geologic history of the deep central Gulf of Mexico basin, in Pilger, R. H., ed., The origin of the Gulf of Mexico and the early opening of the central North Atlantic Ocean: Louisiana State University School of Geoscience Symposium Proceedings, Baton Rouge, p. 3-16.

Buffler, R. T., and Sawyer, D. S., 1985, Distribution of crust and early history, Gulf of Mexico basin: Gulf Coast Association of Geological Societies Transactions, v. 35, p. 333-344.

Chandra, Avinash, 2018, Geological characterization and CO_2 storage potential of Cretaceous sandstone in the DeSoto Canyon Salt Basin of the MAFLA Shelf: Stillwater, Oklahoma State University, unpublished Master's thesis, 66 p.

Charbonneau, Paul, 2018, Geologic framework for the assessment of offshore CO2 storage resources: West Florida Platform: Stillwater, Oklahoma State University, unpublished Master's thesis, 69 p.

Chasteen, H. R., 1983, Reevaluation of the Lower Tuscaloosa and Dantzler Formations (Mid Cretaceous) with Emphasis on Depositional Environments and Time-stratigraphic relationships: Gulf Coast Association of Geological Societies Transactions, v. 33, p. 31- 40.

Damen, K., van Troost, M., Faaij, A., and Turkenburg, W., 2006, A comparison of electricity and hydrogen production systems with CO2 capture and storage. Part A: Review and selection of promising conversion and capture technologies: Progress in Energy and Combustion Science, v. 32, p. 215-246.

Dobson, L. M., and Buffler, R. T., 1997, Seismic stratigraphy and geologic history of Jurassic rocks, northeastern Gulf of Mexico: American Association of Petroleum Geologists Bulletin, v. 81, p. 100-120.

Eaves, E., 1976, Citronelle Oil Field, Mobile County, Alabama: AAPG Memoir 24, p. 259-275.

Esposito, R. A., Pashin, J. C., and Walsh, P. M., 2008, Citronelle Dome: A giant opportunity for multi-zone carbon storage and enhanced oil recovery in the Mississippi Interior salt basin of Alabama: Environmental Geosciences, v. 15, p. 53-62.

Folaranmi, A. T., 2015, Geologic characterization of a saline reservoir for carbon sequestration: The Paluxy Formation, Citronelle Dome, Gulf of Mexico Basin, Alabama: Stillwater, Oklahoma State University, unpublished Master's thesis, 96 p.

Foote, R. Q., 1985, Summary report on the regional geology, petroleum geology, environmental geology, and estimates of undiscovered recoverable oil and gas resources in the planning area of proposed Outer Continental Shelf oil and gas lease No. 94, eastern Gulf of Mexico: U.S. Geological Survey Open-File Report 85-669, 113 p.

Goodman, A., Hakala, A., Bromhal, G., Deel, D., Rodosta, T., Frailey, S., Small, M., Allen, D., Romanov, V., and Fazio, J., 2011, US DOE methodology for the development of geologic storage potential for carbon dioxide at the national and regional scale: International Journal of Greenhouse Gas Control, v. 5, p. 952-965.

Handford, C. R., and Baria, L. J., 2003, Exploration potential and high-resolution sequence stratigraphy of shelf-sand reservoirs, Miocene, south Mississippi: Gulf Coast Association of Geological Societies Transactions, v. 53, p. 309-314.

Handford, C. R., and Loucks R. G., 1993, Carbonate depositional sequences and systems tracts - responses of carbonate platforms to relative sea-level changes, in R. G. Loucks and G. F. Sarg (eds.), Carbonate Sequence Stratigraphy: AAPG Memoir 57, p. 3-41.

Hardie, L. A., 1987, Dolomitization; a critical view of some current views: Journal of Sedimentary Research, v. 57, p. 166-183.

Hills, D. J., and Pashin, J. C., 2010, Preliminary assessment of offshore transport and storage of CO2: Southeastern Regional Carbon Sequestration Partnership Final Report, prepared for Southern States Energy Board, 11 p.

Hovorka, S. D., Meckel, T. A., and Treviño, R. H., 2013, Monitoring a large-volume injection at Cranfield, Mississippi—Project design and recommendations: International Journal of Greenhouse Gas Control, v. 18, p. 345-360.

Koperna, G., Riestenberg, D., Petrusak, R., and Esposito, R., 2009, Lessons learned while conducting drilling and CO2 injection operations at the Victor J. Daniel Power Plant in Mississippi: Society of Petroleum Engineers paper SPE 124003, 26 p.

Koperna, G., Riestenberg, D., Kuuskraa, V., Rhudy, R., Trautz, R., Hill, G.R., and Esposito, R., 2012, The SECARB anthropogenic test: a US integrated CO2 capture, transportation and storage test: International Journal of Clean Coal and Energy, v. 1, p. 13-26.

MacRae, G., and Watkins, J. S., 1996, DeSoto Canyon salt basin: Tectonic evolution and salts [sic] structural styles, in Jones, J. O., and Freed, R. L., eds., Structural framework of the northern Gulf of Mexico: Gulf Coast Association of Geological Societies Special Publication, p. 53-61.

Mancini, E. A., Mink, R. M., Bearden, B. L., and Wilkerson, R. P., 1985, Norphlet Formation (Upper Jurassic) of southwestern and offshore Alabama: Environments of deposition and petroleum geology: American Association of Petroleum Geologists Bulletin, v. 69, p. 881-898.

Mancini, E.A., Mink, R.M., Payton, J.W., and Bearden, B.L., 1987, Environments of deposition and petroleum geology of Tuscaloosa Group (Upper Cretaceous), South Carlton and Pollard fields, southwestern Alabama: American Association of Petroleum Geologists Bulletin, v. 71, p. 1128-1142

Mancini, E.A., and Puckett, T.M., 2002, Transgressive-regressive cycles in Lower Cretaceous strata, Mississippi Interior Salt Basin area of the northeastern Gulf of Mexico, USA: Cretaceous Research, v. 23, p. 409-438.

Mancini, E.A., and Puckett, T.M., 2005, Jurassic and Cretaceous transgressive-regressive (TR) cycles, northern Gulf of Mexico, USA: Stratigraphy, v. 2, p. 31-48.

Mancini, E. A., and Tew, B. H., 1991, Relationships of Paleogene stage and planktonic foraminiferal zone boundaries to lithostratigraphic and allostratigraphic contacts in the eastern Gulf Coastal Plain: Journal of Foraminiferal Research, v. 21, p. 48-66.

Martin, R. G., Case, J. E., 1975, Geophysical studies in the Gulf of Mexico, in Nairn, A. E. M., and Stehli, F. G., eds., The ocean basins and margins v. 3, The Gulf of Mexico and the Caribbean: New York, Plenum Press, p. 65-106.

Meng Jingyao, Pashin, J. C., Nygaard, Runar, and Chandra, Avinash, 2018, Analysis of the stress field in the DeSoto Canyon Salt Basin for ensuring safe offshore carbon storage: International Journal of Greenhouse Gas Control, v. 79, p. 279-288.

Mitchell-Tapping, H.J., 1990, New oil exploration play in Florida—The upper Fredericksburg Dollar Bay Formation: Gulf Coast Association of Geological Societies, Transactions, v. 40, p. 607–621.

Morse, J. W., Arvidson, R. S., and Luettge, A., 2007, Calcium carbonate formation and dissolution: Chemical Reviews, v. 107, p. 342-381.

NETL, 2012, The United States 2012 Carbon Utilization and Storage Atlas (4th Edition): Pittsburgh, National Energy Technology Laboratory, 130 p.

Petrusak, R., Riestenberg, D., Goad, P., Schepers, K., Pashin, J. C., Esposito, R. A., and Trautz, R., 2009, World class CO2 sequestration potential in saline formations, oil and gas fields, coal and shale: The U.S. Southeast Regional Carbon Sequestration Partnership has it all: San Diego, SPE International Conference on CO2 Capture, Storage and Utilization, paper SPE 126619, 18 p.

Pashin, J. C., Guohai Jin, and Hills, D. J., 2016, Mesozoic petroleum systems and structure in the Mobile, Pensacola, Destin Dome, and Viosca Knoll Areas of the MAFLA Shelf, in Lowery, C., Snedden, J. W., and Blum, M. D., eds., Mesozoic of the Gulf Rim and Beyond: New Progress in Science and Exploration of the Gulf of Mexico Basin: GCSSEPM Perkins-Rosen Special Publication, p. 416-449.

Pashin, J. C., Meng Jingyao, Hills, D. G., Guohai Jin, and Mcintyre-Redden, M. R., 2017, SOSRA Data Quality and Coverage Evaluation, Eastern Gulf of Mexico Team: Topical Report, submitted to U.S. Department of Energy through Southern States Energy Board, Subgrant SSEB-SOSRA-981-OSU-2015-001rev, U.S. Department of Energy Cooperative Agreement DE-FE0026086, 9 p.

Pashin, J. C., McIntyre, M. R., Grace, R. L. B., and Hills, D. J, 2008, Southeastern Regional Carbon Sequestration Partnership (SECARB) Phase III: Final Report prepared for Advanced Resources International, 57 p.

Petty, A. J., 1997, Lower Tuscaloosa clastic facies distribution (Upper Cretaceous), Federal and State waters, eastern Gulf of Mexico: Gulf Coast Association of Geological Societies Transactions, v. 47, p. 454-462.

Petty, A. J., 1999, Petroleum exploration and stratigraphy of the Lower Cretaceous James Limestone (Aptian) and Andrew Formation (Albian): Main Pass, Viosca Knoll, and Mobile Areas, northeastern Gulf of Mexico: Gulf Coast Association of Geological Societies Transactions, v. 49, p. 441-450.

Pollastro, R. M., Schenk, C. J., and Charpentier, R. R.,. 2001, Assessment of undiscovered oil and gas in the onshore and state waters portion of the South Florida Basin, Florida—USGS Province 50: U.S. Geological Survey Digital Data Series 69-A, 70 p.

Roberts, Glyn, and Erickson, Joe, 2009, The Norphlet Sandstone and other petroleum plays along and outboard of the Florida Escarpment, eastern Gulf of Mexico: Spectrum Geophysical Technical Paper Reference 20563, 6 p.

Roberts-Ashby, T. L., Brennan, S. T., Merrill, M. D., Blondes, M. S., Freeman, P. A., Cahan, S. M., DeVera, C. A., and Lohr, C. D., 2015, Geologic framework for the national assessment of carbon dioxide storage resources—South Florida Basin: U.S. Geological Survey, Open-File Report 2012-1024-L, 22 p.

Smith, C.C., 1991, Foraminiferal biostratigraphic framework, paleoenvironments, rates of sedimentation, and geologic history of the subsurface Miocene of southern Alabama and adjacent state and federal waters: Alabama Geological Survey Bulletin 138, 223 p.

Southeastern Geological Society, 1986, Hydrogeological units of Florida: Florida Geological Survey Special Publication 28, 8 p.

Story, Chip, 1998, Norphlet geology and 3-D geophysics of Fairway field, Mobile Bay, Alabama, in Allen, J. L., and others, eds., 3-D seismic case histories from the Gulf Coast basin: Austin, Texas, Gulf Coast Association of Geological Societies, p. 123-129.

Winston, G.O., 1976, Six proposed formations in the undefined portion of the Lower Cretaceous section in south Florida: Gulf Coast Association of Geological Societies Transactions, v. 26, p. 69-72.

Mid-Atlantic

Task 2.0: Geologic Overview

Subtask 2.1 - Main Geologic Provinces

The Bureau of Ocean Energy Management (BOEM) has divided the Atlantic Outer Continental Shelf (OCS) area into four planning areas along the Atlantic seaboard as part of their Oil and Gas leasing Program. The Mid-Atlantic region extends from Delaware to North Carolina. The region covers approximately 11,283 acres. Within this area, three main geological provinces can be observed:

- The Baltimore Canyon Trough

The Baltimore Canyon Trough (BCT) is situated off the coast of New-Jersey and extends through the Mid-Atlantic region. Within the Baltimore Canyon Trough, thick Mesozoic and Cenozoic sediment strata up to 18 km thick are present. In Virginia, the thickness of this sediment can reach 12km. The Trough is believed to contain marine sediments, as well as, continental sediment transported from the Appalachian Mountains. During the time of deposition, the region was tectonically active, and each stratum can be attributed to a synrift or postrift phase (Poag, 1979).

Figure 1 presents the geography of the Baltimore Canyon Trough. As mentioned above, the trough's sediments are thick but also their deposition is very wide, up to 200 km. On the outer part of the coastal plains of Virginia, Maryland and Delaware, the Salisbury Embayment can be observed. On the coastal plains of North Carolina, the Albemarle Embayment appears.

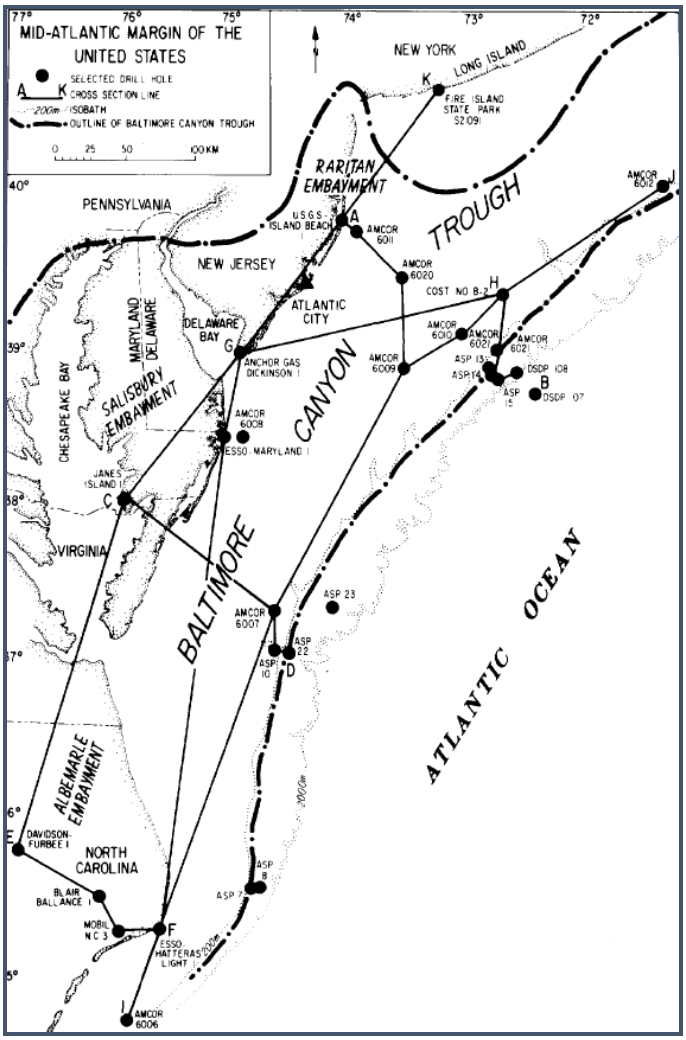

Figure 1. Map of the Baltimore Canyon Trough and Location of Cross-Sections Presented Below (Bayer and Milici, 1987)

Figure 2 displays a cross section between point C and D displayed on Figure 1. The interpretation of well logs identified several layers within the Trough: Upper Cretaceous, lower Cretaceous, Paleocene, Eocene, Miocene, Pliocene and Pleistocene (Poag, 1979).

Lower Cretaceous is usually sandstone and shale with interbedded lignite and coal beds. Although seaward, it might change as there is an indication of the presence of limestone and dolomite which could be a part of a reef complex.

The Upper Cretaceous is primarily marine: marine sandstone, limestone and shale. It remains approximately the same in the entire trough.

The Paleocene sediments formed for primarily limestone rocks which contain multiple marine microfossil. However, the southern part of the Paleocene is different as it gradually becomes a calcareous shallow-marine sandy clay.

Seaward the Eocene is composed on top by impermeable calcareous shale, at the middle by chalky limestone, and at the bottom, shale interbedded with limestone.

Sands predominate in the Miocene layer. In Virginia, some clays can also be encountered.

The Pliocene sediments are mostly shelly sand and silty clay.

The Pleistocene layer is well known as it has been recovered in every core made in the Mid-Atlantic. It can be described as a white to gray and fine to coarse sand in which some silty clay parts can appear.

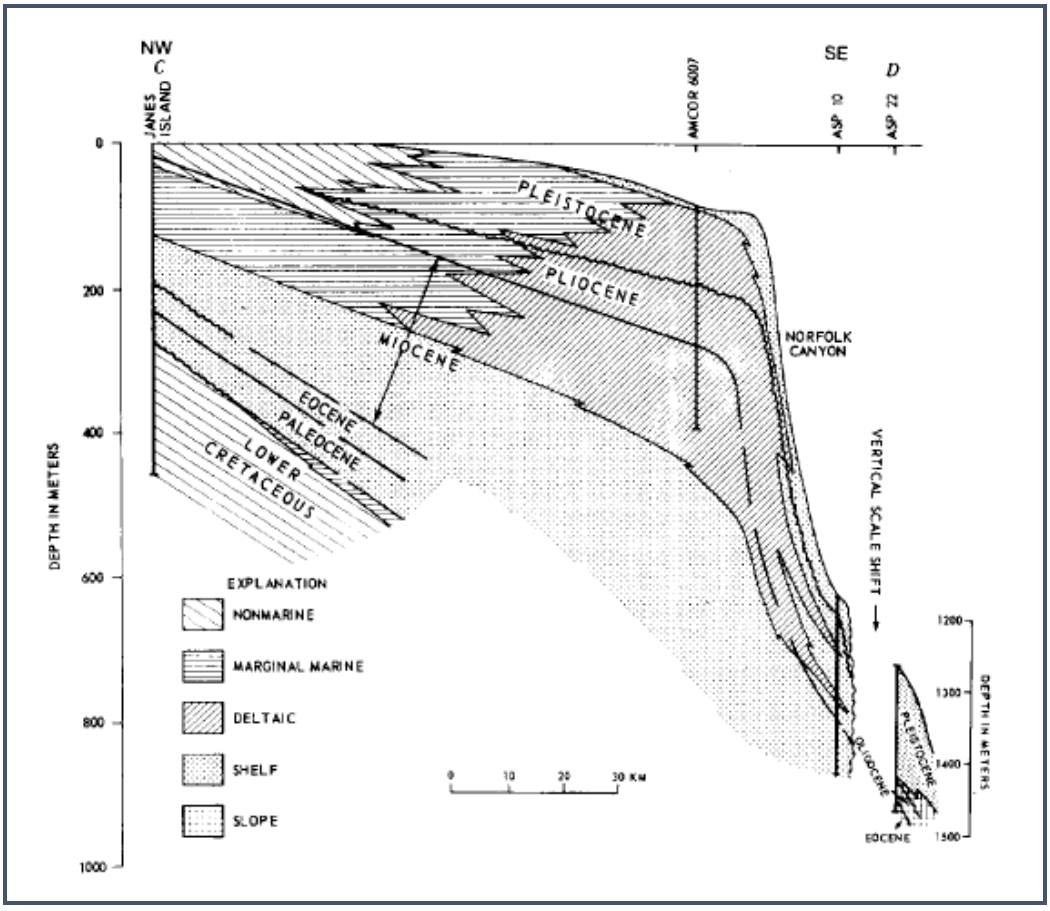

Figure 2. Cross-Section C-D Within Baltimore Canyon Trough (Bayer and Milici, 1987)

Figures 3 and 4 show isopachs of stratigraphic intervals that can be found in the Trough. Figure 3 represents the total thickness of the entire sediment deposition, from sea floor to Lower Cretaceous present in the Trough. While Figure 4, displays only the Upper-Cretaceous thickness contours. The thickness is not homogeneous throughout the trough and becomes thicker at the northern part of the trough (Mattick, 1980).

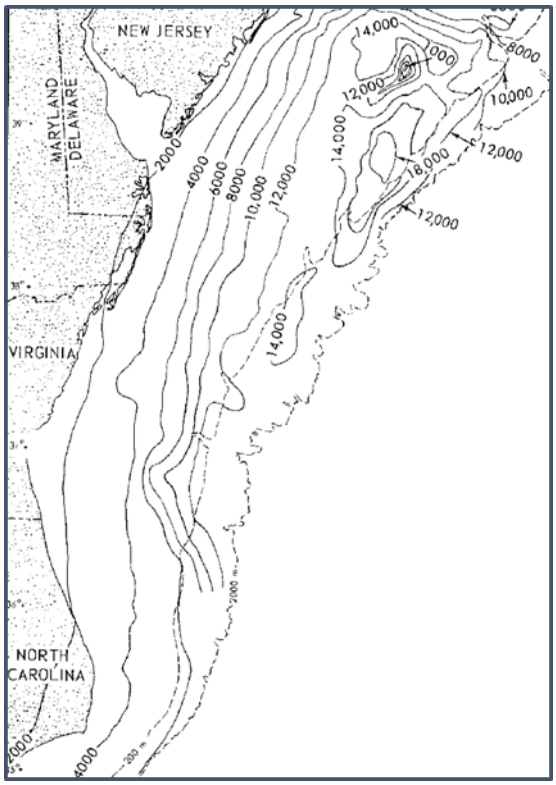

Figure 3. Isopach Total Thickness from Sea Floor to Lower Cretaceous (Mattick, 1980)

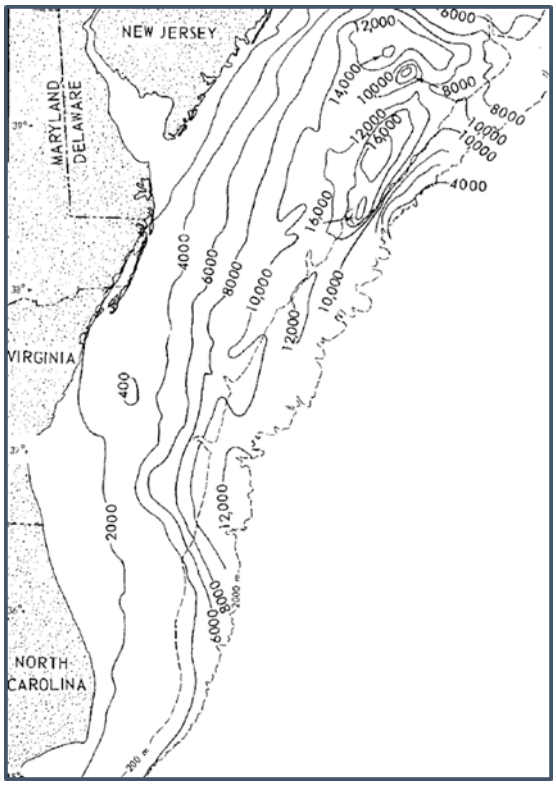

Figure 4. Isopach of the Upper Cretaceous Interval (Mattick, 1980)

- The Carolina Trough

South of the Baltimore Canyon Trough, extending from North Carolina to South Carolina, the Carolina trough (CT) is about 500 km long and 100 km wide. The water depth varies from 180 to 2,100 meters. Studies estimate the sediment thickness to reach up to 12 km thick. Half of the sediment present in the Trough was deposited during the Jurassic.

Unlike the Baltimore Canyon Trough, no wells were drilled in the Carolina Trough and its oil and gas resource potential are not fully assessed. Only its periphery is known from core holes drilled several years ago. This area represents the largest undrilled salt basin of the world. Even if most of the basin is dominated by salt deposits, the Upper and Lower cretaceous appear to be mostly dominated by sandstone, shales chalks and limestone intervals (Carpenter, 1992).

Figure 5 shows the complexity of the Carolina Trough structure. The presence of at least 26 salt diapirs makes the structure complex and prone to oil and gas accumulations. The formation of these diapirs created faults easily identified on seismic data and represented bellow on Figure 5 (Carpenter, 1992).

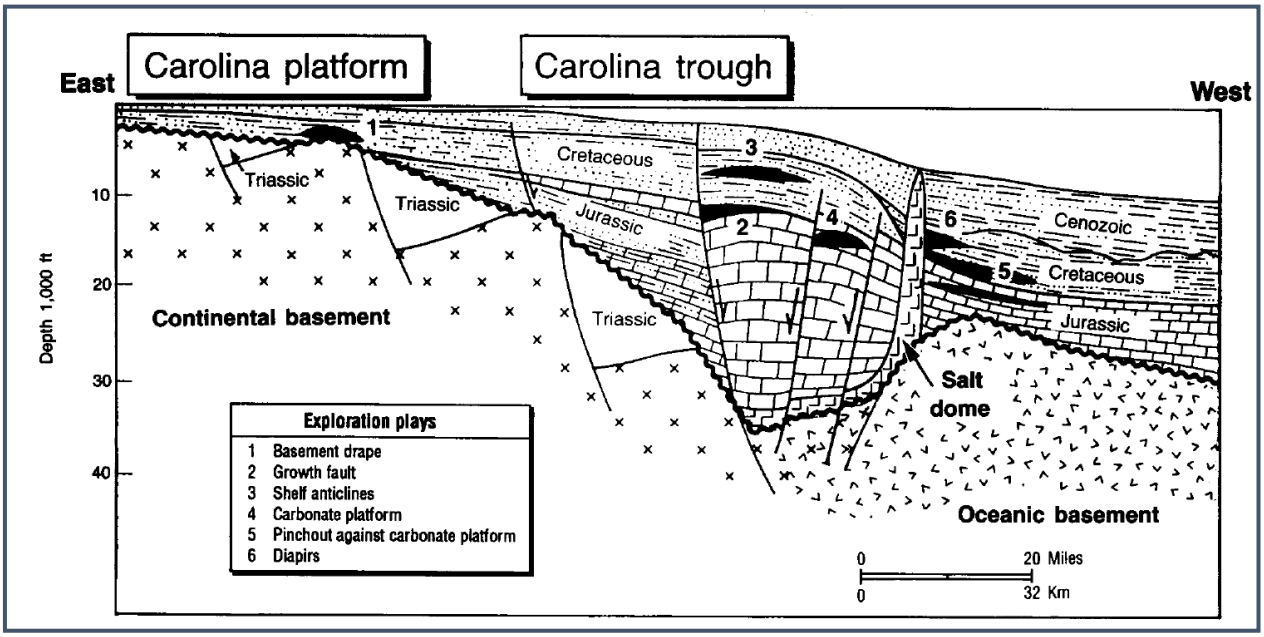

Figure 5. Cross-Section of the Carolina Trough (Carpenter, 1992)

- The Potomac aquifer

Aquifers should be investigated due to their proximity to the coast but also because of the presence of reservoir rock with adequate porosity and impermeable seals confining the aquifer. The storage of brine is only possible if impermeable rock provides a good seal to prevent fresh water from migrating out of the aquifer.

In some places of the Potomac aquifer, potential storage zones can be identified. The mid-Cretaceous sandstone layers could be suitable for CO_2 storage as wells located on the coastal plain of VA and NC highlighted intervals with high porosity and permeability values. Within the Late-Cretaceous interval, fine-grained confining beds could provide an adequate seal for carbon

sequestration. The Potomac aquifer basement bedrock could also be considered a good impermeable underlying boundary. As the Potomac Aquifer is largely faulted, as shown on Figure 6, this issue could represent potential pathways for leakage of fluid (saltwater intrusions or CO_2 migration). All these characteristics should be further investigated to determine if the deeper part of the Potomac aquifer could be a suitable environment for carbon dioxide sequestration (USGS, 2013).

Figure 6 represents the physiology of the Potomac Aquifer and the identified confining zones that could provide insights on identifying zones of interest for carbon dioxide sequestration (USGS, 2013) and prevent any contamination of freshwater aquifers.

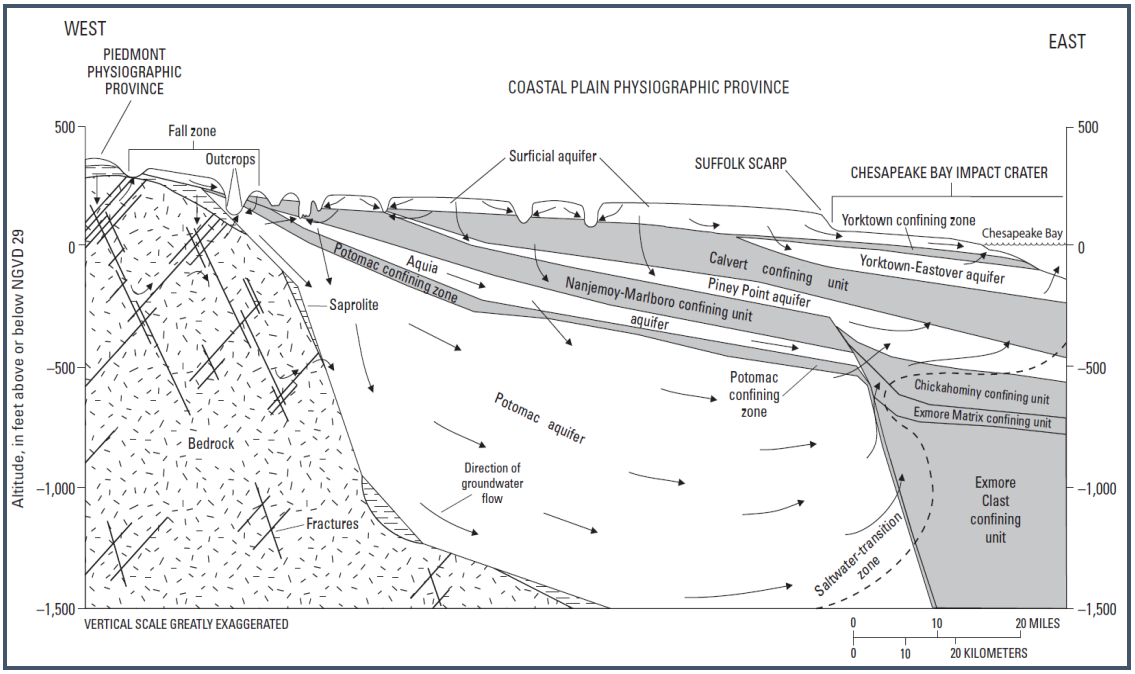

Figure 6. Groundwater Flow of Aquifers located on the Coastal Plain of VA (USGS, 2013)

Subtask 2.2 - Potential Storage Units

Past studies have focused on assessing the oil and gas resource potential of the Atlantic's subsurface. Figure 7 illustrates the potential oil and gas reservoirs that could also be investigated for CO_2 storage. This figure displays two synrift basins, the stratigraphic pinchout of the lower Mesozoic strata, the paleoshelf edge, the Jurassic and Cretaceous carbonate layer and the Cretaceous interval from deltaic origin.

A study from Bayer and Milici (1987) suggests the presence of structural traps in the form of horst and grabens in deeper sections of the Baltimore Canyon Trough (Paleozoic interval). This research also suggests the presence of stratigraphic traps in the form of caprocks, interpreted as carbonate deposits, within the Upper and Lower Cretaceous interval.

Figure 8 shows the possible exploration leads and the possible migration pathways described by Carpenter (1992) in the Carolina Trough. This Trough appears to have more complex geometries, such as the presence of salt deposits, faults and folds. These geometries could provide stratigraphic and structural traps necessary for safe and long-term storage of CO_2. Sandstone intervals present in anticlines show an average porosity of 20% at depth above

2,400 meters which could make these intervals adequate reservoir rocks. The possible seals that are considered in the Carolina Trough are the Cretaceous and the Jurassic (Shale) but also salt, mud-stone and unfractured carbonate rocks (Carpenter, 1992).

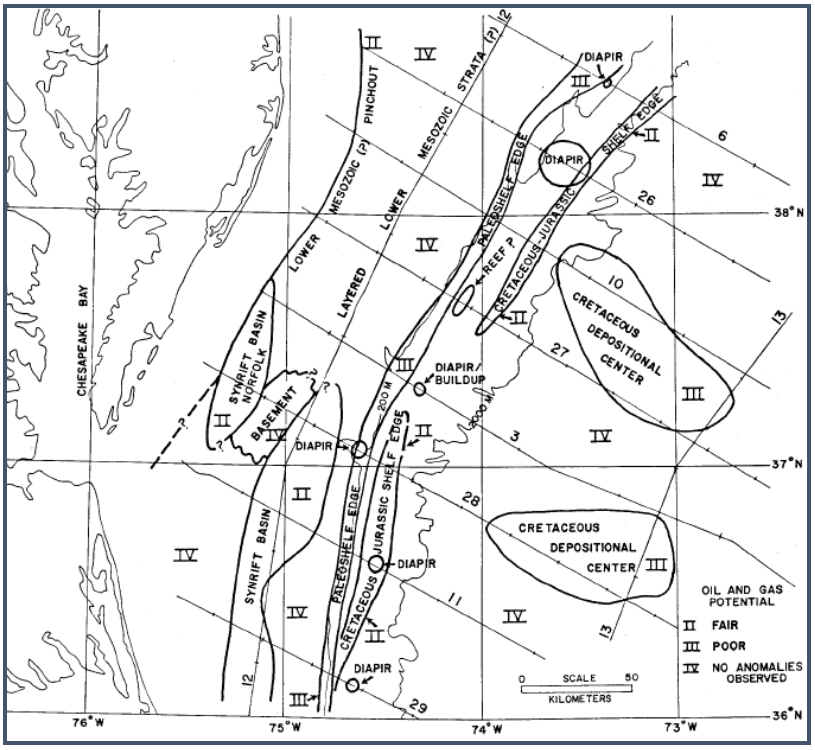

Figure 7. Map of the Oil and Gas Potential of the Mid-Atlantic Area (Bayer and Milici, 1987)

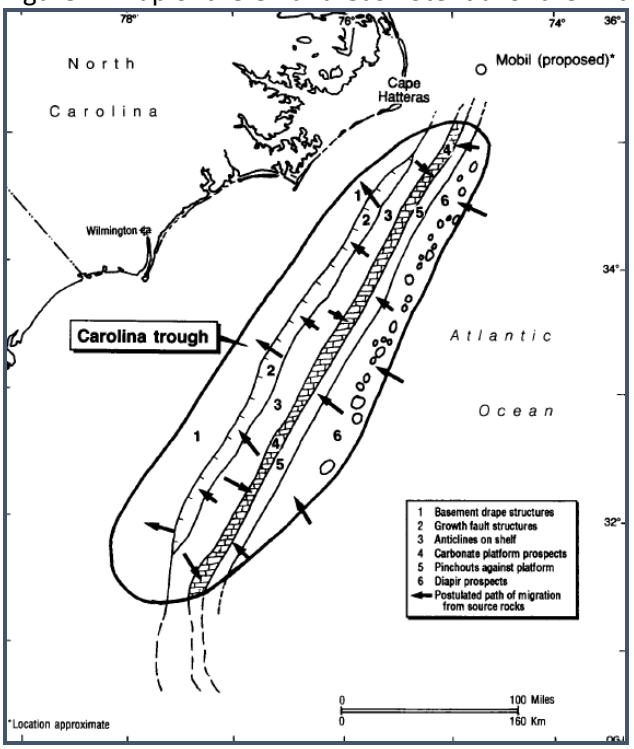

Figure 8. Possible Exploration Leads and Migration Pathways in the Carolina Trough (Carpenter, 1992)

Owing to the proximity of the Atlantic Coastal Plain saline aquifers to the Mid-Atlantic SOSRA study area, a preliminary CO_2 storage assessment by several researchers (Smyth et al., 2008; Szulczewski, 2009; and Reid et al., 2012) was undertaken. Similarly, other offshore reservoirs located to the south on the Carolina Platform and Carolina Trough were assessed (Figure 2A; Smyth et al., 2008).

The two potential CO_2 sinks (Units 1 and 2 shown in Figure 9) identified by Smyth et al. (2008) are located offshore North Carolina in water depths ranging from 50 to 1,000 meters at depths between 500 and 3,000 meters below the seafloor. Unit 90 is an Upper Cretaceous reservoir with an estimated CO_2 storage capacity of approximately 16 Gt and Unit 120 is a Lower Cretaceous reservoir with an estimated CO_2 storage capacity of approximately 178 Gt. Smyth et al. (2008) believed that the lack of extensive drilling along the Atlantic margin can be viewed as either a benefit or a hindrance for CO_2 storage. On one hand, seal integrity should be excellent while the lack of data from drilling limits the amount of analysis that can be performed. The aim of the present study is to make use of all available geologic and geophysical data in order to provide a thorough assessment of potential carbon storage in offshore reservoirs along the U.S. Mid-Atlantic region.

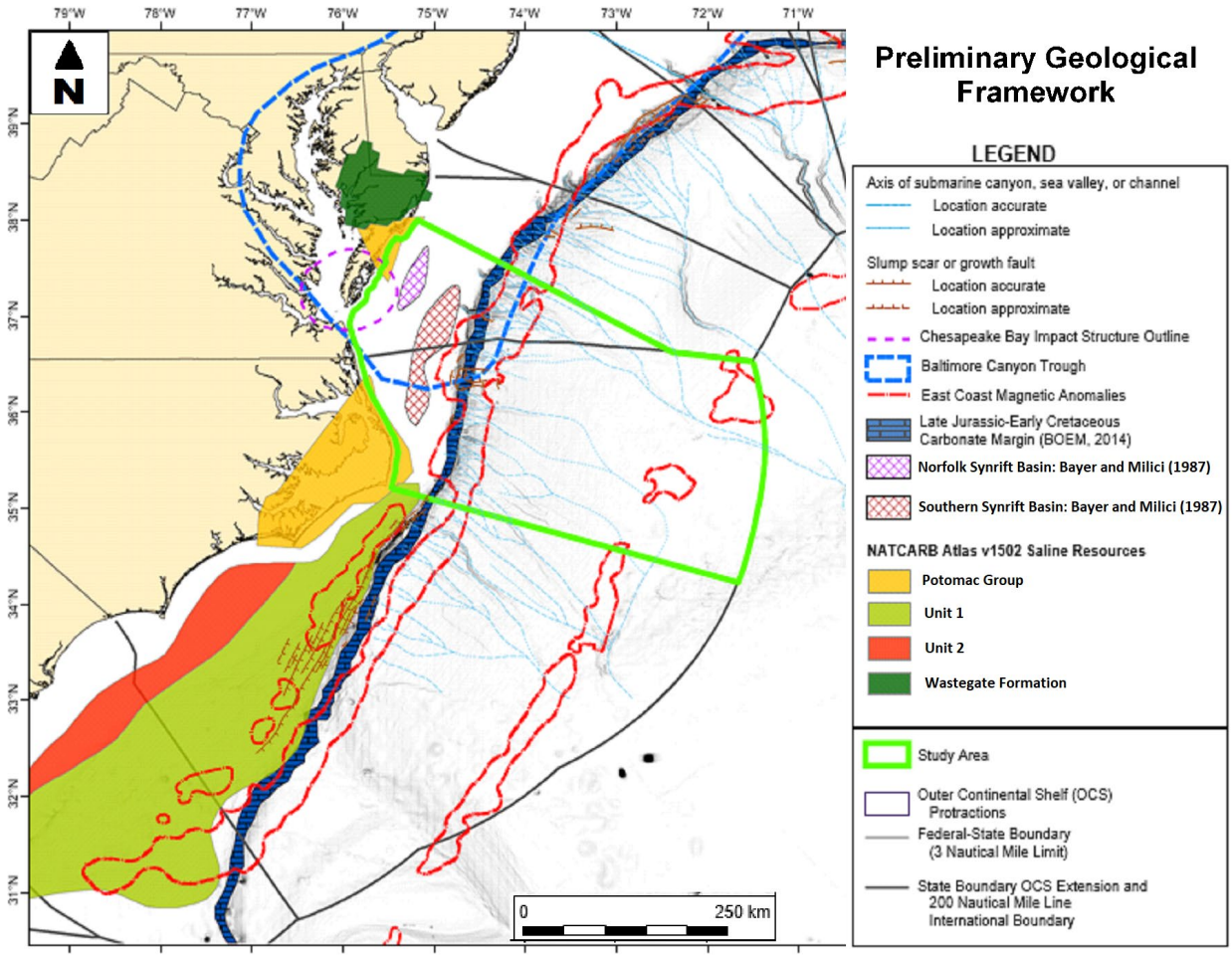

Figure 9. Two potential CO_2 sinks

Subtask 2.3 - Planning Areas

The Mid-Atlantic region encompasses the seafloor off of Delaware, Virginia and North-Carolina. However, state law currently prohibits drilling activities in the Chesapeake Bay and its tributaries. As such, the geological analysis of the Mid-Atlantic region will focus on the seafloor beyond the three-mile state limit.

Task 3.0: Data Collection

Subtask 3.1 - Seismic Databases

A total of 27 seismic surveys were analyzed for the present study. Table 1 lists all the surveys mentioned in this report and the total number of lines and line-metrics for each survey (Fugro, 2017)

Permit or Survey	Year	Client/Research Team	Acquisition Company	Number of Seismic Lines			Approximate Kilometers Acquired		
				Entire Survey	Study Area	VA OCS	Entire Survey	Study Area	VA OCS
S-1-73	1973	USGS	Digicon	3	1	1	949	343	258
S-1-75	1975	USGS	Digicon	7	3	3	3,873	780	235
E14-75	1975	Western Geophysical	Western Geophysical	33	5	0	4,340	227	0
E17-75	1975	Digicon	Digicon	13	1	0	1,125	35	0
E22-75	1975	Teledyne	Teledyne	48	1	1	2,203	60	60
E16-76	1976	Offshore Atlantic Group	Digicon	42	33	17	5,386	3,726	1,590
S-1-77	1977	USGS	Teledyne	10	1	0	4,451	183	0
E02-77	1977	Atlantic Offshore Group	Digicon	29	0	0	10,341	0	0
E11-77	1977	Mid-Atlantic Group	Digicon	64	0	0	3,277	0	0
RC2101	1977	LDEO/ONR	LDEO	11	0	0	1,519	0	0
C-1-78	1978	USGS	GSI	21	3	1	4,866	481	160
E13-78	1978	Chevron	Geosource	10	0	0	184	0	0
E06-79	1979	USGS Conservation Division	Whitehall Corp.	23	5	4	1,721	393	265
E15-79	1979	ARCO	Digicon	14	0	0	1,314	0	0
BGR79	1979	BGR	Prakla-Seismos	21	4	4	4,763	434	360
E01-80	1980	South Atlantic Group	Geosource	159	57	0	6,625	1,866	0
E02-80	1980	South Atlantic Group	Digicon	106	39	0	5,899	1,299	0
E01-81	1981	Exxon	Geosource	107	9	7	7,184	412	306
E07-81	1981	Chevron	Digicon	12	12	0	473	473	0
E02-82	1982	Mid-South Atlantic Group	Geosource	274	113	63	13,835	5,101	2,324
E04-82	1982	Shell	Shell (Assumed)	40	13	5	3,233	859	242
E11-82	1982	ARCO	ARCO	92	46	45	3,855	2,011	1,872
E05-83	1983	Amoco	Norpac	23	12	2	962	374	77
E05-86	1986	Spectrum Resources & Texaco	Teledyne	3	1	1	207	62	62
E03-88	1988	Texaco	GECO	29	17	17	1,176	751	701
VAEDGE	1990	USGS/Various Academic Institutions	GECO	4	4	3	554	554	311
MGL1408	2014	ENAM Community	LDEO	29	17	0	4,634	1,792	0

TOTAL:	**1,009**	**378**	**173**	**99,520**	**22,216**	**8,823**

Table 1. Seismic Data Surveys Collected and Analyzed (Fugro, 2017)

Digicon - Permit E17-75

In 1975, Digicon acquired 13 seismic lines aboard the Gary Chouset. This seismic source allowed the collection of high-resolution data with a one millisecond sampling rate and preservation of high frequencies (as indicated by the 248 Hertz high-cut filter) but limited subsurface penetration and therefore data were recorded for only 3 seconds.

Twelve of the thirteen lines were acquired along the New York/New Jersey OCS with three lines extending from the New Jersey and Long Island, NY shorelines into an area along the shelf break near Hudson Canyon.

No digital SEG-Y files exist for this survey even though navigation files are available from NAMSS. All stacked sections for this survey are available only as scanned images and are of variable quality.

Western Geophysical - Permit E14-75

In 1975, 33 seismic lines were acquired by Western Geophysical extending along the inner shelf from Long Bay, South Carolina northward to offshore Cape Hatteras, North Carolina. The majority of these lines lie landward of the 50-mile “no lease” coastal environmental buffer (BOEM,2014b).

The processing techniques applied, and the order in which they were applied, are not well documented and information comes from a single scanned data label of Line WE-1, which is located outside of the study area in Long Bay, SC. Stacked sections in SEG-Y format are available for all lines from BOEM and the USGS, where the survey is known as W-5-75.

Offshore Atlantic Group (OAG)/Digicon - Permit E16-76

The seismic data acquired for permit E16-76 by Digicon consist of a grid of 42 lines acquired along the continental shelf and slope extending north from offshore Cape Hatteras, North Carolina into southern New Jersey waters. The seismic grid is composed of 35 dip lines and seven strike lines.

Both stacked and migrated seismic time sections in SEG-Y format are available for all lines collected in Virginia waters.

USGS (MMS)/Whitehall - Permit E06-79

Multichannel CDP data collected for the USGS Conservation Division (later to become the MMS), as part of permit E06-79, images the nearshore subsurface in an area running from central Florida to southern New Jersey.

All lines in the study area exist only as scanned copies and only D-100 and D-102, outside of the study area exist as SEG-Y files.

Teledyne - Permit E22-75

The data collected for this permit consists of a dense grid (approximately 2.5 kilometers between lines) of 21 north- south oriented and 11 east-west oriented seismic lines located at the junction of the Delaware, Maryland and New Jersey state boundary OCS extensions near the modern-day shelf break. Fourteen additional lines extend into areas north and east of the dense seismic grid along the NJ OCS shelf and slope. An additional northeast-southwest oriented line runs approximately 300 kilometers from the NJ OCS into the middle of the VA OCS.

The lines collected as part of this permit are available as stacked sections and appear to have undergone amplitude enhancement through a process such as AGC given the lack of amplitude loss with depth.

Atlantic Offshore Group/Digicon - Permit E02-77

A regional grid of 22 dip lines and 7 strike lines were acquired for the Atlantic Offshore Group by Digicon over a large portion of the OCS extending from southern North Carolina to northern Florida and acquiring subsurface data in the Carolina Platform, the Carolina Trough and Blake Plateau.

Migrated SEG-Y files are available for portions of 15 lines of this permit, totaling approximately 17.5% of the line- kilometers acquired by Digicon. For permit E02-77, the only depth section available is for line BP-102 (Plate B-3C). No processing information is detailed in the SEG-Y file and no scanned copy exists so the exact depth conversion processing sequence is unknown.

Mid-Atlantic Group/Digicon - Permit E11-77

The seismic data collected by Digicon for the Mid-Atlantic Group consists of migrated and depth sections at an exploration scale (line spacing between 2 and 3 kilometers) in the central Maryland OCS and a sub-regional scale (line spacing approximately 5 kilometers) along the northeast Maryland and New Jersey OCS. Additionally, 7 strike lines separated from the exploration and semi-regional survey grids were acquired closer to the shoreline. The dense, uniform spacing between lines and the availability of migrated and depth-converted SEG-Y data make interpretation of this dataset ideal for well correlation.

All 64 lines of this permit have migrated SEG-Y files while approximately 56% of the lines have depth converted SEG-Y files. Over 82% of the dip lines and 34% of the strike lines have depth converted SEG-Y files.

South Atlantic Group/Geosource - Permit E01-80

Two seismic surveys were collected in 1980 for the “South Atlantic Group” that covered almost identical areas and often with lines overlapping one another. Geosource collected seismic data as part of permit E01-80 and Digicon acquired data as part of permit E02-80. It is unknown why the two surveys were collected with such similar areal distribution and funded by possibly the same group of industry members. The area surveyed by both Geosource and Digicon for these permits extends from the Southeast Georgia Embayment to the Manteo Protraction east of the Outer Banks of North Carolina.

Both stacked and migrated sections are available for the seismic lines collected as part of this survey.

South Atlantic Group/Digicon - Permit E02-80

As mentioned in the previous survey description, the data collected by Digicon for permit E02-80 covers a geographic extent very similar to the data acquired by Geosource for permit E01-80 and additionally both surveys have very similar line spacing.

The availability of depth sections for permit E02-80 will be valuable as no depth sections are available for the data acquired for permit E01-80.

Exxon/Geosource - Permit E01-81

Data collected for Exxon Exploration by Geosource Inc., as part of Permit E01-81, extends across a large portion of the Eastern U.S. Atlantic Margin.

Chevron/Digicon - Permit E07-81

The 12 lines collected in the North Carolina OCS in water depths of approximately 147 to 8200 ft. (45 to 2500 m) for permit E07-81, image the area that is known as the Manteo Prospect or Manteo Exploration Unit.

Migrated sections using the process of downward continuation (likely Kirchhoff migration) are available as scanned paper copies and in SEG-Y format. Depth migrated sections are available for all lines except Lines 1, 3 and 7 and part A of Line 12.

Chevron/Geosource - Permit E13-78

Chevron contracted Geosource to collect ten lines landward of the BOEM's (2012) Late Jurassic-Early Cretaceous Carbonate Margin Hydrocarbon Play along the Maryland OCS. The data acquired for this permit is made up of a small grid of 3 dip lines and 4 strike lines with 2- to 3-kilometer line spacing and three additional lines to the northeast that form a star-like pattern. Line CPR-78-4 extends along strike from the survey grid intersecting the three lines to the northeast. All ten lines of this survey are available as scanned stacked sections and as stacked and migrated SEG-Y files.

Mid-South Atlantic Group/Geosource - Permit E02-82

Geosource collected approximately 274 seismic lines along the middle and northern Atlantic as part of the geophysical permit E02-82. This large survey covers the offshore New York shelf/slope region just north of the Baltimore Canyon Trough, and a nearly continuous region from offshore southern North Carolina to southern Maryland waters.

Seismic data available for this survey includes SEGY files of stacked sections, migrated sections and depth-converted sections. The migrated and depth-converted sections were purchased from BOEM, while the stacked sections downloaded from the USGS NAMSS website, where the survey is listed as WesternGeco Middle Atlantic (W-4-82-NA).

Shell - Permit E04-82

The 40 lines collected as part of this survey run north of the Southeast Georgia Embayment to Georges Bank Basin, offshore Massachusetts.

Migrated sections and depth-converted sections are available for the five NW-SE oriented lines collected in the Mid-Atlantic.

ARCO - Permit E11-82

In 1982, ARCO Exploration surveyed three Mesozoic Rift Basins as part of Permit E11-82. Near Georges Bank, the Atlantis Basin was surveyed using a relatively tightly-spaced seismic grid with 30 lines as close as 2.5 km apart covering an area of 2800 km^2 and several lines, more sparsely-spaced, imaged the more northerly Franklin Basin.

ARCO/Digicon - Permit E15-79

While navigation information is available for 14 lines acquired for this permit, only 5 lines (PRI-01, PRI-02, PRI-05, PRI-08 and PRI-20) are truly available. These 5 lines are available as stacked section (both as scanned sections and as digital SEG-Y files) and as migrated SEG-Y files. The lines acquired as part of this permit were collected in the Central Baltimore Canyon Trough primarily along the northern Maryland and New Jersey outer shelf to slope. The lines collected form a regional grid of 7 dip lines and 3 strike lines. Additionally, there are 2 oblique lines that run roughly north to south and 2 oblique lines that intersect a northern dip line where multiple wells were drilled near Schlee Dome.

Amoco/Norpac - Permit E05-83

Permit E05-83 consists of 23 sparsely spaced lines collected by Norpac for Amoco in North Carolina, Virginia and Maryland waters in 1983.

The seismic data available from BOEM/BSEE consists of migrated sections and/or depth-converted seismic sections. Unfortunately, much of this information (especially the depth-converted data) exists only as scanned documents and not as digital SEG-Y files. Specifically, only 6 out of 21 depth sections are provided in SEG-Y format and 18 out of 25 migrated sections are available in SEG-Y format.

ONR/LDEO – Cruise RC2101

The seismic data for the RC2101 cruise were acquired by LDEO aboard the Robert D. Conrad in September of 1977 with funding provided by the Office of Naval Research (ONR) for the “COST B-2” project. The objective of the cruise was to acquire data running from the continental shelf to the abyssal plain to allow comparison between MCS and sonobuoy methods for determining sediment velocities in the major physiographic provinces along the eastern seaboard (RC2101 Cruise Report, 1977). The MCS lines were planned to cross the COST-B2 well.

The data available for this survey is available only as raw field data and stacked sections processed by both LDEO (provided by Joyce Alsop) and the USGS. The gaps seen between lines collected for this survey are likely the result of technical difficulties during acquisition and the lack of data for lines 69, 71 and 72 that were either never processed or lost during data transfer from analog tapes. Single-channel sections of the data can be found as scanned seismic negatives from NOAA’s NGDC website for much of the survey, although no digital data is available for the single- channel seismic data.

Spectrum and Texaco/Teledyne - Permit E05-86

Permit E05-86 consists of only three seismic lines: 1) Line 5-YRE extending southeast from the mouth of Chesapeake Bay to the inner continental shelf of Virginia over the southern half of the buried Norfolk Basin, 2) Line OSC-2 running east of Myrtle Beach, SC and 3) Line OSC-3 collected offshore of Charleston, SC.

All three lines have both scanned seismic stacked sections and stacked SEG-Y files.

NSF/LDEO – Cruise MGL1408

The MCS data acquired for Cruise MGL1408 was collected as part of the Eastern North American Margin (ENAM) community seismic experiment (CSE) with the aim of providing open-access onshore/offshore active/passive seismic data across the Mid-Atlantic margin (MGL1408 Cruise Report, 2014). The ENAM CSE was created to progress our understanding of the formation and evolution of rifted margins and related questions highlighted in the GeoPRISMS Science and Implementation Plan.

Migrated and stacked sections are available for the data collected for public use as part of the MGL1408 Cruise. The data was acquired in September and October of 2014 and therefore represents the most recent data available for analysis as part of the SOSRA project. Additionally, raw/field data is also available for this survey so it may be possible to reprocess the data if needed.

Texaco/GECO - Permit E03-88

Permit E03-88 consists of data covering four areas: 1) The Currituck Embayment—with seismic lines labeled 88-16, 2) the Norfolk Basin with seismic lines labeled 88-17, 3) the Long Island Basin with seismic lines labeled 88-18 and 4) the Block Canyon Area with seismic lines labeled 88-19.

There are 20 total SEG-Y files (due to individual lines often being broken up into three separate SEG-Y files) for the Currituck Embayment area and one SEG-P1 navigation file.

USGS/Digicon Survey S-1-73

Three lines were collected during this survey, one across Georges Banks and two across the Baltimore Canyon Trough east of New Jersey and Virginia.

Raw DEMUX SEG-Y files and stacked sections are available for download from the USGS NAMSS website where stacked sections of line 3 are available in its entirety (i.e., line 3 and 3A) as scanned images converted into SEG-Y format, while line 3A is available as it was originally retrieved from the master tape. Details of the migration of SEG-Y data from the “Gulf Seal” master tape indicate that there were numerous problems with the data transfer of line 3 which resulted in the loss of data. This is perhaps the reason why only scanned sections are available for the entire line.

USGS/Digicon Survey S-1-75

The lines collected as part of this survey consist of five dip lines, which infilled data

coverage gaps collected during previous surveys, and two lines running parallel to the continental margin extending from offshore Cape Hatteras, North Carolina into Canadian waters.

For the lines collected in Virginia, unprocessed DEMUX SEG-Y data is available for all lines while only lines 12B, 12C and 13B are available as SEG-Y stacked sections.

USGS/Teledyne Survey S-1-77

Teledyne Exploration acquired 10 seismic lines for the USGS in 1977 aboard the M/V Coral Seal. These long, regional lines were collected to image the Long Island Platform (Line 16, a dip line), the Baltimore Canyon Trough (Lines 14 and 15, both strike lines collected in New Jersey waters), the Carolina Platform (Lines 17 and TD6, both dip lines) and the region extending from the Florida Platform to the Blake Plateau Basin (Lines TD-3, 4 and 5, all dip lines).

Demultiplexed, raw data and stacked sections in SEG-Y format are available for download from the USGS. Scanned stacked sections, observer logs and a final "Seismic Data Acquisition" report is available for download from NOAA's NGDC website.

USGS/GSI Survey C-1-78

Geophysical Services Inc. (GSI) was contracted by the USGS to collect and process the 21 seismic lines making up survey C-1-78. Lines collected as part of this survey provide a substantial amount of information used for the Northern Atlantic Margin portion of the "Geophysical Database of the East Coast of the United States" (Klitgord et al., 1994; Klitgord and Schneider, 1994).

Seismic data are available in SEG-Y format as both unprocessed DEMUX data and as a stacked section.

BGR/Prakla-Seismos 1979 Survey

Four strike lines from the BGR 1979 survey span the Virginia waters. BOEM provided this data with SEG-Y and paper copies of stacked and migrated sections of the four lines acquired in the study area.

Figure 10 displays all the seismic surveys collected and analyzed for this study.

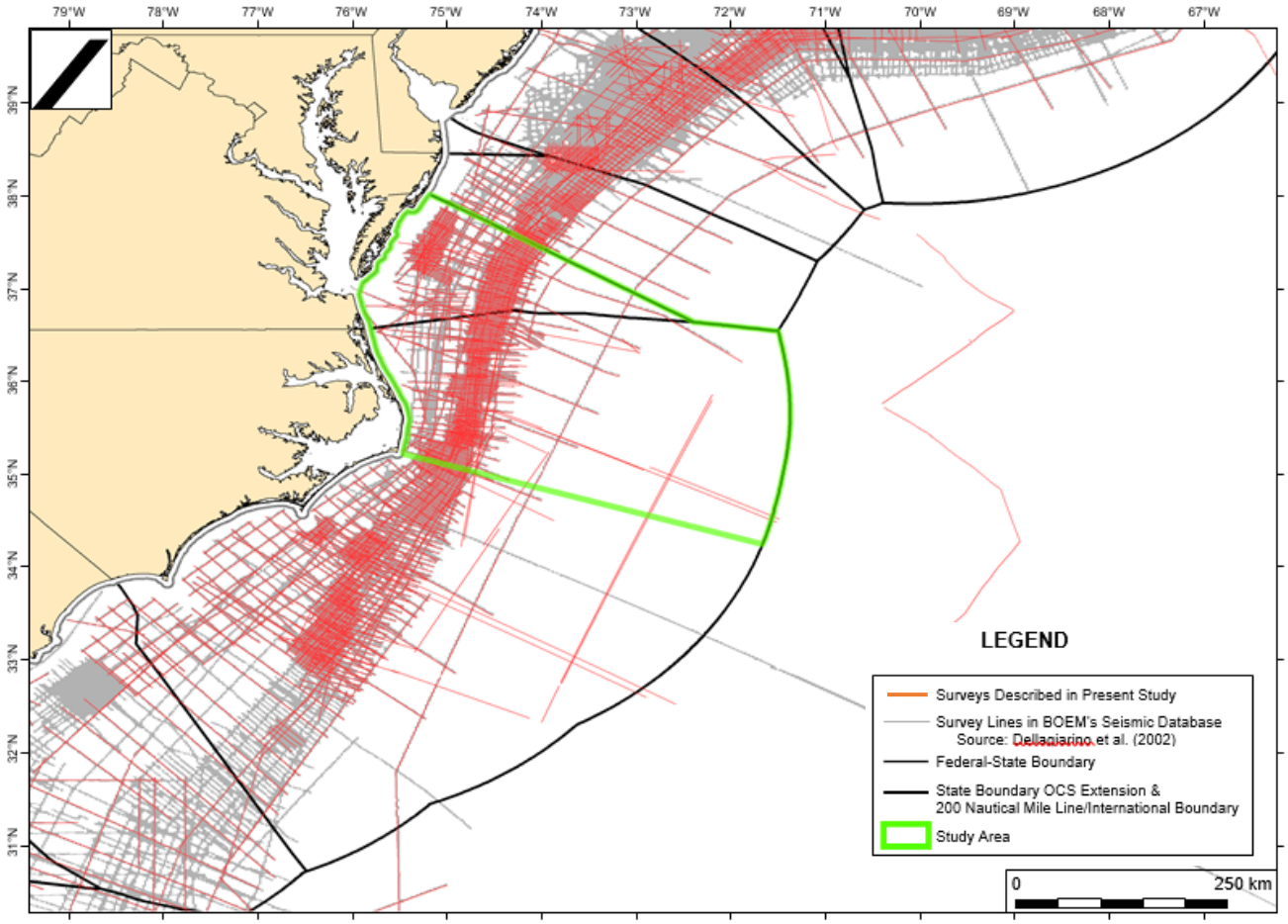

Figure 10. All Seismic Surveys Collected and Analyzed in the Mid-Atlantic (Fugro, 2017)

The majority of the 2-D MCS data for this study was collected during Atlantic OCS exploration during the 1970's and 1980's. It is noted that processed seismic data collected for mineral exploration on the U.S. OCS is made available to the public after a 25-year proprietary moratorium period (based on the permit date). The most recent survey to be released from this moratorium period and made available by BOEM was acquired in 1988. This industry seismic data, along with data from Atlantic OCS exploratory drilling (e.g., well logs), is publicly available for purchase online from the Bureau of Ocean Energy Management (BOEM) at (www.data.bsee.gov). The United States Geological Survey's (USGS) National Archive of Marine Seismic Surveys (NAMSS) maintains a large amount of seismic data that is free to download from their website (walrus.wr.usgs.gov/NAMSS). Recently (i.e., in late 2014 or early 2015), many of the seismic datasets previously available exclusively through BOEM's website became available for download on the NAMSS website.

Subtask 3.2 - Well Logs

Thirty-four wells have been studied for the Mid-Atlantic SOSRA project to aid both seismic correlation of significant stratigraphic tops across the Mid-Atlantic OCS region and provide relevant physical properties needed to assess the CO_2 storage potential of subsurface reservoirs. Descriptions of the wells and the data available for each well are described below. The tables below describe the all the wells and the well logs collected and analyzed for this study.

Deep-Penetrating Atlantic Coastal Plain Wells

Well	County	Latitude	Longitude	Date	Datum	Depth Penetrated	Hole Depth	Digital Logs	Raster Logs
Twiford #1	Currituck	36.30278	-75.92500	1965	4 m (12 ft.)	1,384 m (4,541 ft.)	1,388 m (4,553 ft.)	SP, GR, CAL, RES	VEL
Kellog #1	Currituck	36.11722	-75.85278	1969	5 m (17 ft.)	1,561 m (5,121 ft.)	1,567 m (5,140 ft.)	SP, GR, CAL, RES	VEL, Mudlog
Hatteras Light (Esso #1)	Dare	35.25000	-75.52917	1946	7 m (24 ft.)	3,057 m (10,030 ft.)	3,064 m (10,054 ft.)	SP, RES	
Pamlico Sound (Esso #2)	Dare	35.70351	-75.59795	1947	6 m (21 ft.)	1,924 m (6,312 ft.)	1,930 m (6,332 ft.)	SP, RES	
State of NC #2 (Mobil #2)	Dare	35.43889	-75.57639	1965	7 m (24 ft.)	2,549 m (8,363 ft.)	2,556 m (8,386 ft.)	SP, GR, CAL, DRHO	VEL, RES, DIP, RHOB
State of NC #1 (Mobil #1)	Dare	35.99861	-75.86667	1965	7 m (24 ft.)	1,599 m (5,246 ft.)	1,606 m (5,270 ft.)	SP, GR, CAL, RES, DRHO	VEL, DIP, RHOB
Marshall Collins #1	Dare	35.88333	-75.67083	1965	4 m (14 ft.)	1,914 m (6,280 ft.)	1,919 m (6,295 ft.)	SP, GR, CAL	VEL, RES
Etheridge# 1	Dare	35.92406	-75.67684	1969	8 m (26 ft.)	1,836 m (6,024 ft.)	1,844 m (6,049 ft.)	SP, RES	

Table 2. Wells Located on the Coastal Plain of North Carolina (Fugro, 2017)

Virginia Coastal Plain Wells

Well	County, City or Area	Latitude	Longitude	Date	Datum	Depth Penetrated	Hole Depth	Digital Logs	Raster Logs
Norfolk Water Works	Norfolk	36.87222	-76.20000	1896	5 m (15 ft.)	778 m (2,552 ft.)	782 m (2,567 ft.)		Lith. Log
Chesapeake Bay Bridge-Tunnel	Chesapeake Bay Waters	36.96952	-76.11849	1963	0	447 m (1,467 ft.)	457 m (1,500 ft.)		Lith. Log
Bush Development Corp.	Virginia Beach	36.86667	-75.98083	1964	3 m (10 ft.)	482 m (1,581 ft.)	486 m (1,593 ft.)		SP RES SPR Lith. Log
E.G. Taylor #1-G	Accomack	37.88423	-75.51681	1971	16 m (53 ft.)	1,895 m (6,217 ft.)	1,911 m (6,269 ft.)	GR TEMP	GR SP CAL RES RHOB DRHO VEL Lith. Log
Exmore Corehole*	Accomack	37.58550	-75.81917	1986	9 m (30 ft.)	407 m (1,335 ft.)	416 m (1,366 ft.)		
Jenkins Bridge Corehole*	Accomack	37.93611	-75.60444	1988	2 m (6 ft.)	401 m (1,316 ft.)	402 m (1,320 ft.)	SP TEMP	
Kiptopeke Corehole*	Northampton	37.13527	-75.95223	1989	3 m (9 ft.)	607 m (1,991 ft.)	610 m (2,000 ft.)	SP TEMP	GR SP SPR RES

Cape Charles Corehole*	Northampton	37.25921	-76.01801	2004	2 m (7 ft.)	821 m (2,694 ft.)	823 m (2,699 ft.)		
Eyreville Corehole*	Northampton	37.32147	-75.97518	2005	2 m (8 ft.)	1,764 m (5,787 ft.)	1766 m (5,795 ft.)	SP TEMP	

Table 3. Wells Located on the Coastal Plain of Virginia (Fugro, 2017)

Shallow-Penetrating Offshore Wells
Atlantic Slope Project Wells Analyzed

Well	Location	Latitude	Longitude	Water Depth	Depth Penetrated	Hole Depth*
ASP 07	Offshore North Carolina	35.5583	-74.8100	398 m (1,306 ft.)	305 m (1,001 ft.)	703 m (2,306 ft.)
ASP 08	Offshore North Carolina	35.5450	-74.7867	1,078 m (3,537 ft.)	19 m (62 ft.)	1,097 m (3,599 ft.)
ASP 10	Offshore Virginia	37.0733	-74.5483	616 m (2,021 ft.)	250 m (820 ft.)	866 m (2,841 ft.)
ASP 13	Offshore New Jersey	38.8483	-72.8830	695 m (2,280 ft.)	305 m (1,001 ft.)	1,000 m (3,281 ft.)
ASP 14	Offshore New Jersey	38.8067	-72.8400	1,191 m (3,907 ft.)	305 m (1,001 ft.)	1,496 m (4,908 ft.)
ASP 15	Offshore New Jersey	38.7722	-72.8056	1,493 m (4,898 ft.)	244 m (801 ft.)	1,737 m (5,699 ft.)
ASP 22	Offshore Virginia	37.0417	-74.5483	1,259 m (4,131 ft.)	229 m (751 ft.)	1,488 m (4,882 ft.)
ASP 23	Offshore Virginia	37.3300	-74.1800	1,485 m (4,872 ft.)	305 m (1,001 ft.)	1,790 m (5,873 ft.)

Table 4. Wells Collected for the Atlantic Slope Project Located in the Mid-Atlantic (Fugro 2017)

AMCOR Stratigraphic Test Wells Analyzed

Well	Location	Latitude	Longitude	Datum (KB)	Water Depth	Depth Penetrated	Hole Depth	No. Cores (Recovery)
6006	Offshore North Carolina	34.69	-75.7167	9.7 m (32 ft.)	56.1 m (184 ft.)	89.3 m (293 ft.)	155.1 m (509 ft.)	9 (22%)
6007 & 6007B	Offshore Virginia	37.29983	-74.65267	9.7 m (32 ft.)	85 m (279 ft.)	310.6 (1019 ft.)	405.3 m (1330 ft.)	33 (26%)

Table 5. AMCOR Wells Located in the Mid-Atlantic (Fugro, 2017)

Deep Sea Drilling Project (DSDP)

Leg	Site	Latitude	Longitude	Spud Date	Datum (DF)	Water Depth	Depth Penetrated	Hole Depth	No. Cores (Recovery)
11	105	34.89530	-69.17330	5/13/1970	10 m (33 ft.)	5,251 m (17,228 ft.)	633 m (2,077 ft.)	5,894 m (19,337 ft.)	43 (54%)
93	603	35.49433	-70.02833	5/5/1983	10 m (33 ft.)	4,633 m (15,200 ft.)	833 m (2,733 ft.)	5,476 m (17,966 ft.)	41 (58%)
93	603A	35.49483	-70.02817	5/11/1983	10 m (33 ft.)	4,633 m (15,200 ft.)	-	-	0
93	603B	35.49517	-70.02850	5/12/1983	10 m (33 ft.)	4,633 m (15,200 ft.)	1,585 m (5,200 ft.)	6,228 m (20,433 ft.)	75 (71%)
93	603C	35.49633	-70.03100	5/31/1983	10 m (33 ft.)	4,643 m (15,233 ft.)	366 m (1,201 ft.)	5,019 m (16,467 ft.)	40 (86%)
95	603D	35.49967	-70.02350	9/1/1983	10 m (33 ft.)	4,641 m (15,226 ft.)	640 m (2,100 ft.)	5,291 m (17,359 ft.)	1 (98.6%)

95	603E	35.49967	-70.02283	9/3/1983	10 m (33 ft.)	4,641 m (15,226 ft.)	1,290 m (4,232 ft.)	5,941 m (19,491 ft.)	1 (6%)
95	603F	35.49783	-70.02267	9/10/1983	10 m (33 ft.)	4,640 m (15,223 ft.)	1,546 m (5,072 ft.)	6,196 m (20,328 ft.)	3 (73.8%)

Table 6. DSDP Wells Located in the Mid-Atlantic (Fugro, 2017)

- Oil and Gas Exploration Wells

Drilling for O&G along the Atlantic Margin of the United States resulted in the completion of 51 exploration wells between the years of 1976 and 1984. Three main geographic areas were drilled including: 1) thirty-four wells drilled near Wilmington and Hudson Canyons in the Baltimore Canyon Trough, 2) ten wells drilled in Georges Bank offshore Massachusetts and 3) seven wells drilled in the Southeast Georgia Embayment.

Only one well was drilled along the Maryland OCS, the Shell Baltimore Rise 93-1 well, completed in November 1984 in 1,529 meters of water to a total of 5,407 m True Vertical Depth (TVD). The Shell 93-1 well is approximately 57 km from Virginia waters, being the closest industry well to the Mid-Atlantic SOSRA study area.

Four additional offshore O&G wells drilled in the Baltimore Canyon Trough between 1979 to 1984 have also been selected for analysis as part of the SOSRA project since offshore well control is limited. These wells were drilled along the Mesozoic paleoshelf edge reef trend. These O&G wells will provide the most useful information for carbon storage assessment since they penetrate deep into the subsurface and are positioned near the intersection of numerous seismic lines. There is a suite a well log curves available at each well.

Well Location	Latitude Longitude	Spud Date	Datum	Water Depth	Depth Penetrated	Hole Depth	Digital Logs
Shell 93-1 Baltimore Rise (MD OCS)	37.89306 -73.73583	7/14/1984	15 m (48 ft.)	1,528 m (5,013 ft.)	3,865 m (12,680 ft.)	5,407 m (17,740 ft.)	SP, GR, CAL, SFL, ILM, ILD, DT, DTL
Shell 372-1 Wilmington Canyon (NJ OCS)	38.60028 -72.93694	5/26/1984	15 m (48 ft.)	2,119 m (6,952 ft.)	1,412 m (4,633 ft.)	3,545 m (11,631 ft.)	SP, GR, SGR, CAL, SFL, ILM, ILD, DT, DTL, RHOB, DRHO, NPHI
Shell 386-1 Wilmington Canyon (NJ OCS)	38.40528 -73.21750	12/30/1983	15 m (48 ft.)	1,779 m (5,838 ft.)	3,083 m (10,115 ft.)	4,877 m (16,000 ft.)	SP, GR, CAL, SFL, ILM, ILD, DT, DTL
Shell 587-1 Wilmington Canyon (NJ OCS)	38.38111 -73.16444	8/2/1983	15 m (48 ft.)	1,965 m (6,448 ft.)	2,430 m (7,972 ft.)	4,410 m (14,470 ft.)	SP, GR, CAL, SFL, ILM, ILD, SN, DT
Tenneco 495-1 Wilmington Canyon (NJ OCS)	38.46639 -73.37750	6/12/1979	27 m (88 ft.)	108 m (355 ft.)	5,443 m (17,858 ft.)	5,578 m (18,300 ft.)	SP, GR, CAL, SFL, ILM, ILD, DT, RHOB, DRHO, NPHI

Table 7. Offshore Deep Wells Located in the Mid-Atlantic (Fugro, 2017)

Subtask 3.3 - Additional Data

While not the focus of the present report, there are numerous sources for digital geological and geophysical information that could potentially aid carbon storage assessment along the Mid-

Atlantic OCS. Table 8 lists online sources of information such as bathymetry, gravity, magnetic anomalies, heat flow, thermal gradients, sediment thickness, seismic refraction data, regional geologic maps and geohazards. This information can be used to understand the formation and evolution of the Mid-Atlantic region providing insight into the factors influencing the creation and infilling of the Baltimore Canyon Trough and the Carolina Trough. Figure 11 displays the location of each well and additional information described above in the SOSRA Mid-Atlantic Planning Area.

Table 8. Additional Data Type and Sources (Fugro, 2017)

Product	Website	Data Provider/Funding Agency/Reference
General Bathymetric Chart of the Oceans (GEBCO)	www.gebco.net	International Hydrographic Organization (IHO) & the Intergovernmental Oceanographic Commission (IOC) of UNESCO. Hosted by the British Oceanographic Data Centre (BODC)
Geologic Map of North America	pubs.usgs.gov/ds/424/	USGS in cooperation with the Geological Society of America Reference: Garrity & Soller (2009)
EMAG2: Earth Magnetic Anomaly Grid (2-arc-minute resolution)	www.ngdc.noaa.gov/geomag/emag2.html	Distributor: National Centers for Environmental Information, NESDIS, NOAA, U.S. Department of Commerce Reference: Meyer, B., Saltus, R. & A, Chulliat (2016): EMAG2: Earth Magnetic Anomaly Grid (2-arc-minute resolution) Version 3. National Centers for Environmental Information, NOAA.
CEUS Compilation of Seismic Refraction/Reflection Lines	www.ceus-ssc.com/Report/GIS.html	See metadata on website for compilation from various authors.
Land & Marine Gravity	www.ngdc.noaa.gov/mgg/gravity/1999cd.html	Reference: Land & Marine Gravity CD-ROMs, 1999. Compiled by D. Dater, D. Metzger, & A. Hittelman. U.S. Department of Commerce, NOAA, NGDS, Boulder, CO.
National Geothermal Data System, NGDS	geothermal.smu.edu/gtda/	NGDC aggregates geothermal data collected & curated by the SMU Geothermal Laboratory & its partner organizations. Funding: U.S. DOE awarded to SMU
The Global Heat Flow Database of the International Heat Flow Commission (IHFC)	www.heatflow.und.edu/index2.html	Maintained by the IHFC of the International Association of Seismology & Physics of the Earth's Interior (IASPEI) Website maintained by The University of North Dakota
Total Sediment Thickness of the World's Oceans & Marginal Seas, Version 2	www.ngdc.noaa.gov/mgg/sedthick/	Whittaker, J., Goncharov, A., Williams, S., Müller, RD&G. Leitchenkov (2013) Global sediment thickness dataset updated for the Australian-Antarctic Southern Ocean, Geochemistry, Geophysics, Geosystems. DOI: 10.1002/ggge.20181
Transforms & Spreading Ridges	www.ceus-ssc.com/Report/GIS.html	Reference: Thomas, W.A., 2009, Ouachita Sub-Detachment Structures: presentation given at CEUS-SSC Project Workshop #2, February 18-20, Palo Alto, Calif.

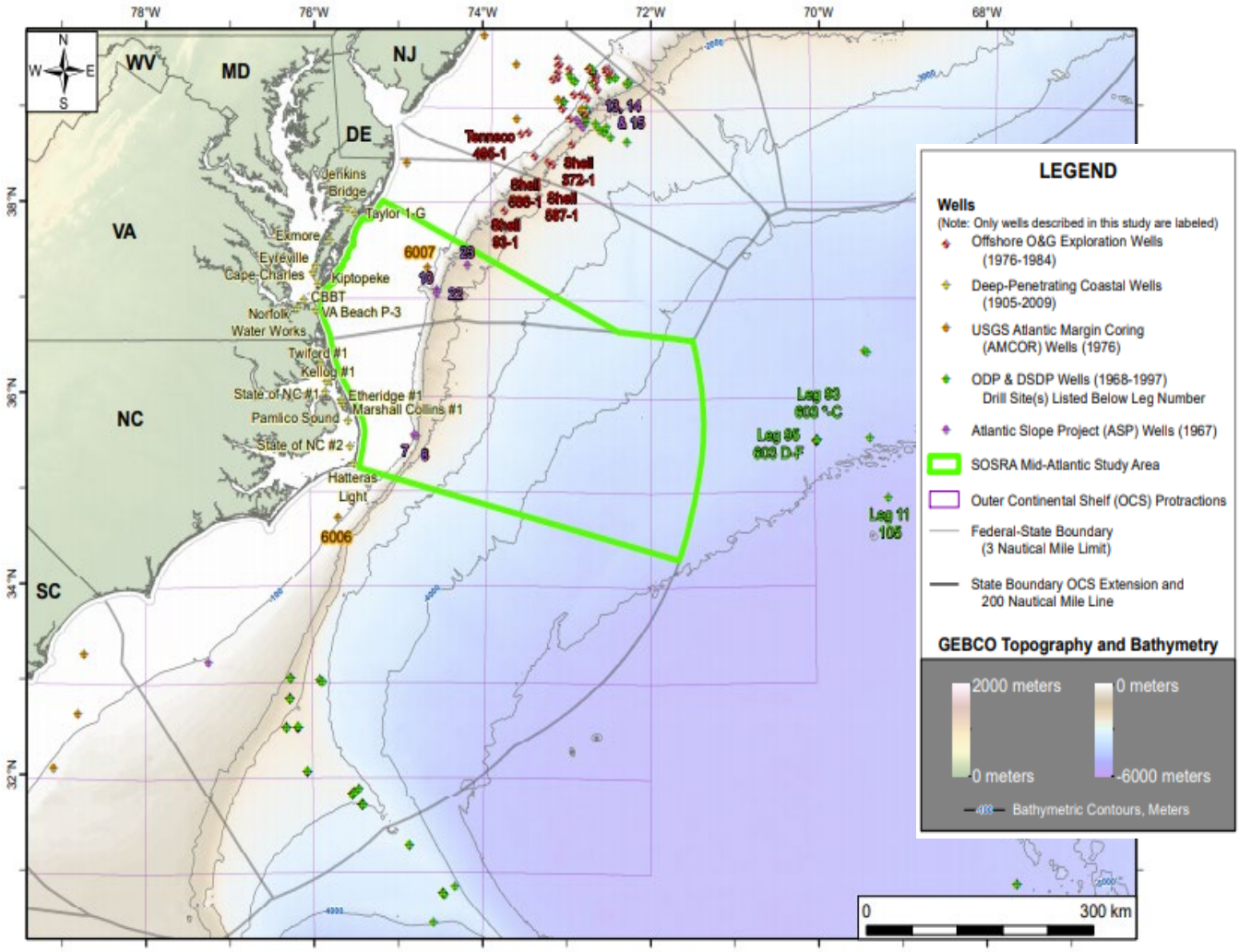

Figure 11. Locations of all Wells Included in this Study (Fugro, 2017)

Task 4.0: Data Analysis

Subtask 4.1 - Quality Assessment

Seismic Data Quality Analysis

Data quality analysis was undertaken to determine the viability of using existing seismic data to help assess the carbon storage potential of the Mid-Atlantic OCS. The ability to properly image the subsurface is largely a function of the seismic survey's design and the data processing steps applied to the recorded data. A seismic survey should be designed to best meet the objective of the investigation. For carbon storage assessment, the emitted seismic wave must possess enough energy to penetrate the strata above a potential reservoir while also preserving the appropriate frequency content needed to properly resolve the geometry of the reservoir.

Acquisition parameters for all seismic surveys analyzed in this report are tabulated in Table 9. Of the many parameters found in Table 9, the cable length, the CDP fold and the acoustic source volume were chosen to provide an assessment of the seismic data quality since these parameters greatly affect the ability to image the subsurface.

During the 1970's and 1980's, the limiting factor in imaging deep targets was often a function of the length of the streamer, which influences the far offset. A rule-of-thumb for seismic acquisition is that the maximum offset should be about the same value as the depth to the target reflection interface (horizon). Modern streamers are typically six to twelve kilometers long whereas the streamers used in the 1970's and 1980's were generally around three kilometers long. Therefore, targets more than three to four kilometers below the sea surface would not have been adequately imaged using the shorter streamers used in these vintage surveys. The cable length for most of the surveys collected within the SOSRA study area are roughly between 3 and 4 kilometers long. Longer streamer lengths used in the E03-88 permit, the VAEDGE 1990 survey and the 2014 MGL survey provide greater imaging at depth and can help analyze the deep stratigraphy in the Mid-Atlantic region.

The CDP fold isn't truly a field parameter, but rather it is controlled by the shot point spacing, the group interval and the number of available channels. Decreasing the shot point spacing and group interval spacing while increasing the number of available channels will allow for an increase in CDP fold resulting from stacking the seismic data during data processing. Stacking involves taking all the traces with a common midpoint (CMP) and summing them together to form a single trace. Stacking therefore reduces the seismic data volume (originally composed of many traces equal to the CDP fold of the data) to single, zero-offset traces that have an increased signal-to-noise (S/N) ratio. Most the seismic data collected in the SOSRA study area have a CDP fold of 36 or 48. Many of the surveys acquired after 1981 have CDP fold values more than 60 and will likely show higher quality imaging of the subsurface. Lines with less than 36-fold are generally from older 1970's surveys and are of a regional nature. Unfortunately, many of these low fold surveys were acquired near the shore and will make offshore correlation of the onshore well data more difficult.

The final field parameter used in the data quality assessment is the acoustic source volume. It is critical to produce a powerful acoustic signal where enough energy is retained to be recorded by near-surface hydrophones after the seismic wave has traveled to, and reflected from, a layer with a thick sedimentary overburden. Each legacy seismic survey's source volume (measured in cubic inches) has been divided into four categories: 1) less than 2,200 cubic inches, 2) between 2,200 and 5,000 cubic inches, 3) greater than 5,000 cubic inches and 4) unknown volumes, sparker arrays or Aquapulse system. In general, there was an increase in the source volume utilized for the legacy seismic surveys with time. All surveys with volumes of less than 2,200 cubic inches were collected in the 1970's, except for the three lines collected by Teledyne Exploration in 1986 for Spectrum/Texaco under permit E05- 86, which utilized the smallest source volume of all surveys described in this report. Surveys collected between 1980 and 1982 used larger source volumes, between 2,220 and 3,060 cubic inches, although the Chevron E13-78 survey used a source volume of 2,680 cubic inches and the ARCO E11-82 survey used a source volume of 5,600 cubic inches. Only four surveys utilized sources with volumes greater than 5,000 cubic inches (Permit E11-82, Permit E03- 88, the VAEDGE 1990 survey and the 2014 MGL1408 survey).

Vertical resolution of the seismic data is another important parameter that dictates the usefulness of the seismic data. Vertical resolution of the data is a function of the frequency content of the data. The frequency content is influenced by acquisition methods, equipment used during acquisition, and signal processing. More specifically, the seismic acoustic source, receiver array channel spacing, shot interval distance, sampling rates, and the frequency response of hydrophones used to record the signal are predominant factors that affect the frequency content of the seismic data.

We performed a frequency content analysis on selected survey lines. The lines analyzed were a sub-set of lines selected from surveys that intersect the various areas of interest, considered to provide a potential tie-in to existing well data, and were deemed to be of the best use for future basin analysis due to the respective survey coverages. Lines analyzed included both strike and dip lines from each survey.

The frequency content can be used to calculate the characteristic “limit of separability” and “limit of detectability” for the seismic data volume. The limit of separability, which is a function of vertical resolution, is defined as the minimum bed thickness for which the top and bottom of the bed can be fully resolved in the seismic data, and is based on the one-quarter acoustic wavelength (λ/4) approximation. The limit of detectability is defined as the minimum bed thickness for which the bed can be detected and is nominally based on one thirtieth of the wavelength (λ/30).

Prior to each analysis, the entire line was reviewed as a vertical display within a Petrel project. A portion of the line was then selected for analysis. The portion was selected on the basis that it was considered to be representative of the line (avoiding any poor-quality sections or steep slopes) and that it incorporates the interval that might be expected to be of most interest during future interpretation, commencing at or close to seabed. The vertical analysis window, selected on the basis outlined above, was usually found to be close to 3 s two-way travel time (TWTT). Exceptions to this, where a significantly smaller interval has been used, typically indicate a geological feature/boundary below which there is very limited penetration. The lateral extents of the selected windows were typically between approximately 10 km and 50 km.

A frequency analysis was conducted to determine the minimum, maximum and dominant frequency for one representative seismic trace and time interval for each survey. The frequencies were then used to calculate the limit of separability S and limit of detectability D. The interval velocities assumed for this analysis are broad approximation of shallower section’s velocities (2000m/s) and deeper section’s velocity (5000m/s) (Ö. Yilmaz, 2001). These velocity estimates are based loosely on the interval velocities described by Klitgord et al. (1994) and are thought to give a reasonable indication of the range of velocities that may be applicable.

Survey	Shotpoint Interval	Acoustic Source			Group Interval	Number of Channels	CDP Fold	CDP Interval	Cable Length	Offset		Sample Rate (ms)	Record Length (Seconds)		Recording System
		Number of Guns	Volume (Cubic Inches)	Pressure (psi)						Minimum	Maximum		No Delay	With Maximum Delay	
S-1-73	100 m	20	1,260	1,800 to 2,000	100 m	24	6, 12 or 24	50 m	2327 m	339 m	2666 m	4	10	11	DFS III
S-1-75	100 m	Unknown	1,700	1,700	50/100 m	48	12 to 48	25 to 50 m	3500 m	348 m	3848 m	2	10	14	DFS III
E14-75	67 m	Aquapulse			67 m	48	24	33.5 m	3152 m	312 m	3464 m	4	5 or 7		DDS-888 COBA I
E17-75	51.2 m	2 Sparker Arrays			34.1 m	24	24	51.2 m	785 m	32.6 m	817.5 m	1	3		DFS III
E22-75	37.5 m	4	Unknown	2,000	75 m	24	48	37.5 m	3,524 m	278 m	3,802 m	4	6.8		DFS IV
E16-76	100 m	18	1,700	Unknown	50/100 m	48	36	50 m	3569 m	338 m	3907 m	4	8	10	DFS III
S-1-77	50 or 100 m	4	2,160	2,000	50/100 m	48	24 or 48	50 m	2700 m	300 m	3000 m	2	12		DFS IV
E02-77	100 m	Unknown	1,700	Unknown	50/100 m	48	36	50 m	3,569 m	240 m	3,809 m	4	7	12	DFS III
E11-77	100 m	Unknown	1,080	Unknown	50 m	48	48	25 m	2,349 m	223 m	2,572 m	2	8		Sercel
RC2101	50 m	4	1,864	2,000	100 m	24	24	50 m	2,300 m	300 m	2,600 m	4	12	16	DFS IV
C-1-78	50 m	Unknown	1,450	2,000	50/100 m	48	48	50 m	3,603m	335 m	3,938 m	4	12		DFS IV
E13-78	67 m	14	5,680	1,800	33.7 m	48	48	33.5 m	3,166 m	600 m	3,766 m	2	7		DFS V
E06-79	50 m	21	2,183	1,800 to 2,000	50 m	64	16	25 m	3,150 m	188 m	3,338 m	4	5		MDS-10
E15-79	50 m	34	1,940	1,850	25/50 m	96	72	25 m	3,562 m	342 m	3,903 m	4	7		DFS IV
BGR79	50 m	"U-Type" Airgun Tuned Array	1,430	1,430	50 m	48	24	25 m	3,350 m	300 m	3650 m	4	10	13	DFS V
E01-80	75 m	14	2,682	1,850	75 m	48	48	37.5 m	3,524 m	223 m	3,747 m	2	8		MDS-10
E02-80	100 m	25	2,220	1,700 to 1,800	25/50 m	96	36	50 m	3,561 m	244 m	3805 m	2	7	9	DFS V
E01-81	22.5 m	14	2,511	Unknown	15/45 m	75	40 to 75	22.5 m	2,940 m	217 m	3,157 m	4	8	9	DFS V
E07-81	100 m	25	Unknown	1,800	25/50 m	96	36	25 m	3,305 m	270 m	3,575 m	2	8		DFS V
E02-82	37.5 m	14	3,060	1,800 to 2,000	37.5 m	96	48	37.5 m	3,562 m	225 m	3,787 m	2	8	9	DFS V
E04-82	30.5 m	Unknown	Unknown	Unknown	Unknown	Unknown	Unknown	30.5 m	Unknown	Unknown	Unknown	4	7	9	Unknown
E11-82	12.5 m	Unknown	5,600	Unknown	25 or 50 m	Assumed: 60 or 120	144 to 240	25 m	2,987 m	329 m	3,316 m	2	7		Unknown
E05-83	25 m	18	Unknown	2,000	25 m	120	60	12.5 m	2,974 m	250 m	3224 m	2	9		DFS V
E05-86	25 m	6	984	2,000	12.5 m	96	48	12.5 m	1,187 m	125 m	1,312 m	2	6		DFS IV
E03-88	25 m	24	6,324	Unknown	25 m	240	70 to 95	25 m	5,975 m	281 m	6,256 m	2	8		DSS/DFS V
VAEDGE	50 m	36	10,800	2,000	25 m	240	60	12.5 m	6,000 m	Unknown	Unknown	2	16		Unknown
MGL1408	25, 37.5, 50, 62.5, 75 or 225 m	2 or 4 Arrays (10 Airguns per array)	3,300 or 6,600	Unknown	12.5 m	480 or 636	480 or 636	25, 37.5, 50, 62.5, 75 or 225 m	6,000 or 8,000 m	307.5 m	6,307.5 or 8,307.5 m	1 or 2	9 or 18		Unknown

Table 9. Field Parameters from Surveys Analyzed in this Study (Fugro, 2017)

$$\lambda = \frac{V}{f}$$

Where λ is the wavelength (m), V interval velocity (m/s) and f frequency (Hz).

$$S = \frac{\lambda}{4}$$

Where S is the limit of separability (m)

$$D = \frac{\lambda}{30}$$

Where D is the limit of detectability (m)

Multiple methods can be used to extract the dominant frequency from a seismic trace. In this study, two methods commonly used by the geophysics community were implemented and compared (Barnes, 1993).

The seismic traces are discrete, real-valued two-way-time t_i and amplitude A_i pairs. Although processed amplitudes are typically unitless, they depict the mechanical energy of the seismic wave relative to an arbitrary zero value. The original signal was then decomposed into discreet, complex-valued frequency f_i and amplitude-time $\tilde{A}_i$ pairs through the discreet Fourier transform (DFT) (Frigo & Johnson, 2005). Again, although the transformed amplitude-time is unitless, it depicts the signal content associated with each frequency. Because the signal content is a complex number, the complex magnitude or absolute value was used to define the magnitude of the signal content.

Method 1 extracted the dominant frequencies ($f_{dom}^{(1)}$) by calculating the average -frequency weighted by the signal content. (Barnes, 1993).

$$DFT\{t_i, A_i\} = \{f_i, \tilde{A}_i\}$$

$$|\tilde{A}_i| = \sqrt{Re(\tilde{A}_i)^2 + Im(\tilde{A}_i)^2}$$

$$f_{dom}^{(1)} = \frac{\sum_i |\tilde{A}_i| f_i}{\sum_i |\tilde{A}_i|}$$

The second method used to extract dominant frequencies also used modified amplitude (signal content). However, for this method, the dominant frequency ($f_{dom}^{(2)}$) represents the average of the squared frequency weighted by the amplitude (Barnes, 1993).

$$f_{dom}^{(2)} = \sqrt{\frac{\sum_i |\tilde{A}_i| f_i^2}{\sum_i |\tilde{A}_i|}}$$

Both methods are considered valid to approximate dominant frequencies and therefore quantify the vertical resolution on 2D seismic reflection profile.

All these steps led to a detailed data quality assessment, which aimed to reduce the dataset volume to the most appropriate data to conduct a regional assessment of the carbon storage potential of offshore Virginia and North Carolina.

Using maximum and minimum frequencies can provide a “best and worst case” values for the limit of detectability and separability. The same analysis was then conducted by using the dominant frequency extracted by the two methods aforementioned. The first methods provided dominant frequencies ranging from 20 (E-16-76) to 31 Hz (E-11-82) whereas the second method extracted higher overall dominant frequencies ranging from 25 (E-16-76) and 40 Hz (E-11-82).

Both methods confirmed that the frequency ranges are still higher for more recent surveys than for older ones. However, modern data with a dominant frequency around 50 Hz, exceeds the quality of all the vintage data. The limits of detectability where calculated by using both dominant frequency extraction method. Both methods provide a limit of detectability and separability in the same order of magnitude.

This complete analysis showed the importance for the interpreter to know the approximated vertical resolution of the dataset used. Some older surveys such as E-16-76 could participate in the construction of a regional geological framework in the study area however, because of the poor resolution of this survey, reservoir identification and mapping cannot be achieved by using these data. Surveys with higher dominant frequencies and therefore smaller wavelength, should be preferred to identify and characterize reservoir in the study area. Overall, the data quality analysis highlighted that the vintage data collected are of fair to poor quality because of the aforementioned field parameters and processing techniques. As a consequence, the depth of penetration, the resolution and the signal to noise ratio of the data were impaired.

The results are displayed on Table 10 and 11.

PERMIT OR SURVEY	CHOSEN LINE	LINE TRACE	TIME WINDOW	LINE TYPE	FREQUENCY RANGE		S				D			
							Min (10%)		Max (90%)		Min (10%)		Max (90%)	
					Min (10%)	Max (90%)	V=2000 m/s	V=5000 m/s	V=2000 m/s	V=5000 m/s	V=2000 m/s	V=5000 m/s	V=2000 m/s	V=5000 m/s
E14-75	we-026_stk	1183	0.5 to 1.5 s	dip	12.7	43.5	39	98	11	29	5	13	2	4
E16-76	MA-032_mig	1005	1s to 2.5s	dip	6.9	32.8	72	181	15	38	10	24	2	5
E02-77	BP-118A_migr	404	0.25s to 1.3s	dip	9	45	56	139	11	28	7	19	1	4
BGR79	bgr79-204a_migr	386	1.5s to 3s	strike	10.9	51.8	46	115	10	24	6	15	1	3
E01-80	56-138_migr	481	0.7s to 1.7s	dip	9.5	41	53	132	12	30	7	18	2	4
E-02-82	PR82-185_migr	134	0.5s to 2s	dip	9.6	40.8	52	130	12	31	7	17	2	4
E-02-80	SA-1142_mig	699	0.5 to 1.8s	dip	8.1	40.5	62	154	12	31	8	21	2	4
E-04-82	18074_migr	247	1s to 2.5s	dip	10.9	42	46	115	12	30	6	15	2	4
E-03-88	88-16-B_migr	2401	0.5s to 1.7s	dip	9.2	43.8	54	136	11	29	7	18	2	4
E-07-81	CSA81-8_migr	199	1s to 2s	dip	13.4	56	37	93	9	22	5	12	1	3
E-11-82	M82-35_migr	601	0.5s to 1.5s	dip	12.5	56.4	40	100	9	22	5	13	1	3
E-01-75	A-243_migr	502	0.7s to 2s	dip	8.4	37.5	60	149	13	33	8	20	2	4

Table 10. Limit of Separability and Detectability

PERMIT OR SURVEY	CHOSEN LINE	LINE TRACE	TIME WINDOW	LINE TYPE	DOMINANT FREQUENCY		S				D			
							Method 1		Method 2		Method 1		Method 2	
					Method 1	Method 2	V=2000 m/s	V=5000 m/s	V=2000 m/s	V=5000 m/s	V=2000 m/s	V=5000 m/s	V=2000 m/s	V=5000 m/s
E14-75	we-026_stk	1183	0.5 to 1.5 s	dip	28.25	32.22	18	44	16	39	2	6	2	5
E16-76	MA-032_mig	1005	1s to 2.5s	dip	20.02	24.73	25	62	20	51	3	8	3	7
E02-77	BP-118A_migr	404	0.25s to 1.3s	dip	27.6	34.35	18	45	15	36	2	6	2	5
BGR79	bgr79-204a_migr	386	1.5s to 3s	strike	26.78	34.75	19	47	14	36	2	6	2	5
E01-80	56-138_migr	481	0.7s to 1.7s	dip	24.9	29.12	20	50	17	43	3	7	2	6
E-02-82	PR82-185_migr	134	0.5s to 2s	dip	24.51	32.66	20	51	15	38	3	7	2	5
E-02-80	SA-1142_mig	699	0.5 to 1.8s	dip	25.33	30.87	20	49	16	40	3	7	2	5
E-04-82	18074_migr	247	1s to 2.5s	dip	25.56	29.9	20	49	17	42	3	7	2	6
E-03-88	88-16-B_migr	2401	0.5s to 1.7s	dip	27.33	32.7	18	46	15	38	2	6	2	5
E-07-81	CSA81-8_migr	199	1s to 2s	dip	31.45	39.56	16	40	13	32	2	5	2	4
E-11-82	M82-35_migr	601	0.5s to 1.5s	dip	31.02	39.13	16	40	13	32	2	5	2	4
E-01-75	A-243_migr	502	0.7s to 2s	dip	24.54	31.75	20	51	16	39	3	7	2	5

Table 11. Limit of Separability and Detectability

Well data quality analysis

Assessing the quality of onshore well logs turned out to be a difficult task due to the absence of digitized logs for deeper section of most wells. Well logs had to be digitized from paper copies prior extracting any information and this process impaired the quality of the data. However, the digitized logs (Gamma Ray, Resistivity, Neutron, Sonic and Density logs) for both onshore and offshore wells are still commonly used and would provide good information to the interpreter.

Well folios publicly available describing petrophysical analysis from cores represent the larger source of information and will be useful for seismic interpretation and reservoir characterization.

Subtask 4.2 - Coverage Assessment

Seismic data coverage

The method used for seismic coverage analysis consisted of describing each seismic survey in terms of line spacing. When exploring for O&G in a frontier basin, it is common for industry to first collect regionally-spaced 2-D seismic lines to initially analyze the basin's hydrocarbon potential. If interpretation of the regional (or semi-regional) seismic data indicates a favorable condition for hydrocarbon accumulation and extraction, seismic data will next be collected at the exploration scale with a much tighter line spacing, or for modern exploration, as a continuous 3-D dataset. To assess the ability of using the available seismic data as part for carbon storage assessment, each survey's scope has been classified as either regional, semi-regional or exploration in scale.

In 1973, the USGS began acquiring long, regional seismic lines to set up the regional framework of the Atlantic Margin by allowing onshore-offshore well correlation and providing insight into the large-scale structural and stratigraphic framework. By 1978, the USGS had collected enough infill lines during multiple seismic programs to produce a regional grid of data extending from offshore Florida to Canada's Exclusive Economic Zone (EEZ). In 1979, the BGR 79 survey was acquired in cooperation with the USGS to further improve the existing offshore data density. In general, seismic surveys collected in the 1980's were more exploratory in nature.

Classifying the line spacing for each survey helps to evaluate how to interpret the available seismic data for the assessment of carbon storage potential. Typically, a first step in this interpretation would be to import the regionally- spaced USGS/BGR datasets into a seismic project on a workstation and incorporate horizons (in TWTT and in depth), faults and interval velocities from the existing USGS publications (i.e., Klitgord et al., 1994) to set up an initial framework. Next, it would be important to interpret lines at semi-regional level by incorporating the semi-regional datasets along with a subset of the exploration size surveys. The final interpretation step would be to focus on identifying and mapping key horizons and faults over all lines that cover the area of interest. Likely, this would be done by first interpreting a single exploration scale survey with the best available coverage (such as E02-82 located along the shelf-slope transition) and then extending that interpretation over lines from other surveys extending across the targeted interval.

Table 12 displays the classification of the main seismic surveys based on the line-spacing used during the collection of the data.

PERMIT OR	LOCATION	SURVEY	SEISMIC DATA	NUMBER OF DIP	TYPICAL DIP LINE	NUMBER OF	TYPICAL STRIKE

SURVEY		SCOPE	TYPE	LINES	SPACING (KM)	STRIKE LINES	LINE SPACING (KM)
E16-76	Cape Hatteras, NC to MD	Semi-Regional	Stacked & Migrated	35	15-04	6	10-25
BGR 79	Northern NC to southern NJ	Regional	Stacked & Migrated	0	NA	4	10-25
	NJ	Regional	Stacked & Migrated	8	13-30	3	40-75
E01-80	Currituck Sound Prospect	Exploration	Stacked & Migrated	16	3-2	6	2-5
	Manteo Prospect	Exploration	Stacked & Migrated	23	5-2	7	3-4
E02-80	Currituck Sound Prospect	Exploration	Stacked, Migrated & Depth	8	5-2	2	7
	Manteo Prospect	Exploration	Stacked, Migrated & Depth	22	5-2	2	10-20
E07-81	Manteo Prospect	Exploration	Migrated & Depth	11	2.5-5	1	NA
E02-82	Northern NC to southern MD	Exploration	Stacked, Migrated & Depth	104	1.5	4	13
E04-82	Northern NC & VA	Regional	Migrated & Depth	9	9-30	0	NA
E03-88	Currituck Sound Prospect	Exploration	Migrated	8	5	1	NA
	Norfolk Basin, VA	Exploration	Stacked	7	5	1	NA
E-14-75	Cape Hatteras, NC to Northern SC	Semi-Regional	Stacked	25	10-20	Variable, 3 to 7	10-20
E02-77	Southern NC to GA	Regional	Stacked, Migrated & Depth	22	20-40	7	Variable, 25-50;120-180
E-11-82	Norfolk Basin, VA	Exploration	Migrated	33	2.5	11	3
	Northern NC to Southern MD	Regional	Migrated	5	25-63	3	7-27

Table 12 Line-spacing for the Main Surveys Covering the Mid-Atlantic (Fugro, 2017)

- Well data coverage

Thirty-four wells were selected to help assess the potential for carbon storage on the Mid-Atlantic. No deep-penetrating wells have been drilled in the OCS waters of the Mid-Atlantic SOSRA study area. While five Atlantic Slope Project (ASP) wells and one AMCOR well were drilled in the study area, these wells penetrate less than 315 meters of the sedimentary section and therefore are of limited use for assessing carbon storage since pressures and temperatures required to reach the CO_2 critical point are typically encountered at depths greater than 800 meters below the seafloor (Smyth et al., 2008). Given the lack of well control in the study area, 17 deep wells located along the Coastal Plain of North Carolina and Virginia as well as five exploratory O&G wells drilled along the Maryland and New Jersey OCS were selected to both improve stratigraphic/lithologic correlation and better understand subsurface reservoir properties that are needed for carbon storage assessment.

Figure 12 displays the main seismic surveys and offshore/onshore wells included in this study. The Mid-Atlantic study area was extended to include deep-penetrating wells and exploration scales surveys. Extending the study area also allowed to create overlap with other study area in the North and South Atlantic, necessary to correlate horizons and validate the developed geomodel.

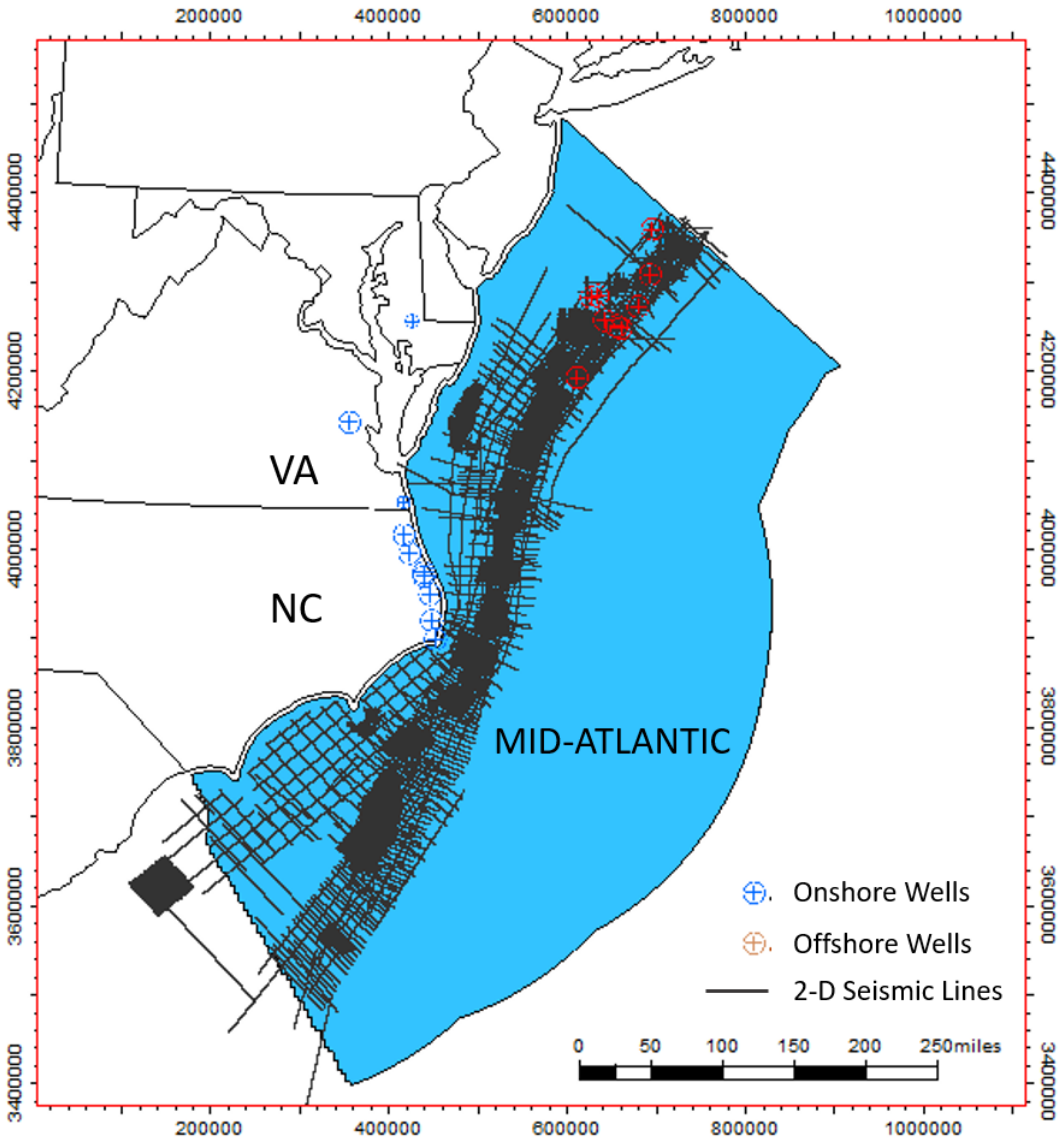

Figure 12. Data Coverage in the Extended Mid-Atlantic Study Area

Subtask 4.3 - Well-Seismic Ties

The correlation of seismic horizons with well-derived information is essential to complete a robust interpretation of the subsurface. Wells provide ground-truth data that cannot be replaced by seismic data. Until a well is drilled, the details of the lithology, rock and fluid properties, and depositional environment of subsurface strata can only be inferred. To help determine the most appropriate line for correlating well and seismic data, a series of tables were created.

Correlating onshore well information into the subsurface of the Mid-Atlantic continental shelf requires the use of dip lines, primarily of 1970's vintage, and interpretation over large (10's of km) data gaps between the onshore well location and the closest seismic line (Table 13).

WELL	SEISMIC SURVEY	SEISMIC LINE	LINE TYPE	LINE PROCESSING	DISTANCE FROM WELL
E.G. Taylor #1-G	E11-82	MAR82-137	Dip	Migrated	35 km
Norfolk Water Works	E03-88	88-16-B	Dip	Migrated	31 km
Norfolk Water Works	E05-86	5-YRE	Dip	Stack	27 km
Norfolk Water Works	E06-79	V105	Strike	Paper (Stack)	32 km
Bush Development Corp	E03-88	88-16-B	Dip	Migrated	13 km
Bush Development Corp	E06-79	V105	Strike	Paper (Stack)	16 km
Twiford #1	E06-79	V104	Oblique	Paper (Stack)	29 km
Kellog #1	VA EDGE	MA-802	Oblique	Paper (Stack)	34 km
State of NC # 1	E14-75	WE-002	Dip	Stack	15 km
State of NC # 1	E16-76	MA-60	Dip	Migrated	17 km
Etheridge #1	E16-76	MA-48	Dip	Migrated	24 km
Etheridge #1	S-1-77	17	Oblique	Stack	18 km
Marshall Collins #1	E16-76	MA-50	Dip	Migrated	27 km
Esso #2	E16-76	MA-54	Dip	Migrated	21 km
State of NC # 2	E14-75	WE-002	Dip	Stack	14 km
State of NC # 2	E14-75	WE-004-1	Dip	Stack	17 km
Hatteras Light	E17-75	DS-13	Dip	Paper (Stack)	4 km
Hatteras Light	E14-75	WE-007-1	Oblique	Stack	6 km

Table 13. Distance from Onshore Wells to the Closest Seismic Lines (Fugro, 2017)

Lines acquired for Permit E11-77 field campaign are the most suitable dataset for correlating all five O&G wells described in this report.

While lines from other seismic surveys are listed as lines for possible well correlation, mostly stacked sections exist for these surveys. Migrated seismic data is often preferred over stacked data for interpretation since migration improves spatial resolution by moving dipping layers and faults to their correct location and collapsing diffractions produced by discontinuities in subsurface strata.

Additionally, for four of the O&G wells, the data collected as part of Permit E11-77 provide correlation in both the strike and dip direction. The additional three lines listed in Table 14 from USGS surveys S- 1-75 and S-1-77 and the BGR-79 survey acquired near Shell 93-1, Shell 586-1 and Tenneco 495-1 will provide alternative routes for regional correlation into the study area or connecting O&G wells not analyzed for this study.

The dense grid of data from Permit E22-75 will aid seismic correlation near the Tenneco 495-1 and allow seismic mapping to extend both landward and into the Mid-Atlantic study area. Lines 25 and 34 from USGS Survey C-1-78 will allow stratigraphic tops from ASP wells 13, 14 and 15 to be extended landward, southwest to the Shell 586-1 well and into deep water where correlation with the RC2101 survey may aid interpretation of the strata encountered at DSDP Sites 603 and 105.

WELL	SEISMIC PERMIT/SURVEY	SEISMIC LINE	SEISMIC LINE ORIENTATION	SEISMIC SECTION FOR CORRELATION	APPROXIMATE DISTANCE FROM WELL
Shell 93-1	E11-77	MA-191	Dip	Migrated or Depth	1 km
Shell 93-1	S-1-75	10	Dip	Stack	1 km
Shell 93-1	E11-77	MA-112B	Strike	Migrated	1 km
Shell 372-1	E11-77	MA-139	Dip	Migrated or Depth	< 1 km
Shell 372-1	E11-77	MA-116A	Strike	Migrated	< 1 km
Shell 386-1	E11-77	MA-151	Dip	Migrated or Depth	2.5 km
Shell 386-1	BGR-79	203	Strike	Migrated	1.5 km

Shell 386-1	E11-77	MA-112B	Strike	Migrated	1 km
Shell 587-1	E11-77	MA-151	Dip	Migrated or Depth	1.5 km
Shell 587-1	E11-77	MA-116A	Strike	Migrated	< 1 km
Tenneco 495-1	E11-77	MA-153	Dip	Migrated or Depth	1 km
Tenneco 495-1	S-1-77	TD15A	Strike	Stack	< 1 km
Tenneco 495-1	E22-75	5044	Oblique	Stack	< 1 km

Table 14. Distance from Offshore Oil and Gas Exploration Wells to the Closest Seismic Lines (Fugro, 2017)

The shallow wells in the study area have lines passing as close as 3 km from them. However due to the poor quality of the data (low resolution), correlating seismic lines to shallow well information may not be possible and therefore might be of little help to the resource assessment.

Subtask 4.4 - Seismic Interpretation

To complete this task, the extended Mid-Atlantic Study area was divided in 2 zones: offshore North Carolina (South) and Offshore Virginia, Maryland and Delaware (North). Two teams worked separately on the interpretation of their assigned study area and correlated their results at the end of the task.

The study area was divided due to the variable seismic and well data coverage in different locations of the Mid-Atlantic. In the North, interpreted horizons were correlated to major well tops identified in various Oil and Gas exploration wells due to the relatively short distance between the study area and these wells. However, in the South, the distance to these wells was deemed too great and therefore, mapped horizons were instead correlated to onshore wells located on the coastal plain of North Carolina. Onshore wells, being less descriptive and older than offshore wells located in the North, provided less information regarding well tops and therefore less horizons could be mapped and correlated in the area. Presented on Figure 13 is the workflow followed in both study areas used to complete the seismic interpretation task.

Seismic stratigraphy has commonly been used by exploration geologists to predict the distribution and characteristics of potential reservoirs and seals at both regional and reservoir scale. Recognizable elements can be observed on seismic data such as stacking pattern, reflector terminations and changes in seismic facies (Mitchum Jr, Vail, & Thompson III, 1977). By applying the principles of seismic stratigraphy, major units can be highlighted, and prediction of sand and shale-prone zones can be achieved (Miller et al., 2017).

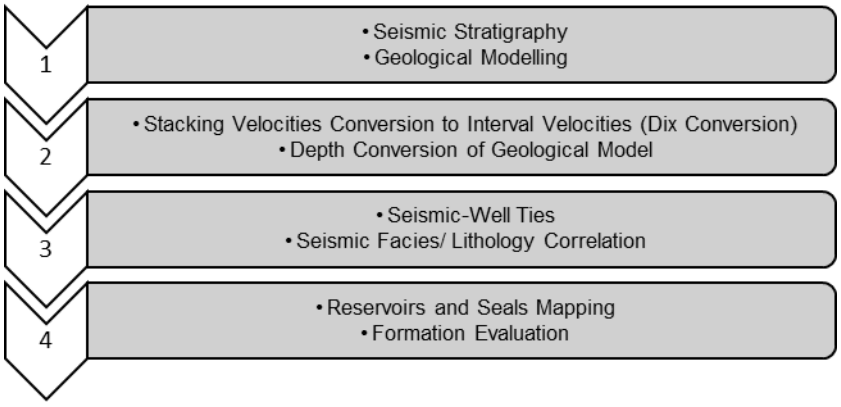

Figure 13. Workflow Developed to Conduct Task 4.4 Seismic Interpretation

Seismic interpretation of the subsurface of North Carolina

Seismic Stratigraphy

The geophysical dataset used was composed of 5 seismic surveys that covered the majority of the study area. To gain well control, information from two onshore stratigraphic test wells (Hatteras Light Esso No. 1, Pamlico Sound Esso No. 2 hereafter Esso-1, Esso-2 respectively) were extracted. Figure 14 displays the dataset used to interpret the subsurface of offshore North Carolina and the two lines represented on Figure 15 and 16.

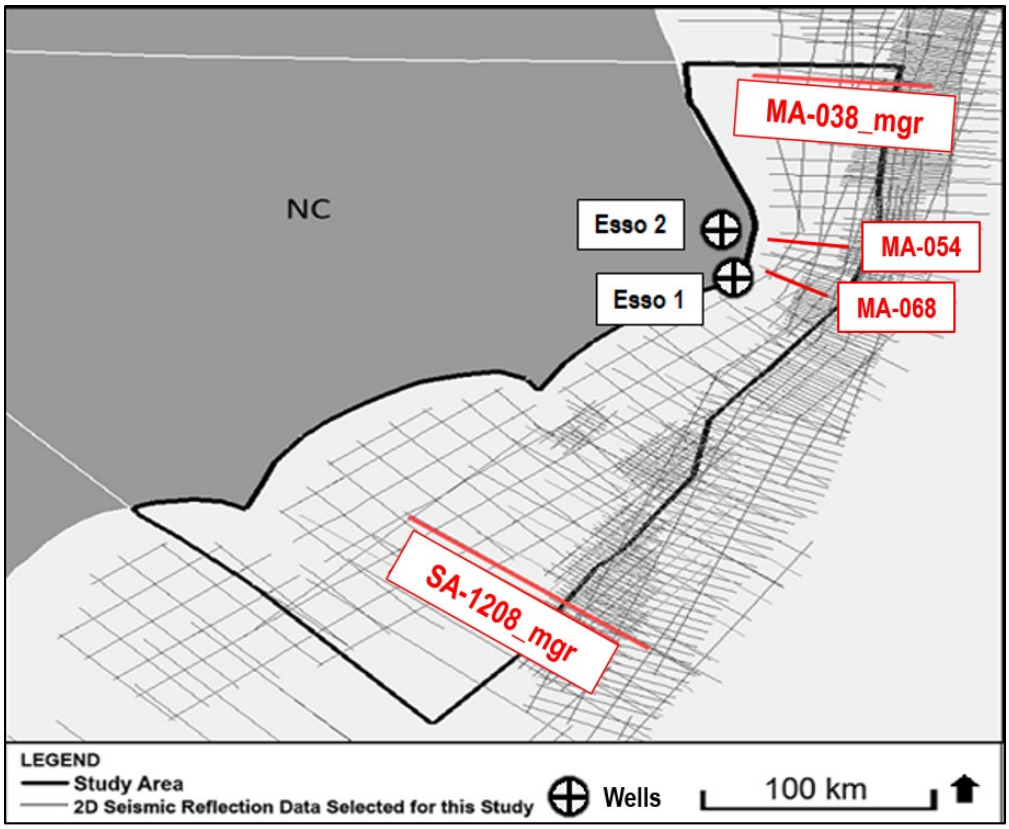

Figure 14. Geophysical Dataset Used in the South of the Mid-Atlantic Study Area

Ten sequence boundaries were identified and mapped across study area, typically. Two seismic profiles, representative of the south of the BCT and CT respectively, are shown in Figure 14 and 15. This interpretation is consistent with past interpretations, as the same patterns were observed by Brown et al. (1972) and Poag (1979). Major growth faults were not identified in the BCT but were present in the CT. The transition zone between siliciclastic-dominated and carbonate-dominated strata cannot be observed on the outer continental shelf of North Carolina due to the limited vertical resolution of the data.

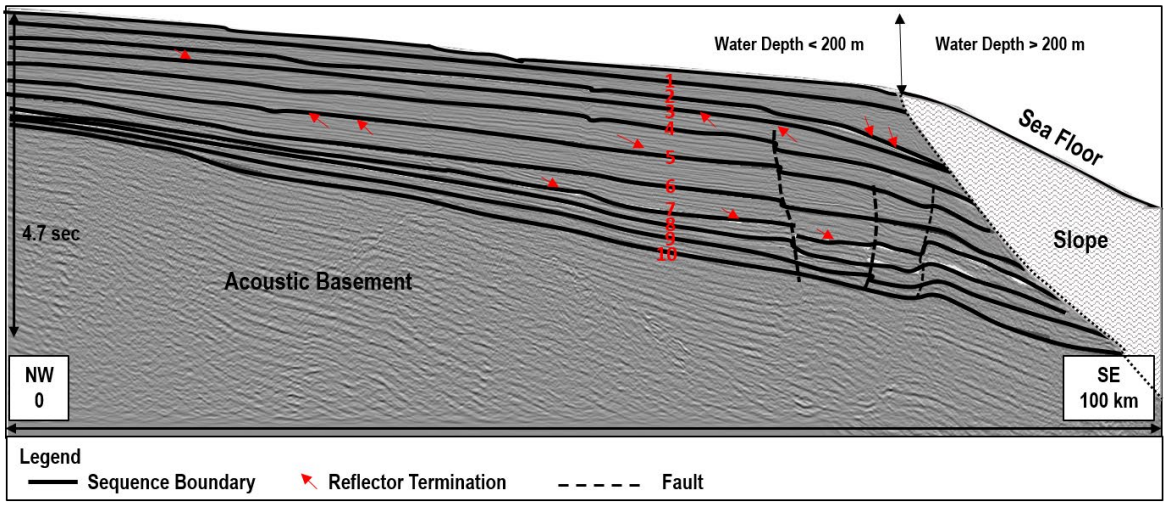

Figure 15. SA-1208 Interpretation

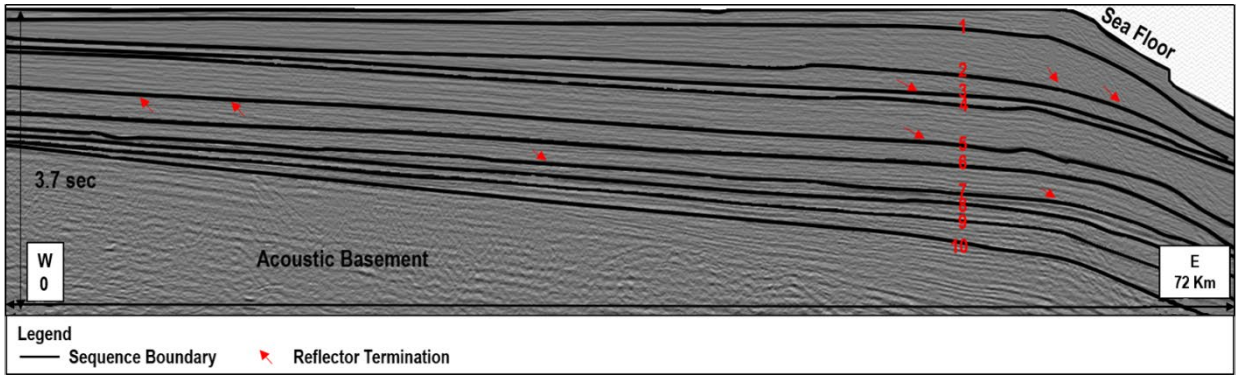

Figure 16. MA-068 Interpretation

Depth Conversion from stacking velocities

Onshore wells did not provide any information regarding interval velocities. However, stacking velocities for three major surveys were available and downloaded from the BOEM website (NAMSS). To convert the geologic model from two-way time (TWT) to depth, a velocity cube was created by using stacking velocities. These velocities were first converted to interval velocities using the Dix conversion (Dix, 1955). This method can be considered accurate for horizontal layers with limited offsets but loses its accuracy for dipping layers and complex geometries (Öz Yilmaz, 2001). The interpretation of the stratigraphy of the outer continental shelf of North Carolina shows an overall shallow dip and overall low structural complexity. Therefore, the Dix conversion was considered acceptable for this study. It is important to note that some uncertainty can be associated with this type of conversion. The interval velocity profile for line SA-1208_migr shot point 1052 is showed below on Figure 17. The time window displayed in this figure is representative of the time between the sea floor and the acoustic basement on the continental shelf.

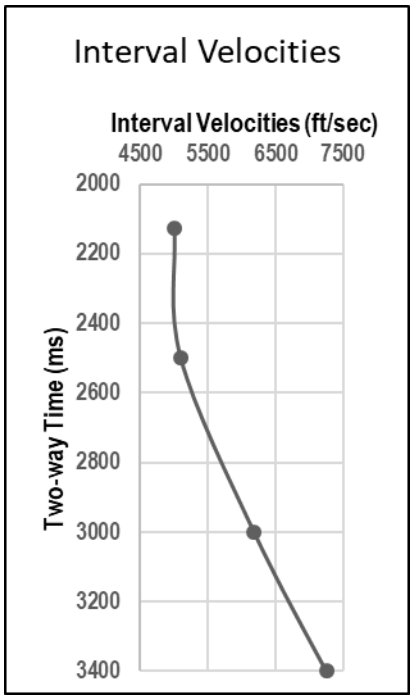

Figure 17

Seismic-Well Ties

The digital well logs for the onshore wells used here are not publicly available. However, some publications provided valuable information to aid in seismic-well ties (Spangler, 1950; Sunde & Coffey, 2009; Swain, 1947).

Formation tops and corresponding lithologies were digitized and correlated to the nearest onshore lines and formation tops described in Swain (1947) were tied to major sequence boundaries. Tying these regionally extensive boundaries to formation tops provided geological ages to each unit. Successful correlations increased the confidence in the seismic interpretation and were used to quality control each picked horizons. Esso-1 penetrated 10,054 ft of sedimentary rocks including the entire Upper and Lower Cretaceous and Upper Jurassic. Esso-2 penetrated into the Lower Cretaceous at 6,410 ft (Swain, 1947). From these wells, seven horizons were successfully mapped across the continental shelf.

Formations of early Jurassic to Pleistocene can be successfully correlated to the closest line and extended through the entire study area (Figure 18 and 19).

An attempt to link seismic facies to lithologies showed limited success due to the vertical and horizontal resolution of the data which did not allow an in-depth analysis of the seismic facies variation.

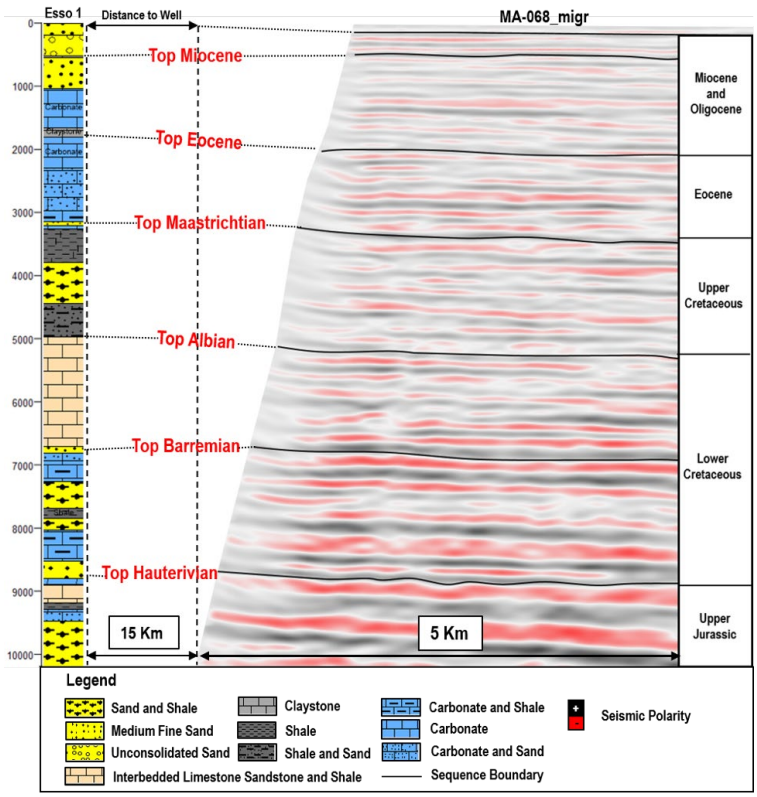

Figure 18. Correlation of Hatteras Light Esso 1 Formation Tops to the Sequence Boundaries Identified on Profile MA-068 (Lithologies from Swain, 1947)

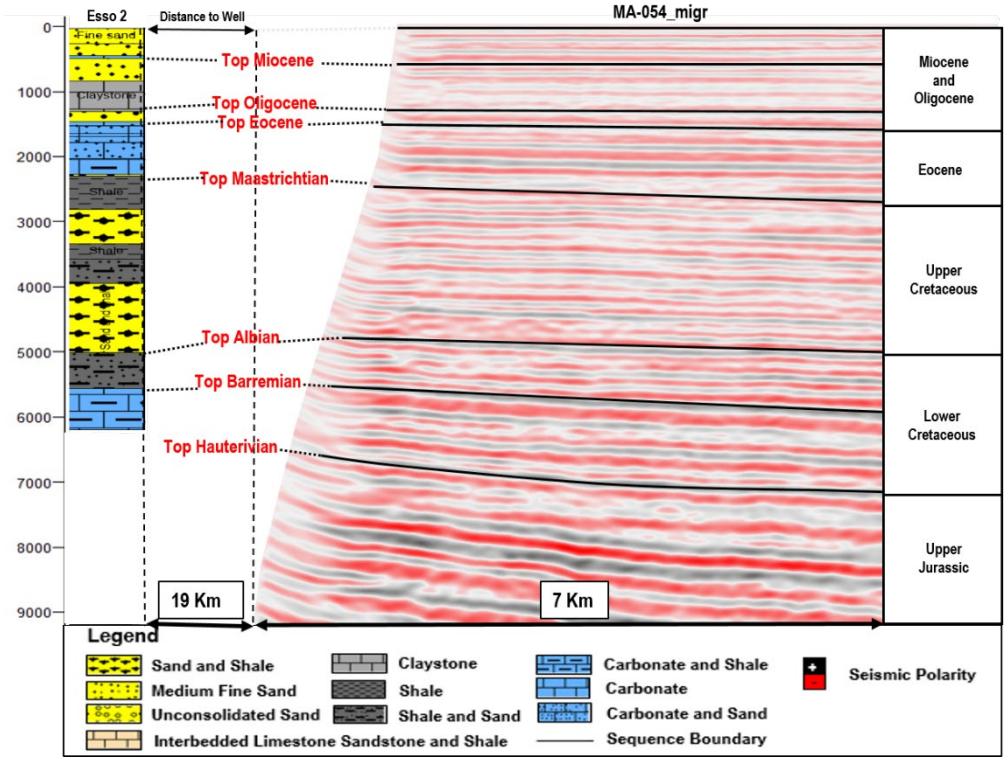

Figure 19. Correlation of Esso 2 Formation Tops to the Sequence Boundaries Identified on Profile MA-054 (Lithologies from Swain, 1947)

Seismic interpretation of the subsurface of Virginia

The same methodology was used to conduct the interpretation task in the North of the Mid-Atlantic. Sequence stratigraphy was conducted first by identifying reflectors terminations and by analyzing seismic facies variations. The sequence boundaries mapped across the study area were then tied to well tops from two main wells located in the North Atlantic: Cost B-2 and Cost B-3. From these ties, correlations between seismic facies and lithologies were made to predict the presence of sand-prone areas within this area.

The results of the interpretation task on two main seismic profiles (dip and strike) are displayed on Figure 21 and Figure 22 and their specific location within the BCT is represented below on Figure 20.

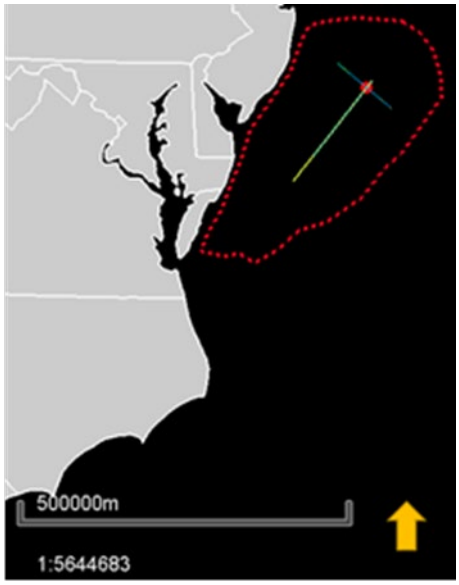

Figure 20. Locations of Two Representative Lines in the Baltimore Canyon Trough (North Area)

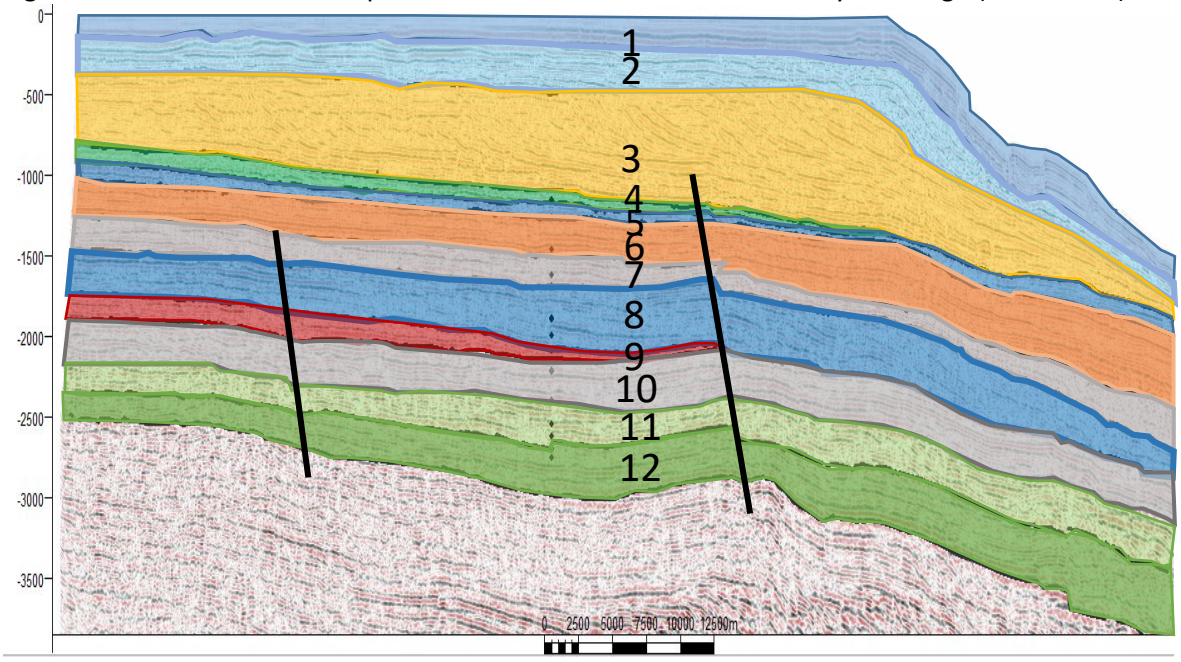

Figure 21. Dip Line Survey E16-76 Interpreted

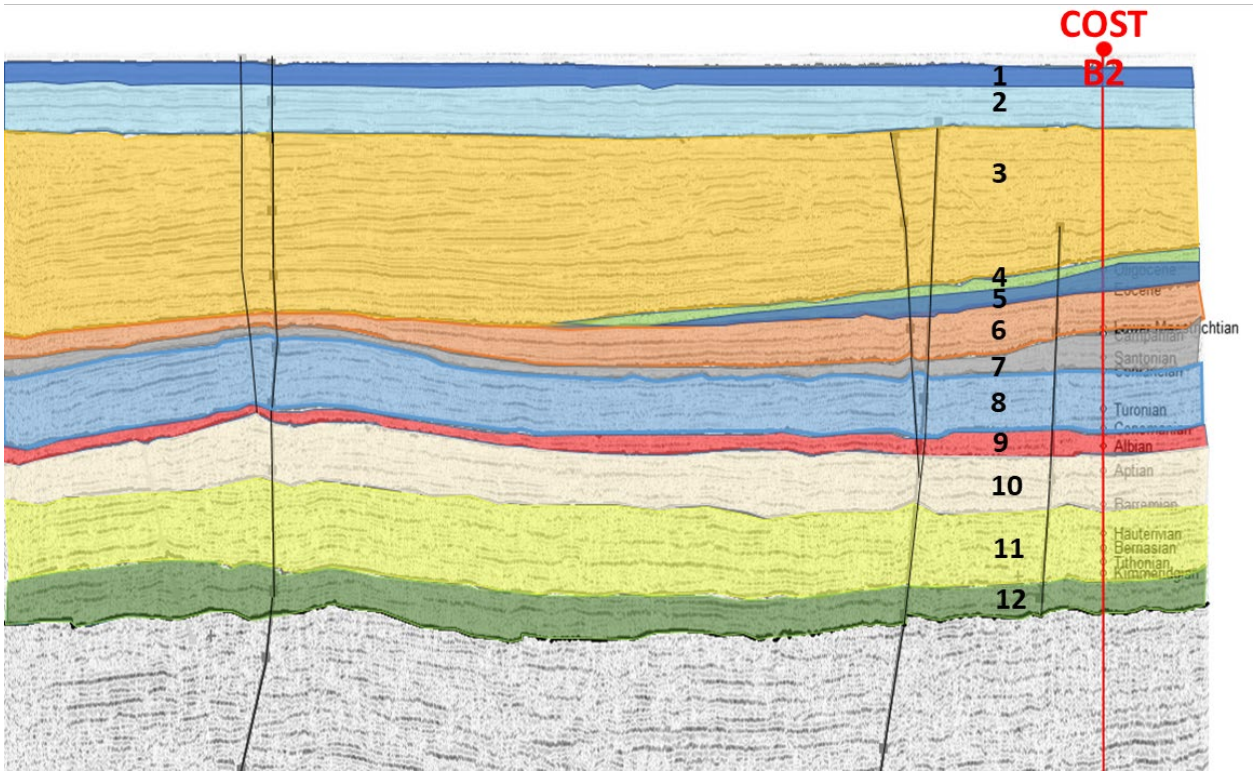

Figure 22. Strike Line Survey E-16-76 Interpreted

12 sequences boundaries were identified in the area, from sea floor to Upper Jurassic formations and were successfully tied to Cost B-2 and Cost B-3. Sub-sequences were also identified close to the wells; however, these sub-sequences could not be mapped across the study area and therefore only the twelve major sequence boundaries were considered in this study. Figure 23 shows the seismic well ties established between the closest line and Cost B-2.

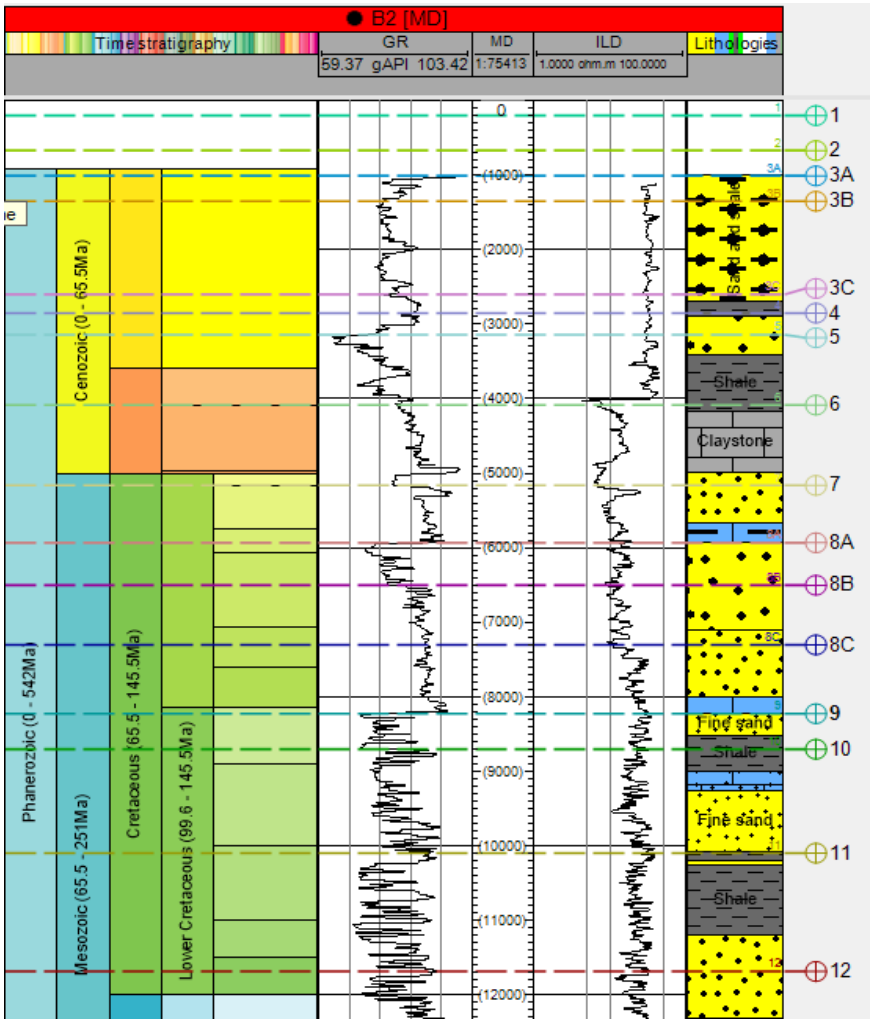

Figure 23. Seismic Well-Ties at Cost B-2

Task 5.0: Geologic Characterization and Volumetric Calculations

Subtask 5.1 - Reservoir Characterization

Boundary Conditions

Carbon storage in geologic formations can only be achieved by injecting supercritical CO_2 into a thick, porous and permeable reservoir. These reservoirs also have to be bounded vertically and laterally, by impermeable seals to prevent migration of CO_2.

Temperatures and bottom hole pressures collected from Esso-1 (Swain, 1947) and also typical geothermal and lithostastic gradients observed in offshore environments, suggest that storage of supercritical CO_2 is possible in the Upper and Lower Cretaceous formations on the outer continental shelf of North Carolina and Virginia. The minimum injection depth should be below 800 meters, making the Upper and Lower Cretaceous intervals suitable for CO_2 storage.

However, due to the potential loss of seal integrity related to shale ductility, the Lower Jurassic was not considered in this study. Based on density logs from 2 offshore wells located on the continental shelf of New-Jersey, COST B-2 and COST B-3 (Amato & Simonis, 1979; Smith et al., 1976), shales become less ductile

and more brittle below 1,600 meters, which consequently can reduce their seal integrity. Interpretation of the Upper Jurassic formation showed that this unit is buried below 2,000 meters and therefore any seals adjacent to reservoir targets may be prone to brittle failure and potential leakage.

In North Carolina and Virginia, suitable reservoirs should be located between the depth of 800 and 1,600 meters to insure the safe and long-term storage of CO_2 in this area.

North Carolina: reservoir parameters

Onshore well logs are not publicly available and therefore reservoir parameters such as porosity, permeability, and net to gross cannot be directly deduced or calculated from well data. Spangler (1950) provided porosity and permeability of major sand units identified in the Esso No. 1. However, no information is available regarding the shales and carbonates encountered in the same well.

This location in the Mid-Atlantic can be complicated to assess due to the lack of basement-penetrating or deep exploration wells offshore, but also due to the distance to other wells located in the Atlantic (COST B-2, B-3, GE-1). As mentioned before, the shelf of North Carolina represents a transition zone between a siliciclastic-dominated shelf to the north and more carbonate-dominated to the south. COST GE-1 in the South Georgia Embayment and COST B-2 in the BCT (New Jersey), highlight the differences in lithologies between the two areas. Therefore, these distant wells cannot be used reliably to provide reservoir parameters for the three units interpreted in the CT. The lateral and vertical variation in seismic facies is not easily observable on seismic data and therefore identifying the extent of the transition zone is problematic. Onshore wells are the only reliable source of subsurface information in this area.

Esso-1 provided porosity and permeability of sand units located between 3,657 feet and 7,191 feet (Swain, 1947). No information regarding the shale and carbonate intervals were collected in this publication and were just broadly described by Spangler (1950). Porosity and permeability vary greatly within the sand bodies located at the Esso-1 well. No strong relationship between porosity or permeability with depth is apparent. However, the average porosity is slightly higher in the upper Cretaceous than lower Cretaceous and higher permeability values can be found in the lower Cretaceous. Due to the absence of deep wells, the porosity and permeability obtained from Esso-1 will be extended to the rest of the study area to estimate the storage potential of each geological unit.

Measured sandstone intervals, shale and limestone are presented in Table 15; these bulk percentages were used to calculate the net-to-gross ratio of reservoir to seal. Only sandstone intervals were considered potential reservoirs (conventional) as carbonate's porosity and permeability were not estimated by previous studies and therefore presented larger uncertainties than sandstone formations. It appears that multiple reservoirs and seals are present within each unit. Between 3,600 ft and 4250 ft, the upper Cretaceous unit identified in some recent publications as the Pleasant Creek Formation (Self-Trail, Prowell, & Christopher, 2004) and as the Black Creek formation in older publications (Richards, 1950; Spangler, 1950) shows great potential for CO_2 storage due to high-porosity sandstone within this interval. This formation is bounded at the top by the Shepherd Grove Formation and at the bottom by the Collins Creek Formation, both dominated by thick shale (Self-Trail et al., 2004). In the Lower Cretaceous formation, carbonates are more abundant, but thick sand intervals are still present, especially the Patuxent Formation, 200 ft thick sandstone at 7,000 ft. The Patuxent Formation is also described as the bottom of Tuscaloosa Formation by Richards (1950).

Formation	% Sand	% Shale	% Limestone
Maastrichtian	37	53	10
Albian	24	38	38
Barremian	27	38	35

Table 15. Lithology Factor for Each Interval in North Carolina

Virginia: reservoir parameters

Cost B-2 and Cost B-3 were used to extract reservoir parameters such as the lithology mix (Table 16), porosity, net-to-gross, net sand and sand intervals' thickness (Table 17). The lithology mix for each interval was based on an extensive analysis of the seismic facies, the continuity of reflectors, the amplitude of the reflectors and on the gamma-ray well log from Cost B-2 and Cost B-3.

SEISMIC FACIES LITHOLOGY ASSOCIATIONS: 1 LITHOLOGY MIX, COST B2 EXTRAPOLATION						
FACIES #	TOP	AGE	SEISMIC FACIES		LITHOLOGY MIX	
				%SS	%SH	%LS (CEMENT)
1.	300	H	High Amp, Continuous Horiz, Low Freq	95	5	
2.	670	PLEIST	High Amp, Semi-Continuous Horiz, High Freq	90	10	
3. A.	1009	PL	Horiz. Low Amp Semi-Cont Horiz->	76	24	
B.	1350		Semi-Cont. Med-High Amp. Sigmoidal ->	61	39	
C.	2600		Horiz, High Amp Cont	41	59	
4.	2850	MIO	High Amp Semi-Cont Horizo	40	59	1
5. A.	3140	OLIG	High Amp Cont Horizo to	35	62	3
B.			Low Amp SemiCont	13	85	2
6. A.	4083	EOC	High Amp Cont Horiz to	13	85	2
B.			Low Amp SemiCont	52	47	2
7. A.	5161	MS/CM/SN/CN	High Amp Cont Horiz to	51	47	2
B.			Low Amp SemiCont Truncated at top	?		
8. A.	5930	TUR	Horiz. Low Amp Semi-Cont Horiz->	56	43	1
B.	6500	CEN	Semi-Cont. Med-High Amp. Shingled ->	54	44	2
C.	7300		Horiz, High Amp Cont	?		
9. A.	8223	ALB	High Amp Cont to	28	62	10
B.			Low Amp SemiCont Horiz, Onlapping	?		
10. A.	8700	APT	High Amp Subparallel SemiCont Horiz to	44	41	15
B.			Gentle Concave Upaward	?		
11. A.	10093	BAR/HAU/VAL	Med Amp Subparallel SemiCont Horiz to	35	48	17
B.			Gentle Concave Upward	?		
12. A.	11680	TITH/KIM	Low Amp Discontin Subhoriz to	24	64	12
B.			High Amp Contin Subhoriz	?		

Table 16. Seismic Facies/ Lithology Associations in Virginia

	OSS No.	GEO. TIME		Top	Op. Seis. Seq.	Gross (Ft)	Sand Numbr.	Net Sand (Ft)	Net/Gross	ϕ (Max.Core Por.)	Porosity - Ft
COST B2	15	NEOGENE	MIOCENE	1100	HO	2500	7	2002	0.80	34.20	685
	14	PALEOGENE	OLIGOCENE	3600	Pg30	1400	6	594	0.42	*55.00	327
	13	CRETACEOUS	MAASTRICHTIAN	5000	K180	2350	8	792	0.34	34.10	270
	12		TURONIAN	7350	K140	1150	4	286	0.25	30.70	88
	11		ALBIAN	8500	K100	500	6	374	0.75	30.60	114
	10		APTIAN	9000	K80	1250	10	836	0.67	30.50	255
	9		BARREMIAN	10250	K50	950	9	704	0.74	26.50	187
	8		HAUTERIVIAN	11200	K40	800	9	528	0.66	25.00	132
	7		VALANGINIAN	12000	K30	4020	22	1122	0.28	23.60	265
	6	JURASSIC	KIMMERIDGIAN	16020(?)	J100(?)						
	5		BATHONIAN		J30(?)						
	4		BAJOCIAN		J20(?)						
	3		AALENIAN		J10(?)						
	2		HETTANGIAN		J0(?)						
	1	TRIASSIC	TRASSIC(BASALT)		Tr80(?)						

Table 17. Core-Seismic Reservoir Parameters from Cost B-2

Subtask 5.2 – Mapping

Isopachs maps of storage intervals suitable for CO_2 storage in North Carolina

Two major units were identified within the Cretaceous interval: 1) Maastrichtian to Albian (Upper Cretaceous), 2) Albian to Hauterivian (Lower Cretaceous). The geological ages of each formation top were obtained from Esso-1 and Esso-2. Thickness maps (isopachs) were created for each interval: Upper Cretaceous shown in Figure 24 and Lower Cretaceous in Figure 25.

Each interval shows potential for CO_2 sequestration due to the presence of thick interbedded sandstones (reservoirs) and shales (seals). Reflectors for the upper limit of Maastrichtian, Albian and Hauterivian cannot be traced below the Onslow Bay. These reflectors may wedge out landward which would indicate the presence of some potential stratigraphic traps. Another explanation could be the poor seismic resolution of the stacked, unmigrated lines acquired from Onslow Bay, limiting the detectability and resolution of some geologic units.

In general, it appears that thickness of all three target intervals increases basinward. The thickness maps show that the upper Cretaceous unit thickens toward the north of the study area, whereas the Albian unit becomes thinner towards the North Carolina-Virginia border. The Barremian unit maintains similar thickness throughout the study area.

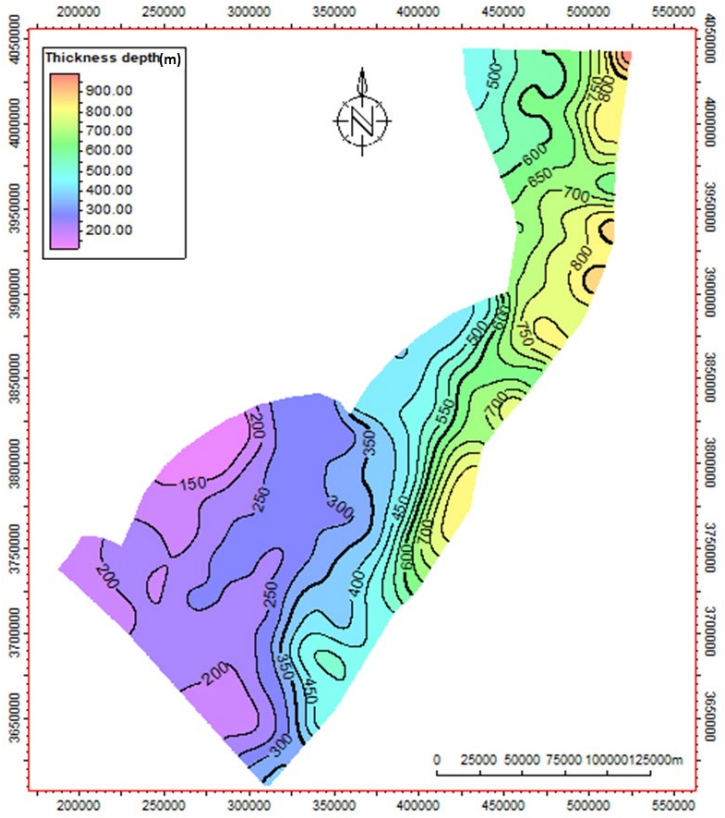

Figure 24. Isopach of the Upper Cretaceous Formation (NC)

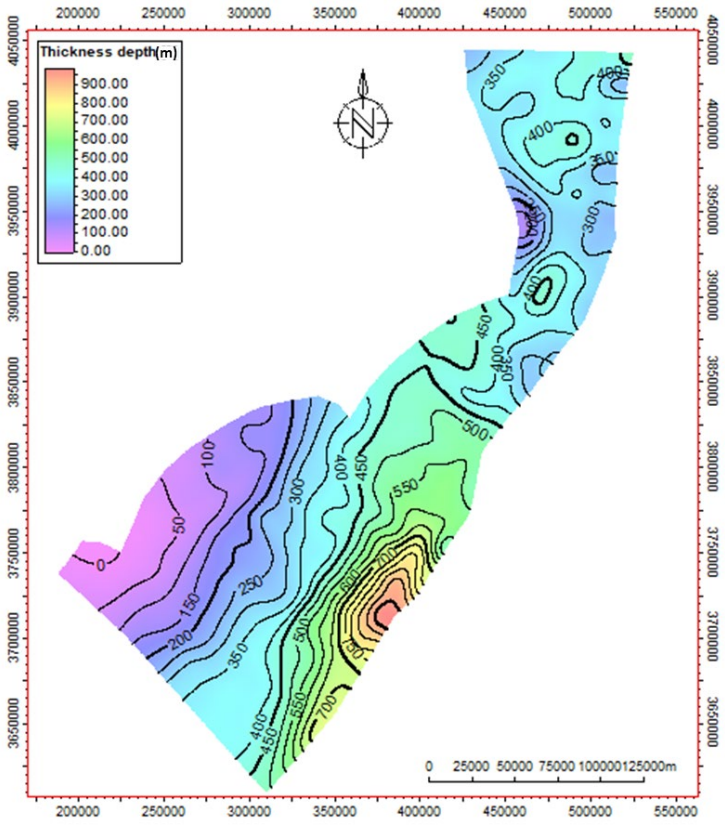

Figure 25 Isopach of the Lower Cretaceous Formation (NC)

Because of the lack of further details regarding the lithology distribution in this area, a lithology factor obtained from onshore wells (Esso-1 and Esso-2) was used to determine the potential thickness of sandstone, shale and limestone intervals. The connectivity of sand-prone areas cannot be predicted with the current available datasets and therefore these lithology factors were applied to the isopachs represented on Figure 23 and 24 to estimate the storage potential of both major formations aforementioned.

Isopachs maps of storage intervals suitable for CO_2 storage in Virginia

A more in-depth assessment of potential reservoirs suitable for CO_2 storage was done in this location, due to the increased amount of available well data and an improved quality and density of seismic data.

6 intervals, within the injection zone (defined by applying the boundary conditions) mentioned above, were identified as suitable for CO_2 storage.

In the Upper Cretaceous Formation, 4 distinct intervals were identified and isopachs were created for each:
- Maastrichtian (Figure 26)
- Santonian (Figure 27)
- Coniacian (Figure 28)
- Cenomanian (Figure 29)

In the Lower Cretaceous Formation, 2 intervals were mapped:
- Albian (Figure 30)
- Barremian (Figure 31)

The sandstone estimated thicknesses for each interval are displayed in Figure 32 to 37.

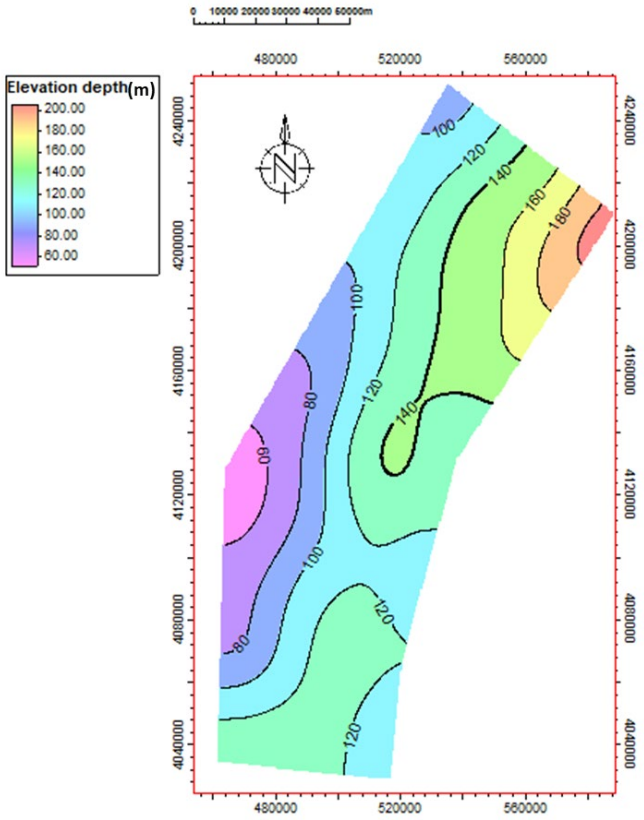

Figure 26. Isopach of the Maastrichtian Interval Within the Upper Cretaceous Formation

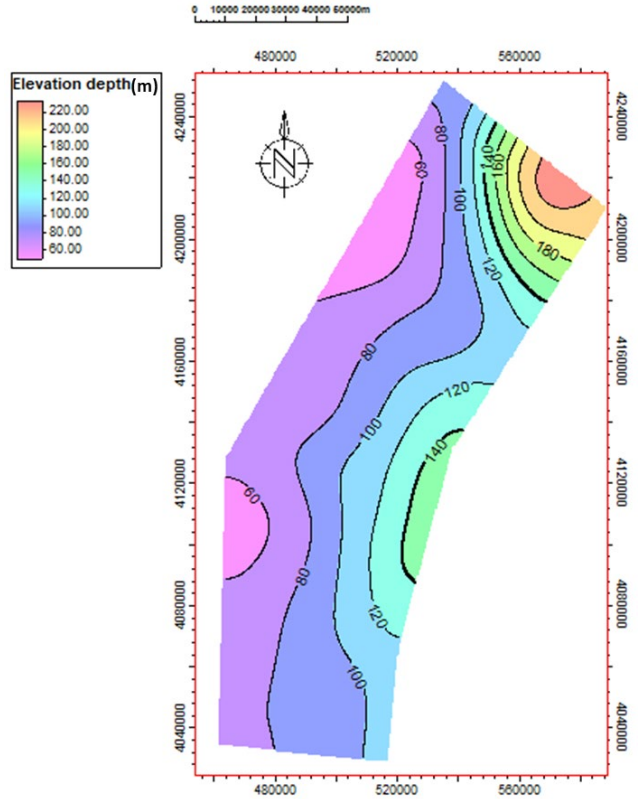

Figure 27. Isopach of the Santonian Interval Within the Upper Cretaceous Formation

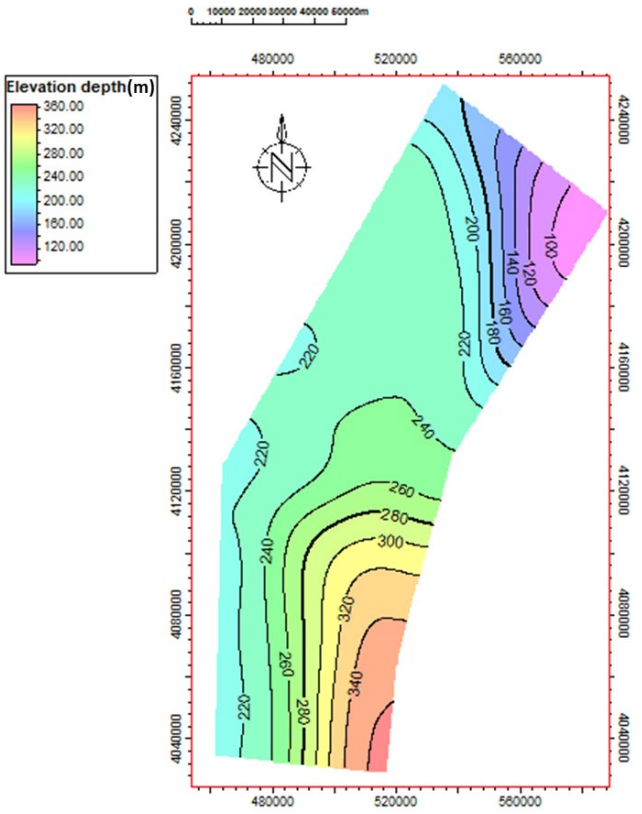

Figure 28. Isopach of the Coniacian Interval Within the Upper Cretaceous Formation

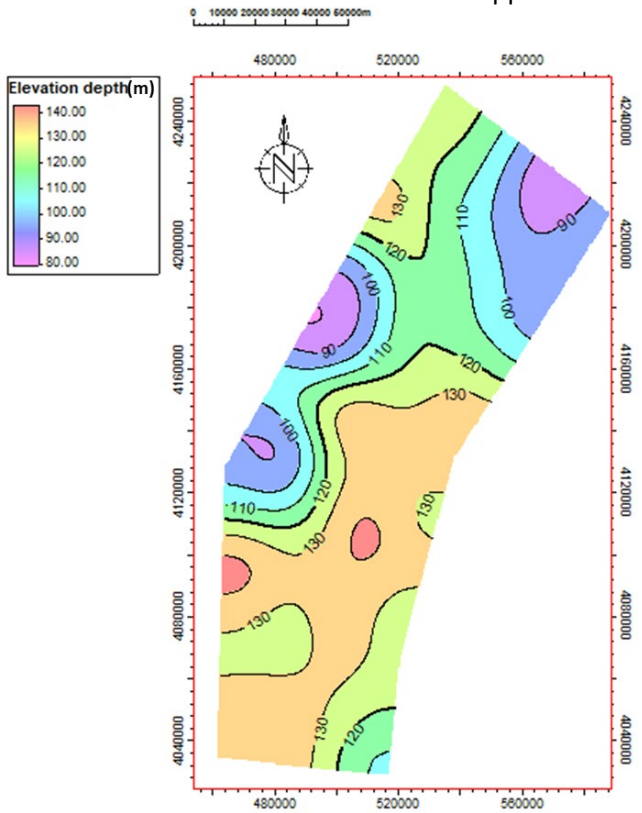

Figure 29. Isopach of the Cenomanian Interval Within the Upper Cretaceous Formation

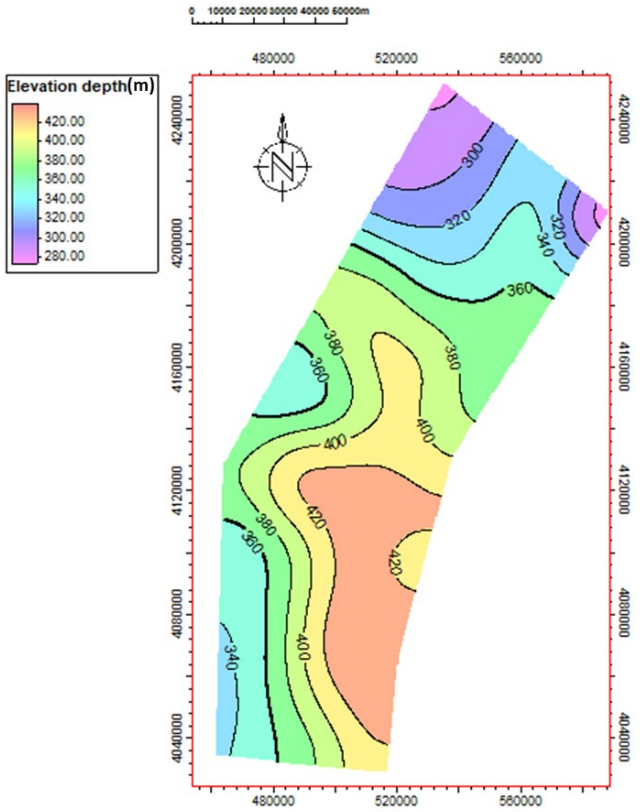

Figure 30. Isopach of the Albian Interval Within the Upper Cretaceous Formation

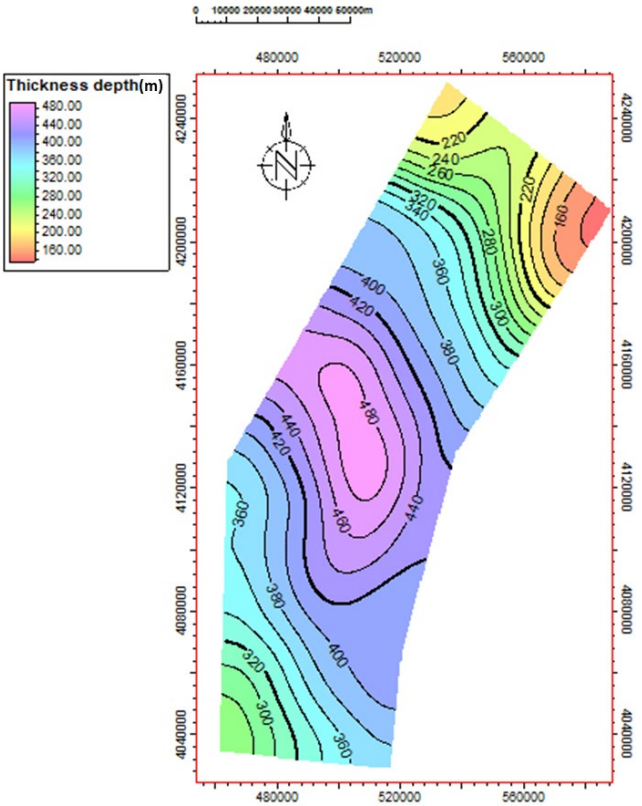

Figure 31. Isopach of the Barremian Interval Within the Upper Cretaceous Formation

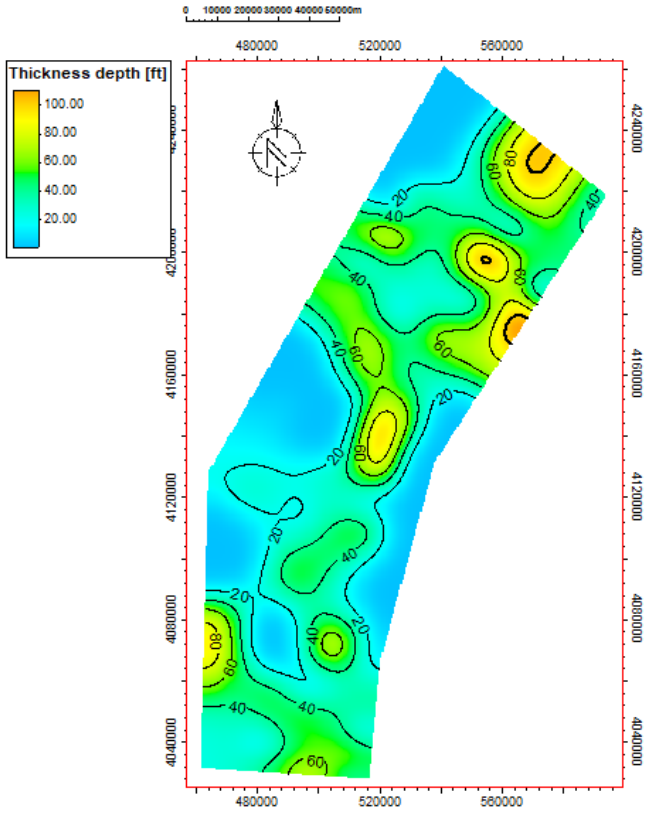

Figure 32. Estimated Sandstone Thickness Within the Maastrichtian Interval

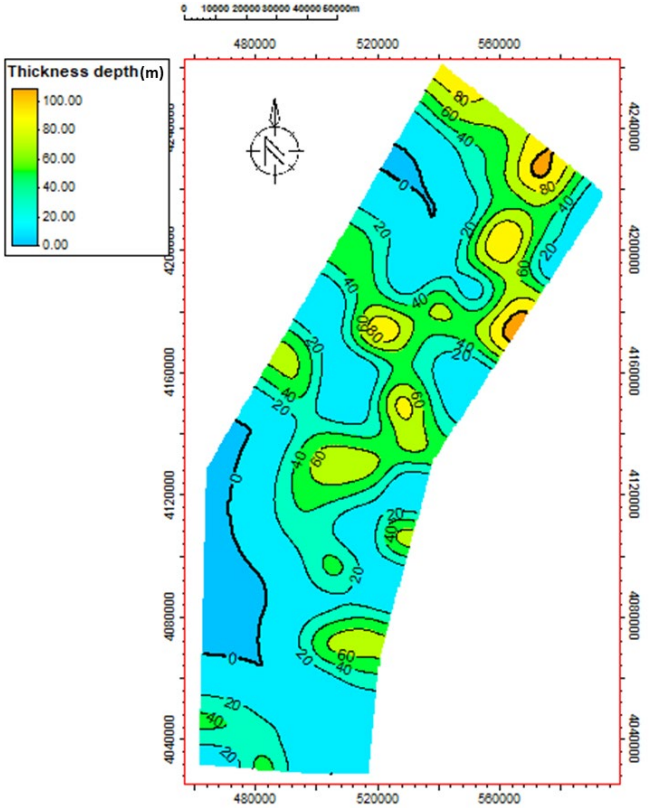

Figure 33. Estimated Sandstone Thickness Within the Santonian Interval

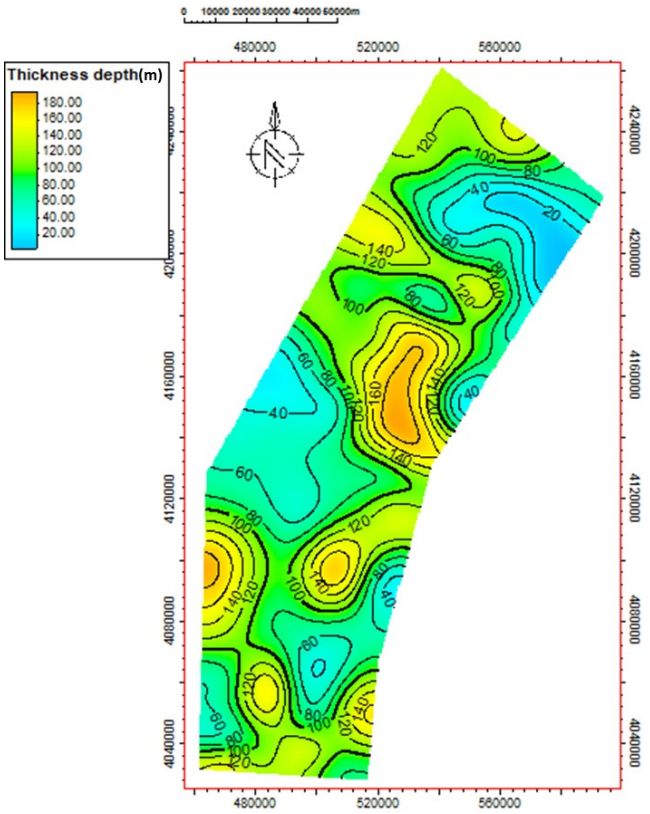

Figure 34. Estimated Sandstone Thickness Within the Coniacian Interval

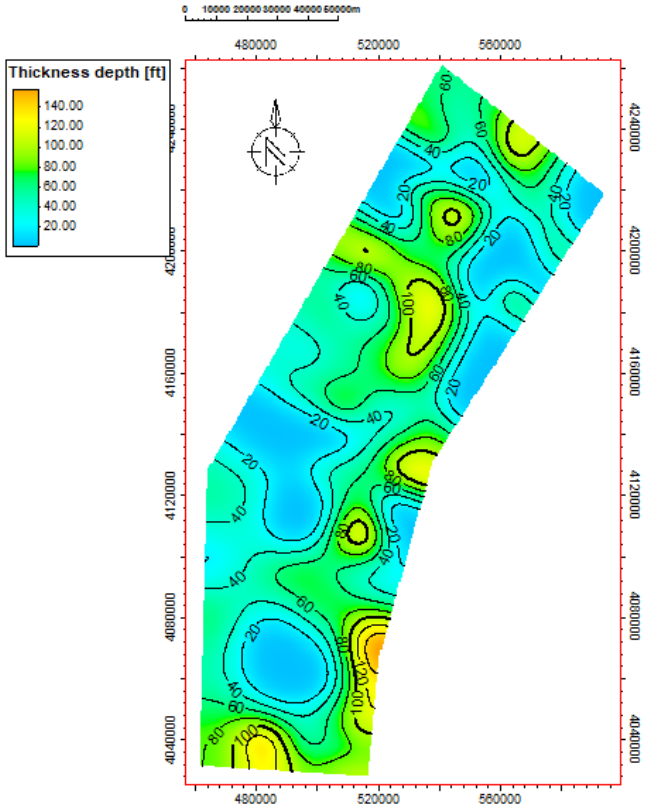

Figure 35. Estimated Sandstone Thickness Within the Cenomanian Interval

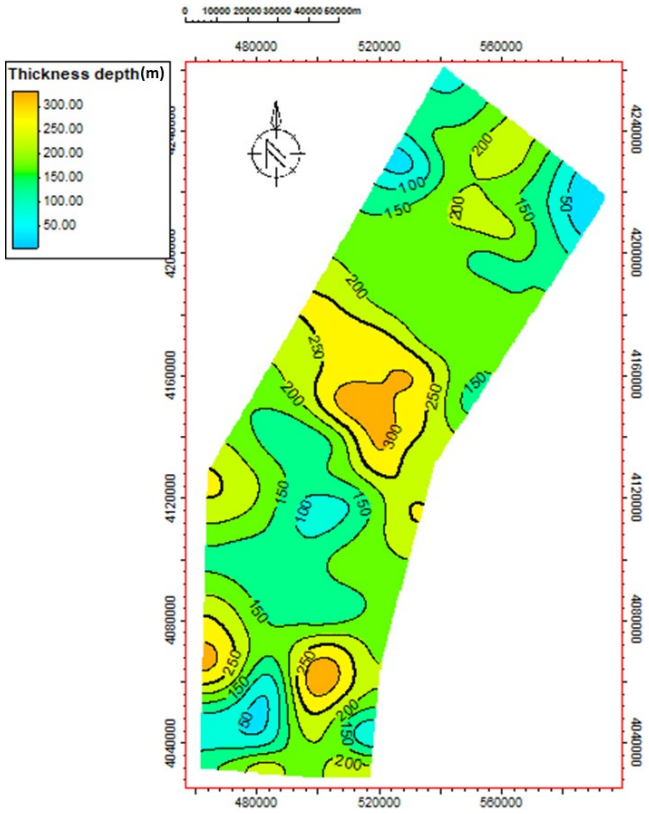

Figure 36. Estimated Sandstone Thickness Within the Albian Interval

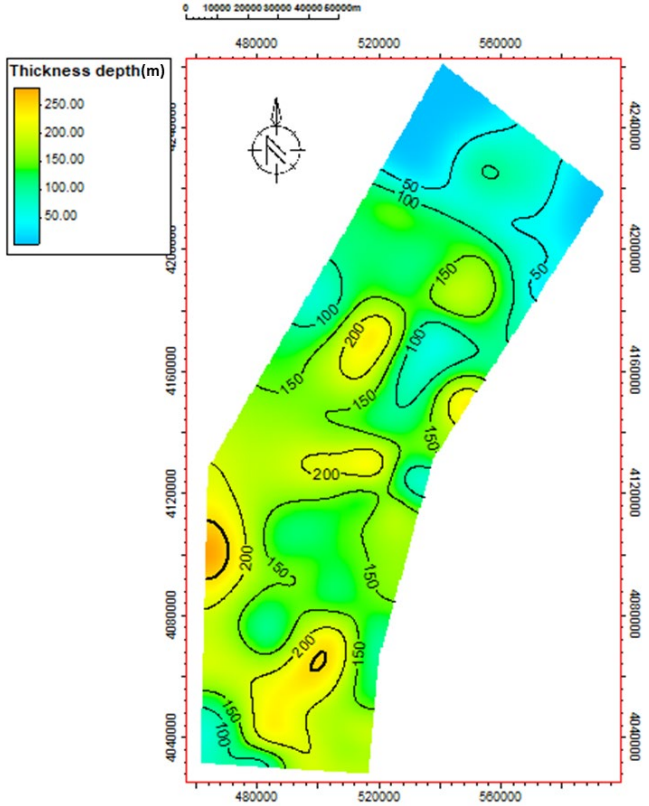

Figure 37. Estimated Sandstone Thickness Within the Barremian Interval

Subtask 5.3 - CO_2 Storage Resource

North Carolina
Based on the net-to-gross calculated from the literature, volumetric calculations were conducted for the three main target intervals identified here. Net-to-gross values were given to each interval and were extended across the study area. The model did not consider lithofacies changes within the study area, mostly because of the lack of data in other parts of the seismic polygon.

The boundary conditions applied to determine the suitable injection depth, reduced the area and depth of injection within the North Carolina study area. The Upper and Lower Cretaceous Formations located at depth between 800 and 1,600 meters are located within the area shown on Figure 38.

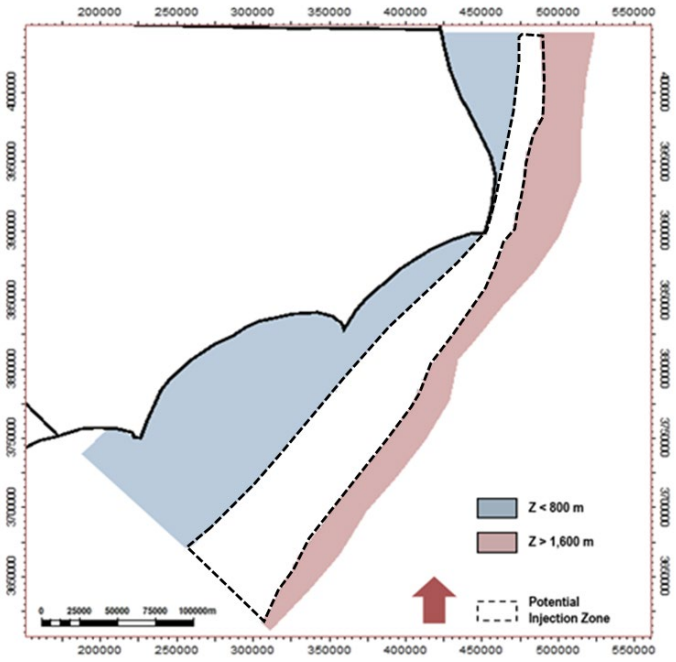

Figure 38. Potential Injection Zone for the Upper and Lower Cretaceous Formations in North Carolina

The volume of each reservoir within the potential injection zone was calculated and used to estimate the storage capability for the three identified reservoirs (methodology described above). An average porosity based on the core analysis described in Swain (1947) was used. The density of 700 kg/m^3 for supercritical CO_2 was used for the calculation. The storage efficiency refers to that of saline formations in clastic reservoirs described in Goodman et al. (2011). This coefficient represents the fraction of pore volume that will realistically be occupied by carbon dioxide. Probabilities show that this coefficient can range between 0.5% and 5.4% (10th and 90th percent probability) Goodman et al. (2011). The value for 50th percentile was also added to the calculations. The results are presented in Table 18.

						Storage Coefficient			Storage Potential (Gt)		
Formation	**Volume (m3)**	**Net Sand**	**Net to Gross**	**Density (kg/m3)**	**Porosity**	P10	P50	P90	P10	P50	P90
Maastrichtian	2.27E+12	0.37	0.9	700	0.32	0.005	0.02	0.054	**0.94**	**3.76**	**10.16**
Albian	2.55E+12	0.24	0.8	700	0.25	0.005	0.02	0.054	**0.54**	**2.14**	**5.78**
Barremian	2.83E+12	0.27	0.8	700	0.35	0.005	0.02	0.054	**0.94**	**3.75**	**10.12**
									2.41	**9.65**	**26.05**

Table 18. Storage Resource Potential of the Subsurface of North Carolina

Virginia

Core data from Cost B-2 and Cost B-3 were used to extract the average porosity, net-sand and net-to-gross ratios (Table 17). The same methodology used to assess the storage resource potential of North Carolina was used in Virginia. The area was reduced by applying the same boundary conditions to define the area and volume of each interval identified. The isopach maps below shows the area within the injection zone for each interval, that was used to calculate the volume of each potential sandstone interval and therefore the storage resource potential of Virginia (Figure 39, 40, 41, 42, 43). The Barremian interval was considered too small to display on a map but was still used to calculate the storage resource potential of Virginia.

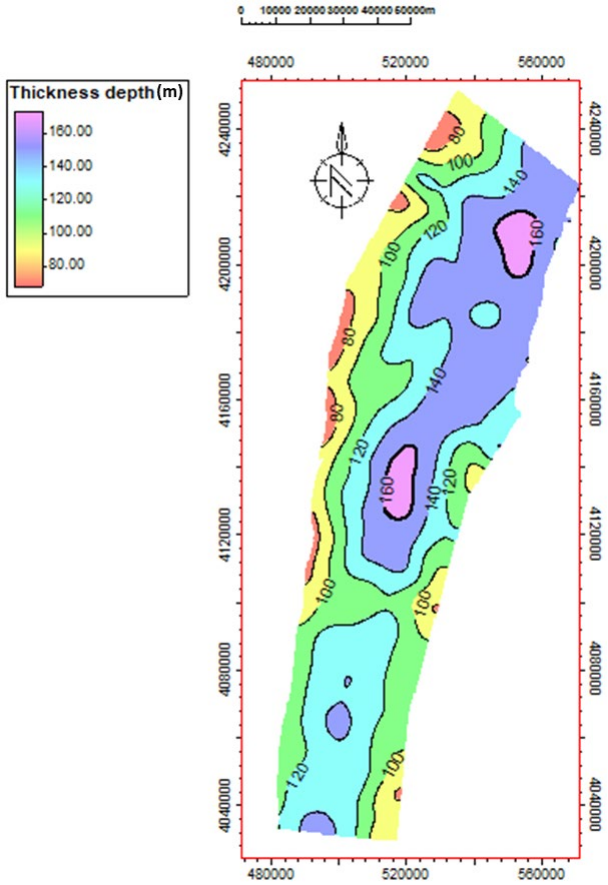

Figure 39. Isopach of the Maastrichtian Interval Within the Potential Injection Zone

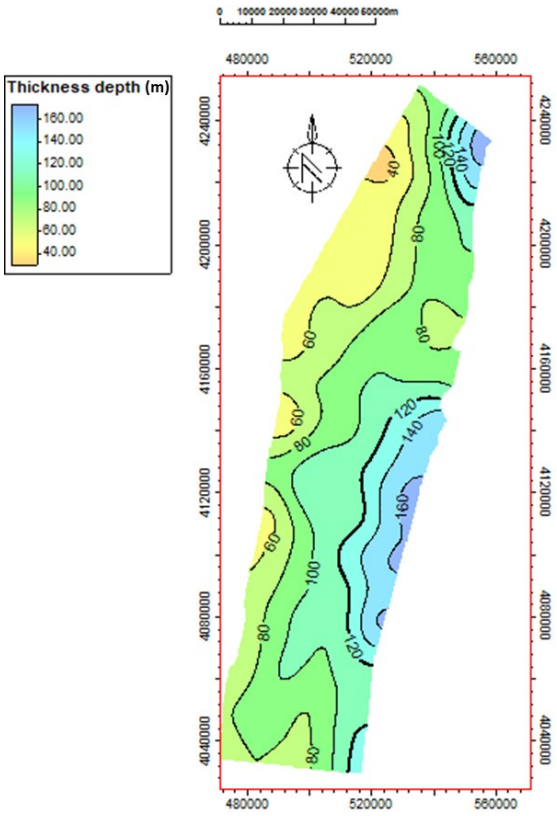

Figure 40. Isopach of the Santonian Interval Within the Potential Injection Zone

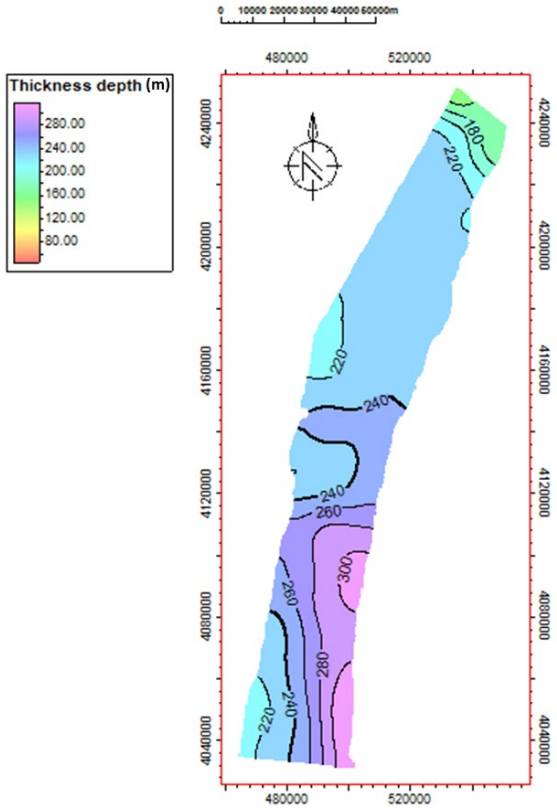

Figure 41. Isopach of the Coniacian Interval Within the Potential Injection Zone

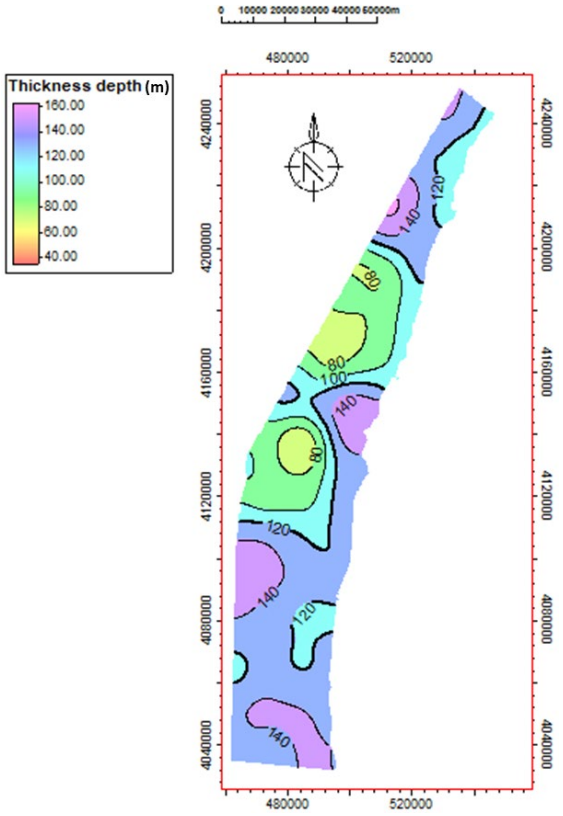

Figure 42. Isopach of the Cenomanian Interval Within the Potential Injection Zone

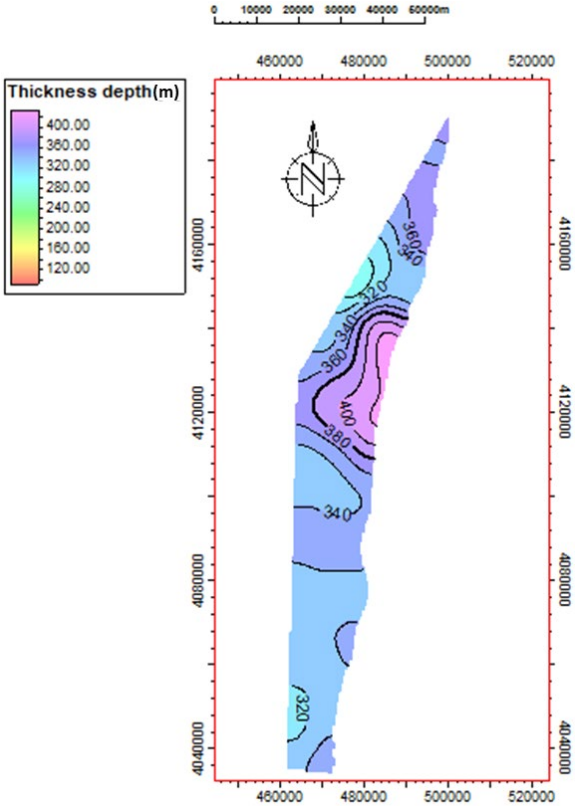

Figure 43. Isopach of the Albian Interval Within the Potential Injection Zone

The volumetric calculation for the Virginia study area is represented in Table 19.

						Storage Coefficient			Storage Potential (Gt)		
Formation	Volume (m3)	Net Sand	Net to Gross	Density (kg/m3)	Porosity	P10	P50	P90	P10	P50	P90
Maastrichtian	1.63E+12	0.3	0.9	700	0.32	0.005	0.02	0.054	**0.49**	**1.97**	**5.32**
Santonian	1.37E+12	0.27	0.9	700	0.3	0.005	0.02	0.054	**0.35**	**1.40**	**3.78**
Coniacian	3.21E+12	0.41	0.9	700	0.27	0.005	0.02	0.054	**1.12**	**4.48**	**12.09**
Cenomanian	1.65E+12	0.43	0.9	700	0.24	0.005	0.02	0.054	**0.54**	**2.15**	**5.79**
Albian	2.55E+12	0.24	0.8	700	0.19	0.005	0.02	0.054	**0.64**	**2.56**	**6.92**
Barremian	2.83E+12	0.27	0.8	700	0.21	0.005	0.02	0.054	**0.84**	**3.35**	**9.06**
									3.98	**15.91**	**42.96**

Table 19. Storage Resource Potential of the Subsurface of Virginia

Subtask 5.4 - Identification of Target Development Areas

The continental shelf of North Carolina was chosen to pursue this investigation. The unexplored oil and gas potential of this area and the geometry of the subsurface make this location a more interesting environment for the deployment of large-scale CO_2 storage projects. The distance between exploration wells in the North Atlantic and the Virginia study area makes the interpretation and reservoir characterization much more uncertain than in the North Atlantic.

Large sandstone deposits have been observed within the Upper Cretaceous Formation at the Esso-1 well. These deposits are bounded by two thick shale intervals providing top and bottom confining to the potential sandstone reservoirs (Figure 44).

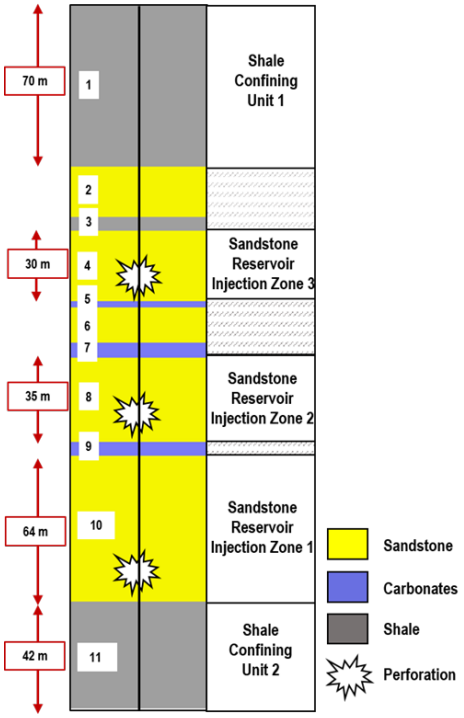

Figure 44. Cross-Section of Geomodel Representing the Sandstone Reservoirs and Confining Units

The Upper Cretaceous Formation was divided in 11 zones, each one dominated by a particular facies: sandstone, shale or carbonates (Table 20). These ratios were estimated from Esso-1 stratigraphic log presented in Brown, Miller, and Swain (1972). In this report, only sandstone reservoirs are considered suitable for carbon storage. These stacked reservoirs are represented by 3 sandstone intervals: Interval 4, 8 and 10, confined by two seals (shales) at the top and the bottom of the formation (Figure 43).

Facies %	1	2	3	4	5	6	7	8	9	10	11
Sandstone	1	95	0	90	0	95	5	90	0	90	0
Shale	99	5	95	5	5	5	0	5	5	5	99
Carbonate	0	0	5	0	95	0	95	0	95	0	1

Table 20. Facies Distribution in Each Zone of the Geomodel

Subtask 5.5 – CO_2 Storage Capacity

Reservoir simulations were conducted on multiple grids to determine the storage capacity and the efficiency factor after long period of injection of CO_2. The reservoir simulations presented below focused on a 200 km^2 area, located in the northern part of the Carolina Trough (CT), 10 km away from the shore of NC. A circular grid, with 50x50 grid blocks, was created to model the formation at depth between 1,030 to 1,440 meters below sea floor (SSD).

The reservoir was considered homogenous and therefore, average values of porosity, permeability and net-to-gross (NTG) were calculated for each facies, from the core analysis results of Esso-1 and Esso-2, published in Swain (1947). The reservoir parameters are presented in Table 2. Rock compressibility for sandstone was set as $4x10^{-10}$ bars (Zimmerman, 1990) and brine salinity as 10%. To prevent geomechanical failures and preserve borehole stability, a fracture pressure was estimated at 300 bars (30,000 kPa).

Facies	Porosity	Permeability IJ (mD)	Permeability K (mD)	Net-to-Gross
Sand	0.2	100	10	0.8
Shale	0.3	0.005	0.0005	0.2
Carbonate	0.25	0.02	0.002	0.15

Table 21. Petrophysical Properties of the Homogeneous Grid

The reservoir initial conditions were based on typical geothermal and hydrostatic gradient, of respectively 25°C/km and 0.1 bars/m. At 1,200 meters, the reservoir temperature was set as 35°C and the pressure as 120 bars.

Each simulation consisted of 50 years' continuous injection of CO_2, with a bottom hole pressure (BHP) limit set as 90% of the estimated fracture pressure (270 bars). The BHP reference depth is located at the bottom of the deepest reservoir (Injection Zone 1). Each interval was perforated and opened at different time during the injection to increase the storage capacity of each interval. During the first 25 years, CO_2 was injected in the lowest interval (Injection Zone 1), then for 15 years in Injection Zone 2 and finally 10 years in Injection Zone 3. This strategy was developed to optimize the storage of CO_2 in the deepest and thickest interval and prevent large accumulation of CO_2 below Confining Unit 1 which would decrease the risk of leakage. The initial flowrate was set a 1 million metric tons per year (MT) and constrained by the maximum BHP of 270 bars (27,000 kPa).

The numbers of wells as well as the well spacing varied for each run to determine which scenario would optimize the storage capacity of CO_2 (Figure 45) and range between 1 to 10 wells with a spacing between 2 to 8 km. Five combinations of wells were tested for each run (1, 2, 3, 5 and 10 injector wells) and are described in Table 22.

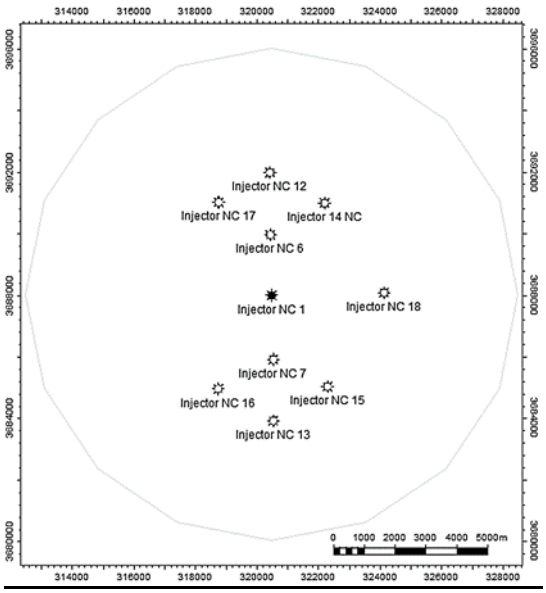

Figure 45. Well Distribution and Spacing on the 200 km^2 Grid

# of Wells in Runs	NC 1	NC 6	NC 7	NC 12	NC 13	NC 14	NC 15	NC 16	NC 17	NC 18
1	x									
2	x	x								
3	x			x	x					
5	x	x	x	x	x					
10	x	x	x	x	x	x	x	x	x	x

Table 22. Well Combination for Variable Number of Wells Used in Runs

Laterals boundaries were not identified by this study and therefore both cases of open and confined system must be investigated.

Confined Aquifer Results

To simulate a confined aquifer, a no flow-boundary condition was selected to prevent any fluid migration outside of the reservoir. The storage capacity of a homogeneous confined aquifer was estimated for multiple injection scenarios and a sensitivity analysis was then conducted to determine the effect of reservoir dimensions, well spacing and rock compressibility on the storage capacity.

Storage Capacity Estimation in Homogeneous Aquifer

Five different cases were run on a homogeneous grid. Table 23 describes the estimated storage capacity in this type of aquifer for these five cases with a well spacing of 2 km.

Boundary Condition No flow			*200 km² Grid*		
Simulation Scenario	**Target Injection Rate (MT/Year/well)**	**# of Wells**	**Max BHP (bar)**	**Storage Capacity (MT)**	**Injection Rate (MT)/ Year**
Case 1	1	1	266	50	1
Case 2	1	2	270	61	1.22
Case 3	1	3	270	62.6	1.25
Case 4	1	5	70	63.5	1.27
Case 5	1	10	270	64.5	1.29

Table 23. Storage Capacity Estimations in a Homogeneous 200 km^2 Aquifer

Only Case 1 maintained the set injection rate for the entire injection period. The results show that the injectivity is greater for Case 1 as increasing the number of wells only increase the storage capacity by 25 to 30% each year. The pressure constraint set at 270 bars, limit the injection for cases with more than one well injecting at the same time for wells spaced 2 km apart. These observations can be explained by the large pressure build-up observed in the aquifer when other wells are added to the simulation. This pressure build-up affects each well, as the BHP reaches its limit early on during the injection. Therefore, to remain below the pressure limit, the injection rate is adjusted in all wells affected by the pressure build-up.

Effect of Well Spacing on Storage Capacity

In the previous section Case 2 was identified as the best-case scenario for multi-wells injection strategies in this type of aquifer (Table 23). However, to potentially increase the storage capacity in this aquifer, the effect of well spacing on the storage capacity was investigated. Scenarios with two wells spaced by 4 km (NC 6 and NC 7) and 8 km (NC 12 and NC 13) were tested (respectively Case 6 and Case 7) and compared to Case 2 (2 km well spacing) (Figure 46).

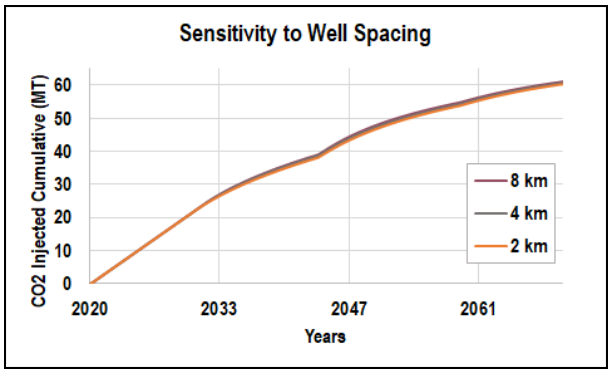

Figure 46. Comparison of Storage Capacity Estimation for Variable Well Spacing (2,4 and 8 km)

Figure 46 highlights that the well spacing does not impact the storage capacity in this type of aquifer. The pressure constraint set at 270 bars limits the flowrate of CO_2 for the three different cases presented above and average 0.6 MT/ year per well. These results confirm that the communication of pressure has an effect over long distances (2,4 and 8 km). To prevent geomechanical failures in the borehole and in the aquifer, the flowrate needs to be limited early on for multi-wells injection strategies for any type of well spacing.

Sensitivity to Aquifer Dimensions

Reservoir dimensions were then tested to quantify the effect of variable distance to lateral boundaries on the storage capacity of a confined aquifer. A 100 km^2 and 300 km^2 grid were designed to reduce and extend the reservoir dimensions. Table 24 shows that a reduction of 50% of the aquifer size, decreases the storage capacity by 33 to 45%. Whereas, an expansion of the aquifer (300 km^2), increases the storage capacity due to the increase productivity of additional wells (up to 60%) (Table 25).

Boundary Condition No flow			*100 km² Grid*		
Simulation Scenario	**Target Injection Rate (MT/Year/well)**	**# of Wells**	**Max BHP (bar)**	**Storage Capacity (MT)**	**Injection Rate (MT)/ Year**
Case 1	1	1	270	33.6	0.67
Case 2	1	2	270	34.5	0.689
Case 3	1	3	270	34.7	0.693
Case 4	1	5	270	34.8	0.696
Case 5	1	10	270	35	0.7

Table 24

Boundary Condition No flow			*300 km² Grid*			
Simulation Scenario	**Target Injection Rate (MT/Year/well)**	**# of Wells**	**Max BHP**	**Storage Capacity**	**Injection Rate / Year**	**% Variation from 200 km²**
Case 1	1	1	218	50	1	**0%**
Case 2	1	2	270	87	1.74	**+42.6%**
Case 3	1	3	270	93.7	1.87	**+49.7%**
Case 4	1	5	270	102	2.03	**+60.6%**
Case 5	1	10	270	103	2	**+59.7**

Table 24. Storage Capacity Estimations in a Homogeneous 300 km^2 Aquifer

These results demonstrate the importance of knowing the reservoir dimension to estimate the storage capacity but also determine which injection strategy should be implemented. In a 100 km^2 aquifer, the injection of less than 1 MT/year appear to be the safest option (maximum flowrate of 0.67 MT/year) whereas on a larger grid (200 km^2 and 300 km^2), injecting 1MT/ year can be done while remaining below the fracture pressure. In the largest aquifer (200 and 300 km^2), a higher flowrate than 1 MT/year can be considered, as the BHP limit was not reached in both cases.

Determination of Maximum Injection Rate in 100 km^2, 200 km^2 and 300 km^2 Aquifers

On the original 200 km^2 aquifer, a different maximum injection rate was tested for the case with the best productivity (Case 1). This case was given a target flowrate of 2 MT per year with the same pressure constraint previously used. These simulations were run to quantify the maximum injection rate a single well can support in variable aquifer geometries. The results are presented in Table 26.

Boundary Condition No flow			*100 km² Grid*			*200 km² Grid*			*300 km² Grid*		
Simulation Scenario	**Target Injection Rate (MT/Year/well)**	**# of Wells**	**Max BHP (bar)**	**Storage Capacity (MT)**	**Injection Rate (MT)/ Year**	**Max BHP (bar)**	**Storage Capacity (MT)**	**Injection Rate (MT)/ Year**	**Max BHP (bar)**	**Storage Capacity (MT)**	**Injection Rate (MT)/ Year**
Case 1	2	1	270	34	0.7	270	57.5	1.15	270	83.5	1.67

Table 26

The maximum injection rate in a small aquifer (100 km^2) cannot exceed more than 0.7 MT/year. Another simulation showed that a 200 km^2 aquifer could support a flowrate of 1.15 MT/year which represent a 64% increase in storage capacity each year compared to a small aquifer. Then, a larger confined aquifer showed the capability to store up to 1.67 MT/year, or a 31% increase from the storage capacity of a medium size aquifer.

The dimensions and geometry of a potential geological target play a crucial part in determining the storage capacity of a confined saline aquifer. However, for all the tested cases, it appears that a single vertical injector well provides the best injectivity under the given conditions used for these simulations. Due to the fast diffusion of pressure over long distances in the aquifer, additional wells appear to be unnecessary as the injection in one well at the maximum injection rate estimated above (Table 26) lead to a higher injectivity than 2 or more combined wells.

Storage Capacity Sensitivity to Sandstone Compressibility

Lastly, sandstone reservoir total compressibility represents one of the main unknown parameters and can vary greatly depending on the composition of the formation. A sensitivity analysis of this parameter was conducted on all cases described in Figure 46. Compressibility values were adjusted by one order of magnitude with a minimum sandstone compressibility of 9x10^{-11} Pa^{-1} and a maximum value of 2x10^{-9} Pa^{-1} to assess the impact of this parameter on the storage capacity (Zimmerman, 1990).

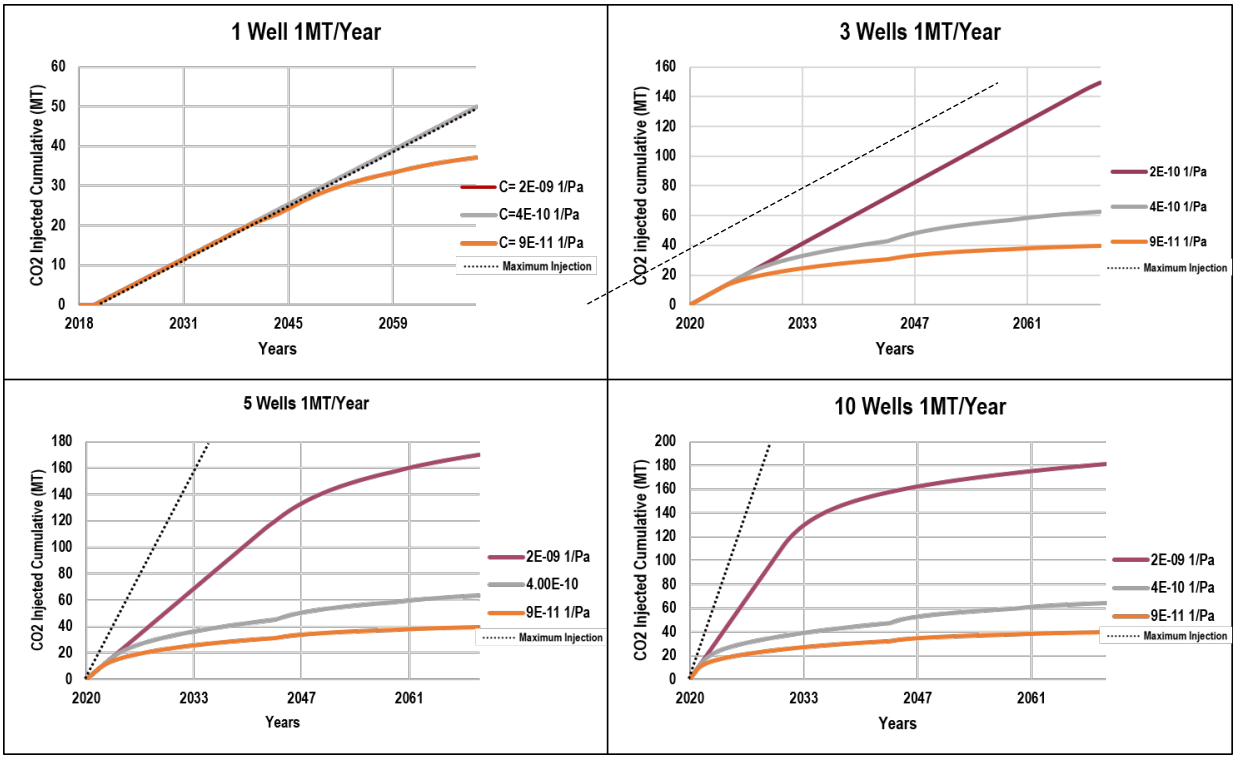

Figure 48. Effect of Rock Compressibility on the Storage Capacity of a Confined Aquifer

The results of these simulation presented in Figure 48, show a high impact of the rock compressibility on the storage capacity of a 200 km^2 confined homogeneous aquifer especially on multi-wells runs. The dotted line represents the slope of the storage capacity if the injection rate was maintained at 1 MT/year for 50 years. Every multi-well simulation showed an adjustment of the CO_2 flowrate after a short period of time for every compressibility tested. However, higher compressibility value can drastically increase the storage capacity of this aquifer by 130% for 3 wells runs and 180% for 10 wells runs. Whereas, a lower value can reduce this

capacity by 40% on average. These results can be explained by a variable change in available pore volume due to formation and brine compressibility and increased fluid pressure during the injection. The rock compressibility directly impacts the pore volume multiplier and therefore the variation of reservoir pore volume under increased pressure conditions observed during CO_2 injection. For higher rock total compressibility values, when the fluid pressure increases, the bulk and fluid in place adjust their state to accommodate the increased fluid volume providing more available pore space. This increase in pore space limits the pressure build-up in the aquifer and allows a higher injectivity of CO_2. Inversely, lower compressibility values lead to a limited injectivity in all scenarios due to less pore space available at higher-pressure conditions.

Storage capacity predictions for a homogeneous confined aquifer widely depend on the knowledge of the aquifer. These scenarios ran in this section showed the sensitivity of the storage capacity to two main parameters: reservoir dimensions and rock compressibility. However, other should be mentioned such as the estimated fracture pressure, which depends on the geological specificity of the injection site. The sensitivity to this parameter was not investigated for this publication.

Case study of heterogeneous reservoir

To understand the effect of heterogeneity of reservoir parameters in the same type of aquifer on the storage capacity, a range of reservoir parameters was randomly distributed in the geomodel. Ranges for permeability (IJK), porosity and Net-Reservoir for the three lithologies present in the geomodel were extracted from publications and publicly available data (Brown et al., 1972; Spangler, 1950; Swain, 1947). Identical injection scenarios were run on the heterogeneous model; however, perforations depth was adjusted to fit in sandstone's high permeability and high porosity zones.

Model and Simulation Set-up

To obtain a realistic range of reservoir properties that could potentially apply to the study area, core data from wells located on the coastal plain of North Carolina were analyzed to extract reservoir properties for the 3 lithologies present in the geomodel (Table 27). This range was calculated to consider zone with lower reservoir quality as well as zone with above average reservoir quality.

Upper Cretaceous Formation	Sandstone	Shale	Carbonate
Porosity Range	0.1-0.4	0.2-0.3	0.1-0.2
Permeability (mD) Range	1-500	0.01-0.1	0.01-0.1
Net-to-Gross Range	0.6-0.9	0.1-0.3	0.1-0.3

Table 25. Range of Reservoir Properties for Sandstone, Carbonates and Shale

Figure 48 displays the distribution of these parameters in one of the sandstone reservoirs (Injection Zone 1). The well's locations remained unchanged from the previous simulation in the homogeneous aquifer. Only the perforation's depth was adjusted to zone with better reservoir quality (higher permeability and porosity zones) to provide the highest storage capacity.

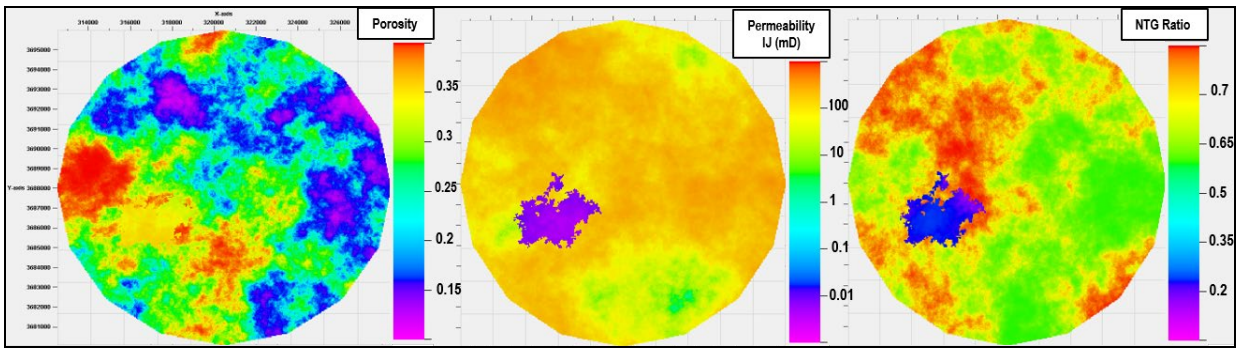

Figure 48 Reservoir Property Distribution at 1,270 meters in a 200 km^2 Aquifer

A net-to-gross (NTG) ratio was added to consider the presence of non-reservoir rocks within each sandstone reservoir. Including this ratio to the storage capacity calculation prevents overestimation of the storage capacity and can provide a more conservative estimation of the storage potential of an area.

Storage Capacity Estimation in Heterogeneous Aquifer

The results presented in Table 28 showed that in a heterogeneous 200 km^2 aquifer, a single vertical injector well still remain the best option as simulation showed that one well can successfully inject 100% of the target injection rate of 1MT/year for 50 years. Multi-wells run highlighted the difficulty for this type of aquifer to support more than one well as the addition of other well limits the injection rate from 1 to 0.7MT/year/well for Case 2, 0.5 Mt/year/well for Case 3 and 0.38 MT/year/well for Case 4. The injection of 1 MT of CO_2/year, in the 3-stacked aquifers allows the diffusion of pressure from the borehole to the aquifer at a sufficient rate to limit the BHP increase and maintain the flowrate to its initial target. However, for the multi-well cases, the diffusion of pressure in the aquifer impacts the injectivity of additional wells after a short injection time. The pressure build-up can be observed in all the confined aquifer and therefore CO_2 flowrate are adjusted for the BHP to remain below the fracture pressure limiting the storage capacity of this aquifer. These observations are similar to the one observed in a homogeneous aquifer.

Boundary Condition No flow			***200 km² Grid***		
Simulation Scenario	**Injection Rate (MT/Year)**	**# of Wells**	**Max BHP (bar)**	**Storage Capacity (MT)**	**Injection Rate (MT/ Year**
Case 1	1	1	246	50	1
Case 2	1	2	270	71.5	1.42
Case 3	1	3	270	75	1.5
Case 4	1	5	270	76	1.52

Table 26. Storage Capacity Estimations in a Heterogeneous 200 km^2 Aquifer

Comparison Between Storage Capacity of Homogeneous and Heterogeneous Aquifers

Heterogeneous aquifers showed an increased storage capacity compared to the homogeneous aquifer for multi-wells run (Figure 48). This increase in injectivity can be attributed to the presence of higher permeability zones in the aquifer. Higher permeability areas, in proximity to the wellbore, increase the diffusion of pressure, allowing the injection of CO_2 at a higher flowrate over time.

Compared to the homogeneous aquifer, a 200 km^2 heterogeneous aquifer can store 17% more CO_2 for a 2 wells injection strategy, 19% more for 3 wells and 20% more for 5 wells run. Including heterogeneity for storage capacity calculation greatly impacts the obtained results for multi wells simulation. However, the

storage capacity remains the same for Case 1 as in both homogeneous and heterogeneous cases, the injection rate remain unchanged at 1MT/year.

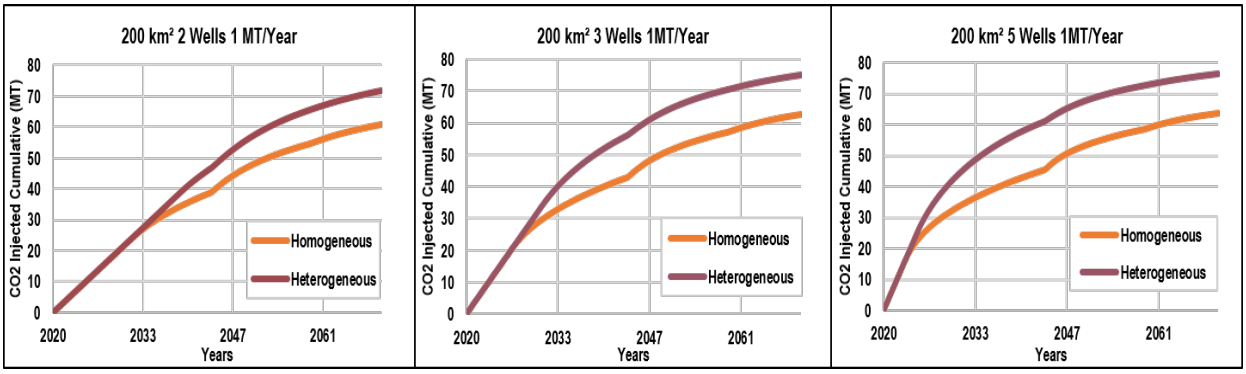

Figure 49. Comparison of Storage Capacity (MT) in a Homogeneous(orange) and Heterogeneous Aquifer (maroon).

Sensitivity to Aquifer Dimensions

A similar sensitivity test of aquifer dimension was conducted on a heterogeneous aquifer. The trend observed is equivalent to the one observed in a homogeneous aquifer.

A smaller aquifer (100 km^2) will store between 25 and 51% less CO_2, than a 200 km^2 aquifer. However, Case 1 injection rate increased from 0.67 MT/year in a homogeneous aquifer to 0.75 MT/year in a heterogeneous aquifer, which represent a 15% increase of storage capacity in 100 km^2. Case 1 remains the most adequate injection strategy in a heterogeneous aquifer with an area of 100 km^2. Multi-wells simulations are constrained by the BHP pressure limit and therefore limit the total storage capacity (Table 29) also observed in a homogeneous aquifer.

Boundary Condition No flow			***100 km² Grid***			
Simulation Scenario	**Target Injection Rate (MT/Year/well)**	**# of Wells**	**Max BHP (bar)**	**Storage Capacity (MT)**	**Injection Rate (MT)/ Year**	**% Variation from 200 km^2**
Case 1	1	1	270	37.3	0.75	**-25.4%**
Case 2	1	2	270	37.9	0.756	**-47.0%**
Case 3	1	3	270	38.1	0.76	**-49.2%**
Case 4	1	5	270	38.3	0.77	**-51.4%**

Table 29

In a 300 km^2 aquifer, similar results are observed in both homogeneous and heterogeneous reservoirs (Table 30). In both cases, Case 1 showed no injection rate adjustment which allowed the storage of 50MT of CO_2 after 50 years of injection. For multi-wells cases, increasing the aquifer sizes, also increase the storage capacity by 23 to 40% depending on the number of wells in each run. However, compared to an identical size homogeneous aquifer, the storage capacity in a heterogeneous aquifer only increased by 1.6 to 6%. In a larger aquifer, the effect of heterogeneity is less important than in smaller size aquifers. This result can be explained by a decrease in pressure build-up and therefore a BHP below the limit for longer periods, allowing a higher flowrate of CO_2 in both types of aquifer. The limited increase in storage can be attributed to higher permeability zones, which provide a better diffusion of pressure close to the wellbore.

Boundary Condition No flow			*300 km² Grid*			
Simulation Scenario	Injection Rate (MT/Year)	# of Wells	Max BHP (bar)	Storage Capacity (MT)	Injection Rate (MT)/ Year	% Variation from 200 km²
Case 1	1	1	221	50	1	**0%**
Case 2	1	2	270	88.4	1.77	**+23%**
Case 3	1	3	270	98.5	1.9	**+31%**
Case 4	1	5	270	107	2.15	**+40%**

Table 27. Storage Capacity Estimations in a Heterogeneous 300 km^2 Aquifer

In a heterogeneous aquifer, the storage capacity appears to be greater than a homogeneous aquifer. However, the aquifer dimensions and the distance to lateral boundaries still plays a crucial part in determining the storage capacity of an aquifer.

Determination of Maximum Injection Rate in 100 km^2, 200 km^2 and 300 km^2 Heterogeneous Aquifers

The injection scenario presenting the most successful injectivity remains Case 1 in a heterogeneous aquifer. Only in a smaller aquifer (100 km^2), the flowrate is lowered to 0.75 MT/year on average to maintain the BHP below 270 bars (Table 29). When the target injection rate is raised to 2MT/year, as predicted in a 100 km^2 aquifer, the injection rate remains unchanged at 0.75 MT/year. However, on a 200 km^2 aquifer and 300 km^2 aquifer, the injection rate average is respectively 1.4 and 1.7 MT/year. These injection rates represent the maximum flowrate a single injector can support while remaining below the estimated fracture pressure (Table 31). The effect of heterogeneity is especially observed on a 200 km^2 aquifer, where the maximum injection rate increases by 22% compared to the one estimated on a homogeneous aquifer. This injection rate rises from 1.15 MT/year to 1.4 MT/year. In this type of aquifer, the higher permeability zones compensate the pressure build-up, allowing the injection of CO_2 at higher flowrate than on a homogeneous aquifer.

Boundary Condition No flow			*100 km² Grid*			*200 km² Grid*			*300 km² Grid*		
Simulation Scenario	Injection Rate (MT/Year)	# of Wells	Max BHP (bar)	Storage Capacity (MT)	Injection Rate (MT)/ Year	Max BHP (bar)	Storage Capacity (MT)	Injection Rate (MT)/ Year	Max BHP (bar)	Storage Capacity (MT)	Injection Rate (MT) / Year
Case 1	2	1	270	**37.7**	0.75	270	69.7	1.4	270	85	1.7

Table 28. Maximum Injection Rate for a Single Injector Strategy

To estimate the storage capacity of a large area such as the ones presented above, the heterogeneity present in sandstone reservoirs plays a major role. This simulation highlighted the impact of heterogeneity on the storage capacity in multiple injection scenarios and with variable aquifer dimensions. The heterogeneous distribution of permeability provides high permeability zones capable of enhancing the diffusion of fluids in the reservoir and therefore diffuse the pressure away from the injection well, increasing the flowrate of CO_2 and therefore the total storage capacity.

However, to include a heterogeneous distribution of reservoir parameters in the calculation of storage capacity, a higher degree of knowledge of the aquifer is needed to prevent any overestimation or underestimations compared to a homogeneous distribution. Average values carry less uncertainty at this stage of exploration as those values are based on observed data at specific locations. In this case, core data were obtained from onshore wells located on the coastal plain of North Carolina, 15 km away from the considered aquifers. Extrapolating averaged reservoir parameters over these distances carries high uncertainty, but also provide a more conservative approach than a heterogeneous distribution of reservoir parameters.

Comparison of Storage Capacity Between Static and Dynamic Approach

The continental shelf of North Carolina represents a total area of 46,600 km^2. However, to store CO_2 under supercritical state, any potential reservoirs should be buried below the 800 m limit. Preserving seal integrity is also a crucial part of long-term geological storage of CO_2. Based on density logs from 2 offshore wells located on the continental shelf of New-Jersey, COST B-2 and COST B-3 (Amato & Simonis, 1979; Smith et al., 1976), shales become less ductile and more brittle below 1,600 m, which consequently can reduce their seal integrity. This two boundary conditions described in more depth in (Mullendore, Parent, Schlosser, & Romans, 2018), reduce the study area to a 12,400 km^2 zone (Figure 50). A small polygon of this area was removed from the volumetric calculations due to its too close proximity to the shore and its limited width (grey area on Figure 7).

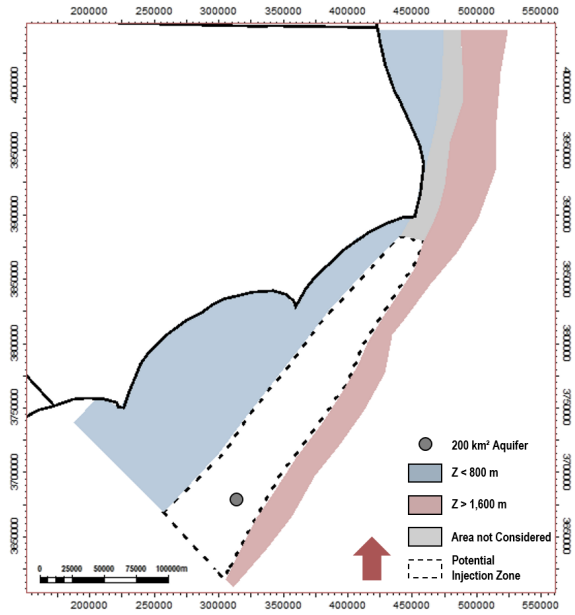

Figure 50. Potential Injection Zone Defined on the Continental Shelf of North Carolina

To estimate the storage capacity of the identified injection zone, two approach can be applied: static and dynamic. Dynamic volumetric calculations are based on reservoir numerical modelling and simulations. The storage capacity estimated in this final report are the results of the dynamic approach applied to small portions (100, 200 and 300 km^2) of the potential injection zone (Figure 50). However, During the early stages of exploration, volumetric calculation can be conducted by following a static approach.

Static Volumetric Calculation

DOE-NETL developed a static method to estimate the storage capacity of saline aquifer while incorporating an efficiency factor proper to clastic reservoirs (Equation 1). This efficiency factor was calculated by following a Monte Carlo approach based on data acquired from various clastic reservoirs and ranges between 0.5, 2.0 and 5.4 % (10th, 50th and 90th percentile) (Goodman, Sanguinito, & Levine, 2016). Other static approaches have been developed by other authors and have been summarized in (Goodman et al., 2016). To estimate the storage capacity of a saline clastic aquifer, a straightforward equation can be used (Equation 1).

$$G(CO2) = A * h * \emptyset * \mathrm{NS} * \mathrm{NTG} * \rho * E \qquad (1)$$

With:

G (CO_2): calculated storage capacity of CO_2 in GT
A: total area of the reservoir (12,400 km^2)
h: stratigraphic thickness of sandstone reservoir interval(s)
Ø: average estimated porosity of the formation)
NS: Net sandstone in the reservoir interval
NTG: Net to gross ratio
ρ: density of CO_2 at supercritical state (700 kg/m^3)
E: estimated CO_2 storage efficiency factor in clastic saline aquifer (Goodman et al., 2016)

							Storage Coefficient			Storage Potential (Gt)		
Formation	**Volume (m3)**	**Area (m2)**	**Net Sand**	**Net to Gross**	**Density (kg/m3)**	**Porosity**	P10	P50	P90	P10	P50	P90
Injection Zone 1	7.94E+11	1.24E+10	0.90	0.8	700	0.2	0.005	0.02	0.054	**0.40**	**1.60**	**4.32**
Injection Zone 2	4.34E+11	1.24E+10	0.90	0.8	700	0.2	0.005	0.02	0.054	**0.22**	**0.87**	**2.36**
Injection Zone 3	3.72E+11	1.24E+10	0.90	0.8	700	0.2	0.005	0.02	0.054	**0.19**	**0.75**	**2.02**
										0.81	**3.22**	**8.71**

Table 29 Storage Capacity Estimation Calculated with Static Approach (DOE-NETL)

The results of this approach show that for all 3 intervals combined, the storage potential ranges between 0.81 and 8.71 GT of CO_2 (Table 32).

Dynamic Volumetric Calculations

The reservoir simulations conducted in the section above only estimated the storage capacity of a limited area of the total injection zone identified on Figure 50 (100, 200 and 300 km^2). For all three aquifer dimensions, reservoir simulations identified a maximum injection rate for a scenario with a single injection well (Table 31). To extend the storage capacity to the total injection zone, the number of aquifers of each dimension that could cover the entire injection zone was calculated. The results showed that 62 aquifers with an area of 200 km^2 could be considered for CO_2 storage, 41 aquifers for 300 km^2 and 124 for 100 km^2 to cover the entire injection zone shown on Figure 49. Based on the results displayed in previous section (confined heterogeneous aquifer), the total storage capacity was estimated for the total injection zone for all three aquifer sizes (Table 33).

Aquifer Dimensions	Storage Capacity in 1 Aquifer (MT)	# of Potential Aquifers in Total Injection Zone	Total Storage Capacity (GT)
100	37.7	124	4.67
200	69.7	62	4.32
300	85	41	3.48

Table 30. Maximum Storage Capacity in the Total Injection Zones for 3 Aquifer Dimensions

The storage capacity estimations obtained by using a dynamic approach are consistent with the results obtained with the static methodology and approach the storage capacity estimated by using the P_{50} value of the efficiency factor. The efficiency factor for each aquifer was calculated individually by following the methodology described in Figure 50. The total rock compressibility provided a pore volume multiplier as a function of pressure. The efficiency factor was calculated for all three aquifers sizes and for three different rock compressibilities.

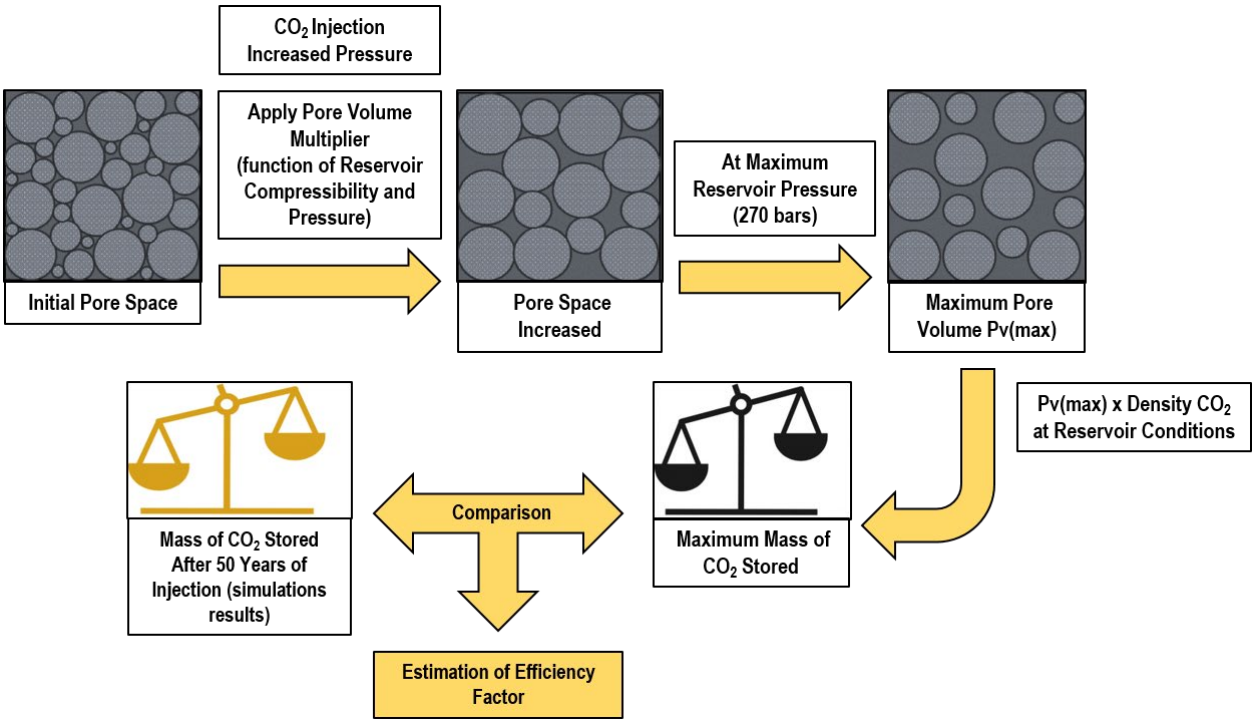

Figure 51. Methodology Used to Estimate the Storage Capacity of Each Aquifer

The efficiency factor estimated by the dynamic approach (reservoir simulation), considered a pressure gradient in the reservoir and also the variation in density of CO_2 under different pressure conditions. Including these parameters, provides an accurate estimation of the maximum mass of CO_2 that could be stored in the 3 sandstone intervals. When compared to the actual mass of CO_2 injected after 50 years of continuous injection estimated by reservoir simulations, an efficiency factor proper to this type of formation and reservoir conditions can be calculated (Table 34).

Compressibility	Aquifer Dimension	Mass of CO2 Stored After 50 Years of Injection (GT)	Maximum Mass of CO2 Stored (GT)	Efficiency %
4E-10 bars-1 (medium)	100 km2	1.28	0.03	2.34
	200 km2	2.45	0.06	2.44
	300 km2	3.84	0.08	2.08
2E-09 bars-1 (high)	100 km2	1.31	0.09	6.89
	200 km2	2.52	0.10	3.96
	300 km2	3.95	0.10	2.53
9E-11 bars-1 (low)	100 km2	1.27	0.02	1.63
	200 km2	2.44	0.04	1.69
	300 km2	3.82	0.05	1.39

Table 31. Efficiency Factor (%) for all Aquifer Dimensions and all Compressibility

Reservoir conditions with higher rock compressibility values present a higher efficiency corresponding to values between the P_{50} and P_{90} percentile of the efficiency factor value calculated by Goodman et al. (2016). A lower compressibility decreases the efficiency factor to a value ranging between the P_{10} and P_{50} percentile of the value estimated by Goodman et al. (2016). Results also showed that for median and low compressibility, the 200 km^2 aquifer presents the higher efficiency factor.

Comparing the storage capacity obtained by static volumetric calculation to the storage capacity estimated by reservoir simulation is a way for engineers to validate geomodel and initial reservoir parameters. In this case,

the results obtained by reservoir simulation are consistent with the one obtained by using the DOE-NETL methodology. In most cases, the efficiency factor estimated varied within the range provided in Goodman et al. (2016) for clastic aquifers.

To refine this analysis, additional data could be used to update the geomodel and initial reservoir conditions. The uncertainty associated with sandstone intervals' thicknesses and the associated reservoir parameters could be reduced by collecting additional high-resolution 3D seismic surveys and by drilling stratigraphic tests.

Case Study of Open Aquifer System

The lateral boundaries of the confined aquifers mentioned above were not observed on seismic data. The hypothesis of their presence was based on the poor resolution of the 2D seismic reflection data interpreted. The lateral boundaries such as stratigraphic or structural traps were believed to be below the resolution of the seismic and therefore not observable and mappable. However, in the case of absent trapping mechanisms or at too far distances, simulations were conducted in an open aquifer system. For this type of aquifer, challenges shift from pressure management to plume migration management. The overall objective of the simulation was to optimize the storage capacity while maintaining the CO_2 plume to a small area. The concerns associated with CO_2 storage in an open aquifer are various and range between unwanted migration of CO_2 and freshwater contamination but also infiltration of brine in fresh water aquifer in the coastal plain. On the East coast of the U.S, and especially in the coastal plain of North Carolina, saltwater intrusion has already been identified as problematic for freshwater aquifers. This issue is mostly attributed to over-pumping of drinking water in this area, which promotes lateral and upward migration of brine into freshwater aquifers (US-Geological-Survey, 2000). Injecting CO_2 in the subsurface on the continental shelf could enhance this issue by increasing the flow of brine away from the injection zone and towards the continental shelf. Injection strategies developed in this section are focused on limiting the CO_2 plume and therefore limit the diffusion of brine away from the injection zone.

Storage capacity in a Heterogeneous Open Aquifer System

To model a heterogeneous open aquifer system, a constant pressure boundary condition was added to the simulation to allow the evacuation of fluids outside the grid. All simulation cases tested previously on a confined aquifer, were tested on a 200 km^2 to show the storage potential of this type of aquifer. The results are presented in Table 35.

Results showed the large storage potential of this type of aquifer as all cases reached 100% injectivity for 50 years of continuous injection.

Table 32. Storage Capacity of a 200 km^2 Heterogeneous Open Aquifer

Boundary Condition Constant Pressure			***200 km² Grid***		
Simulation Scenario	**Injection Rate (MT/Year)**	**# of Wells**	**Max BHP**	**Storage Capacity**	**Injection Rate / Year**
Case 1	1	1	163	50	1
Case 2	1	2	178	100	2
Case 3	1	3	200	150	3
Case 4	1	5	213	250	5

The large storage potential of this type of aquifer is due to the limited pressure build-up in the aquifer and to the diffusion of brine outside the grid. From the initial reservoir pressure set as 140 bars, the maximum increase in reservoir pressure is observed in Case 4 when 5 wells are injecting CO_2 simultaneously for 50

years (213 bars). In all cases the pressure remains below the fracture pressure (270 bars) and therefore does not affect the injectivity of the active wells. However, as mentioned above, injecting large amount of CO_2 carries the risk of displacing large amount of brine towards to coastal plain and increase the risk of saltwater intrusion in freshwater aquifers. Any additional wells should be placed in the N-S plane from Injector 1 to increase the storage potential and limit the displacement of brine.

CO_2 Migration (Plume) In an Open Aquifer System

For the reasons mentioned above and with the objective of performing long-term monitoring of the injection zone, it is important to contain the CO_2 plume to a controlled area. Typically, 3D and 4D seismic surveys are used to monitor injector zones and can cover limited area. The plume was analyzed and quantified for a single well injection strategy with a flowrate of 2 MT/year, to understand the migration of CO_2 in a heterogeneous open aquifer. The total storage capacity of this well after 50 years of injection successfully reached 100 MT. The distribution of reservoir parameters remained unchanged from the one used in a confined aquifer.

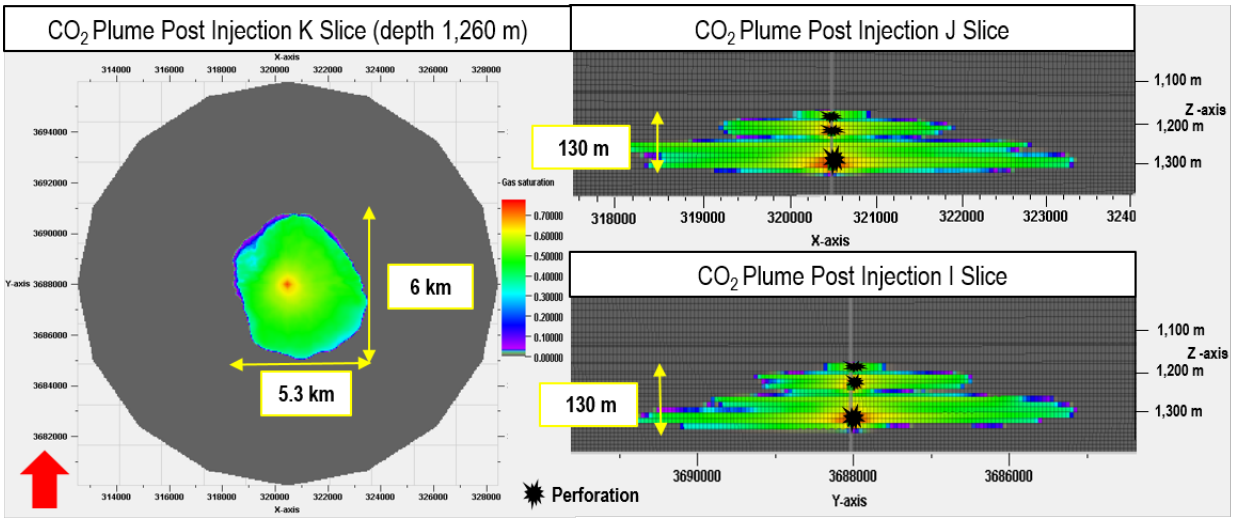

Figure 52. Plume After 50 Years of Continuous Injection at a Rate of 2 MT/year

Figure 52 shows that after 50 years of injection, the plume extension reaches approximately 5 km diameter in the N-S and E-W directions. The longer injection period in Injection zone 1 lead to a larger plume in the deepest reservoir. The upward migration of CO_2 is contained by Confining Unit 1. The thin carbonate formations present in the model act as short-term seal as they slow down the upward migration of CO_2 and encourage the lateral extension of the plume in between each injection zone. After 50 years, Confining Unit 1 remain unperturbed by the injection and appear to maintain its sealing integrity.

Despite the CO_2 plume being contained to a limited area, the “pressure plume” affects the entire grid and extend further than the grid boundaries located at an 8 km radius from the injection well. Figure 53 displays the “pressure plume” after 50 years of continuous injection. On the left, the pressure is represented at 1,260 meters below sea floor (Injection Zone 1) and shows the pressure affects the entire reservoir. On the right, a lateral view of the geomodel shows the diffusion of pressure upward and laterally. In Injection Zone 1, the pressure only increased by 40 bars from the initial pressure at the end of the injection due to the absence of lateral confinement and to the mobility of the water outside the grid.

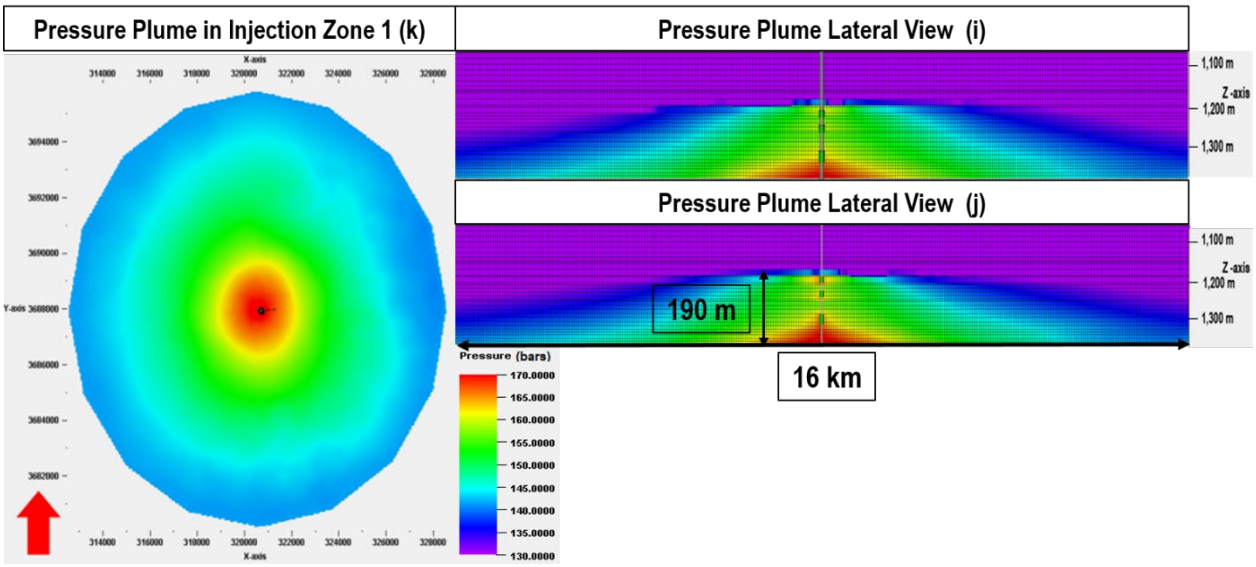

Figure 53. Pressure Plume Extension in a 200 km^2 Open Aquifer After 50 Years of Continuous Injection

Sensitivity to Net-Reservoir Ratio

The reservoir parameters used in these simulations represents a large part of the uncertainty of this study. The extrapolation of well data from onshore wells over long distances carries large uncertainty. One of the main unknowns of this study remains the presence and thickness of sandstone reservoirs. Due to the resolution of the interpreted seismic data, seismic facies analysis is difficult and therefore the interpretation relied heavily on sequence stratigraphy to predict sand deposit in this formation. The prediction obtained with this method were then combined with well data to approximate the thickness of the reservoirs and confining units to obtain the facies distribution presented in Figure 43. However, to account for this uncertainty, a sensitivity analysis was conducted to quantify the effect of a Net-to-Gross ratio or Net-Reservoir on the plume extension in an open aquifer system. A factor of ± 30% was applied to the NTG already used in the previous simulations. The results are presented in Figure 54.

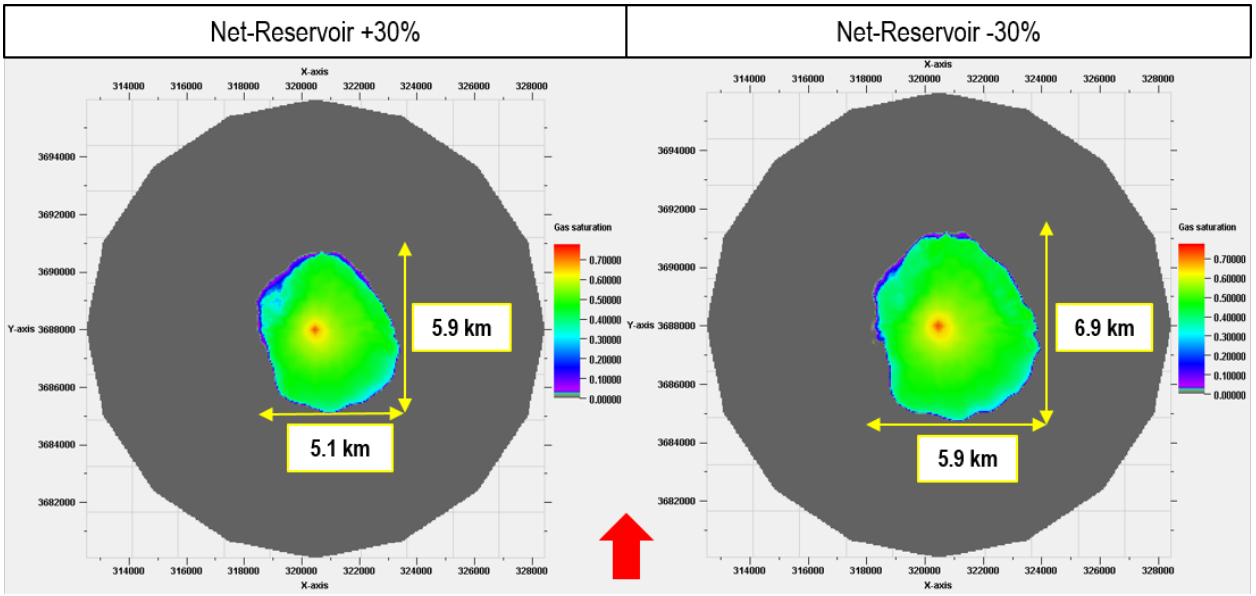

Figure 54. Plume Extension on a 200 km^2 Open Aquifer with a Factor ± 30% Applied on the NTG Ratio

The plume is not impacted much by an increase in the NTG ratio; however it increased the gas saturation in the plume as more reservoir is available in proximity to the wellbore. A decrease in the NTG ratio expands the plume by 15% in the N-S direction and 11% in the E-W direction. This observation confirms the impact of the knowledge of the aquifer to predict plume extension as much as it did on the storage capacity of a confined aquifer.

Sensitivity to Reservoir Parameters: Porosity and Permeability

A similar sensitivity analysis was then conducted to observe the effect of variable porosity and permeability in the aquifer. A factor of ± 30% was added to these properties and an identical injection strategy was tested to compare the plume extension when reservoir parameters are altered.

Figure 55 shows that a decrease in permeability, allows a limited increase in the lateral diffusion of CO_2 and therefore an extension of the plume in all directions (5% in the N-S direction and 2% in the E-W direction). Inversely, an increase in permeability slightly decreases the plume size. This analysis showed that the variation in the range of permeability has a limited impact on the plume extension.

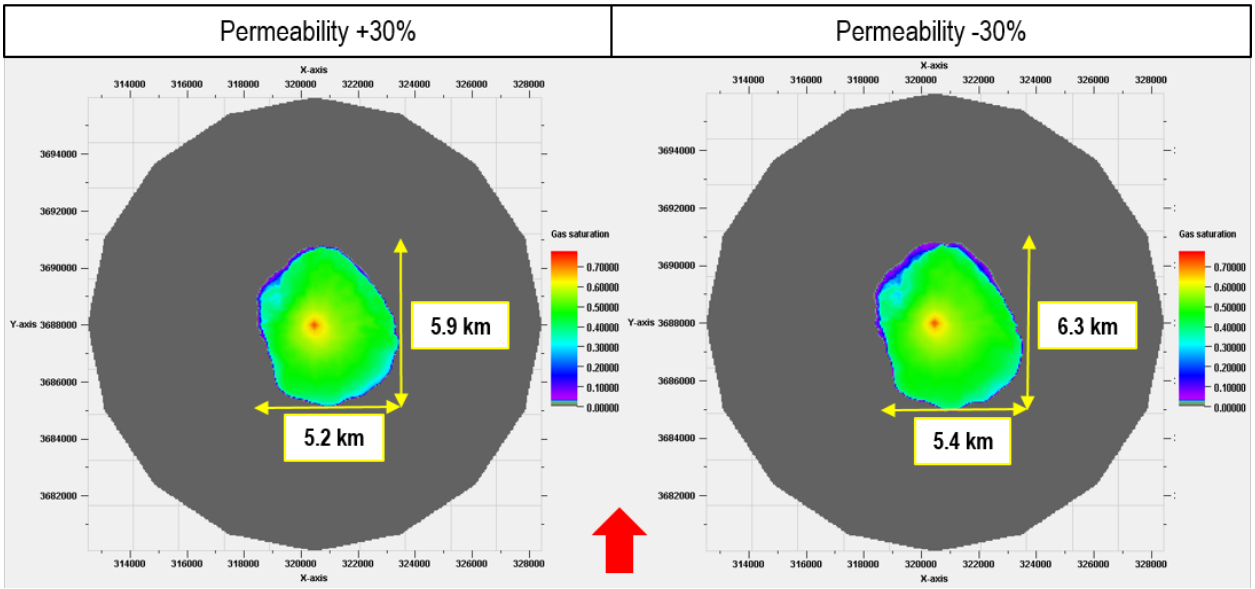

Figure 55. Plume Extension on a 200 km^2 Open Aquifer with a Factor ± 30% Applied on the Permeability

The last parameter tested for this sensitivity analysis is the porosity of the reservoir. A factor of ± 30 % was applied on this property and the results showed in Figure 55, highlight the important impact of this property on the plume extension in this type of aquifer.

An increased overall porosity can reduce the plume extension by 10% in the N-S direction and 11% in the E-W direction. Similarly, decreasing the porosity can enhance the plume extension by 13% in all directions. These results can be easily explained by the variation in available pore space occupied by CO_2. Increasing the porosity, increase the storage capacity in proximity to the wellbore, limiting the lateral expansion of the CO_2 plume.

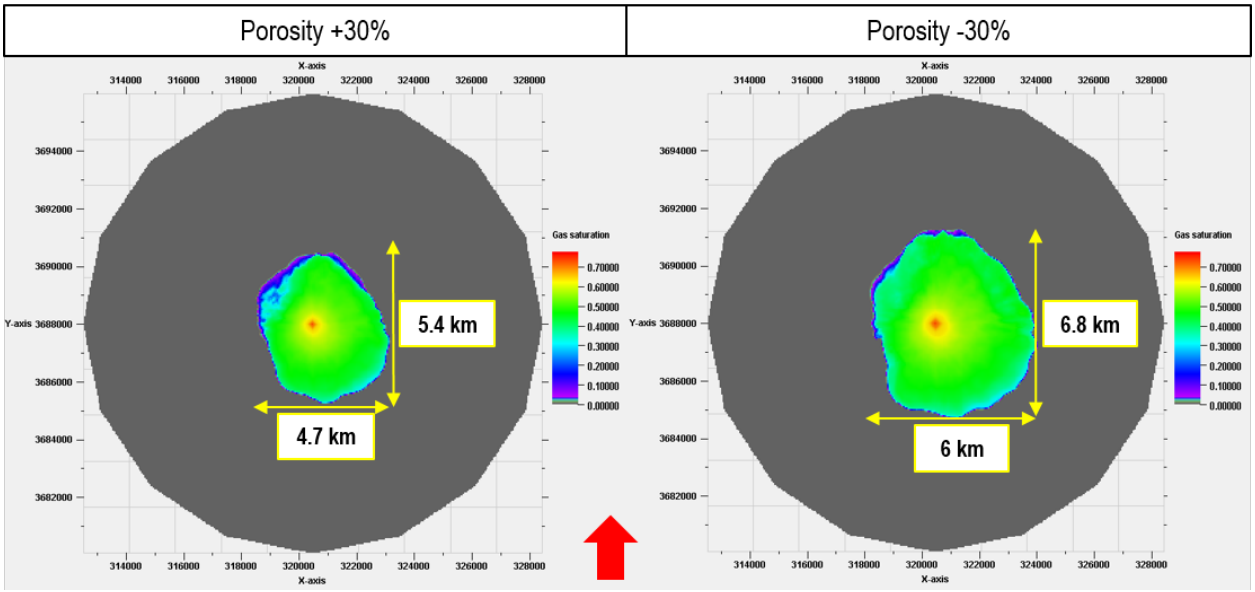

Figure 56. Plume Extension on a 200 km^2 Open Aquifer with a Factor ± 30% Applied on the Porosity

This sensitivity analysis was necessary to understand the impact of each parameter on the plume extension. The NTG ratio as well as the porosity values estimated in this paper have a large impact on the plume migration. Predicting the plume migration is as crucial as predicting the storage capacity prior to any field development. These predictions can influence the development of injection strategies that should be implemented in this type of aquifer. In this case, these simulations confirmed that any additional wells should be located in the N-S plane to prevent an increase in diffusion of brine and CO_2 towards the coastal plain. This analysis also highlighted the importance of gathering as much data as possible, as any variation in the reservoir properties impacts the plume extension and therefore the positioning of additional wells.

Uncertainty Analysis

This analysis provided the basis to understand the potential of the continental shelf of North Carolina for the geological storage of CO_2. For both types of aquifers (confined and open), the storage capacity estimations as well as the plume extension depend greatly on the density and quality of the data gathered for this assessment. At this stage of exploration, it is common to rely any resource assessment on limited datasets. However, it is important to understand that these assessments carry large uncertainties due to the lack of data. Pursuing the exploration of a study area by collecting additional data, can refine the storage capacity estimations and the prediction of plume extension.

At this stage, the main uncertainties associated with the results presented in this final report are for the most part related to the presence, extent and quality of the sandstone reservoirs. The geomodel presented is based on extrapolation of onshore or distant wells information and on sparse, low-resolution 2D seismic data analyzed and interpreted in previous publication (Mullendore, Parent, et al., 2018; Mullendore, Schlosser, Ripepi, & Xu, 2018).

Another major uncertainty lies with the estimation of the fracture pressure. The fracture pressure refers to the tensile failure pressure (Zhang & Yin, 2017) in an impermeable case, in this case the wellbore. In the eventuality of the BHP rising above the fracture pressure, the wellbore could be submitted to tensile failure and therefore lose its integrity. This parameter is important for CO_2 storage as leakage from the lack of well integrity is considered a major issue. This final report highlighted the importance of this parameters as it determines the BHP pressure limit used to calibrate the flowrate of CO_2. In a confined system, this BHP pressure limit was set to maintain borehole stability and prevent leakage from the borehole itself and from the

formation. The results showed a strong influence of this limit on the maximum flowrate for each case tested and therefore on the storage capacity. The estimation of this fracture pressure was based on geomechanical studies conducted on borehole stability. To estimate the "formation breakdown pressure", Haimson and Fairhurst (1967) proposed the model presented in equation 2.

$$P_{Max} = 3\sigma_h - \sigma_H + T \qquad (2)$$

With:
P_{Max}: the formation breakdown pressure or fracture pressure
σ_h: minimum horizontal stress
σ_H: maximum horizontal stress
T: tensile strength

Both horizontal stresses (maximum and minimum) were assumed equals in this case due to the limited data. The tensile strength was assumed to be null. Estimating the vertical stress can be deduced from the stratigraphic column and the estimated thickness and depth of each strata. The horizontal stress can be estimated by using the ratio k between vertical stress and horizontal stress described by Sheorey's model.

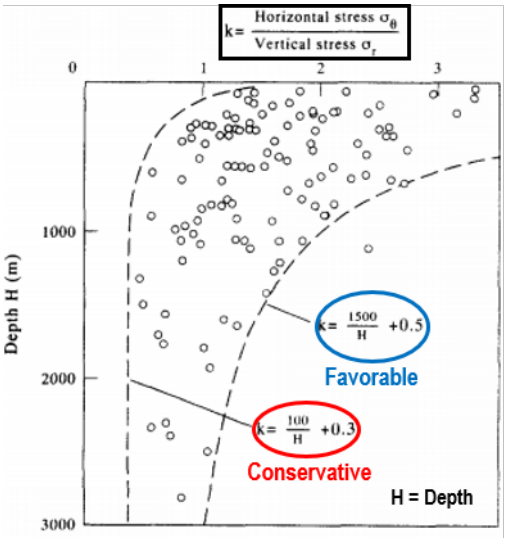

Figure 57. Ratio Between Vertical and Horizontal Stress vs Burial Depth modified from Sheorey (1994) Based on Measurements by Hoek and Brown (1980)

These two ratios (conservative and favorable) are then used to estimate the horizontal stress and deduce a conservative and favorable minimum fracture opening pressure also referred as fracture pressure (Equation 3).

$$P_{Max} = 2\sigma_V k \qquad (3)$$

With:
σ_V: vertical stress
k: ratio obtained by Sheorey's model

An average value between the conservative and favorable fracture pressure (P_{max}) calculated was chosen to determine the fracture pressure to be used in the reservoir simulations. The BHP pressure limit (270 bars) represents 90% of the estimate fracture pressure.

Many assumptions were made to obtain the estimated fracture pressure which impact the storage capacity calculated by reservoir simulations. A sensitivity analysis to this specific parameter should be conducted to quantify its effect on a storage resource assessment. Additional data could also contribute in refining the estimation of the fracture pressure by determining the stress regime on the continental shelf of North Carolina and provide a more accurate estimation of the vertical stress.

Task 8.0: Outreach

Subtask 8.1 – Public Outreach

Links to all presentations & posters can be found in the Appendix

Meetings with presentations:

1. March 2016, Southeast Offshore Storage Resource Assessment (SOSRA) – Mid-Atlantic Project Update; 11th Annual SECARB Stakeholder's Meeting, Atlanta, Georgia
2. March 2018, Southeast Offshore Storage Resource Assessment (SOSRA) – Mid-Atlantic Project Update; 13th Annual SECARB Stakeholder's Meeting, Atlanta, Georgia
3. May 2018, Southeast Offshore Storage Resource Assessment (SOSRA); Virginia Center for Coal & Energy Research Advisory Board Meeting, Kingsport, Virginia
4. August 2018, Southeast Offshore Storage Resource Assessment (SOSRA): Mid-Atlantic and Eastern Gulf of Mexico Project Update; NETL Carbon Capture, Utilization, Storage, and Oil & Gas Technologies Review Meeting, Pittsburgh, Pennsylvania
5. March 2019, SOSRA Project Overview: Mid-Atlantic Region; 14th Annual SECARB Stakeholder's Meeting, Atlanta, Georgia

Poster presentations:

1. April 2016, Southeast Offshore Storage Resource Assessment: Mid-Atlantic; International Workshop on Offshore Geologic CO_2 Storage, Austin, Texas
2. February 2019, SOSRA Reservoir Simulation Results; Society of Mining, Metallurgy and Exploration (SME) Annual Conference, Denver, Colorado

Subtask 8.2 - Knowledge Sharing and Technology Transfer

Links to all publications can be found in the Appendix

Publications:

1. Mullendore, M., Schlosser, C., Tang, X., Gilliland, E., Ripepi, N., 2018, Assessment of Geophysical Data Quality and Coverage for the Continental Shelf of Virginia and North Carolina: Geosciences, *in review*
2. Mullendore, M., Schlosser, C., Ripepi, N., 2018, CO_2 Storage Capacity Assessment in the Outer Continental Shelf of North Carolina: International Journal of Greenhouse Gas Control, *in review*

Task 9.0: Closeout and Reporting

Subtask 9.1 – Modeling-based MVA Recommendations
Information regarding this task and deliverable is reported under the Eastern Gulf of Mexico chapter.

Subtask 9.2 – Infrastructure Development Recommendations
Information regarding this task and deliverable is reported under the Eastern Gulf of Mexico chapter.

Subtask 9.3 – Target Development Recommendations
At the time of writing, a moratorium on offshore drilling and related activities in the Atlantic precludes oil and gas exploration activity that would support carbon capture, utilization, and storage characterization efforts. There is no strong indication when this moratorium will expire, and recent legislative action has indicated an interest in extending the moratorium, perhaps in perpetuity. Therefore, target development recommendations assume no coincident oil and gas development.

Existing seismic data in the Atlantic is limited to legacy 2D seismic surveys collected circa 1970-1980. Although there is an abundant inventory of legacy seismic data on the continental slopes of Virginia and North Carolina, which is a promising location for oil and gas resources, there is little to no coverage on the continental shelf which is more ideal for CO_2 storage. Additionally, these surveys lack sufficient resolution at depths suitable for CO_2 storage to warrant exploration and development activities beyond additional regional surveys.

To address these issues, a campaign of modern 3D seismic surveys should be performed to the identify and characterize extensive sand bodies that could provide a large storage capacity. This would lead into drilling of exploration boreholes to obtain reservoir properties and storage capacity estimates.

References Cited

Barnes, A. E. (1993). Instantaneous spectral bandwidth and dominant frequency with applications to seismic reflection data. Geophysics, 58(3), 419-428

Brown, P. M., Miller, J. A., & Swain, F. M. (1972). Structural and stratigraphic framework and spatial distribution of permeability of the Atlantic Coastal Plain, North Carolina to New York (2330-7102).

Dix, C. H. (1955). Seismic velocities from surface measurements. Geophysics, 20(1), 68-86.

Frigo, M., & Johnson, S. G. (2005). The design and implementation of FFTW3. Proceedings of the IEEE, 93(2), 216-231

Fugro Consultants Inc., 2015, Virginia offshore oil and gas readiness study, prepared for the Commonwealth of Virginia Department of Mines, Minerals and Energy, Fugro Project No. 04.8114.0015, 270

Fugro Consultants Inc., 2017, Mid-Atlantic outer continental shelf, Virginia and North Carolina: Geological and geophysical analysis report, prepared for Virginia polytechnic institute and state university Mining and Minerals Engineering Department, Fugro Project No. J02.16031051

Klitgord, K. D., and C. Schneider, 1994, Geophysical database of the East Coast of the United States Northern Atlantic Margin: Velocity analyses: US Geological Survey

Klitgord, K.D., Poag, C.W., Schneider, C.M., and North, L., 1994, Geophysical database of the East Coast of the United States: northern Atlantic margin - cross sections and gridded database (Georges Bank Basin, Long Island Platform, and Baltimore Canyon Trough), U.S. Geological Survey Open-File Report 94-637, 190 p

Miller, K. G., Browning, J. V., Sugarman, P. J., Monteverde, D. H., Andreasen, D. C., Lombardi, C., . . . Kopp, R. E. J. J. o. S. R. (2017). Lower to Mid-Cretaceous Sequence Stratigraphy and Characterization of CO2 Storage Potential in the Mid-Atlantic US Coastal Plain. 87(6), 609-629.

Mitchum Jr, R., Vail, P., & Thompson III, S. (1977). Seismic stratigraphy and global changes of sea level: Part 2. The depositional sequence as a basic unit for stratigraphic analysis: Section 2. Application of seismic reflection configuration to stratigraphic interpretation

Mullendore, M., Schlosser, C., Ripepi, N., & Xu, T. (2018). Overview of the Coverage and Quality of Publicly Available Vintage Geophysical Data Located on the Continental shelf of Virginia and North Carolina as Part of the Southeast Offshore Storage Resource Assessment

Poag, C. W. (1979). Stratigraphy and depositional environments of Baltimore Canyon Trough. AAPG Bulletin, 63(9), 1452-1466.

Smyth, R.C., Hovorka, S.D., Meckel, T.A., Breton, C.A., Paine, J.G., Hill, G.R., Herzog, H., Zhang, H., Li, W., 2008, Potential sinks for geologic storage of carbon dioxide generated by power plants in North and South Carolina: The University of Texas at Austin, Bureau of Economic Geology, 57 p., 4 appendices. GCCC Digital Publication Series #08-24

Spangler, W. (1950). Subsurface geology of Atlantic coastal plain of North Carolina. AAPG Bulletin, 34(1), 100-132.

Sunde, R. F., & Coffey, B. P. (2009). Lithology-Based, Sequence Stratigraphic Framework of the Mixed Siliciclastic-Carbonate Lower Cretaceous Sediments, Atlantic Coastal Plain, Eastern United States. Paper presented at the Frontiers+ Innovation, CSPG CSEG CWLS Convention.

Swain, F. (1947). Two recent wells in coastal plain of North Carolina. AAPG Bulletin, 31(11), 2054-2060.

Yilmaz, Ö. (2001). Seismic data analysis: Processing, inversion, and interpretation of seismic data: Society of exploration geophysicists.

South-Atlantic

Task 2.0: Geologic Overview

Subtask 2.1 - Main Geologic Provinces

The geology of the offshore area of the Southeastern United States is complex (Poag, 1978), therefore, a detailed description of the Atlantic Continental Shelf is included in this report. Following the latest collisional event of Laurentia and Gondwana at the end of the Paleozoic (Alleghenian), continental rifting began in the Early Mesozoic as part of the breakup of the supercontinent Pangea. Locally, this involved tectonic subsidence in restricted extensional basins, followed by thermal subsidence along the Eastern North American margin that still continues today (Dillon and Popenoe, 1988). The thermal subsidence probably ended before the Cretaceous but certainly, before the Coastal Plain sediments were deposited. Stratigraphic sequences on this passive margin are characterized by extensive lateral continuity and relatively minor structural disruption. The oldest post-rift sediments, above a regional unconformity known as the “post rift unconformity”, are of Jurassic age and are the product of rapid clastic sedimentation from erosion followed by a period of evaporite deposition and subsequent initiation of widespread, shallow water carbonate deposition with some terrigenous input (Dillon and Popenoe, 1988). Geophysical and stratigraphic studies suggest that the Jurassic section is at least 4.6 miles thick in the basins, and thickens seawards (Dillon et al., 1979). The Cretaceous section is characterized by more clastic sedimentation in the north and more carbonate deposition in the south, forming a large carbonate platform over the Blake Plateau and offshore Florida. In Upper Cretaceous, the Suwanee Strait provided clastic sedimentation to the Blake Plateau creating a distinct facies change to the neighboring offshore Florida and Bahamas carbonate platforms (Pinet and Popenoe, 1985). Strong paleo-currents controlled the sedimentation in large portions of the offshore region from the Upper Cretaceous to the Cenozoic. The Suwannee Strait eventually evolved into today’s Gulf Stream providing strong erosive power that eroded most of the Paleogene sediments on the Blake Plateau and prevented deposition off the Florida-Hatteras slope where it continues to the north along the shelf edge (Pinet and Popenoe, 1985). The major sedimentary deposits from north to south include the Carolina Trough, the Southeast Georgia Embayment, and the Blake Plateau Basin, which range in sediment column thicknesses from 10,000 to 23,000 ft (Maher and Applin, 1971).

Carolina Trough

The Carolina Trough is a long, narrow sedimentary basin located at the edge of the Atlantic Continental Shelf directly east off the coast of the Carolinas (Figure 1). The trough is roughly linear and positioned in a SW-NE trend parallel to the Eastern North American coastline. The Carolina Trough formed from initiation of rifting during the Triassic-Jurassic periods. During this time, evaporites were deposited in the trough, followed by a clastic deposition at the end of the Jurassic through the Cretaceous. This gave rise to salt diapirism as the salt beds mobilized and deformed the overlying sediments. The salt dome deformations are visible on the ocean floor, and are emplaced at a depth of 9,800 ft under water (Book, 1982). The deformations are characterized by major faults centered on the dome structures. Throughout the Cenozoic, the Gulf Stream eroded many of the sediments from the area; however, around a total of 7.5 miles of sediments is believed to have been accumulated in the Carolina Trough (Book, 1982).

Southeast Georgia Embayment

The Southeast Georgia Embayment is a broad depression plunging eastward from the Atlantic Coastal Plain (Figure 1). It is a major structural feature of the Florida - Hatteras Shelf, but is considered a minor sedimentary geologic unit compared to the other sedimentary basins in the region. Based on cores recovered from the COST GE-1 well, Paleozoic rocks sit at a depth of 10,560 ft and are overlain by probable Jurassic non-marine clasts, dolomites, coal, and anhydrite. This sedimentary sequence continued throughout the Mesozoic, until carbonate sedimentation took over in the Cretaceous. Sedimentation in the Southeast Georgia Embayment is still likely ongoing today (Dillon et al., 1975; Book, 1982).

Florida-Hatteras Slope

The Florida-Hatteras Slope is a prominent geological feature, but is not a “true’ continental slope (Figure 1). This feature separates the North American Continental Shelf from the Blake Plateau and was formed by mainly erosive processes of the Suwanee Strait. This prevented deposition on the eastern margin of the shelf while coastal margin sedimentation was unaffected, resulting in a slope-like feature (Book, 1982).

Blake Plateau Basin

The Blake Plateau Basin (Figure 1) is a major sedimentary basin formed at the same time and by the same processes that resulted in the formation of the Carolina Trough. The basin lies at depths ranging approximately from 2,000 to 3,300 ft., and its subsidence depth is much greater than the Carolina Trough. Blake Plateau has a complex geology and tectonic history (Poag, 1978). The Blake Plateau basin is separated into two parts, northern and southern, and is cut across by an east - west trending fracture system terminating at the Blake Spur on the western margin of the plateau (Dillon et al., 1979). The southern portion of the plateau is characterized by increased subsidence relative to the northern portion and is the product of new oceanic crust created during rifting. The seaward margin of the southern portion consists of reef development from the Cretaceous time. In contrast, the northern seaward margin was developed from erosional sedimentation (Book, 1982).

Subtask 2.2 - Potential Storage Units

The study area has multiple potential storage geologic units within the Cenozoic and Mesozoic, especially the Cretaceous and Upper Jurassic. In order to assess the potential CO_2 storage units offshore in the Atlantic, we performed the following preliminary geologic characterization:

- Identification and characterization of main geologic provinces and potential CO_2 storage units within the study area,
- Assessment of the stratigraphic framework, depositional setting, tectonic framework, geologic history, spatial extents, key formations, and the implications of these characteristics for carbon storage.
- Preliminary assessments of porosity and permeability, spatial extents, presence of seals and traps, proximity to other potential storage units, and other site-specific factors.

The main factors that play a significant role in the entrapment of CO_2 are porous reservoir rocks, impermeable seals, and stratigraphic and/ or structural traps. At COST GE-1 well, the reports indicate that there are impermeable beds that could act as seals for CO_2 entrapment. The thick shales and calcareous shales between 3,600 and 5,700 ft (1,100-1,750 m), as well as thinner shales and anhydrite beds in the deeper parts, are the best potential seals. In the form of shales, seals are present throughout the COST GE-1 well section. In addition, anhydrite beds, which would act as seals, are present below about 6,000 ft (1,800 m) (Scholle, 1979). Although sandstone strata are present below 10,000 ft (3,050m), they are tightly cemented and, in spite of some gas shows in GE-1, must be considered as non- reservoir units in offshore hydrocarbon exploration. Stratigraphic trapping through lateral facies changes may be of greater interest in this area than in other basins along the Atlantic offshore margin (Scholle, 1979).

Subtask 2.3 - Planning Areas
Southeast Georgia Embayment

Our efforts have focused on the Southeast Georgia Embayment (SGE) which is a broad depression plunging eastward from the Atlantic Coastal Plain (Figure 1A). It is a major structural feature of the Florida-Hatteras Shelf, and is considered a minor sedimentary geologic unit compared to the other sedimentary basins in the region (Book, 1982), but with significant storage potential. The SGE represents a transitional zone between a predominantly clastic depositional province north of Cape Hatteras and a carbonate province that includes Florida and the Bahamas.

Based on cores recovered from the COST GE-1 well (Figure 1B; Amato, 1978), Paleozoic rocks sit in the embayment at a depth of ~10,560 ft and are overlain by probable Jurassic non-marine clasts (rocks fragments), dolomites, coal, and anhydrite (Edgar, 1981). This sedimentary sequence continued throughout the Mesozoic until carbonate sedimentation took over in the Cretaceous. Sedimentation in the SGE is still likely ongoing today (Dillon et al., 1975; Book, 1982). The lithology in the COST GE-1 well has two main prospective intervals: (1) the interval from 3,300 to 4,600 ft includes Upper Cretaceous, Paleocene, and lower Eocene strata and consists of limestone and calcareous shales, and (2) the interval from 4,600 to 7,200 ft consists of limestone and dolomites interbedded with sandstones. Carbonate- cemented, feldspathic, and glauconitic sandstones at a depth of 5,800 ft indicate a major regression phase between the shallow-water restricted-shelf carbonates and the overlying fine-grained open- marine limestones. In more detail, the depth interval from about 5,700 ft to 7,200 ft contains a varied shallow marine sequence of generally medium-grained calcarenites, dolomite, and anhydrite with significant amounts of quartzitic sandstone, pyrite, and glauconite. Common rock types include oolites, fossiliferous calcarenites, dolomite, micrite, and anhydrite (Scholle, 1979).

Table 1. Wells used for acoustic impedance inversions and formation evaluations.

Well name	Long. X	Lat. Y	Water Depth (ft)	KB (ft)	TD (ft)	TVD (ft)
COST GE-1	-80.2997	30.619	136	99	13254	13254
Exxon 564-1	-80.25583	30.43972	145	81	12863	12863
Transco 1005-1	-80.2439	30.9928	134	101	11635	11635

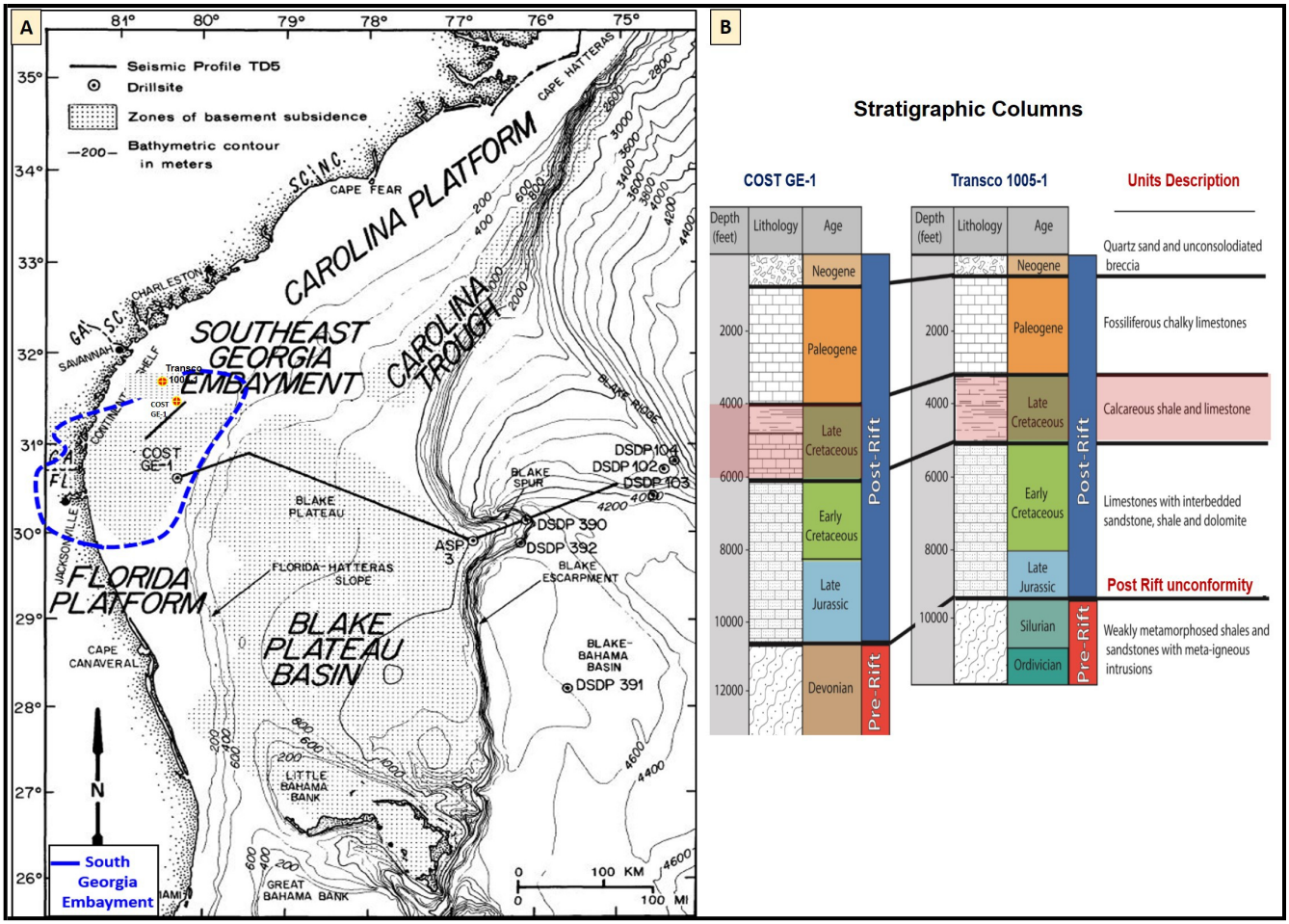

Figure 1. [A] Location map showing the main regional geologic provinces within the offshore areas considered for potential storage of CO_2, modified from (Smyth et al., 2008; Dillon, et al., 1976). [B] stratigraphic columns and lithology description at COST GE-1 and Transco 1005-1 wells, located at Southeast Georgia embayment, modified from (Pollack, 2014).

Task 3.0: Data Collection

Subtask 3.1 - Seismic Databases

The geophysical data used for this analysis include two-dimensional (2D) multichannel seismic reflection data collected on the Atlantic Margin in the late 1970's as part of geophysical and geological exploration of oil and gas prospects on the U.S. Outer Continental Shelf. The seismic dataset ID is *E08-76* and the Bureau of Ocean Energy Management (BOEM) acquired the profiles.

Hersey et al., 1959, Katz & Ewing, 1956, and Sheridan et al., 1966 provided refraction data with stratigraphic units picked. The refraction data points were acquired using 128 recording stations. 538 data points indicating stratigraphic units at various locations and depths were published. The refraction data points serve as control for the depths estimated when using the velocity model. Hersey et al., 1959 published tops of specific formations found in the refraction study. On the other hand, Katz & Ewing, 1956 and Sheridan et al., 1966 published more ambiguous data points for formations. In these 2 papers, the data points published are not tops, but rather points somewhere within the formation associated with each data point. Pre-stack data acquired in 1975 by the Institute for Geophysics at the University of Texas at Austin provides an opportunity to perform velocity analysis. The velocity analysis points serve as further control on the velocity model.

Subtask 3.2 - Well Logs

Seven exploratory wells were drilled in the south Atlantic (Figure 2), most of which providing the following logs: Borehole Compensated Sonic Log, Compensated Formation Density Log, Compensated Neutron Formation Density, Computed Log, Continuous Diameter, Dual Laterolog, Temperature Log, and Sonic Log (Table 1). For the COST GE-1 well, the USGS published a geological study in 1979 containing several key datasets such as velocity data and formation tops (Scholle, 1979). Five Atlantic Margin Coring (AMCOR) shallow wells are also present with a maximum depth of 308 m.

Three of the seven wells have the digital logs necessary to implement acoustic impedance inversion and conduct integration with seismic data (Table 1); the others have reports. All the depth references in this report are based on Kelly Bushing (KB).

Subtask 3.3 - Additional Data

In addition to seismic and well data, COST GE-1 core samples from the Delaware Geological Survey (DGS) were studied at the NETL Lab in Morgantown (WV) for both destructive and non-destructive petrophysical analyses for the purpose of comparing and calibrating with rock properties from seismic inversion as described later in the report.

From the existing COST GE-1 drill core collection at the Delaware Geological Survey (DGS), specific depth intervals were loaned and decided upon from prospective reservoir and seal recommendations in previous SOSRA studies. In total, 23 boxes and 57.1 feet of core were loaned for this study.

¾-slabbed core: The following data were generated from analyses on all 57.1 feet of ¾-slabbed core.

1. Core Photographs: Before any analyses were conducted, high-resolution and low-resolution photographs of the loaned core were taken.
2. Medical X-Ray Computed Tomography (CT) scans: These non-destructive images captured the entire 57.1 feet of loaned core at a 0.35-0.55 millimeter resolution. These data were collected in parallel to #3.
3. Multi-Sensor Core Logger (MSCL): This non-destructive analysis measured P-wave velocity, gamma density, fractional porosity, and X-Ray fluorescence (XRF) for the entire 57.1 feet of core. These data were collected in parallel to #2.

Core Plugs: The following data were generated from analyses on 7 core plugs (1” D x 2”L) extracted from the ¾-slabbed core. The specific depth of each core plug was chosen using lithologic interpretations in Scholle, 1979 and results from Medical CT scans targeting high porosity, high permeability zones as well as low-porosity, low permeability zones.

1. Industrial CT scans: These non-destructive images were generated for each core plug at a 30-42 micrometer resolution.

2. Permeability Tests: Permeabilities were collected for each core plug using a Temco UltraPerm 500 on permeable samples and a Pulse-Decay Permeameter (PDP) on impermeable samples.
3. Porosity Tests: Porosities were collected for each core plug using a Helium Porosimeter.
4. Dynamic Mechanical Tests: Each core plug underwent dynamic testing in an NER AutoLab 1500 to simulate in-situ reservoir and seal confining pressure conditions.

Task 4.0: Data Analysis

Subtask 4.1 - Quality Assessment; Subtask 4.2 - Coverage Assessment

Methodology and Data Analysis
Acoustic impedance (AI), a product of rock density and compressional velocity, can be used as an indicator of lithology and porosity, which are important for CO_2 storage assessment (Alshuhail et al., 2009; Veeken, 2007). AI provides a more detailed sub-surface geologic image than the conventional seismic section because the reflectivity coefficient (RC) on the conventional seismic section captures the layer interfaces while the AI (a layer-based property) focuses on the layers themselves (Schlumberger, 2017). However, extracting acoustic impedance properties from seismic data requires seismic inversion which implies converting seismic reflection amplitudes into impedance profiles (Alshuhail et al., 2009; CGG, 2016). This process involves removing the band-pass filter (wavelet) intrinsic to seismic acquisition and processing. In addition, it includes estimation of a background impedance model (low-frequency model), which incorporates well log data (P-wave and density) and interpreted horizons. Also, it involves wavelet extraction and inversion analysis by synthetic seismogram and finally, seismic inversion (Vukadin and Brnada, 2015; CGG, 2016; Figure 3). In this study, a series of post-stack inversion algorithms were applied to the data in order to provide a most accurate acoustic impedance model. They include Colored, Sparse-Spike, Band-Limited, and Model-Based Inversion.

Model-Based Inversion
Model-Based Inversion (MBI) starts with the convolutional theory which states that the wavelet can be convolved with the Earth's reflectivity series to generate the seismic trace after addition of noise. MBI uses well control and seismic data (interpreted horizons) to build an initial low-frequency estimated model of the acoustic impedance distribution (Maurya and Sarkar, 2016). Using an estimate of the source wavelet, the model response, in the form of synthetic seismograms, is then compared to the actual seismic traces, usually by means of cross correlation. This process is iterated several times until the model response error falls within the acceptable range that is determined by the difference between the synthetic traces calculated from the inversion and the original seismic composite trace (Lee, 2013; CGG, 2016). The MBI is implemented through the following workflow: (1) select a proper seismic line and extract the input wavelet (a critical key for a successful post stack inversion result), (2) select and correlate the well using the interpreted horizons, (3) build the initial model and apply inversion analysis, and (4) apply the inversion result to the multi 2D seismic lines.

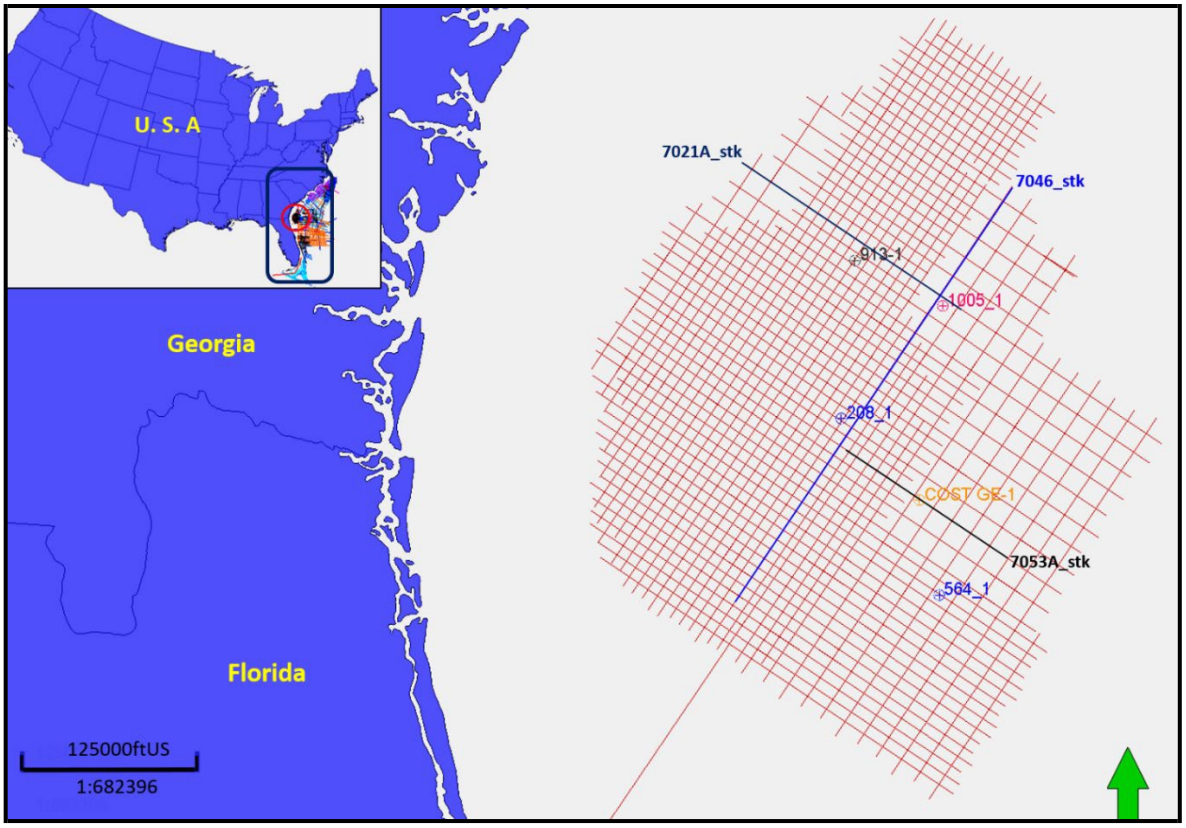

Figure 2. Location map of seismic survey and exploratory wells within the Southeast Georgia Embayment (SGE). Seismic lines used in the acoustic inversion analysis are bold.

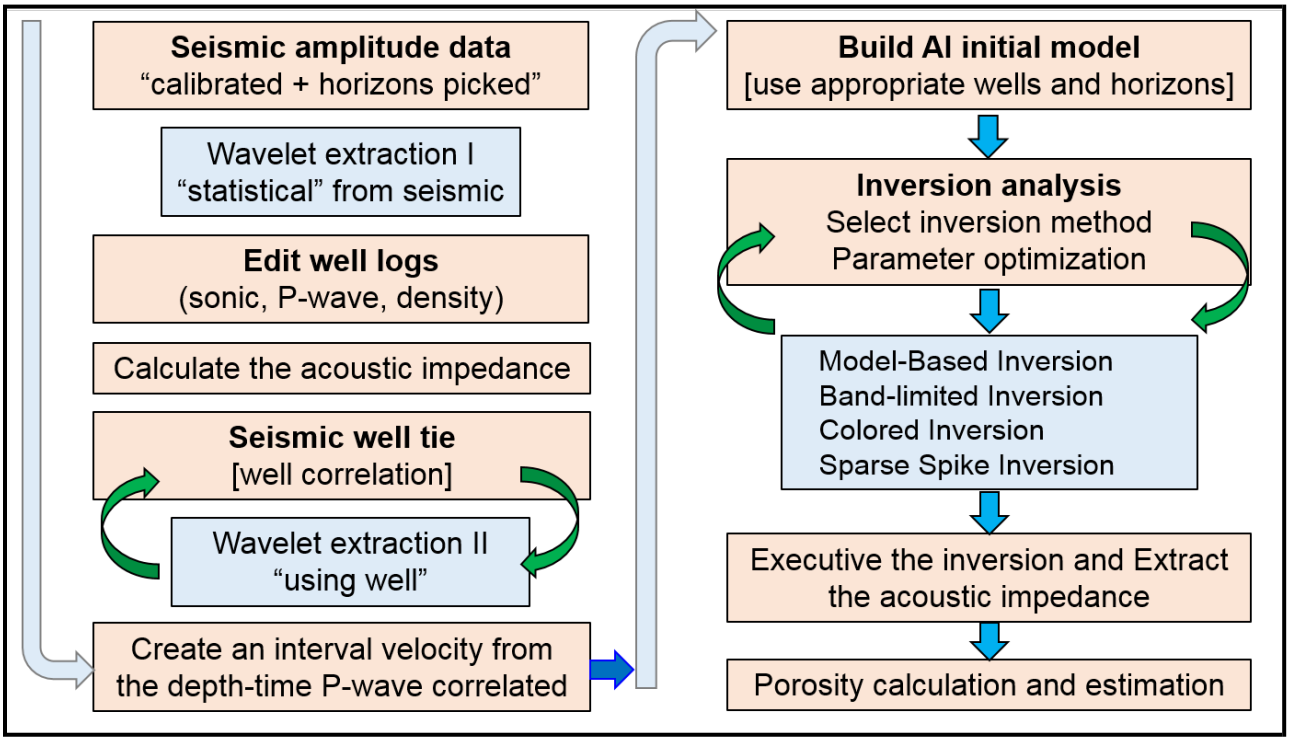

Figure 3. Flowchart outlining the seismic inversion workflow to extract the acoustic impedance.

Extract Wavelets

Two main steps were used to extract the proper wavelet.

Extract a Statistical Wavelet: a statistical wavelet (zero phase) is extracted using a nearby seismic line (Figure 4A). This involves correlating the initial synthetic seismogram with the seismic trace until getting a low correlation error percent. The algorithm extracts the wavelet amplitude spectrum by analyzing the autocorrelation of a group of traces within a selected time window that ranges from 400 to 1,500 ms. The required parameters for extracting the statistical wavelet were specified as: sample rate (4 ms), wavelet length (200 ms), phase type (constant and zero phase), and taper length (25 ms). After creating the depth-time relationship, the sonic and density logs were used to create the reflectivity series that was convolved with the wavelet to generate the synthetic seismic trace from the well logs (Lee, 2013; CGG, 2016; Maurya and Sarkar, 2016).

Extract a Wavelet from Wells: both available wells and near seismic data are used to extract another wavelet to correct the phase (Figure 4B). It extracts the wavelets by finding an operator which is convolved with reflectivity series from the well. This extracts the actual wavelet phase from the data, but it is very sensitive to the correlation quality between well logs and seismic data (Lee, 2013; CGG, 2016).

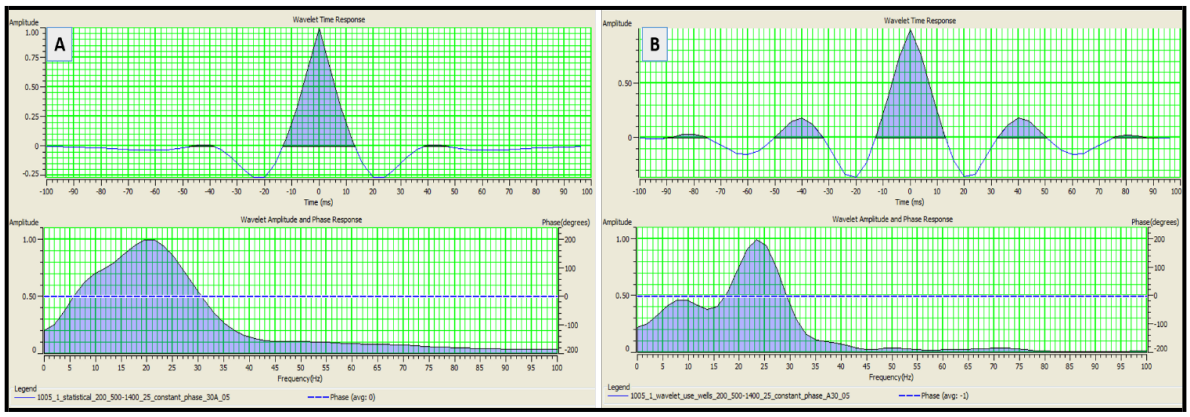

Figure 4. Extract statistical wavelets. [A] using seismic line # 7021A; and [B] using the 1005-1 well.

Generate Synthetic Seismograms

The seismic forward modeling involves convolving the seismic reflectivity series R(t) calculated from the P-wave velocity and density well logs with the wavelet W(t) extracted from the seismic data at the well location (Figure 4B) to generate a synthetic seismic trace S(t) that is subsequently correlated with the real seismic trace (Figure 5). This procedure assumes that the well logs are accurate and the velocity varies only with depth. It is also assumed that the geological structure is horizontal (Liner, 2004).

$S(t) = R(t) * W(t)$

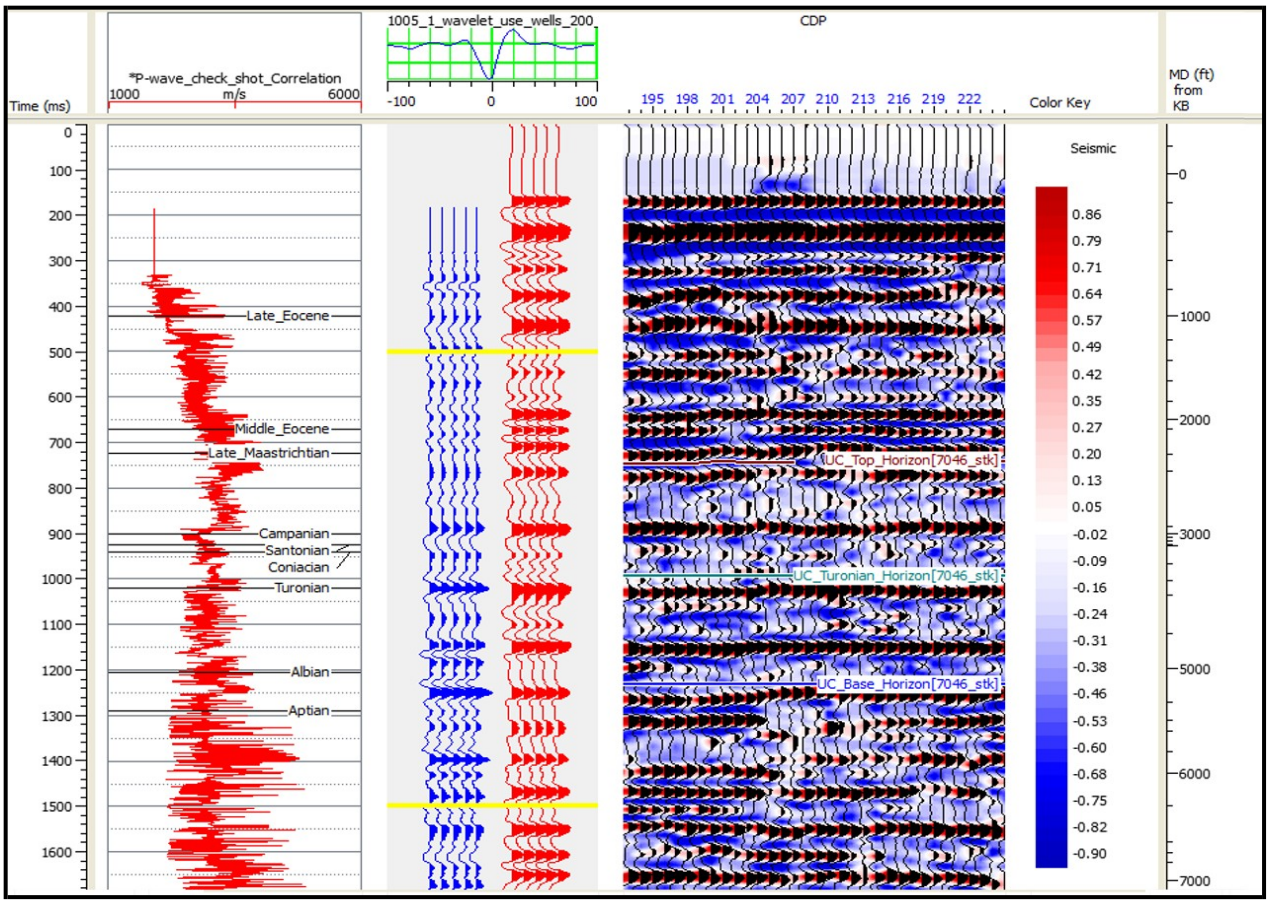

Figure 5. Seismic-well correlation achieved by matching events on the synthetic traces with the same events on the seismic traces (Transco 1005-1 well).

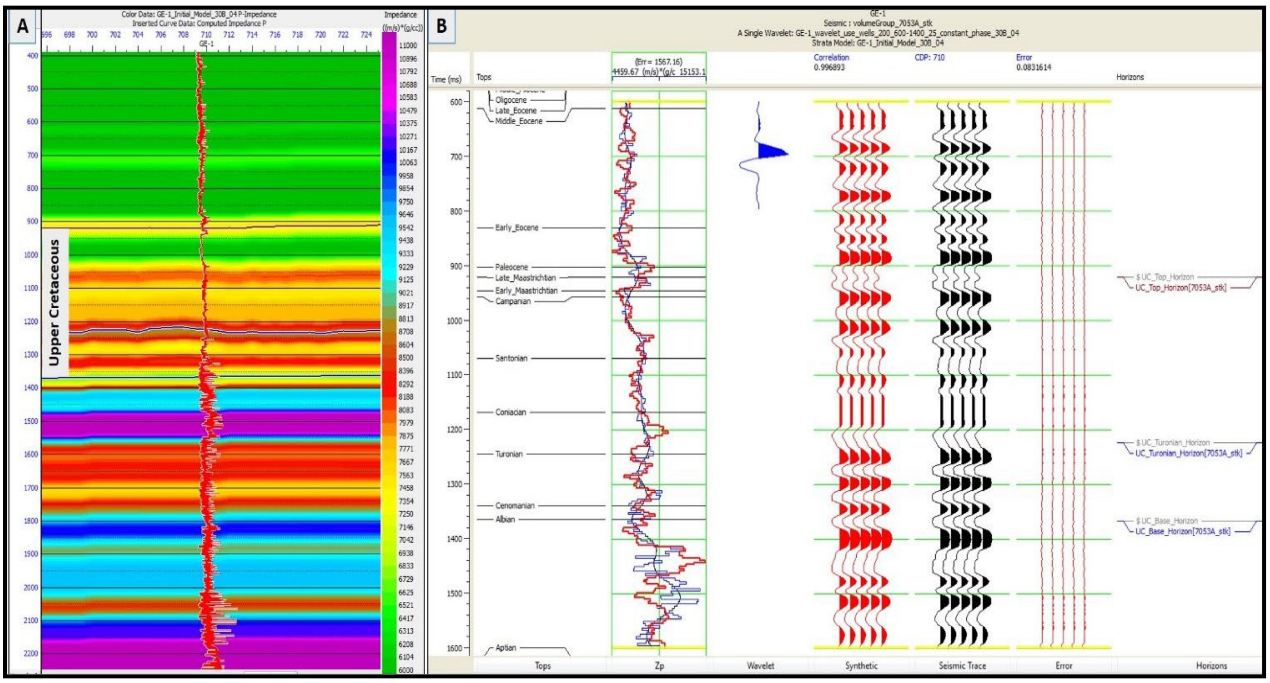

Figure 6. [A] Acoustic impedance Initial model, and [B] post stack seismic inversion analysis at the COST GE-1 well.

Subtask 4.3 - Well-Seismic Ties

Seismic-Well Correlation

It is important to relate horizon tops identified in the well logs with specific reflectors on the seismic data in order to provide acoustic impedance values for the potential reservoir and seal intervals to further estimate porosities. Therefore, seismic-well tie analysis has been conducted to compare well logs (measured in depth units), with seismic data (measured in time units), by creating a time depth relationship using the sonic log and the check shots to improve and adapt the depth-time conversion. The correlation applied included (1) using key well tops to match peak–peak or trough–trough, (2) using bulk shift to tie synthetic to seismic or variable time shift to move and stretch two or more horizons, and
(3) using the alignment points to make small adjustments between the synthetic and real seismic data (Cubizolle, et al., 2015; Figure 5).

Build Initial Model and Inversion Analysis

The initial impedance model is generated by using the P-wave impedance logs calculated from the sonic and density logs with a low-pass filter. This filter passes all frequencies up to 10 Hz, filters all frequencies above 15 Hz, and interpolates the filter between those limits (Lee, 2013; CGG, 2016). The next step is to generate a 2D impedance model by interpolating the impedance at the well location using interpreted horizons to guide the interpolation (Figure 6 A). The extrapolation at the top and bottom of the well log curve depends on compaction trends in the well. The program uses a least square fit to determine a trend to use for the top and bottom of the well. The MBI analysis was performed initially at the location of the 1005-1 and COST GE-1 wells to QC the inversion results and optimize the inversion parameters, properly. It runs on the target window that ranges from 400 to 1,600 ms and evaluates the efficacy of the inversion by comparing the impedance at the well with the impedance inverted from the seismic data for each initial model (Alshuhail, 2009; Lee, 2013; CGG, 2016; Maurya and Sarkar, 2016). Figure (6 B) shows a reasonable match between the inverted acoustic impedance (in red) and the computed impedance from the well (in blue). The black curve indicates the low frequency impedance extracted from the acoustic impedance log. The synthetic traces calculated from this inversion (in red) are side-by- side with the original seismic composite traces (in black; Figure 6 B). The far-right track represents the error traces or the difference between the two previous results and it shows a low correlation error percent.

Subtask 4.4 - Seismic Interpretation

Porosity Analysis

Porosity and permeability distribution versus depth are critical factors to assess the strata for CO_2 storage. Here, porosity is calculated at the wells, extrapolated with QC to the available core data and extracted from the acoustic impedance as discussed below. As described above, a series of post-stack inversions were applied to the data in order to provide a more accurate acoustic impedance model. Figure 7 shows a comparison of all different inversions results including Colored, Sparse-Spike, Band-Limited, and Model-Based Inversion.

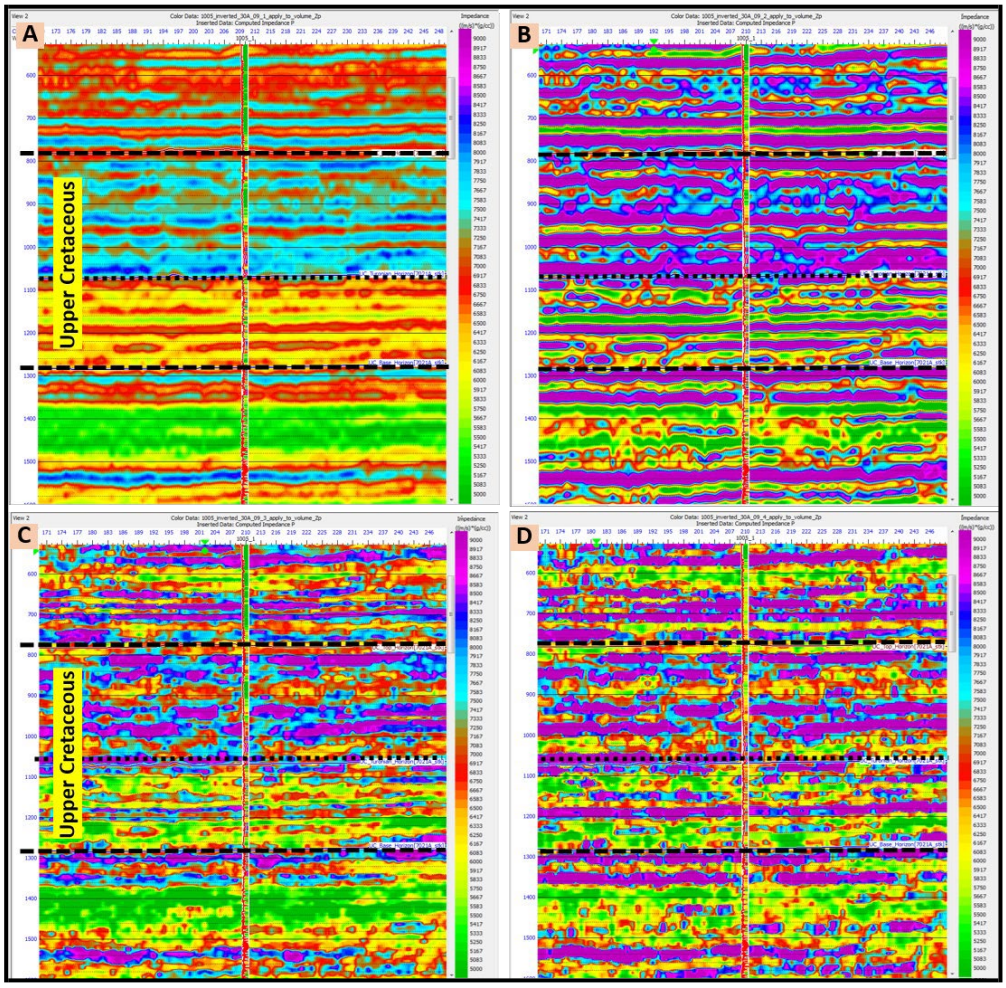

Figure 7. Comparison results of different post stack inversion algorithm that cover the Upper Cretaceous strata using seismic line # 7021A and the Transco 1005-1 well. [A] bandlimited inversion, [B] colored inversion, [C] linear programming sparse spike, and [D] maximum likelihood sparse spike.

Using Density and Neutron Logs

Density logs provide a continuous record of the formation's bulk density, which is a function of formation porosity, fluid content in the pore spaces, and matrix density (Asquith et al., 2004). It is commonly used to calculate porosity. However, the neutron log provides fluid-filled porosity and measures hydrogen concentration in a formation. Although sonic porosity logs are still used, the two predominant porosity measurements are density porosity and neutron porosity. Density tools emit medium-energy rays into a borehole wall. The gamma rays collide with electrons in the formation, lose energy and scatter after successive collisions. The number of collisions is related to the number of electrons per unit volume, also called the electron density. The electron density for most minerals and fluids encountered in oil and gas wells is directly proportional to their bulk density.

The bulk density measured by tools (ρ_{log}) result from the combined effects of the fluid (porosity) and the rock (matrix) and is used to compute density porosity ($\emptyset_{density}$) (Smithson, 2012). Using density and Neutron logs (CGG, 2016), total porosities were calculated at COST GE-1, Exxon 564-1 and Transco 1005-1 wells, (Figure 8), in two steps:
Using density porosity:

$$\emptyset_{den} = \frac{\rho matrix - \rho bulk}{\rho matrix - \rho fluid}$$ (Serra, 1984)

Here, formation bulk density (ρ_{bulk}) is a function of matrix density (ρ_{ma}), porosity, and formation fluid density (ρ_f). The estimated matrix density is 2.65 g/cc for sandstone, 2.71 g/cc for limestone, and 2.87 g/cc for dolomite, and the fluid density is 1.09 g/cc for brine (Smithson, 2012).

Using neutron and density logs:

$$ND_{\emptyset} = \sqrt{\frac{(N_{\emptyset})^2 + (\emptyset_{den})^2}{2}}$$ (Gaymard and Poupon, 1968)

Here, $ND_{\emptyset}$ is neutron density porosity, $N_{\emptyset}$ is neutron porosity, and $\emptyset_{den}$ is density porosity.

Porosity Extrapolation

Another way to estimate porosity distribution is the derivative from simultaneous inversion. In this process, inversion property builder tools in CGG Hampson Russell were used to provide a porosity model, (Figure 9 A, B) by involving the porosity log, the top and the base of the horizons and the acoustic impedance as a guide model for geometry (Schlumberger, 2016; 2017). Since well logs provide critical information about geologic formations such as lithology and stratigraphy, the gamma-ray (GR) log measures the natural radioactivity in different rocks and is overlaying the porosity section in Figure 9 A (thick line) to determine the shale strata interval. Shale has high radioactive elements that elevate the gamma-ray values (Asquith, 2004). However, the porosity measured from the core at the GE-1 well matches well the inverted 2D porosity section (Figure 9 A and B) which is important for quality control.

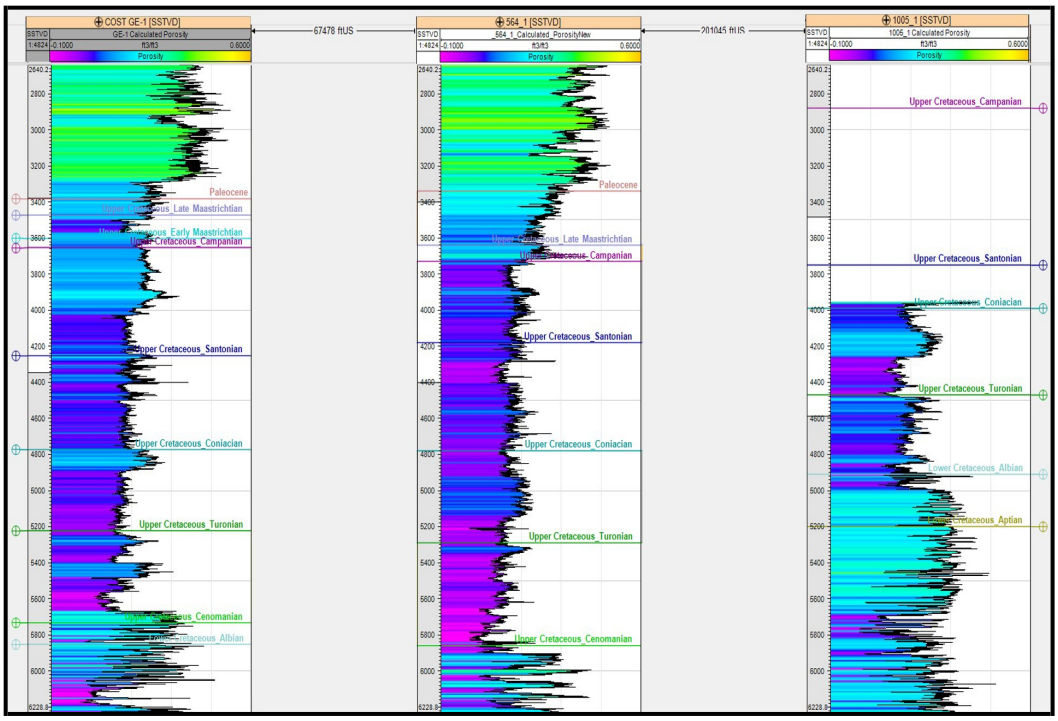

Figure 8. Calculated porosity logs at COST GE-1, Exxon 564-1, and Transco 1005-1 wells.

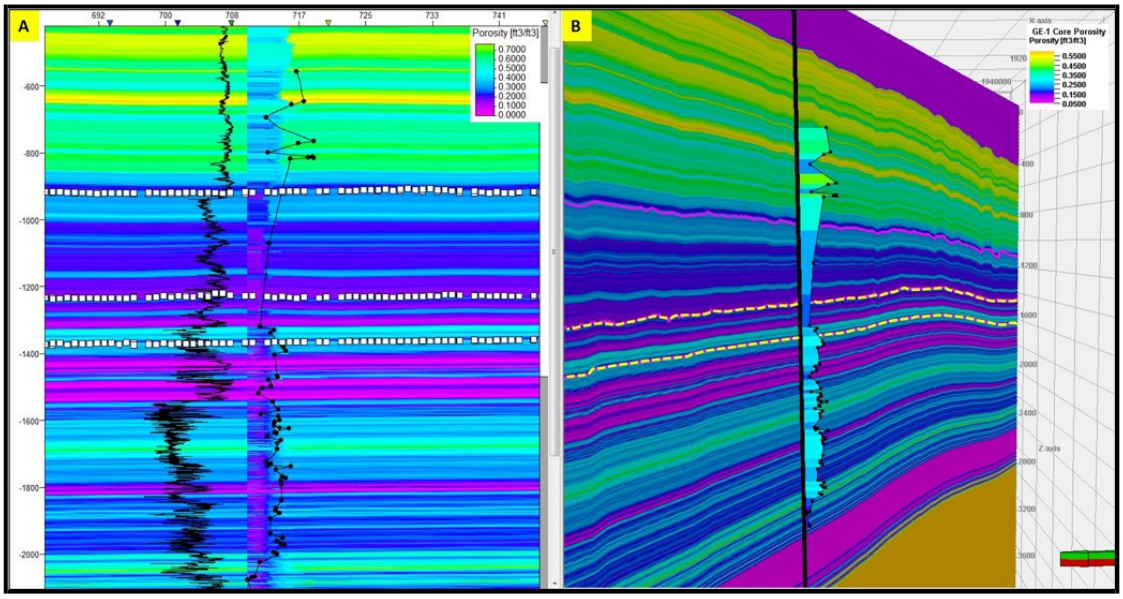

Figure 9. Extrapolated porosity using inversion property builder at the well GE-1.

Acoustic Impedance Inversion

Acoustic impedance (AI) inversion techniques were used to estimate porosity from seismic data. It indicates that the Upper Cretaceous strata at Southeast Georgia Embayment (SGE) has two prospective intervals at the Transco 1005-1 well. The first interval represents an impermeable seal which is the layer between the top of Upper Cretaceous and the Turonian surface that gives high impedance (low porosity). The second layer represents the interval between the Turonian surface and the base of the Upper Cretaceous (Figure 10). These two intervals are suggested to be the significant reservoirs for CO_2 storage (Almutairi et al., 2017),

since they show low impedance values or high porosity (acoustic impedance varies invers proportionally with porosity). These results are similar to the impedance inversion values at COST GE-1 well which has two strata intervals within the potential reservoir (Figures 11 and 12). In addition, the lowest impedance values are located where the highest porosity is and vice versa. Furthermore, it is correlated with the core's porosity at different wells for quality control. Therefore, with a proper workflow and analysis, the acoustic impedance inversion appears to be a most successful tool to discriminate lithology and estimate porosity especially where well data are sparse.

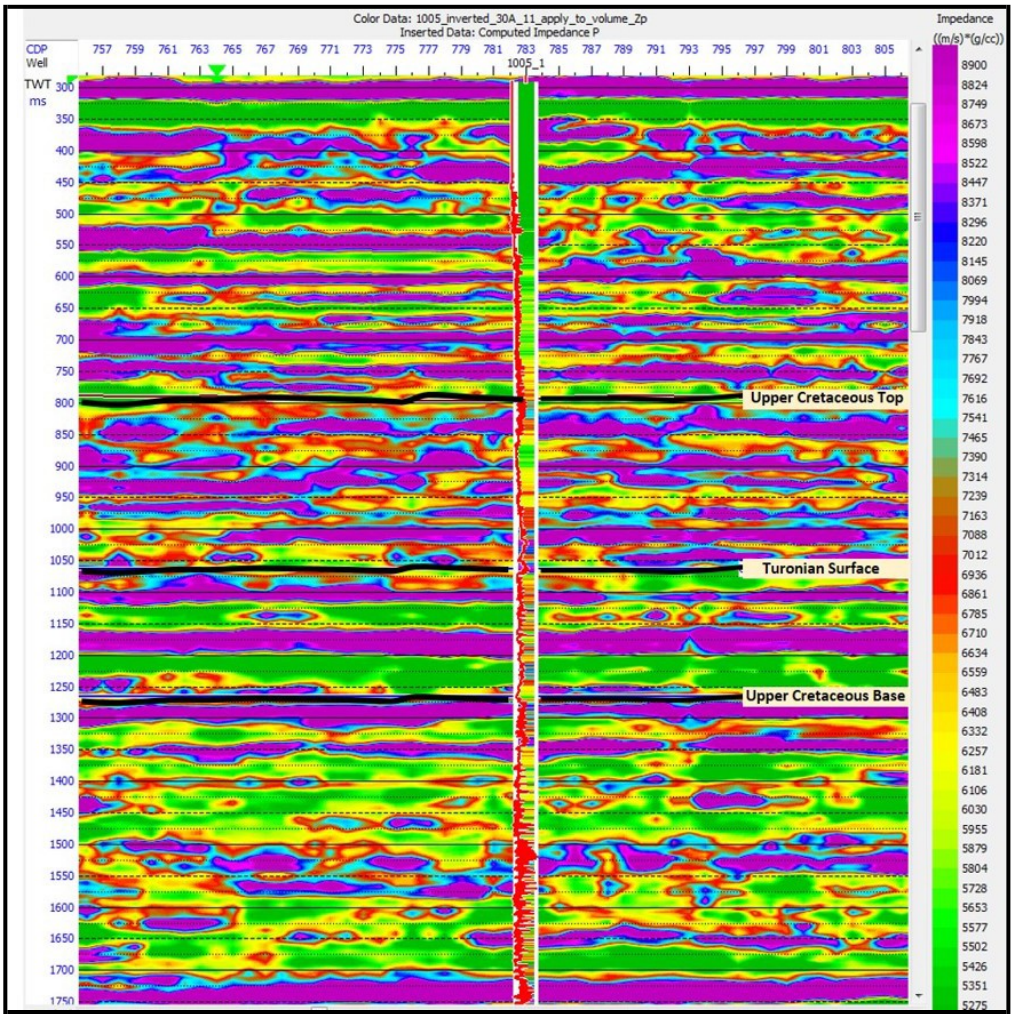

Figure 10. Acoustic impedance at the Transco 1005-1 well.

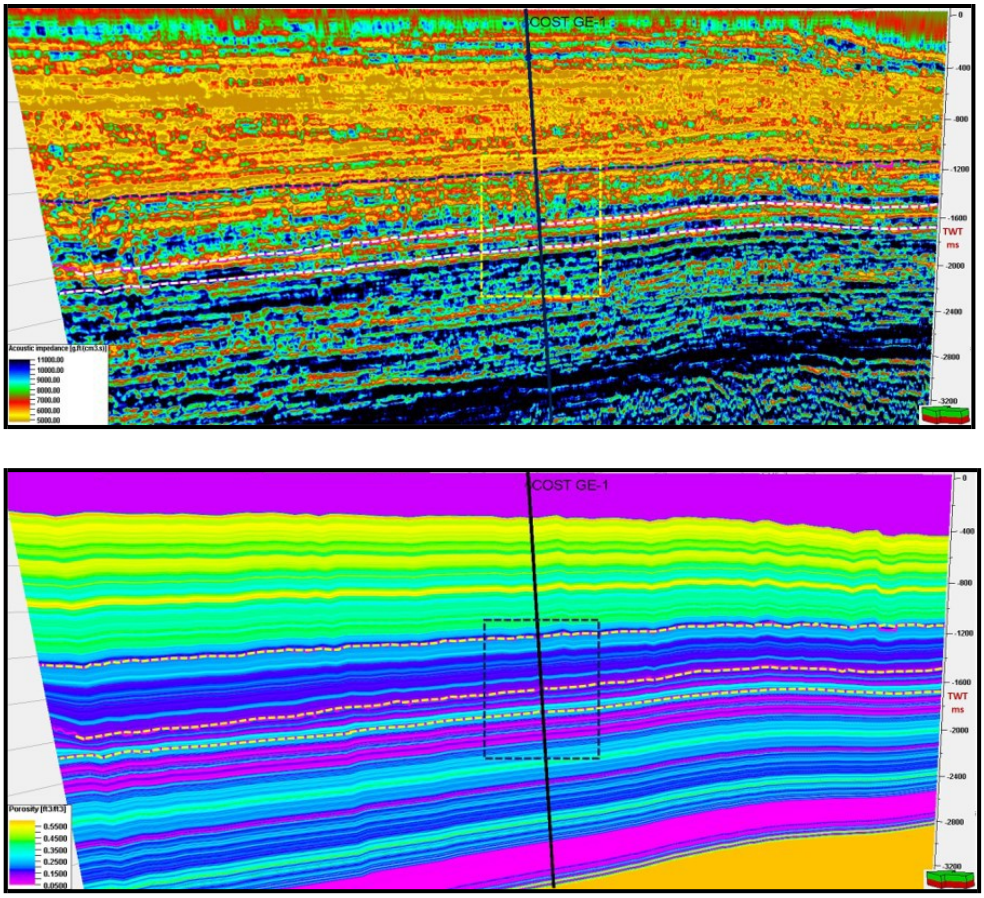

Figure 11. 3D view of the acoustic impedance (top) and the extrapolated porosity (bottom), using seismic lines # 7053A across the COST GE-1 well.

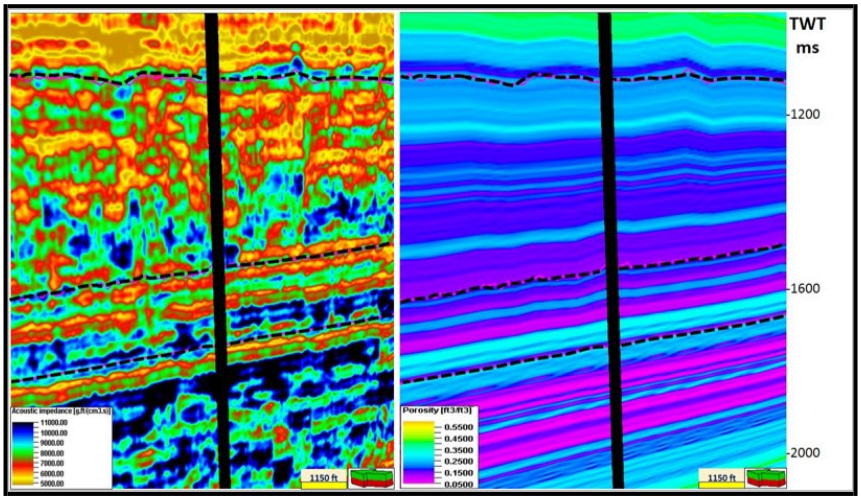

Figure 12. Zooming in for the acoustic impedance and the extrapolated porosity (see Fig. 11).

Porosity and Acoustic Impedance Relationship

Cross plotting is an effective method to link the acoustic impedance with porosities that were either calculated from the density and neutron logs or measured from the cores (Kumar, 2016). Figures 13 and 14 show a linear regression between acoustic impedance and porosity at the COST GE-1 and Transco

1005-1 wells. This reasonable correlation between porosity and acoustic impedance from logs and core data in the Upper Cretaceous strata indicates a robust transform function for application to seismic inversion results. It helps to understand the porosity regimes that are critical for CO_2 storage assessment. Also, the inverted impedance is a good indicator for porosity changes and gives confidence when indicating porosities from impedance. In addition, it is a viability study to know whether porosity can be extracted from the impedance or not. Figure 13 A shows high porosities and low impedance in the lower strata of the Upper Cretaceous interval which is an indication of a potential porous reservoir overlaid by an impermeable seal interval with high impedance values. Based on this relationship and the stratigraphic analysis, it appears that the most suitable reservoir strata for CO_2 storage are within restricted shelf carbonates with high primary and secondary porosity and good permeability occurring between 5,700 and 7,200 ft (Scholle, 1979). It has low to moderate acoustic impedance values which reflect high to moderate porosity values. In addition, it has the best permeability encountered below 1,000 ft in the COST GE-1 well (Scholle, 1979; Almutairi et al., 2017). This depth interval (5,700 and 7,200 ft), dominated by sandstone, shows porosities that vary widely and unsystematically with depth from 25% to 30% (probably due to variation in diagenesis), and the permeability is as high as 4,000 mD.

Although characterized by good porosity and low acoustic impedance, the fine-grained limestone above 5,700 ft is likely too impermeable to make the strata interval a candidate for reservoir rocks unless they are widely fractured or contain undetected permeable horizons. Data suggest that the rocks between 1,000 to 5,700 ft have a permeability of 3 mD or less (Scholle, 1979) which gives low acoustic impedance values (Figure 13A). The porosity and acoustic impedance relationships for wells COST GE-1 and Transco 1005-1 are compatible with the core data where high porosity strata have low impedance values. At the Transco 1005-1 well, the acoustic impedance and porosity relationships were tested at different depth intervals to get the best correlation that is 0.68 at the interval between 4,046 to 6,000 ft (Figure 14).

Extract Porosity from Acoustic Impedance

Using the porosity and acoustic impedance relationship, the porosity distribution is extracted using linear regression with the best correlation (Dolberg and Helgesen, 2000). Therefore, seismic data predicts porosity with a maximum correlation (R) of 0.75. Figures 15 and 16 show the estimated porosity using the relationship between acoustic impedance and porosity at the COST GE-1 and Transco 1005-1 wells, respectively.

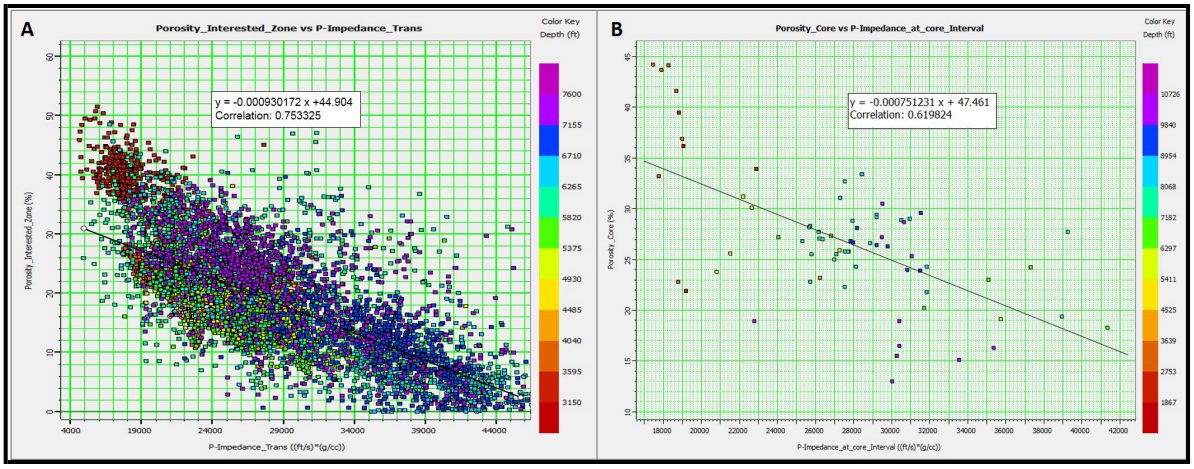

Figure 13. [A] Acoustic impedance relationship with calculated porosity at an interested zone [3,150-7,600] ft of the COST GE-1 well where the correlation coefficient is 0.75, however, [B] is the acoustic impedance and measured porosity relationship for the entire well, where the correlation coefficient is 0.62.

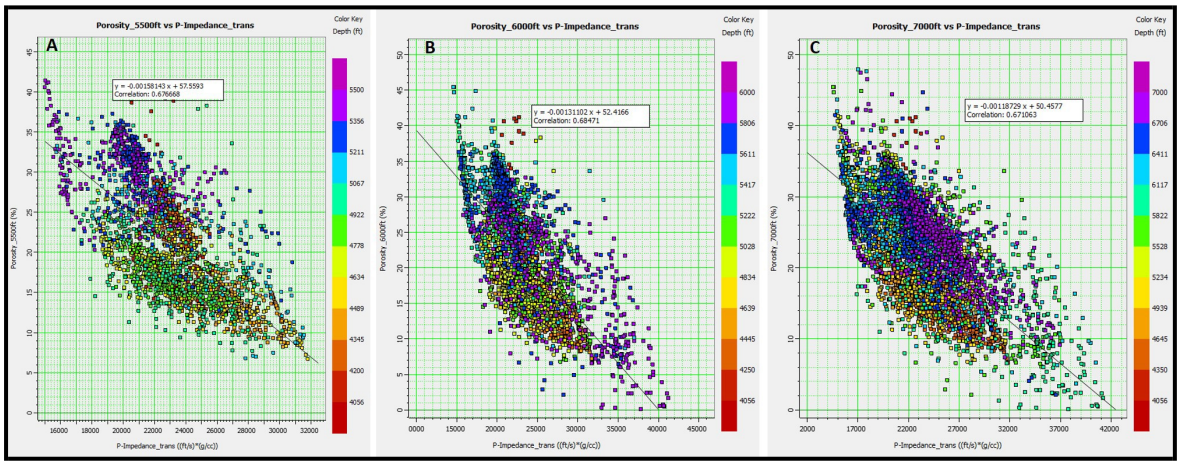

Figure 14. Acoustic impedance versus calculated porosities from density and neutron logs at three different depth intervals at the Transco 1005-1 well, where the best correlation coefficient achieved is (0.6847) at the interval between 4,046 to 6,000 ft.

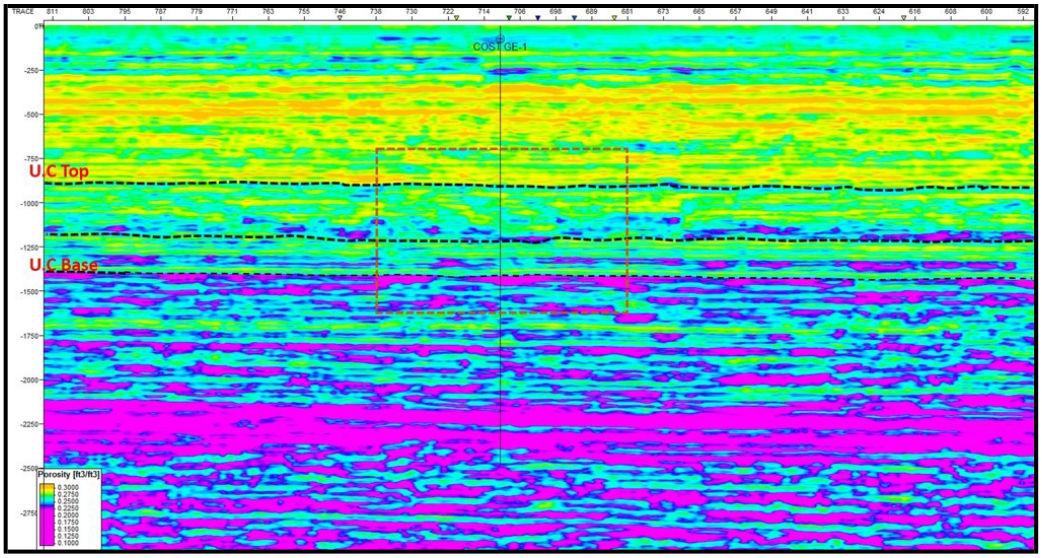

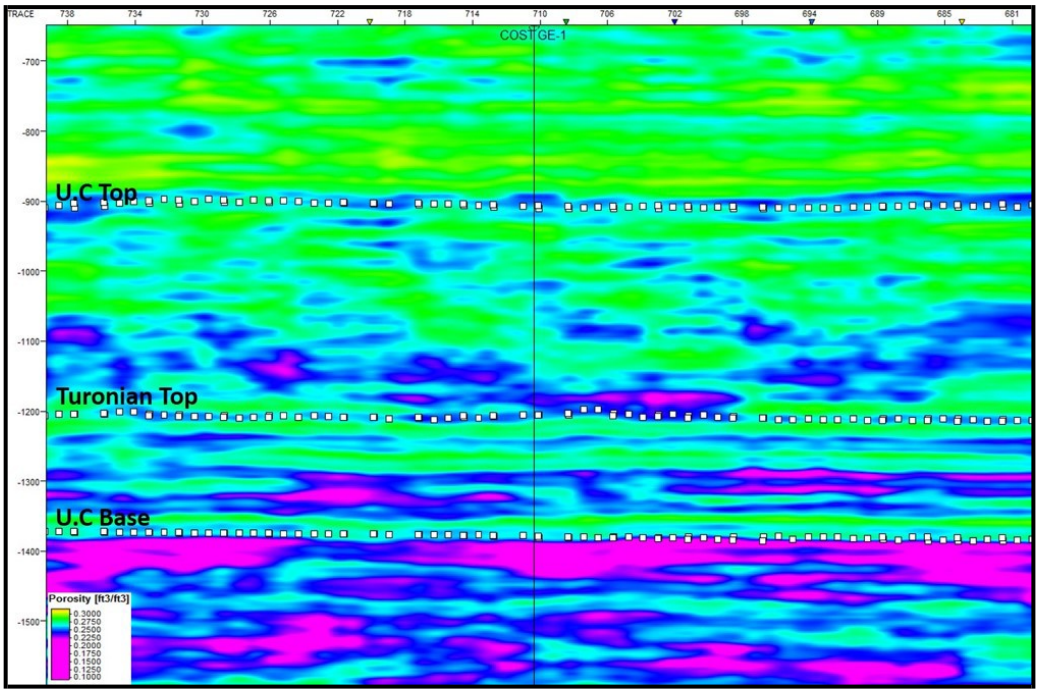

Figure 15. Extracted Porosity from the acoustic impedance at the GE-1 well using the linear regression relationship of: [Porosity = (-0.0018164*AI) + 73.137], where the correlation coefficient is 0.75.

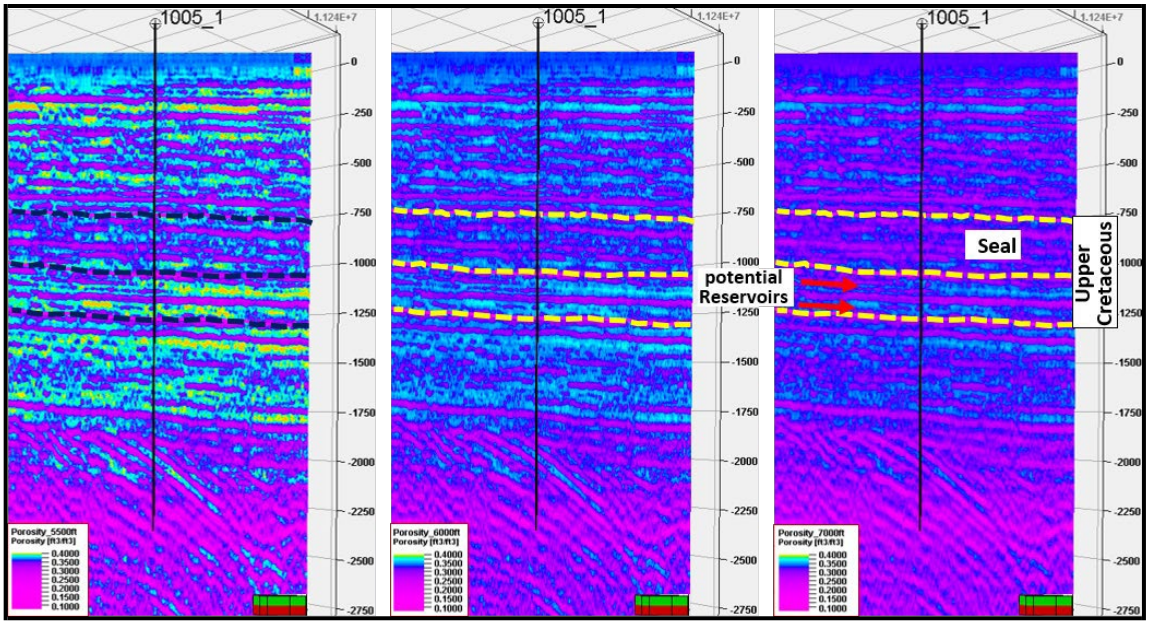

Figure 16. Extracted porosity from the acoustic impedance at three different intervals at the Transco 1005-1 well. Two strata within the potential reservoir intervals in the Upper Cretaceous are identified.

Porosity - Permeability Relationships

Understanding porosity and permeability spatial distributions are critical for characterizing a potential CO_2 reservoir and its seal. Values calculated from well logs show an irregular pattern perhaps due to cementation and facies changes. COST GE-1 well data, for instance, shows a clear decrease of porosity with depth down to ~5,700 ft. Plotting the porosity versus depth for the upper portion of the COST GE-1 well (Figure 17 A), shows that the fine-grained carbonates appear to behave similarly to chalks with respect to porosity change with depth. Some of these carbonates are not strictly true chalks because of their argillaceous matrix. The porosity and permeability depth relationship for the upper 5,700 ft of the COST GE-1 well indicates that the Upper Cretaceous section has a porosity range of 12% to 23% from 3,500 ft to about 5,500 ft; and the approximate matrix permeability is in the range of 0.15 to 0.6 mD.

Porosities and permeabilities from conventional and sidewall cores at the COST GE-1 well show that very high porosities (25 to 40%) are encountered in the Cenozoic age chalks in the 1,000 to 3,000 ft depth interval, and the corresponding permeabilities for these fine-grained limestones are predictably low (Amato and Bebout, 1978). However, the lower part of the Upper Cretaceous interval (5,500 ft) has porosities of 20-35% and high permeability (450 mD) which makes it a candidate for reservoir rock since it is capped by thick low permeability strata.

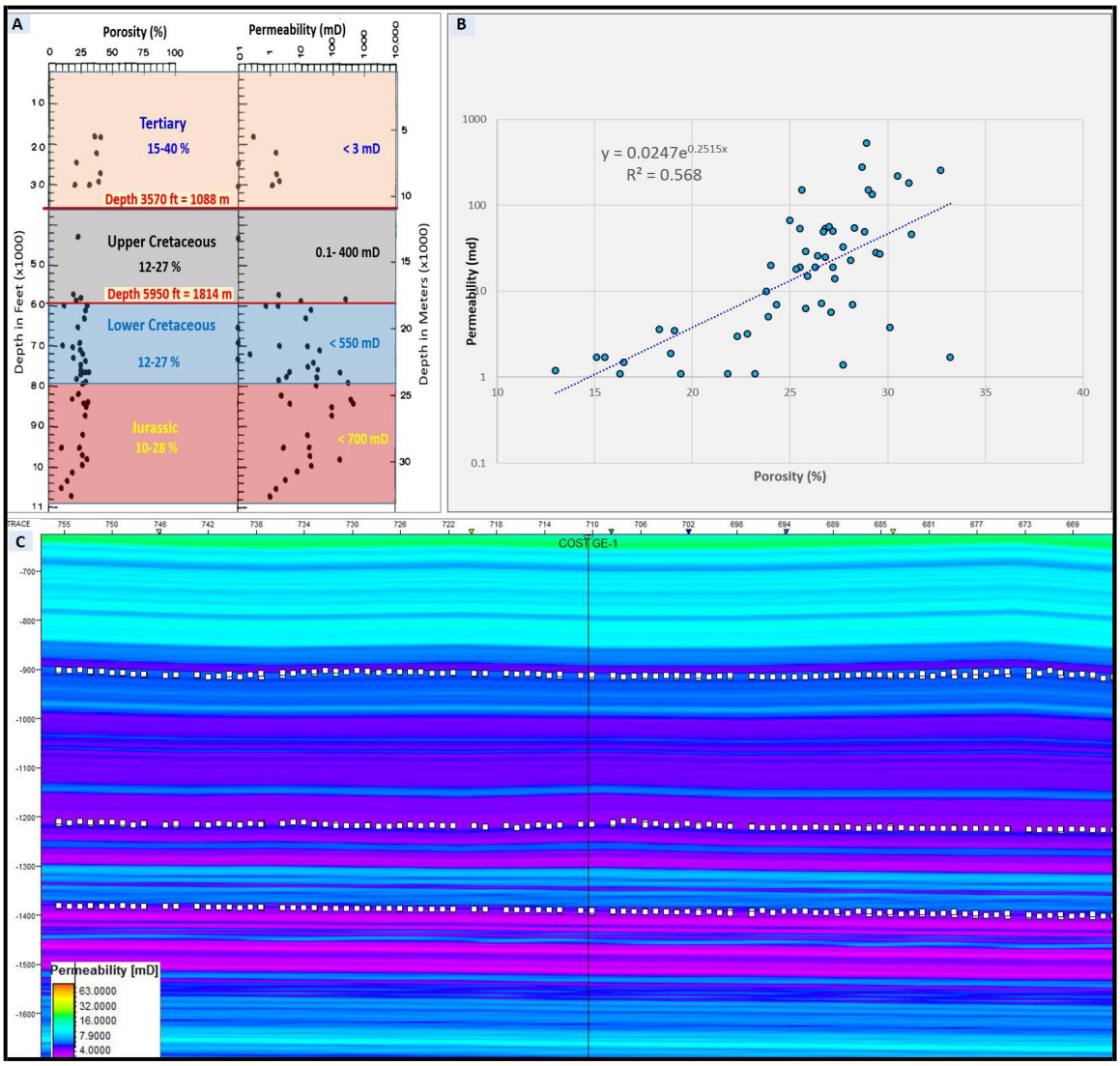

Figure 17. Porosity and permeability relationship at the COST GE-1 well: [A] values measured on conventional and sidewall cores as a function of depth (Amato and Bebout, 1978; Almutairi et al., 2017); [B] cross plotting core porosities versus core permeabilities for the entire well, data (from Scholle, 1979). [C] permeability distribution using the core's porosities and permeability relationship.

Figure 17 B shows the core's porosity and permeability relationship as a function of depth. This relationship supports the previous study conducted by Almutairi et al. (2017) which proposed that the Upper Cretaceous strata has two significant potential storage reservoirs for CO_2 including limestones with significant interbedded sandstone and shales and dolomite (Scholle, 1979). Thick sediments seal these strata, mainly shale interbedded with limestone (Figure 19). The cross plotting relationship of porosity against permeability and acoustic impedance provides more evidence that the best two potential reservoirs are located in the lower part of the Upper Cretaceous section with high values of primary and secondary porosity, low acoustic impedance, and best permeability. The first potential reservoir is between 5,320 to 5,600 ft, which is sealed by about 725 ft. thick shale. The second between 5,760 to 5,950 ft, which is sealed by 160 ft thick shale. However, permeability distribution is estimated using the regression relationship between the core's porosity and permeability (Nelson, 1996; Gilles, 2000). The equation of the least square exponential fit was used to predict the permeability distribution as a function of porosity that was extracted previously from the acoustic impedance. Figure 17 C shows the estimated permeability using the estimated porosity from the acoustic impedance of seismic line # 7053A and the COST GE-1 well data, as an example.

Permeability = $0.0247e^{0.2515\ x}$ where the correlation coefficient R^2= 0.568, and x is the estimated porosity

Task 5.0: Geologic Characterization and Volumetric Calculations

Subtask 5.1 - Reservoir Characterization; Subtask 5.2 – Mapping

Significant markers in the Upper Cretaceous, Lower Cretaceous, and Jurassic sections were identified for potential reservoirs and seals within the SGE. The main potential units were selected based on paleontological data, depths versus geologic series or stage. These units are (1) Maastrichtian, representing the top of Upper Cretaceous (Figure 18 A), (2) Turonian, (Figure 18 B) and (3) top Albian, representing the base of Upper Cretaceous, (Figure 18 C) (Amato and Bebout, 1978; Almutairi et al., 2017). Since SGE has conformable deposition, lateral facies changes may be of greater interest in this study area than in other basins along the Atlantic offshore margin (Scholle, 1979). Therefore, acoustic impedance inversion conducted for providing more detail on the critical properties such porosity and permeability, leads to more clear lithology discrimination for the potential reservoirs and seals. However, CO_2 sequestration requires reservoir and associated seal with a minimum depth and thickness (NETL, 2015; IEA, 2007; 2008). The depth to the top of Upper Cretaceous strata varies approximately from 3,000 ft to 4,500 ft at the SGE. The prospective reservoir, strata interval between the Turonian strata and the base of Upper Cretaceous, has a depth range from 4,000 ft to 7,000 ft and a thickness from approximately 250 ft to 1,200 ft (Figure 18 E). Nevertheless, the sediment column between the top of the Upper Cretaceous and the Turonian strata, mostly shales with low permeability, would serve as a thick (800 to 2,600 ft) seal (Almutairi et al., 2017; Figure 18 D). Therefore, such depths and thicknesses are suitable for CO_2 sequestration. Since geologic CO_2 sequestration requires suitable porosities and permeabilities for the reservoir and the seal, the relationship between the acoustic impedance and porosity cross-plotted with permeability (Figure 19) indicates two main reservoirs capped by impermeable strata:

- The first potential reservoir, located at depths between 5,400 to 5,580 ft, and composed of siderite, some pyrite quartz, limestone, with high porosity (17-23%) and high permeability (3.5 to 447 mD) are encountered. It is overlain by thick seal layers, located at depths between 4,400 to 5,400 ft, composed of shale, fine bedding, and has porosity of 23.5% and low permeability (0.1 mD).
- The second potential reservoir which is composed of sandstone, quartzose silt, dolomite loose sand, coal, siltsone, and is located at 5720 to 5950 ft depth. The estimated porosity is 19 to 30.1% and the permeability is between 3.5 to 447 mD (Scholle, 1979; Almutairi et al., 2017). However, it is capped by seal strata, composed of calcareous shale, fine-med silt, and biomicrite, and located at a depth range of 5,580 to 5,720 ft. Its average porosity is 12% and has less permeable clayey sequence.

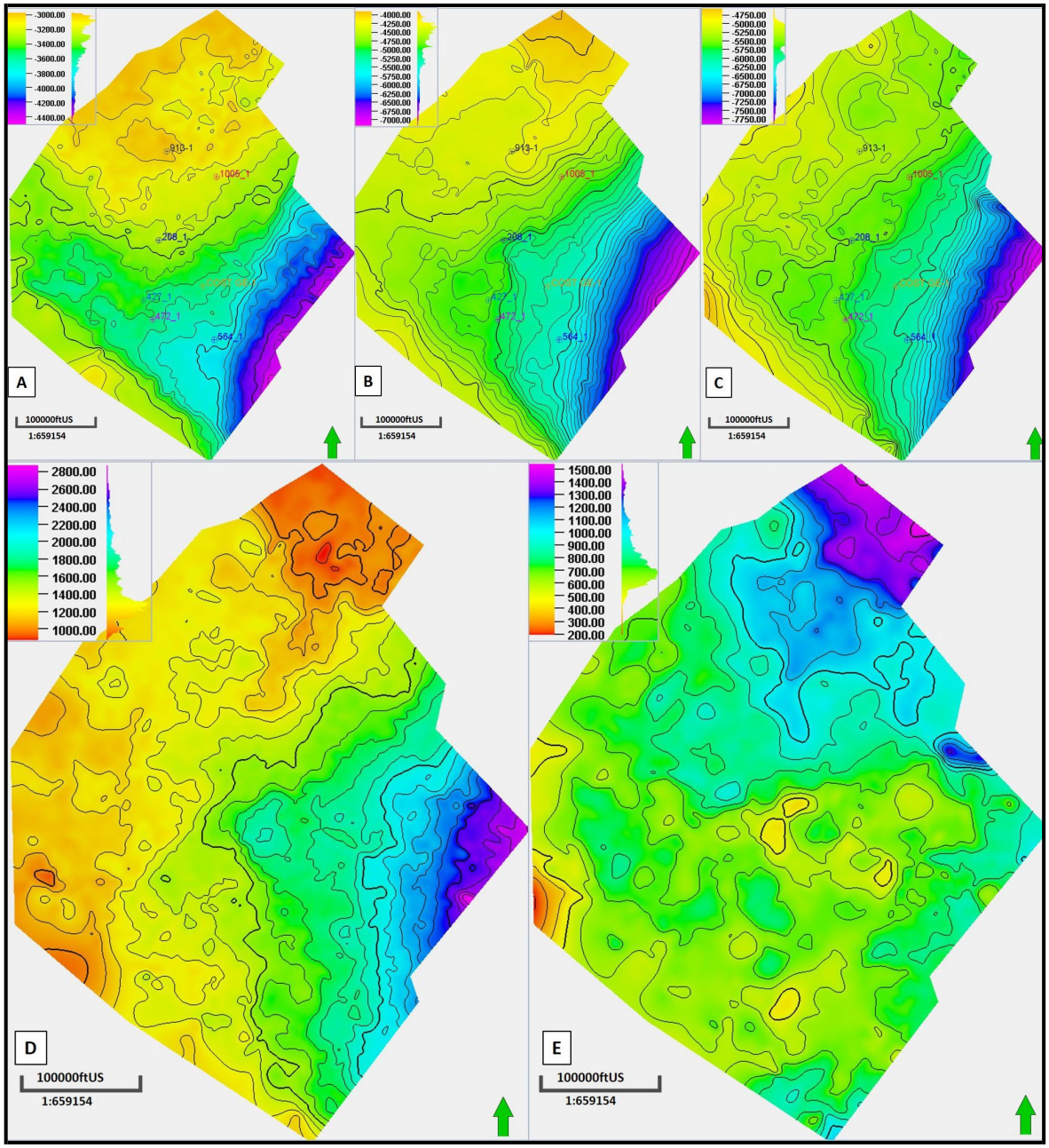

Figure 18. Structure maps (in feet) for [A] top of Upper Cretaceous [Late Maastrichtian], [B] Turonian, and [C] base of Upper Cretaceous [Albian]. Thickness maps (isochores) in feet for [D] prospective seal and [E] potential reservoir within the offshore of Southeast Georgia Basin (Almutairi et al., 2017).

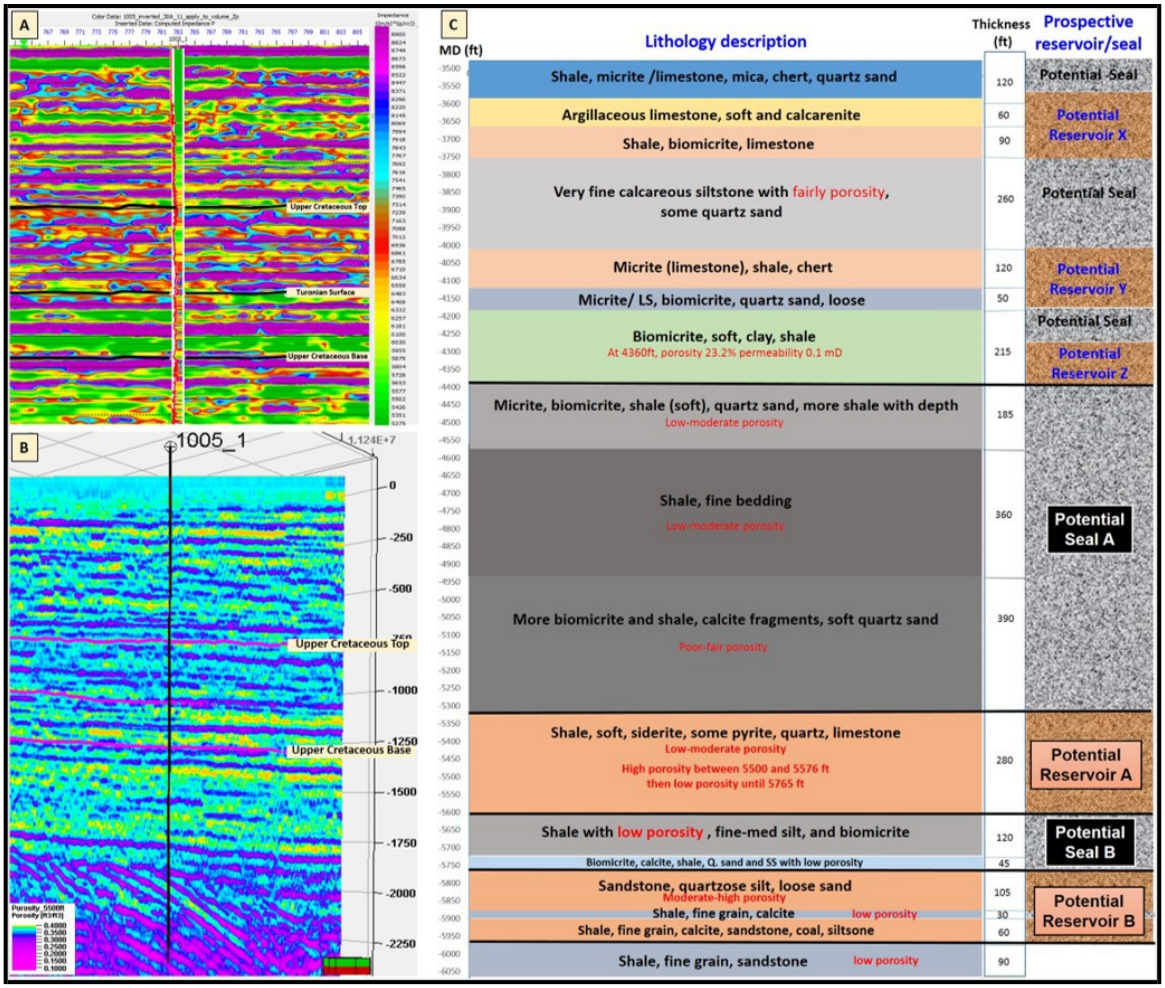

Figure 19. [A] Acoustic impedance, [B] extracted porosity and [C] lithology description with a geological model for the main two potentials reservoirs and seals at the Upper Cretaceous strata at South Georgia Embayment, modified after Almutairi et al, (2017); data from (Scholle, 1979).

Subtask 5.3 - CO_2 Storage Resource; Subtask 5.4 - Identification of Target Development Areas; Subtask 5.5 – CO_2 Storage Capacity

The acoustic impedance (AI) and porosity relationship is defined by:
Porosity = (-0.0018164*AI) + 73.137
where the correlation coefficient is R^2= 0.75.
However, the relationship between porosity and permeability is defined by: Permeability = $0.0247e^{0.2515\ x}$], where the correlation coefficient is R^2= 0.568.
The extracted values of porosity and permeability are close to the measured values from the well cores at the Upper Cretaceous strata interval. Correlation coefficients in the linear regressions between the acoustic impedance, the porosity and the permeability are within the range of similar studies that relate to CO_2 sequestration and porosity prediction such as Alshuhail (2011), Patricia (2014), and Hills and Pashin (2010). The high impedance zones observed in the seismic section of Upper Cretaceous have low porosity. Since Almutairi et al. (2017) proposed two significant storage reservoirs for CO_2 at the Upper

Cretaceous strata, the seismic inversion and the regression between the acoustic impedance and porosity closely agreed with those results. The potential reservoir zones give low impedance and high porosity. Comparing the low impedance zone with the well lithology description, the reservoir is comprised of limestone with significant interbedded sandstone, shale, and dolomite (Scholle, 1979). Thick sediments seal it, mainly shale interbedded with limestone, which have high impedance and low porosity values (Almutairi et al., 2017). From the acoustic inversion analyses and physical property relationships, the Upper Cretaceous strata have mainly two potential reservoirs and extend within the South Georgia Embayment (SGE). The shallow potential reservoir, located at depths between 5,400 to 5,580 ft, and composed of siderite, some pyrite quartz, limestone, with high porosity (17-23%) and high permeability (3.5 to 447 mD) are encountered. However, it is overlain by thick seal layers, located at depths between 4,400 to 5,400 ft, composed of shale, fine bedding, and has porosity of 23.5% and low permeability (0.1 mD). Nevertheless, the deep potential reservoir which is composed of sandstone, quartzose silt, dolomite loose sand, coal, siltsone, located at depth 5,720 to 5,950 ft. The porosity is (19 to 30.1%) and the permeability is between 3.5 to 447 mD, (Scholle, 1979; Almutairi et al., 2017). However, it capped by a seal interval, composed of calcareous shale, fine-med silt, and biomicrite, located at a depth range of 5,580 to 5,720 ft. Its porosity is 12% and has less permeable clayey sequence at the GE-1 well.

Southeast Georgia Embayment - Upper Cretaceous

For estimation of CO_2 storage capacity, a theoretical approach based on the DOE- NETL equation (DOE, 2008) was used to estimate the saline reservoir storage capacity. It estimates CO_2 storage capacity (GCO_2) based on the following expression:

$GCO_2 = A \times h \times \emptyset \times \rho \times E$

where:

A: total area covered by target reservoir and seal, h: Reservoir thickness

$\emptyset$: Reservoir porosity

ρ: Density of supercritical CO_2

E: CO_2 Storage efficiency factor

Regional CO_2 storage capacity is estimated using the interpolated surfaces with geographical total area of 19x1010 m^2. The average reservoir thickness is about 263 ft (80 m). This estimate depends on the regional thickness map for the prospective reservoir. The average porosity values from the core within the reservoir interval is 15%. A density of 700 kg/m^3 was used for supercritical CO_2 (NETL, 2015). The storage efficiency factor E is an important source of uncertainty for capacity assessment. It reflects a fraction of the total pore volume that would be occupied by the injected CO_2. For saline formations, the storage efficiency coefficients range between 1.41 and 6.0 % over the P_{10} and P_{90} percent probability range. Comparing with different methods, efficiency factors range between 1.2 and 4.1% over the P_{10} and P_{90} percent probability range. Therefore, the storage efficiency value of 2.0% was used which represents the probability level P50 in the limestone by the Monte Carlo method (Goodman et al., 2001).

Locally, within the offshore SGE, CO_2 storage capacity is estimated with high confidence in the areas reasonably covered by seismic and well data. The geographical total area that covers the two-significant potential reservoirs (named A and B) is 15.9x109 m^2 (Figure 21). The total net thickness of the two significant reservoirs is about 470 ft (143.3 m) determined from the well logs. The average porosity value, from the core data, within the two reservoirs is 25.83%. Therefore, the CO_2 storage capacity is approximately 31.92 GT, regionally. The local storage capacity for the two significant reservoirs in the Southeast Georgia Embayment provides 8.79 GT of that amount (Table 2).

Table 2: CO_2 storage capacity estimation in GT using different storage efficiency factors for the saline reservoirs (%): P_{10} = 0.51, P_{50} = 2.0, and P_{90} = 5.4 (NETL, 2015; Peck et al., 2014).

		CO_2 Storage Capacity in GT	
Storage Efficiency Factor (E)		South Georgia Embayment	Regional Scale (South Georgia Embayment, Carolina Trough and Blake Plateau basins)
P10	0.0051	2.25	8.97
P50	0.02	8.79	31.92
P90	0.055	24.2	96.76

Southeast Georgia Embayment - Lower Cretaceous

Integration of three well logs at the COST GE-1 well (GR, RHOB, and Porosity) with values for porosity and permeability data from core analysis is shown in Figure 20. These well logs were derived from core samples for laboratory analysis obtained during the COST GE-1 well drilling operations into the carbonates at the Southeast Georgia Embayment. The correlation of these three well logs with the laboratory core analysis is used to identify three potential reservoirs in the Lower Cretaceous section, each one associated with an overlying seal (Table 3).

Table 3: Potential sinks and their seals within the Lower Cretaceous units of the offshore Southeastern U.S.

Depth in COST GE-1 Well (ft)		**Total Average Thickness (ft)**	**Area (ft^2)**	**Volume (ft^3)**	**Porosity %**	**Permeability (md)**	**Potential Strata**
from	to						
5840	5988	295.01	$4.61*10^{12}$	$1.36*10^{15}$	18	0.8	seal
5988	6520	428.26	$4.61*10^{12}$	$1.97*10^{15}$	18-34	3- 450	reservoir
6520	6900	360.09	$4.61*10^{12}$	$1.66*10^{15}$	20-25	0.1-4	seal
6900	7200	264.64	$4.61*10^{12}$	$1.22*10^{15}$	20-28	0.1-300	reservoir
7200	7360	451.19	$4.61*10^{12}$	$2.08*10^{15}$	18--22	0.1-9	seal
7360	8665	731.02	$4.61*10^{12}$	$3.37.*10^{15}$	28-36	70-650	reservoir

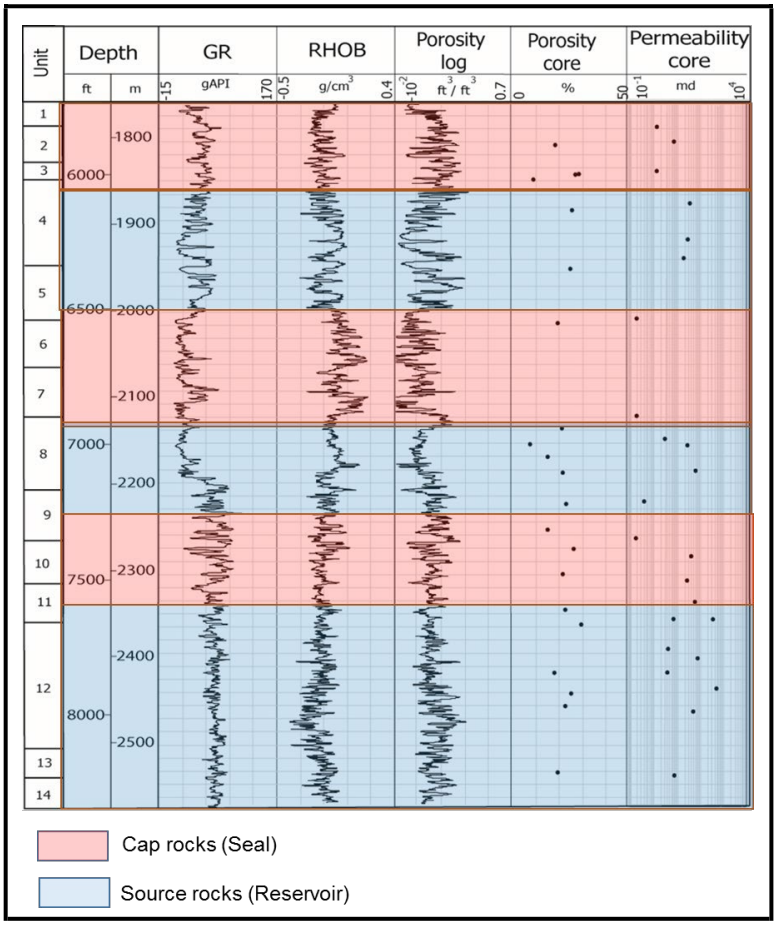

Figure 20: Correlation of three logs: gamma ray, density, and porosity with porosity and permeability values calculated from sidewall cutting and core analysis at COST GE-1 well for the fourteen lithological units in the Lower Cretaceous section.

Adequate core sample analysis has been conducted in order to determine effective porosity and permeability values on sidewall core samples from the COST GE-1 well. The porosity ranges between 15 and 30% and the permeability ranges between 0.01 mD and 550 mD within the Lower Cretaceous strata (Scholle, 1979). The Lower Cretaceous section between depths of 5,900 ft (1,798 m) and 7,200 ft (2,195m) was divided into fourteen lithological units which are mainly composed of varying proportions of calcite, clay, shale, sandstone, limestone, and dolomite (Lizarralde et al., 1994; Poag, 1978; and Poppe et al., 1995; Table 4).
Table 4: Lithological column based on sidewall core analyses from the COST GE-1 well (Scholle, 1979).

Core interval	**Depth**		**Lithology**	**Porosity**
	ft	**m**		
1	5900	1798	Shale, gray, silty, calcareous, micaceous, and sandstone	poor
2	5990	1826	Shale, silty, calcareous, micaceous, non-calcareous sandstone.	very poor

3	6080	1853	More shale, slightly calcareous, carbonaceous, fossiliferous.	low
4	6320	1926	Coarse to medium crystals, dense, and fossil fragments.	low to high
5	6500	1981	Partly sandy, dense silty, hard, calcareous to non-calcareous	moderate
6	6800	2073	Sandstone, shell, sandstone, anhydrite, and gypsum.	low to high
7	6890	2100	Limestone, shale, very fine grained calcareously cemented sandstone, and anhydrite with denes dolomite.	moderate
8	7020	2140	Dolomite, finely crystalline to dolomite, limestone increasing with depth, shale, and sandstone,	fair to good
9	7070	2155	Limestone, fossifillerous, dolomite, and non-calcareous.	fair to good
10	7160	2182	Shale and sandstone, much calcareous cement.	moderate to low
11	7200	2195	Shale, sandstone, and silty shale with calcareous cement. Limestone, some dolomite, and fossifillerous to non-fossifillerous	high
12	7400	2256	Shale, some gravel trace, dolomite and fossifillerous to non-fossifillerous.	high
13	7490	2283	Lithology like unit 12 with decreasing shale, increasing dolomite,	high
14	7910	2411	Shale to fine sandstone, gravel, faintly calcareous, and shale non-calcareous, dolomite with some clayey coatings, non-fossifillerous, much coal, anhydrite, and sandy dolomite.	moderate

Chadwick et al. (2008) previously identified ideal CO_2 geological storage criteria for reservoir properties such as porosity, permeability, depth, and thickness of the reservoir. COST GE-1 well has described lithology and rock properties for fourteen core samples. Dolomite rocks are the most dominant rocks in this section. Based on porosity and permeability properties, three reservoirs separated by three seals have been marked as target CO_2 geologic repositories within the Lower Cretaceous section. The Lower Cretaceous section ranges in depth between 5900 ft and 8330 ft and consists of dolomite interbedded with sandstones and calcareous silty shales. Scholle (1979) pointed out that there are impermeable shales with calcareous shale layers interbedded with the highly permeable dolomite layers in the COST GE-1 well. However, a few samples of sandstone were marked between 5800 ft and 8300 ft, with high primary and secondary porosity and high permeability that makes it suitable to be a reservoir rock for CO_2 sequestration. This section is dominated by dolomites with porosities that vary widely and unsystematically with depth from 17 % to 32 %, and permeability between 0.3 and 550 mD. Porosity logs were derived and calculated from well logs to fill in the hiatus between the core interval data. Structure maps at the top of the prospective storage horizons are shown in Figures 21 to 23.

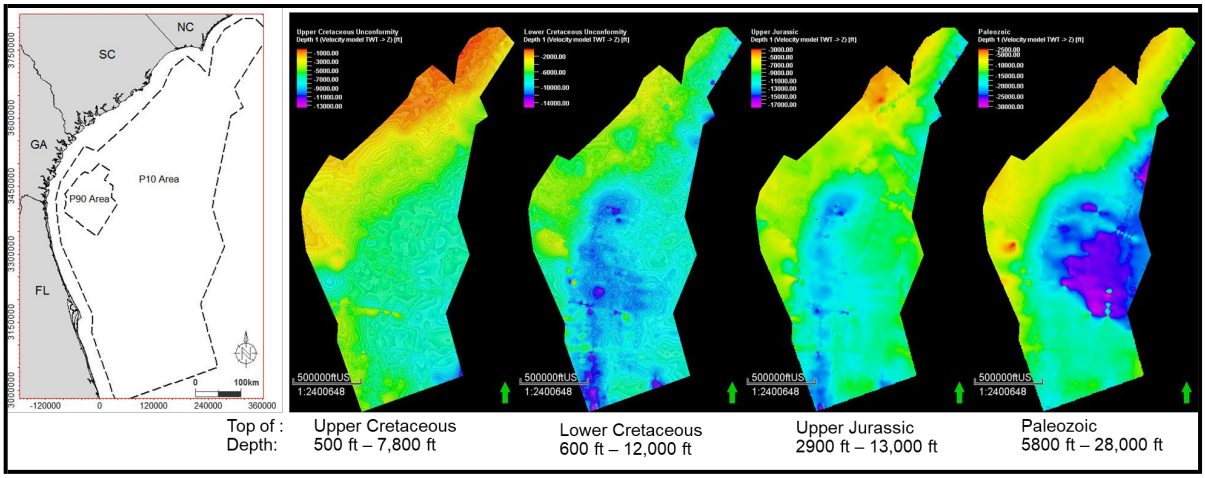

Figure 21. Structure maps of the top of the U. Cretaceous, L. cretaceous, U Jurassic, and Paleozoic sections.

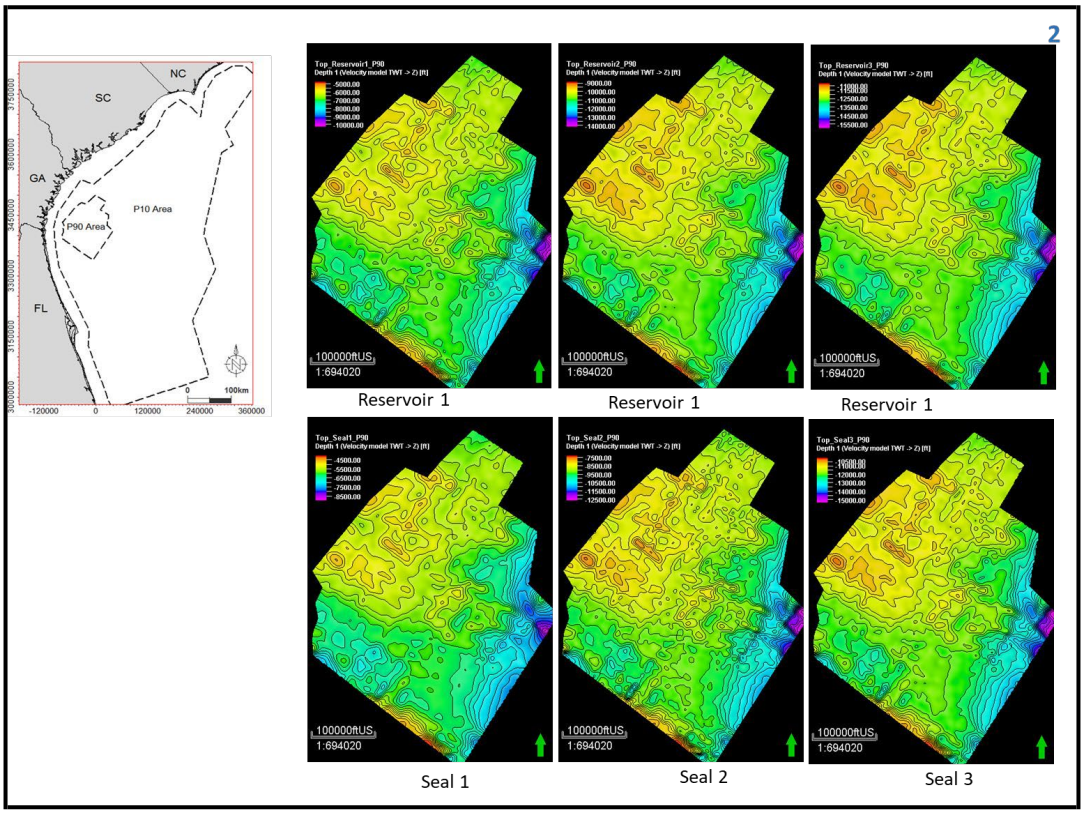

Figure 22. Structure maps for the three reservoirs and three seals in the Lower Cretaceous section of the SGE at P_{90}.

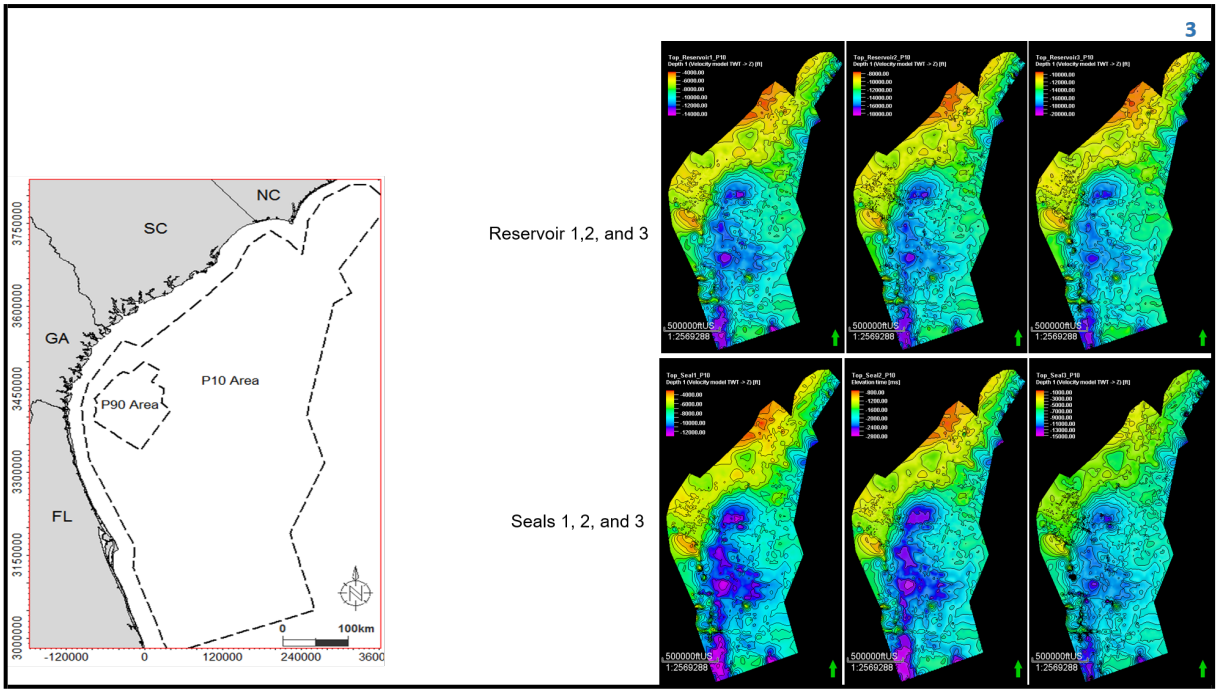

Figure 23. Structure maps for the three reservoirs and three seals in the Lower Cretaceous section of the SGE at P_{10}.

The same DOE-NETL equation was used to estimate the CO_2 storage capacity in the Lower Cretaceous section. Figure 20 shows the storage potential of the three reservoirs identified within the Lower Cretaceous section of the Southeast Georgia Embayment. Combined, these three reservoirs have a significant total capacity.

The US DOE equation is mathematically expressed as:
$G_{co2}=A_t\ h_g\ \varphi_t\ \rho^E$ (USDOE equation)
Where:
Gco_2 – Total mass of CO_2 in Gt (G_t)
A – Target area (m^2)
h – Gross strata thickness (m)
φ – Effective porosity (%)
ρ – CO_2 density (kg/m^3)
E – Efficiency factor (%)

The parameters A, h, and φ are the yield of the total pore volume of the interesting section. The ρ parameter is the volume conversion to the mass of CO_2 and the efficiency factor (E) is reducing the total CO_2 mass for storage to an accurate realistic value. Related to the specific aquifer, the efficiency factor has been determined by several factors (Goodman et al., 2011). The potential capacity of the several reservoirs of the whole Lower Cretaceous section has been calculated using all parameters in the US DOE equation. The team used the Monte Carlo method for saline formations. The efficiency factors at the formation scale were improved by Goodman et al. (2011). The capacity for CO_2 storage potential of the Lower Cretaceous was calculated based on the net thickness of the porous and permeable layers. The average porosities of the upper, middle, and lower reservoirs were 27.4%, 28.1% and 28.7%, respectively. The dolomite efficiency factors (E) of P_{10}, P_{50}, and P_{90} were 2.2 to 3.4% described earlier. Table 5 shows P_{90} potential capacity of the three target reservoirs within the Lower Cretaceous strata. Table 6 shows P_{90} potential capacity of the three target reservoirs within the Lower Cretaceous strata. The calculated storage capacity is 746 Gt of CO_2 at P_{50} that could be stored securely in $4.61*10^{12}$ cubic ft. The total average thickness is 1425 ft (Table 7).

Table 5. Estimates of the Lower Cretaceous P_{90} CO_2 Storage Capacity (> 0.003 Gt per mi2).

Potential	Area (m^2)	Thickness (m)	Porosity	Storage efficiency E	Density (kg/m^3)	G (Kg)	G (Gton)	Area ($mile^2$)
R1	1.1148E+10	134	0.23	0.02	700	4.8103E+12	4.810296444	
R2	1.1148E+10	91	0.28	0.02	700	3.9768E+12	3.976844691	
R3	1.1148E+10	93	0.25	0.02	700	3.6288E+12	3.628792742	
Total		318					12.41593388	4285.7

Table 6. Estimates of the Lower Cretaceous P_{10} CO_2 Storage Capacity (> 0.006 Gt per mi2).

Potential	Area (m^2)	Thickness (m)	Porosity	Storage efficiency E	Density (kg/m^3)	G (Kg)	G (Gton)	Area ($mile^2$)
R1	2.04943E+11	134	0.317	0.036	700	2.1938E+14	219.3805223	
R2	2.04943E+11	91	0.282	0.036	700	1.3253E+14	132.5331457	
R3	2.04943E+11	93	0.324	0.036	700	1.5562E+14	155.618765	
Total		318					507.532433	79130

Table 7: Estimates of CO_2 storage capacity for the three reservoirs within the Lower Cretaceous section in the study area (P_{50}).

Element	Volume ft^3	Porosity θ	ρ*E	ρ*E*θ	CO_2 (kg)	kg-ton	CO_2 ton	CO_2 Gt
Reservoir I	1.36E+15	0.18	Seal					
	1.97E+15	0.26	0.3964	0.103064	2.03E+14	0.001102	2.24E+11	203
Reservoir II	1.66E+15	0.23	Seal					
	1.22E+15	0.24	0.3964	0.095136	1.16E+14	0.001102	1.28E+11	116
Reservoir III	2.08E+15	0.2	Seal					
	3.37E+15	0.32	0.3964	0.126848	4.27E+14	0.001102	4.71E+11	427

Southeast Georgia Embayment Upper Jurassic

Figure 24 shows well logs and a stratigraphic column of the three potential reservoirs separated by four seals within the Upper Jurassic strata in the Southeast Georgia Embayment.

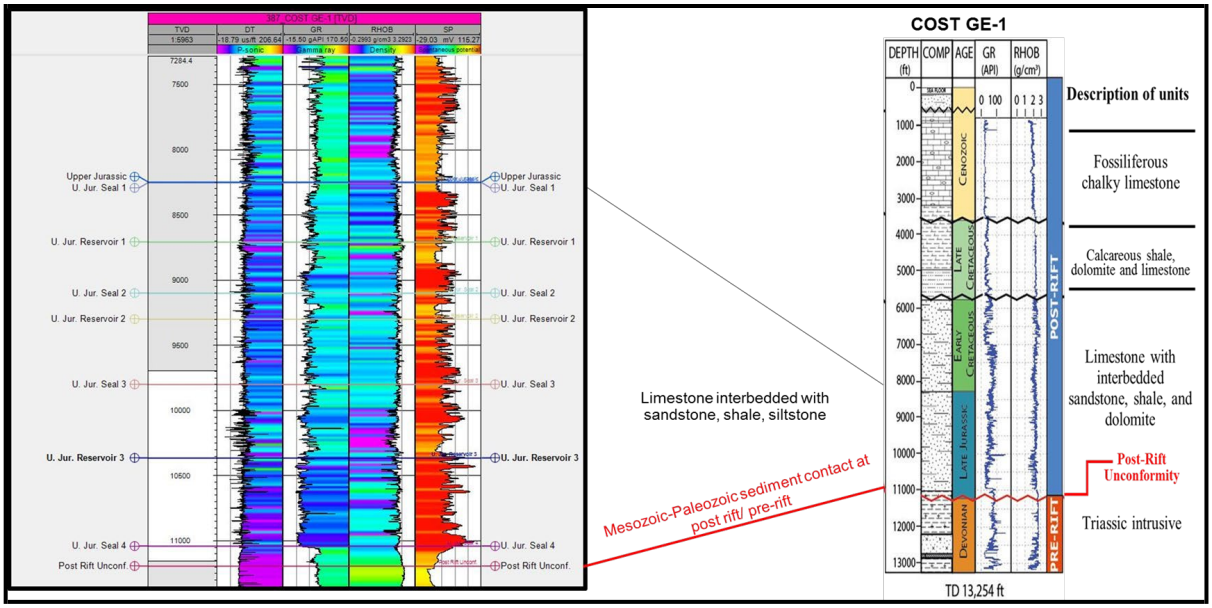

Figure 24: Three potential reservoirs separated by four seals within the Upper Jurassic strata in the Southeast Georgia Embayment.

Figure 25 shows the COST GE-1 well tie to the MME 101 seismic line for the Jurassic section of the Southeast Georgia Embayment. The Upper Jurassic section is bound at the bottom by the Triassic post- rift unconformity.

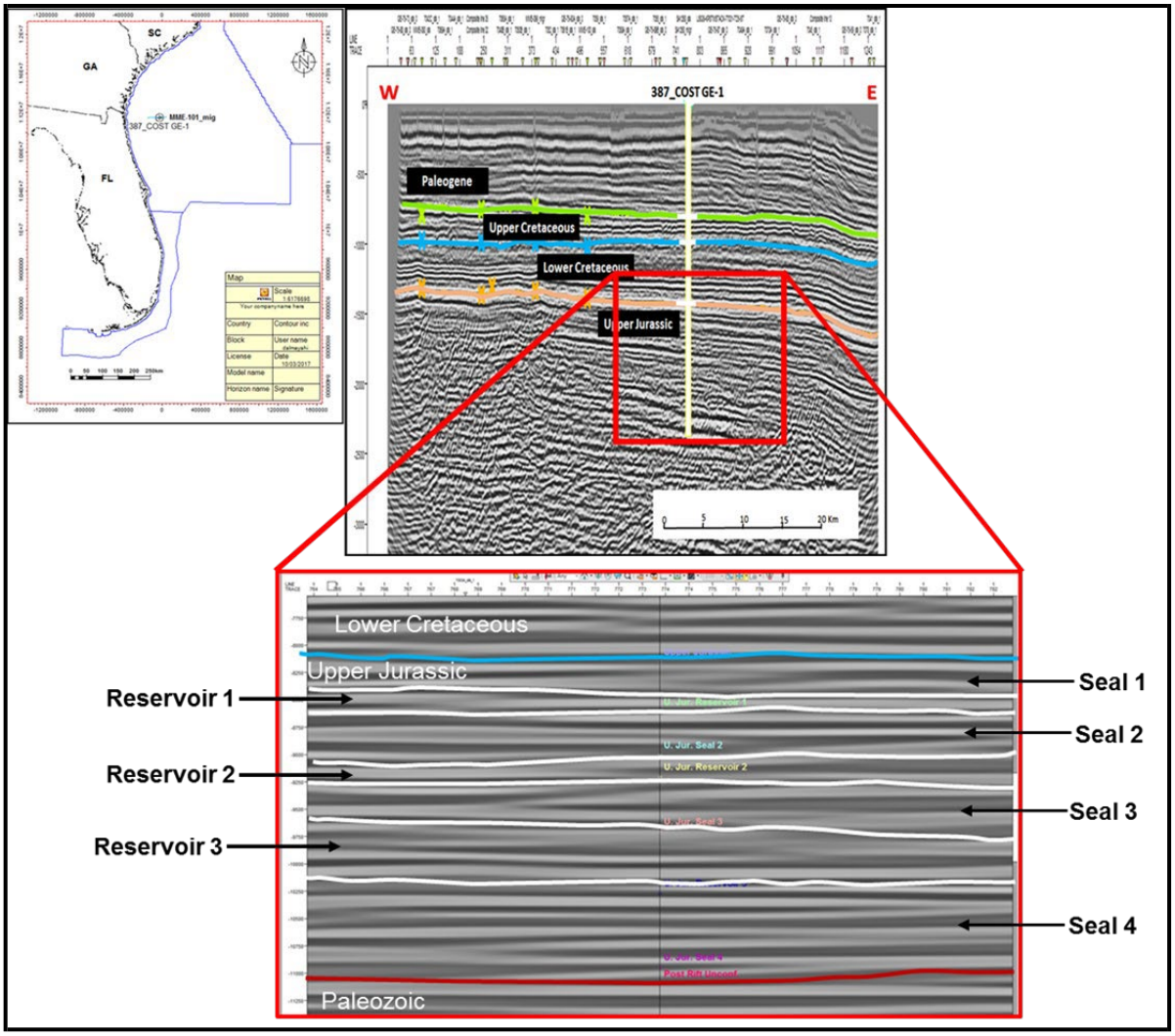

Figure 25: Correlation of the COST GE-1 well with the MME 101 seismic line (upper left inset) for the Jurassic section of the Southeast Georgia Embayment (SGE).

Table 8: Three reservoirs separated by four seals within Upper Jurassic strata in the SGE.

Storage Element	Depth (ft)	Thickness (ft)	KB (ft)	Elevation Z (ft)
Seal I	8240	468	99	-8141
Reservoir I	8708	392	99	-8609
Seal II	9100	200	99	-9001
Reservoir II	9300	490	99	-9201
Seal III	9790	920	99	-9691
Reservoir III	10710	90	99	-10611
Seal IV	10800	400	99	-10701
Post Rift Unconformity	11200			

Table 9. Upper Jurassic Storage Capacity at P90 (> 0.008 Gt per mi2).

	Potential	Area (m^2)	Thickness (m)	Porosity	Storage efficiency E	Density (kg/m^3)	G (Kg)	G (Gton)	Area ($mile^2$)
	R1	1.1148E+10	392	0.21	0.02	700	1.2848E+13	12.84826746	
	R2	1.1148E+10	490	0.26	0.02	700	1.9884E+13	19.88422346	
	R3	1.1148E+10	90	0.24	0.02	700	3.3713E+12	3.371265516	
	Total		972					36.10375644	4285.7

Geomechanical and Computed Tomography Data Collection and Analyses

Motivation

The South Georgia Embayment (SGE) of the Atlantic Continental Margin is well covered by legacy 2D seismic reflection and refraction data, however well control is scarce. A total of seven wells have been drilled in the 11,000+ mi^2 region. While all seven wells have available wireline logs, only one well has existing intact core. This study aims to ground-truth the geophysical studies and constrain volumetric estimates by performing a comprehensive data collection from existing COST GE-1 drill core for experimental rock physics evaluation. More specifically, this study collected X-ray Fluorescence (XRF) and medical X-ray Computed Tomography (CT) images on whole-core samples, and industrial CT images, porosity, permeability, dry rock density, grain density, P-wave velocity, S-wave velocity, and elastic moduli for plug samples within potential reservoir and seal depth intervals. These data provide a better understanding of in-situ geomechanical response and rock properties of both reservoir and seal lithologies to constrain CO_2 storage suitability within the SGE.

Data Collection from COST GE-1 Core

SOSRA geophysical studies conducted by Almutairi 2018 and Almayahi 2020 (in prep) yielded depth intervals that demonstrate potential reservoir and seal qualities in Upper Cretaceous, Lower Cretaceous, and Jurassic strata. All geomechanical and rock property testing described in this study occurred on COST GE-1 drill core within these recommended intervals.

Delaware Geological Survey (DGS) currently houses and curates COST GE-1 drill core and core-derivative products, including ¾-slabbed drill core, sidewall core, prepared materials such as powdered samples and thin section slides, and washed and unwashed cuttings. Only 363 feet of core was originally recovered from the COST GE-1 well and exists in the DGS collection. Due to the rarity of this core and its significance to the geological understanding of the region, a data collection methodology was created to minimize destructive analyses and maximize physical returns to the DGS repository.

In February 2019, requests were made to DGS to loan portions of ¾-slabbed drill core within potential reservoir and seal intervals for further geomechanical and rock property testing. For specific requested interval depths, refer to Table 10. In total, 23 boxes of 57.1 feet total were loaned for this study. Every reference of depth in this study is measured from the Kelly Bushing (KB).

Table 10. Depth intervals of COST GE-1 drill core requested from DGS.

Depth Intervals (ft)	Number of Core Boxes	Sample Types (as listed in DGS Inventory)
6607-6614	3	Slabbed Core
6647.5-6655.4	4	
7040-7048	3	
7091-7098.9	3	
8352-8361	3	
9453-9460.9	3	
9501.8-9506.1	2	
10545.9-10551	2	
Total Depth of Core (ft)	**Total Number of Core Boxes**	
57.1	23	

All analyses conducted on the COST GE-1 core were performed at National Energy Technology Laboratory (NETL) in Morgantown, WV and Pittsburgh, PA between April and May 2019 and are detailed below. These experiments were conducted by trained employees and were designed on a brisk schedule to maximize data collection while also minimizing machine downtime and delays to ongoing projects at NETL. For a data collection summary, refer to Table 11.

- **¾-slabbed core:** The following data were generated from analyses on all 57.1 feet of ¾-slabbed core.

    1. Core Photographs: Before any analyses were conducted, high-resolution and low-resolution photographs of the loaned core were taken.

    2. Medical CT scans: These non-destructive images captured the entire 57.1 feet of loaned core at a 0.35-0.55 millimeter resolution. These data were collected in parallel to #3.

    3. Multi-Sensor Core Logger (MSCL): This non-destructive analysis measured P-wave velocity, gamma density, fractional porosity, and X-Ray fluorescence (XRF) for the entire 57.1 feet of core. These data were collected in parallel to #2.

- **Core Plugs:** The following data were generated from analyses on 7 core plugs (1” D x 2”L) extracted from the ¾-slabbed core. The specific depth of each core plug was chosen using lithologic interpretations in Scholle 1979 and results from Medical CT scans targeting high porosity, high permeability zones as well as low-porosity, low permeability zones.

    1. Industrial CT scans: These non-destructive images were generated for each core plug at a 30-42 micrometer resolution.

    2. Permeability Tests: Permeabilities were collected for each core plug using a Temco UltraPerm 500 on permeable samples and a Pulse-Decay Permeameter (PDP) on impermeable samples.

    3. Porosity Tests: Porosities were collected for each core plug using a Helium Porosimeter.

4. Dynamic Mechanical Tests: Each core plug underwent dynamic testing in an NER AutoLab 1500 to simulate in-situ reservoir and seal confining pressure conditions.

Table 11. A summary table of data collected in this study.

Experiment	Date Generated On:	Data Volume	Derivative Rock Properties
Core Photographs	Slabbed Core	238 MB	
Medical CT scans	Slabbed Core	14 GB	Bulk Density
MSCL	Slabbed Core	11 MB	XRF, gamma density
Industrial CT Scans	Plug	152 GB	Fractures, effective porosity, mineralogy
Permeability Tests	Plug	155 KB	Permeability
Porosity Tests	Plug	19 KB	Porosity
Dynamic Mechanical Tests	Plug	8 MB	In-situ P-wave, S-wave, Young's Modulus, Poisson's Ratio

Table 12. Depths of extracted core plugs.

Depth Interval (ft)	Depth of Extracted Core Plug (ft)
6607-6614	6608.5
6647.5-6655.4	6654
7040-7048	7046
7091-7098.9	7096.9
8352-8361	8360.5
9453-9460.9	9456.4
9501.8-9506.1	-
10545.9-10551	10550

Data Analysis & Preliminary Results

Generated medical CT images have a resolution in the millimeter range. Individual images were processed and stacked within an open-source software called Image to create 3D volumetric representations of the cores and 2D cross-sections through the middle. These 3D volumes are called TIF stacks. Scans have voxel resolutions of 0.35 x 0.35 mm in the XY plane and 0.50mm along the core axis, and typically have greater than 1400 XY slices.

Loaned intervals of COST GE-1 drill core showcase highly variable lithologies with alternating beds of limestone, shale, and sandstone in the Lower Cretaceous and Jurassic strata as described in Amato 1978 and Scholle 1979. When dealing with heterogeneous potential reservoirs like these where visual inspection is insufficient, CT imaging is crucial in the selection of core plug samples (Skinner, 2015).
In addition to capturing heterogeneity in core, CT scans have other benefits. CT images produce greyscale values, or CT numbers, which can be used as a proxy for density and chemical composition. In each CT image, the greyscale value corresponds to the X-ray linear attenuation coefficient. Higher density and higher atomic numbers result in higher attenuation of X-rays, thus making it possible to

identify density from medical CT scans (Tanaka, 2011). CT images are also useful for bulk characterization of core, fault identification, and changes in bedding structure (Crandall, 2017).
In Figure 26, CT scans of loaned core at 8352-8361 feet is shown next to a normal photograph. The heterogeneous nature of the geology is immediately discernible. The photograph displays areas of lighter and darker red sandstone and siltstone. Upon CT examination, differences in densities become apparent especially between 8353-8354 feet. This difference in density is captured in Figure 27 which shows a 3D representation of 8352-8355 feet with a filter applied. This filter, called a Thermal LookUp Table (LUT) filter, is a rendering option and plugin within ImageJ that color codes the gradation of image intensity to create a “heat map” ranging from blue (lowest relief) through green and yellow to red (highest relief). Simply put, this filter characterizes heterogeneity by highlighting differences in densities.

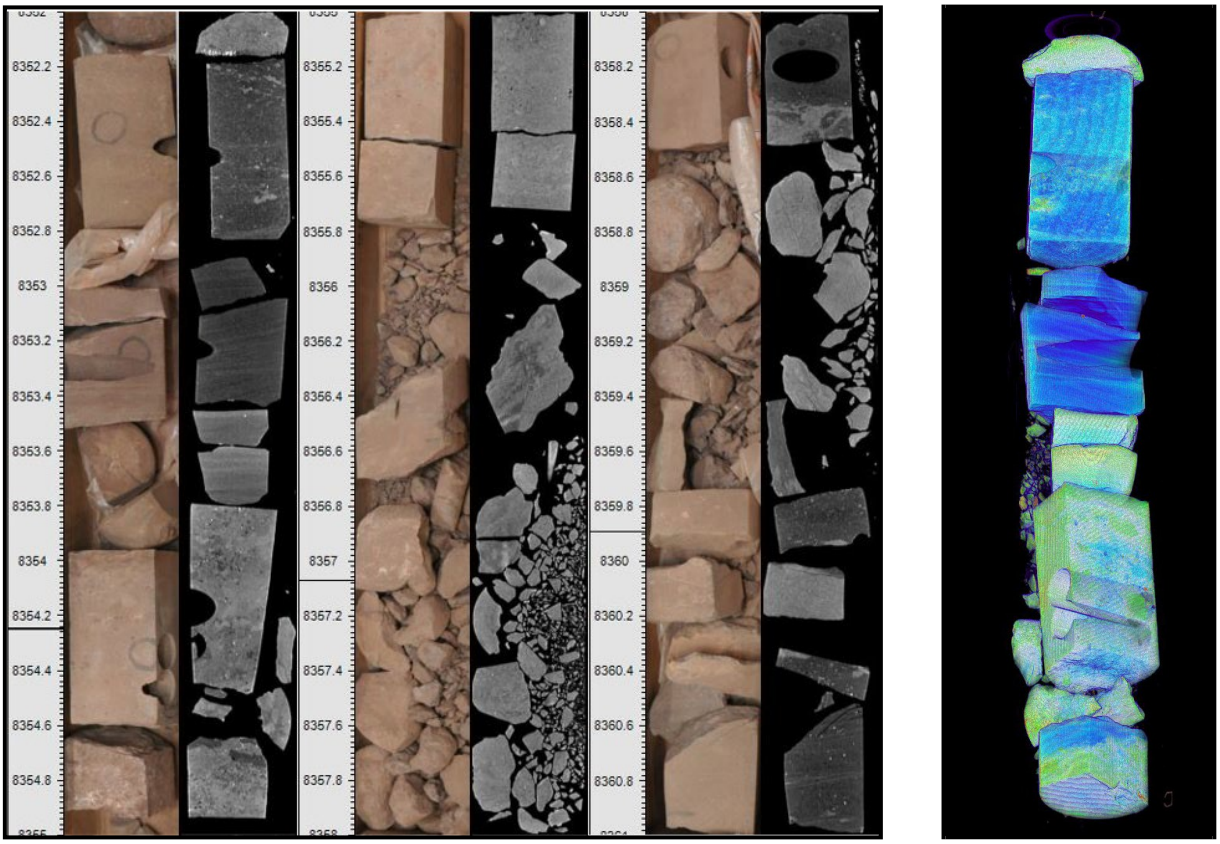

Figure 26. 8352-8361 ft interval displaying core photographs (left) and X-ray CT scans (right) with a depth track.

Figure 27. 3D representation of 8352-8355 ft interval with Thermal LUT filter applied displaying difference in densities.

Given that medical CT images generated during this study can be used as a proxy for rock density, is was important to compare the greyscale values to wireline bulk density values. In Figure 28, 6648.9-6655.5 ft interval is displayed with depth, core photograph, CT scan, and RHOB. In the CT image, whiter greyscale values indicate areas of higher density and vice versa, displaying a high density at the top of the image, low density in the middle, and high density at the bottom. RHOB mirrors this response showing higher density values toward the top of the interval decreasing towards the middle and increasing towards the

bottom. This correlation of CT greyscale values to RHOB values are virtually universal throughout all samples.

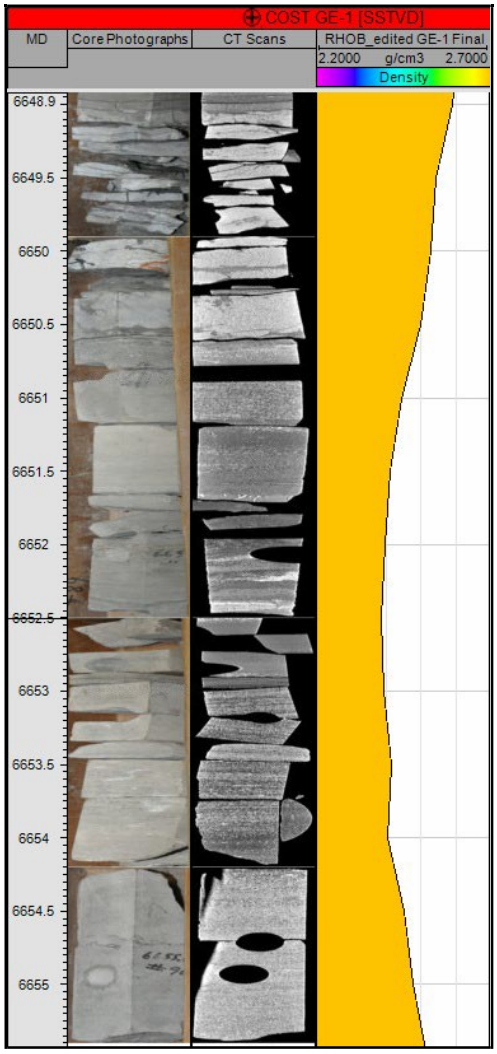

Figure 28. A comparison between 6648.9-6655.5 ft interval CT image and wireline RHOB, which are in general agreement.

In addition to medical X-ray CT scans, high-resolution industrial CT images were generated on each core plug prior to any geomechanical or rock property tests. Resolution of industrial CT images range from 30-42 µm per pixel and allow for a better understanding of specific features. For the purpose of this study, industrial CT scans yield a unique, previously unseen high-resolution perspective of interconnected porosity and fracture networks within potential reservoirs and seals. Using plugins within Image, it is possible to process each CT image to create a TIF stack, isolate pore space and fractures within a core plug, and create a 3D representation of each core plug to quantify connected porosity in 3D space (Figures 29 and 30).

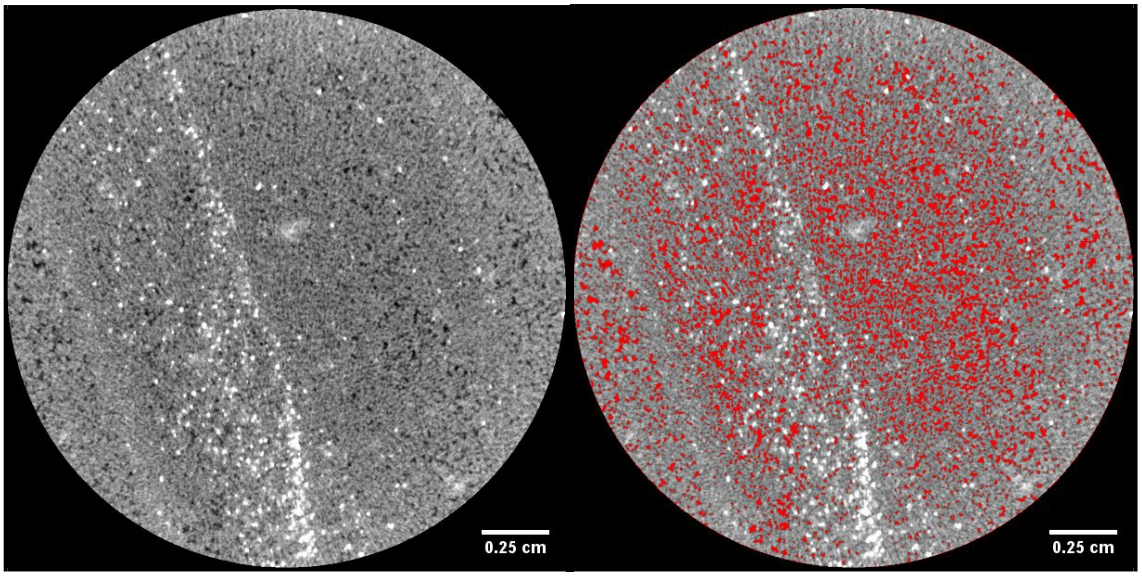

Figure 29. Industrial CT TIF stack of core plug 8360.5. (Left) Bright greyscale values indicate a band of dense minerals while dark greyscale values indicate pores. (Right) A threshold was applied to highlight pores in red.

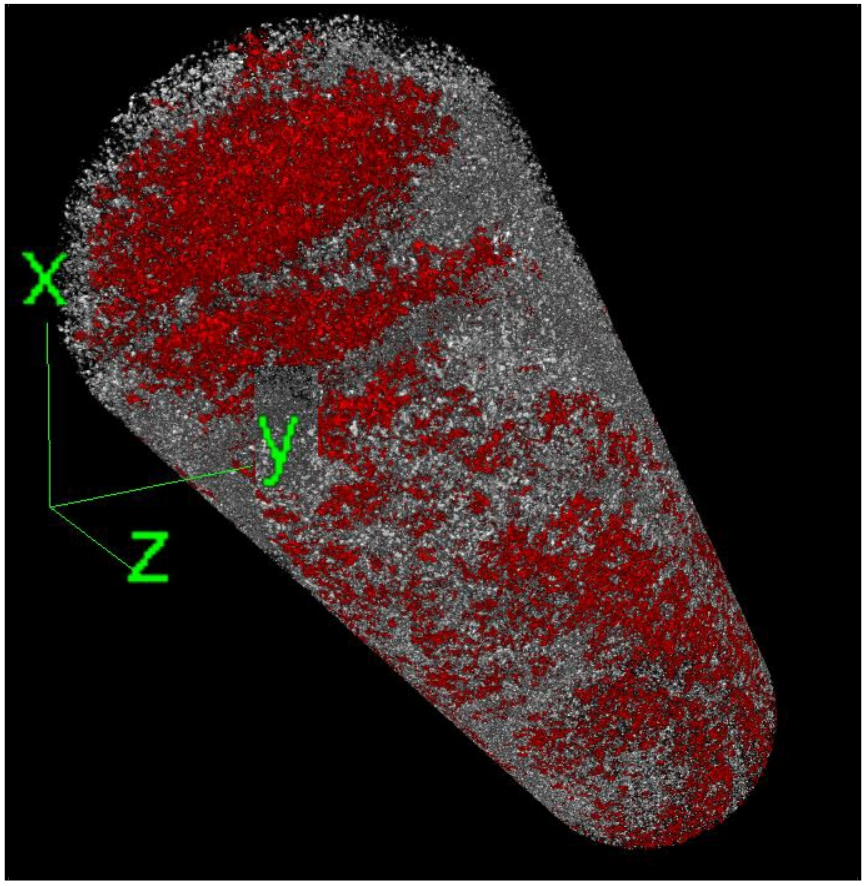

Figure 30. A 3D representation of isolated pores (grey) and connected pores (red) of core plug 8360.5.

Processing each TIF stack of each core plug for connected porosity allows for a more precise estimation of effective porosity. Effective porosity is the interconnected porosity that contributes to fluid flow or permeability in a reservoir. Due to time constraints on this study, flow-through experiments of brine or

CO_2 were not conducted and effective porosity cannot be calculated. However, quantifying connected porosity can produce a close estimate to effective porosity in the absence of a fluid flow experiment.
In geologic carbon storage volumetric calculations across the globe, there are cases where geologic variables, such as effective and total porosity, are extremely over- or underestimated (Gorecki, 2009). If actual values of these variables are known, they should be used in CO_2 storage volumetric equations to obtain a more precise and formation-specific estimates. Below is the U.S. Department of Energy volumetric approach and equation to estimate mass CO_2 storage (G_{CO2}) in saline formations (Goodman, 2016):
where: A_t = total area of reservoir
h_g = gross thickness of reservoir

$$G_{CO2} = A_t * h_g * \varphi_{tot} * \rho * E_{saline}$$

φ_{tot} = total porosity in reservoir volume ρ = density of CO_2 at storage conditions E_{saline} = CO_2 storage efficiency factor
For most regional estimates of CO_2 storage volumes without specific geologic variables, Monte Carlo simulations are used to estimate E_{saline}, which can be broken down into specific geologic variables like this:

$$E_{saline} = E_A E_h E_\varphi E_v E_d$$

where: E_A = net-to-total area
E_h = net-to-gross thickness
E_φ = effective-to-total porosity
E_v = volumetric displacement efficiency
E_d = microscopic displacement efficiency

A major objective of this ground-thruth study is to constrain the previous geophysical SOSRA volumetric estimates using reservoir-specific values of connected-to-total porosity instead of relying on Monte Carlo simulations for E_φ.

Following industrial CT scanning, each core plug was desiccated and basic dimensions including diameter, length, mass, bulk volume and density were captured. Using a Helium Porosimieter, total porosity, pore volume, grain volume and grain density were measured. Permeability of each plug was captured with a Pulse Decay Permeameter for impermeable samples or an Ultra-Perm 500 for permeable samples. These rock properties can be seen summarized in Table 11.

Table 11. Dimensions, porosity, and permeability measurements for each core plug sample.

Core Plug (ft)	Mass (g)	Bulk Volume (cm^3)	Bulk Density (g/cm^3)	Porosity (%)	Pore Volume (cm^3)	Grain Volume (cm^3)	Grain Density (g/cm^3)	Permeability (md)

6608.5	68.864	27.958	2.463123	9.66	2.701333	25.25667	2.726567	2.34
6654	72.237	28.693	2.517583	11.15	3.2	25.493	2.833601	0.048
7046	90.56	35.669	2.538899	6.25	2.23	33.439	2.708215	0.022
7096.9	62.531	31.319	1.996584	21.29	6.668	24.651	2.536652	269
8360.5	60.985	28.488	2.140726	17.47	4.976	23.512	2.593782	365
9456.4	75.391	28.292	2.664746	4.93	1.3944	26.8976	2.802889	0.003
10550	63.773	27.807	2.293415	11.26	3.1308	24.6762	2.584393	6.38

AutoLab Results for 6608.5

Event	Conf	Pore	Diff	Temp	V_p	$V_s^{(1)}$	$V_s^{(2)}$	Young's Modulus	Poisson's Ratio
	MPa	MPa	MPa	°C	m/s	m/s	m/s	GPa	
0	12.6	0.1	-1.3	28.6	4155	2465	2488	37.00	0.225
1	16.5	0.1	-1.6	28.9	4281	2510	2547	38.81	0.232
2	20.4	0.1	-1.7	28.9	4311	2565	2594	40.03	0.221
3	24.5	0.1	-1.8	29.0	4384	2595	2606	40.93	0.229
4	28.5	0.1	-1.9	29.2	4409	2626	2653	41.90	0.221
5	32.5	0.1	-2.0	29.1	4448	2683	2702	43.24	0.211
6	36.5	0.1	-2.1	29.2	4480	2717	2712	43.92	0.210
7	40.4	0.1	-2.3	29.3	4509	2723	2731	44.39	0.212
8	44.5	0.1	-2.1	29.4	4509	2741	2745	44.71	0.206
9	48.5	0.1	-2.2	29.4	4542	2764	2747	45.21	0.209
10	52.4	0.1	-2.3	29.4	4551	2772	2766	45.56	0.206
11	48.5	0.1	-2.5	28.7	4547	2779	2750	45.43	0.207
12	44.5	0.1	-2.2	28.2	4521	2770	2739	45.03	0.205
13	40.4	0.1	-2.1	27.8	4520	2745	2739	44.77	0.209
14	36.4	0.1	-2.1	27.4	4498	2728	2733	44.38	0.208
15	32.5	0.1	-1.9	27.2	4459	2704	2702	43.53	0.210
16	28.5	0.1	-1.9	26.9	4431	2669	2680	42.76	0.213
17	24.4	0.1	-1.7	26.8	4374	2621	2633	41.40	0.218
18	20.5	0.1	-1.4	26.6	4324	2567	2614	40.33	0.220
19	16.5	0.1	-1.5	26.5	4272	2529	2574	39.21	0.223
20	12.5	0.1	-1.3	26.4	4227	2479	2520	37.89	0.231
21	16.4	0.1	-1.5	27.1	4240	2532	2564	38.93	0.217
22	20.4	0.1	-1.5	27.7	4330	2580	2601	40.37	0.221
23	24.4	0.1	-1.7	28.1	4363	2639	2641	41.59	0.211
24	28.4	0.1	-2.0	28.3	4432	2662	2656	42.45	0.219
25	32.4	0.1	-1.8	28.5	4455	2706	2701	43.51	0.209
26	36.5	0.1	-2.1	28.6	4496	2733	2729	44.37	0.208
27	40.4	0.1	-2.2	28.7	4509	2747	2742	44.74	0.206
28	44.5	0.1	-2.3	28.8	4524	2758	2761	45.16	0.204
29	48.4	0.1	-2.4	28.7	4539	2781	2764	45.53	0.202
30	52.5	0.1	-2.6	28.9	4547	2796	2764	45.74	0.202
31	48.4	0.1	-2.4	28.1	4554	2778	2764	45.62	0.206
32	44.4	0.1	-2.3	27.6	4533	2755	2750	45.08	0.208
33	40.5	0.1	-2.2	27.1	4524	2731	2733	44.60	0.213
34	36.4	0.1	-2.2	26.8	4495	2731	2722	44.27	0.209
35	32.5	0.1	-1.9	26.7	4470	2712	2706	43.74	0.210
36	28.5	0.1	-1.9	26.5	4459	2670	2675	42.91	0.220
37	24.4	0.1	-1.7	26.4	4380	2616	2670	41.77	0.214
38	20.5	0.1	-1.6	26.3	4368	2603	2624	41.09	0.221
39	16.5	0.1	-1.4	26.2	4297	2522	2570	39.26	0.230
40	12.5	0.1	-1.5	26.2	4239	2474	2491	37.62	0.239

Figure 31. AutoLab 1500 results from two confining pressure ramps on plug 6608.5.

Following porosity and permeability tests, dynamic tests were conducted using a New England Research Group (NER) AutoLab 1500 automatic servo hydraulic triaxial system, which simulated in-situ pressure conditions for each core plug and measured P-wave and S-wave velocities. As seen in Figure 31, each

plug underwent two confining pressure ramps up to 52.4 MPa. P-wave and S-wave velocities were measured for each pressure interval, and Young's Modulus and Poisson's Ratio were derived from velocities. Due to time constraints on this study, pore pressure was excluded.

Upon crossplot of AutoLab generated Young's Modulus and Poisson's Ratio values, an intriguing result is displayed, seen in Figure 32. Virtually all common materials, natural or manmade, become narrower in cross section when they are stretched. This is an example of a positive Poisson's Ratio. In contrast, materials with a negative Poisson's Ratio expand laterally and become fatter when stretched. Although rare in nature, rocks exhibiting this geomechanical characteristic are termed "auxetic rocks" (Gercek, 2007). Core plug 9456.4 exhibits a negative Poisson's Ratio, making it auxetic. Research on auxetic natural materials determined that negative Poisson's Ratios can occur in highly anisotropic rocks (Gercek, 2007), or in samples with high concentrations of open cracks with large q-ratios (Zaitsev, 2017).

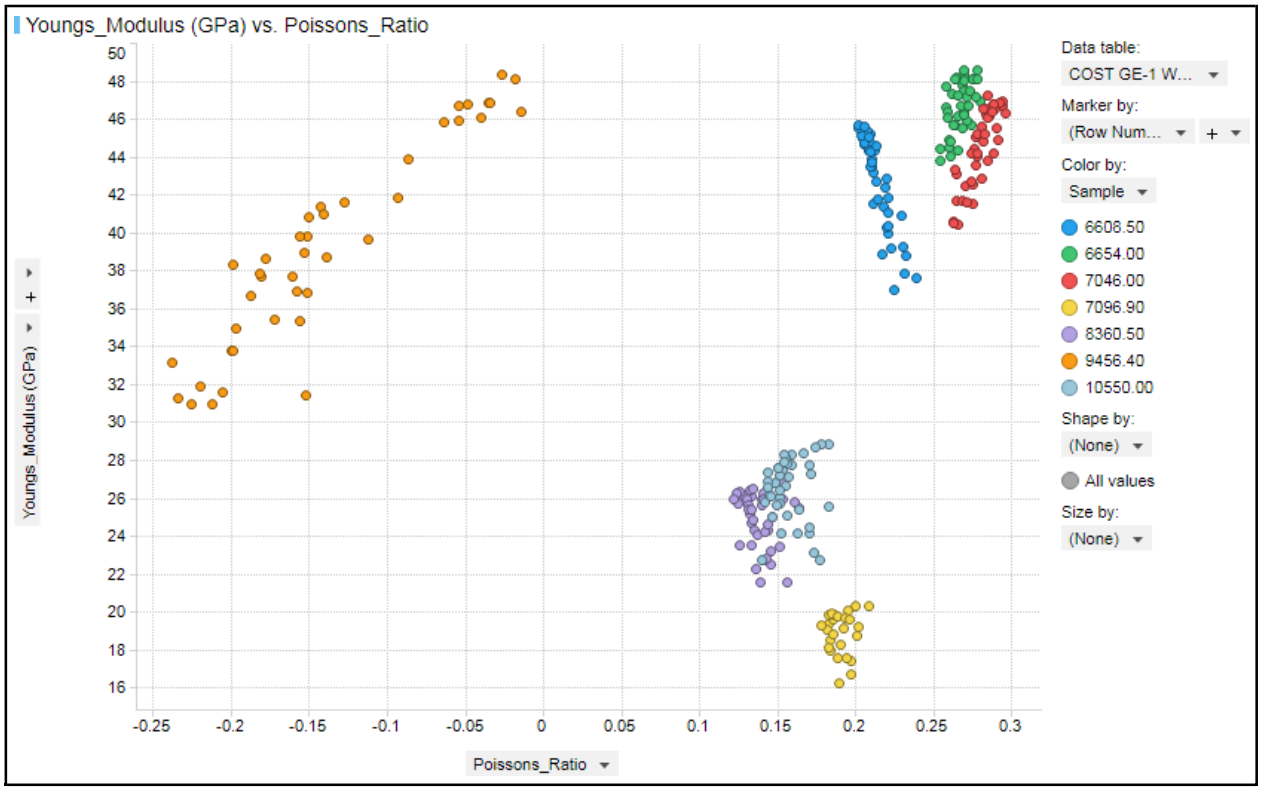

Figure 32. Crossplot of Young's Modulus in GPa and Poisson's Ratio collected during two confining pressure ramps on each core plug. Plug 9456.4 (orange) exhibits a negative Poisson's Ratio.

Analysis of all data collected, including XRF, is still ongoing and will be covered in depth in the forthcoming thesis entitled *Geophysical, Geomechanical, and Computed Tomography Characterization of Potential Reservoirs and Seals for CO_2 Storage: Southeast Georgia Embayment* (Bean et al., in prep).

The CO_2 storage capacity of the South-Atlantic study area is approximately 31.92 GT, regionally. A complete and comprehensive storage resource assessment would include economic and regulatory considerations, which are beyond the scope of this project. Due to the lack of exploration data, a level of uncertainty exists within the South Atlantic study area. Currently there are no active oil & gas or research exploration leases in the Atlantic area. There is no existing infrastructure and all previously drilled wells have been abandoned. Drilling and exploration in the Atlantic would need to be authorized by the U.S. government in order for subsea bed CO_2 sequestration to progress.

Task 8.0: Outreach

Subtask 8.1 – Public Outreach

The project team enhanced outreach and education through the development of a project website. The website incorporated the project goals, methods, and accomplishments. The website is hosted by the South Carolina Geological Survey and has the added benefit of being able to continue after the project is completed and become a part of the S.C. Department of Natural Resources' growing resource database.

The web resources were developed to disseminate project information to stakeholders and other users and include narratives of the project's goals, web maps and data viewers, and other resources making it possible to locate relevant project information. Additionally, the website hosts five story maps that are served through ESRI's story map website. Links on the SCGS webpage will direct viewers to the story maps. The Story Map format is used to provide information on climate history, CO_2 production in the U.S., carbon storage techniques, carbon capture technologies, and SOSRA data and analysis.

http://www.dnr.sc.gov/SCO2/offshore.html

Links to all presentations & posters can be found in the Appendix

Meetings with presentations:

1. March 2016, Southeast Offshore Storage Resource Assessment (SOSRA); 11th Annual SECARB Stakeholder's Meeting, Atlanta, Georgia
2. July 2016, South Georgia Rift - Implications of Rock Physics for Tectonics, Society of Exploration Geophysicists; American Geophysical Union Joint Workshop on Upper Crust Physics of Rocks, Hilo, Hawaii
3. July 2016, SOSRA: Southeast Offshore Storage Resource Assessment - North Carolina to Florida; American Geophysical Union Joint Workshop on Upper Crust Physics of Rocks, Hilo, Hawaii
4. December 2016, The Quest for Carbon Sequestration in the Southeastern United States; American Geophysical Union Meeting, San Francisco, California
5. December 2016, Southeast Offshore Storage Resource Assessment (SOSRA): Evaluation of CO_2 Storage Potential on the Continental Shelf from North Carolina to Florida; American Geophysical Union Meeting, San Francisco, California
6. December 2016, Impact of Permeability and Mineralization on an Injected Carbon Dioxide Plume in the South Georgia Rift Basin; American Geophysical Union Meeting, San Francisco, California
7. December 2018, Carbon Storage Assessment of the Southeastern United States Continental Shelf; American Geophysical Union Meeting, San Francisco, California
8. December 2018, Velocity Model for CO_2 Sequestration in the Southeastern United States Atlantic Continental Margin; American Geophysical Union Meeting, San Francisco, California
9. December 2018, Evaluation of Carbon Dioxide Sequestration in the Southeastern United States Continental Shelf; American Geophysical Union Meeting, San Francisco, California
10. March 2019, Southeast Offshore Storage Resource Assessment (SOSRA) South Atlantic Team, 14th Annual SECARB Stakeholders Meeting, Atlanta, GA

Poster presentations

1. June 2017, Progress of South Atlantic Seaboard Research; Second International Offshore Workshop - Gulf Coast Carbon Center, Beaumont, Texas

Subtask 8.2 - Knowledge Sharing and Technology Transfer
Information pertaining to this task was reported in the SSEB chapter.

Task 9.0: Closeout and Reporting

Subtask 9.1 – Modeling-based MVA Recommendations
Information regarding this task and deliverable is reported under the Eastern Gulf of Mexico chapter.

Subtask 9.2 – Infrastructure Development Recommendations

Injection Simulation
The lack of robust regional well control and knowledge of lateral lithologic variations within the stratigraphic section introduce considerable uncertainty into any traditional reservoir modeling approach. Extrapolation of lithologies and physical properties (porosity, permeability) from existing well control over the regional extent of the study area is problematic at best, and suggests that estimates of bulk storage capacity presented above are likely as good as any modeling effort. Nonetheless, we have performed several model runs on a subset of the study area in the vicinity of the existing well control in the Southeast Georgia Embayment.

This study is considering results from the previous geophysical (Almutairi et al., 2017, Almutairi, 2018, and Almayahi, in prep.) and geological studies at the COST GE-1 well by USGS. The stratigraphic columns characterized by two main boreholes (COST GE-1 and Transco 1005-1) show that a sequence of seal and reservoir strata exist in the Upper Cretaceous section in the South Georgia Embayment (SGE) and these have a porosity/ permeability of 17-23%/ 3.5-477 mD (reservoir) and 23.5% and 0.1 mD (seal), respectively. The seal zone located at a depth of 4400 to 5400 feet consists of thick layers of shale fine bedding while the reservoir consists of sandstone, dolomite coal and siltstone and is located between 5720-5950 ft depth. The other candidate reservoir for CO_2 storage is the upper part of the Lower Cretaceous below 6000 ft depth. The petrophysical parameters like porosity and permeability are 25% and 10 mD respectively, and this is a safer location to store CO_2. Consequently, we have two models for the same location that are candidates to CO_2 storage.

The model has been built using the Computer Modelling Group Ltd. (CMG) reservoir simulation software platform. The main model covered 3,600 km^2 with a resolution of 10,000 cells. We extracted two small, low-resolution models from the main model to explain the distribution of CO_2 in the reservoir in both the Upper and Lower Cretaceous strata.

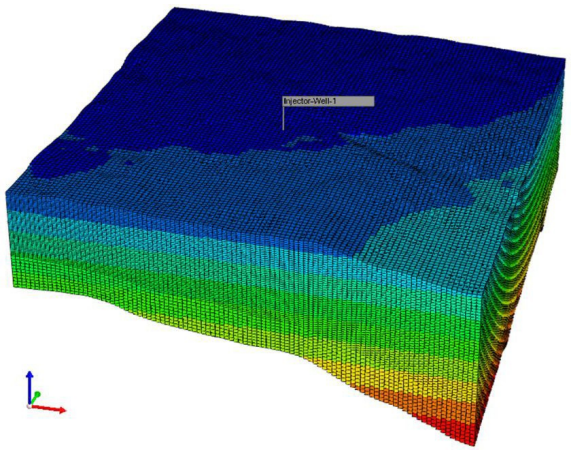

Figure 33. View of reservoir conceptual model for the Upper and Lower Cretaceous strata within the South Georgia Embayment, with 10,000 cells

Three scenarios have been considered to explain the CO_2 behavior in the injection zone in both age intervals. The model includes injecting a low rate of CO_2, 100,000 ft^3 for 30 years and 200,000 ft^3 for 15 years while the third scenario explains the impact of injecting 1,000,000 ft^3 for 15 years. The total simulation time is between 100 to 200 years, which is the most important period to examine the benefit of CO_2 sequestration.

Table 12: Explanation of model runs for the Upper and Lower Cretaceous target intervals.

Model	Injection rate Cubic feel	Shut down
Upper Cretaceous	100,000	After 30 years
	200,000	After 15 years
	1000,000	After 15 years
Lower Cretaceous	100,000	After 30 years
	200,000	After 15 years
	1000,000	After 15 years

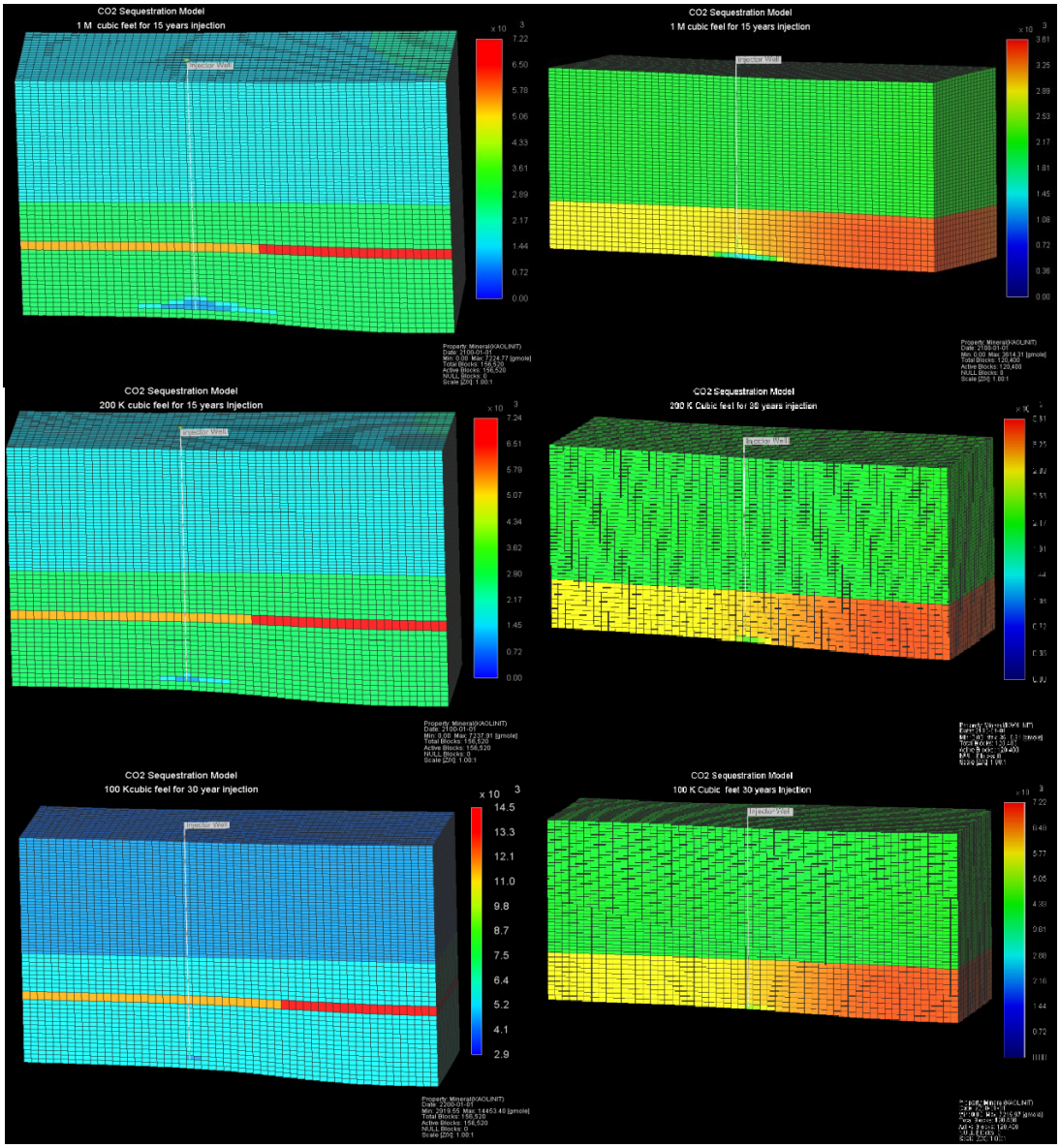

Figure 34. Preliminary results from model runs, showing the variation in calcite mineralization according to three scenarios 1M cubic feet of carbon dioxide, 200 K cubic feet, and 100 K cubic feet. From top right to down right, the Upper Cretaceous models and top left to bottom left are the Lower Cretaceous models, respectively.

The Upper Cretaceous models in Figure 34 (right side) show dissolution over a greater area comparative with the Lower Cretaceous models on the left. This is an indicator that carbonate rocks dissolve more efficiently at lower depths. The second observation is the depositional area. The aqueous component of CO_2 tends to deposit in the higher porosity area in the same horizon in addition to being located in the east part of the model where the depth is relatively higher. We also see the vertical variation of mineralization which is proportional to porosity and permeability for every layer of the Cretaceous models.

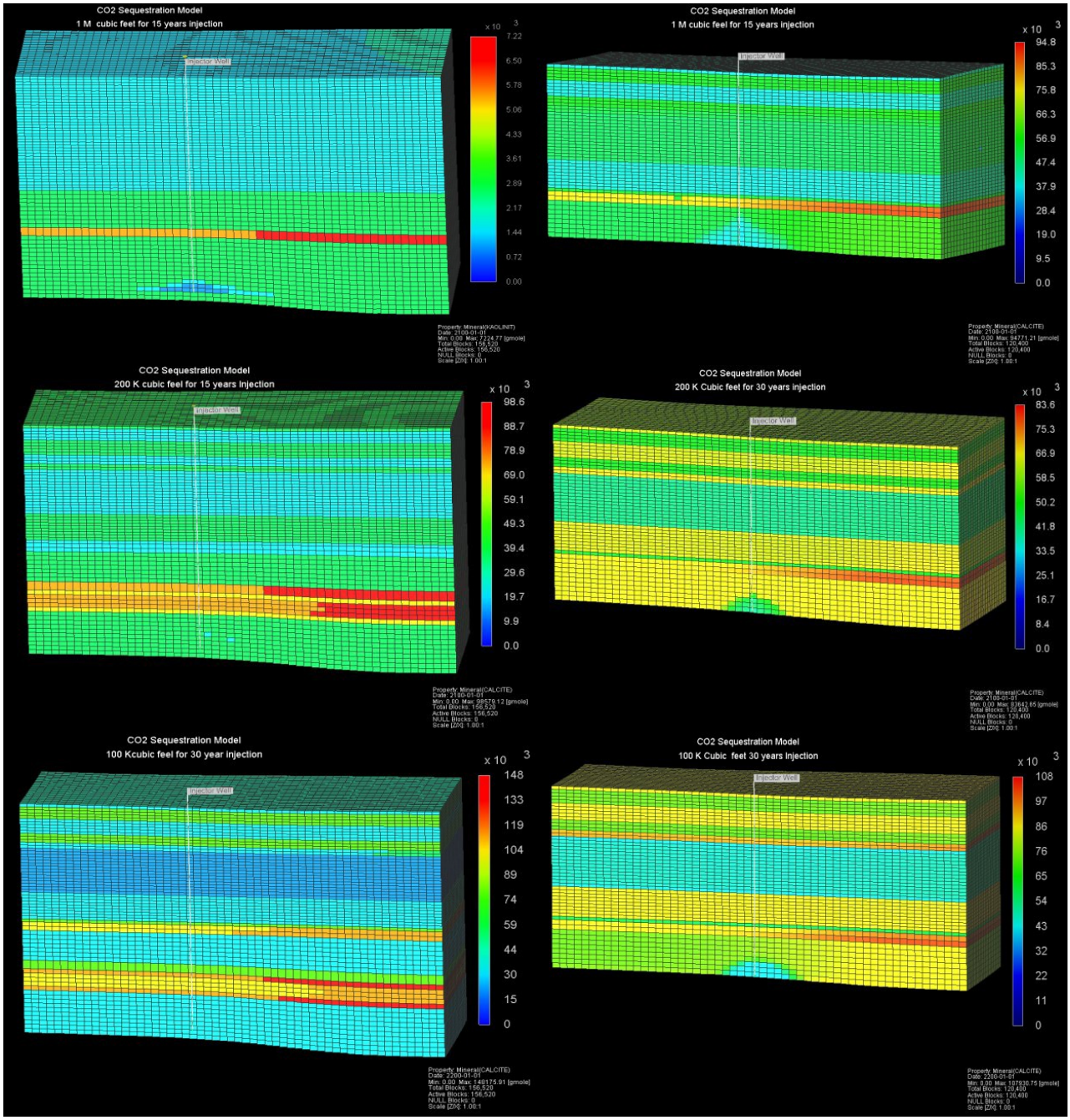

Figure 35. These models show the differences between the two main injection zones. Lower Cretaceous models to the left and Upper Cretaceous, to the right. All of them have mineralization of kaolinite.

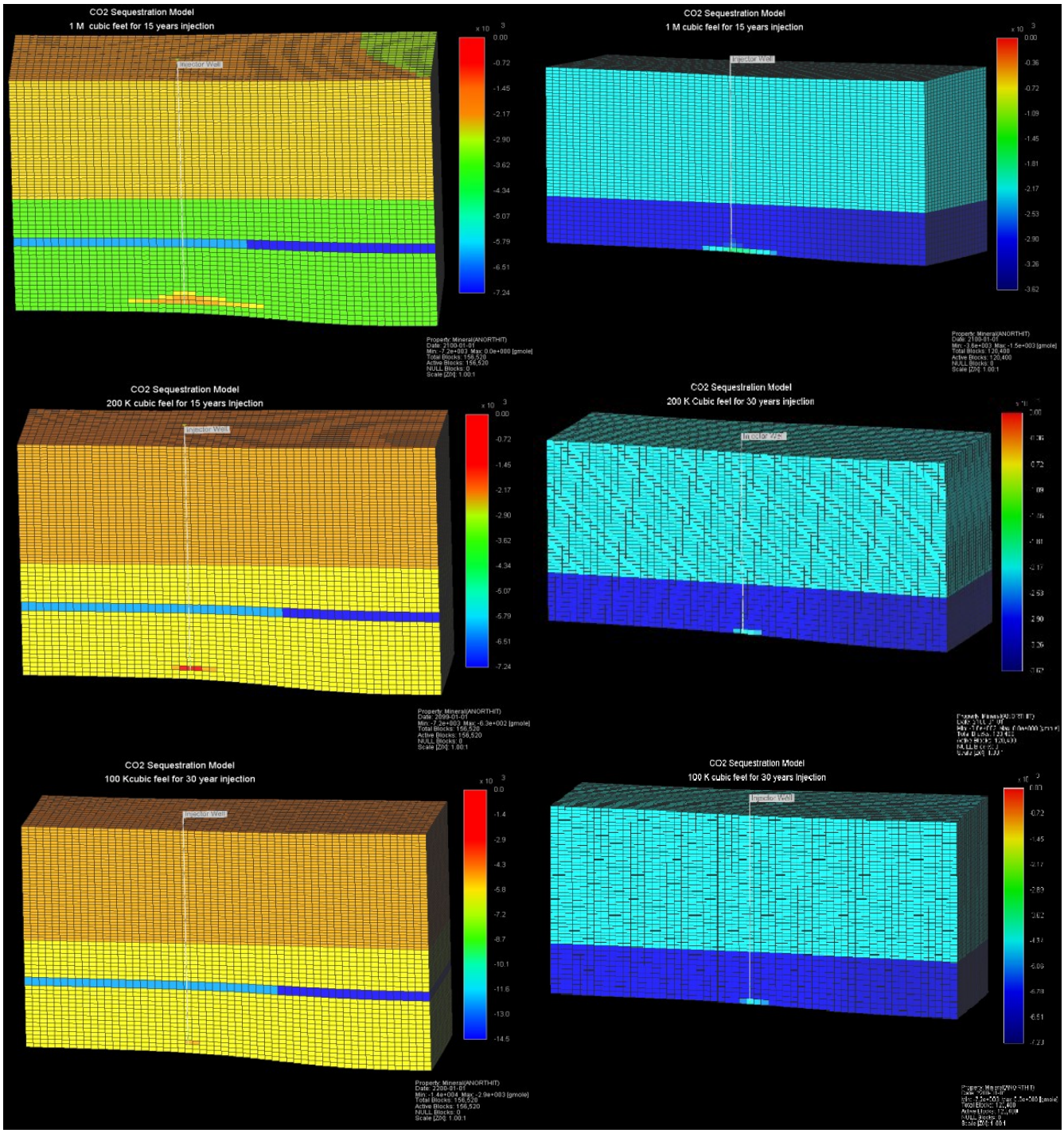

Figure 36. Distribution of anorthite in both the Upper Cretaceous and Lower Cretaceous models where the anorthite dissolves and the calcite and kaolinite deposit. The negative values reflect the dissolution which takes place in all layers.

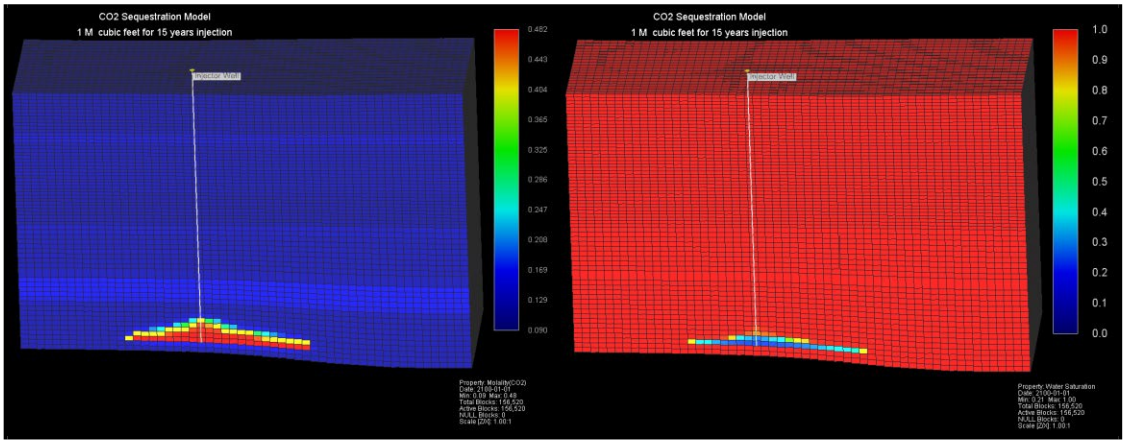

Figure 37. Relationship between the water saturation and CO_2 saturation. The volume of CO_2 plume in the injection area seams larger than the low water saturation.

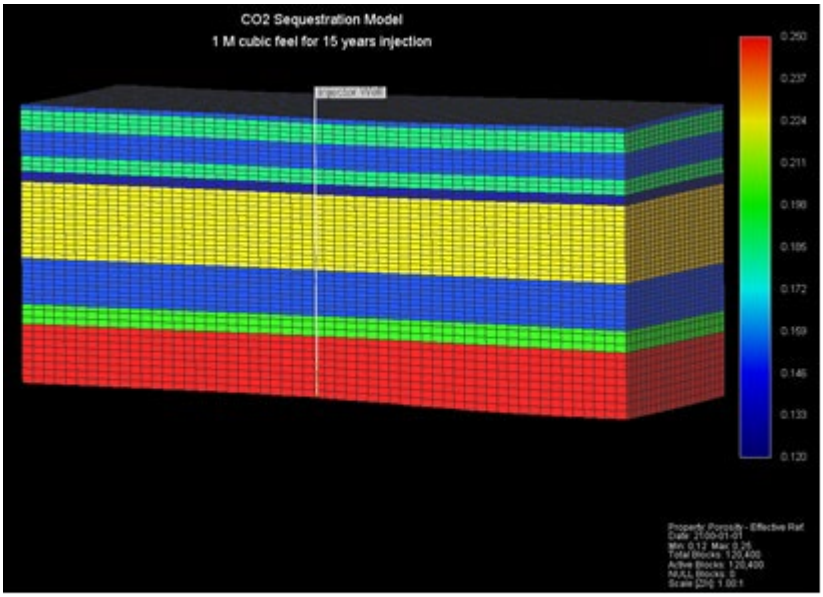

Figure 38. Distribution of porosity for the Upper Cretaceous model extracted from COST-GE-1. The red color corresponds to high porosity and is a candidate for a CO_2 injection while the blue zone represents the seal part of the model. The other zones are likely candidates for potential reservoirs and seals dependent on the porosity and permeability values.

Next, we modeled the expansion of conductive fracture through the tensile failure due to increasing pore pressure. The total normal stress due to constant CO_2 injection will force the rock to compact and decrease in size while increasing the pore pressure. Within that decreasing rock volume, the small channels between the grains (which affect the permeability) become active and more connected, potentially leading to failure within the seal zone above the injected reservoir. The permeability is expected to increase because of increasing CO_2 injection. The Barton-Bandis Fracture Permeability Model (Karakaş, 2008) comes in handy to demonstrate the fracture permeability model within injection simulation of three-dimensional models in the potential Cretaceous sequences.

The Barton-Bandis Fracture Permeability Model is a complex system. The parameters included in the three-dimensional simulation are Poisson's ratio, Young's modulus, rock compressibility, pressure, porosity, dual permeability values and a three-dimensional distribution of the seal rock. There is a local variation in permeability values through depth for all depths from 11000 to 3500 feet. Consequently, applying the Barton-Bandis Fracture Model will show us that vertical variation of cap leakage. According to the geophysical and core data analysis, there are local variations in permeability values at all depths from 3500 to 11000 ft. Consequently, applying the Barton-Bandis Fracture Permeability Model will help us assess the vertical variation of cap leakage properties.

In order to apply the Barton-Bandis Model, we needed to define the natural fracture system as a very small fracture permeability value to start with based on the seismic data. Also, there are many physical parameters that should be accounted for in the model (Tables 13 and 14). The 2D model was built by a 100*1*33 grid mesh with two seal horizons to show the effect of tension failure and was located on layers 6 and 12 of 33 layers in the z direction. The other layers, except the contact with deformed layers 6 and 12 will not be defined just to optimize the results.

Table 13. Petrophysical properties of the simulation model. The initial value of the area that represents the Barton-Bandis zone is very small in order to optimize the results after failure occurs later. Permeability values are in mD.

1	porosity	0.13
2	porosity fracture	0.13
2	permeability	15
4	permeability fracture	15
5	permeability fracture at 6^{th},12^{th} layers	0.0000001
6	porosity	0.13

Table 14. Additional parameters that affect the stress-strain deformation in rock 1, the Barton model and rock 2 the contact layers.

parameter	**Rock 1**	**Rock 2**
Young's elastic modulus KPa	5.00E+06	861845
Poisson' ratio	0.25	0.3
pressure dependence of formation porosity /compressibility kPa	1.28E-01	1.28E-05

The last parameters associated with the mineralization process are the numerical parameters and mineral species reactions. When CO_2 is injected in a reservoir, a chemical reaction is expected to occur. The surface area of the grain and the rate of reaction in addition to the temperature and the released energy is required to know in order to predict the path of dissolution /precipitation of new minerals.

Table 15. Mineral parameters associated with the chemical reaction with CO_2.

Mineral reaction	Reactive Surface Area	Log10(Rate Constant)	Activation Energy J/mol	Reference Temperature
Anorthite + $8H^+$ = Ca^{++} + 2 Al^{+++} + 2 SiO 2(aq) + 4 H2O	88	-12	67830	25 C°
Calcite + H^+ = Ca^{++} + HCO_3^-	88	-8.79588	41870	25 C°
Kaolinite + $6H^+$ = 5H2O + 2SiO2(aq) + 2 Al^{+++}	17600	-13	62760	25 C°

The injection scenario demonstrates injection of 73 million cubic meter /year of supercritical CO_2 for five years into a reservoir associated with saline aquifer, then shut down the injection well to detect the fate of CO_2 migration and the tension failure of the seal after increasing the pressure, accordingly.

The simulation results show that free phase of CO_2 moves up within the two years and start to generate the pore pressure on the first seal of the Barton-Bandis model against constant total stress (Figure 40). At the same time, the effective normal stress that is already present before the injection time starts to drop down gradually due to the increasing injection pressure (Figure 39). Subsequently, due to decreasing effective stress, the fracture for the small value of permeability starts to change and open new pathways through the seal for gas to escape into the overburden layers (Fig. 41) causing seal failure and leakage.

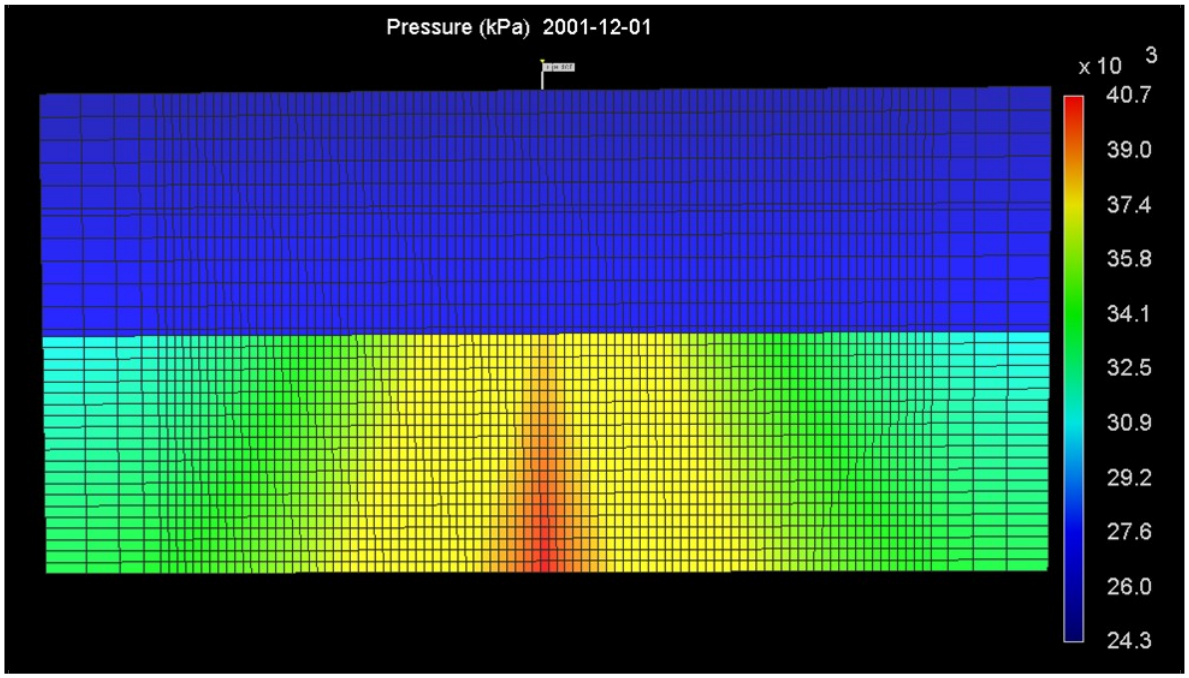

Figure 39. 2D model shows increasing the pore pressure on the seal before the failure moment within two years only. The red color is the maximum values of pressure near the injection area.

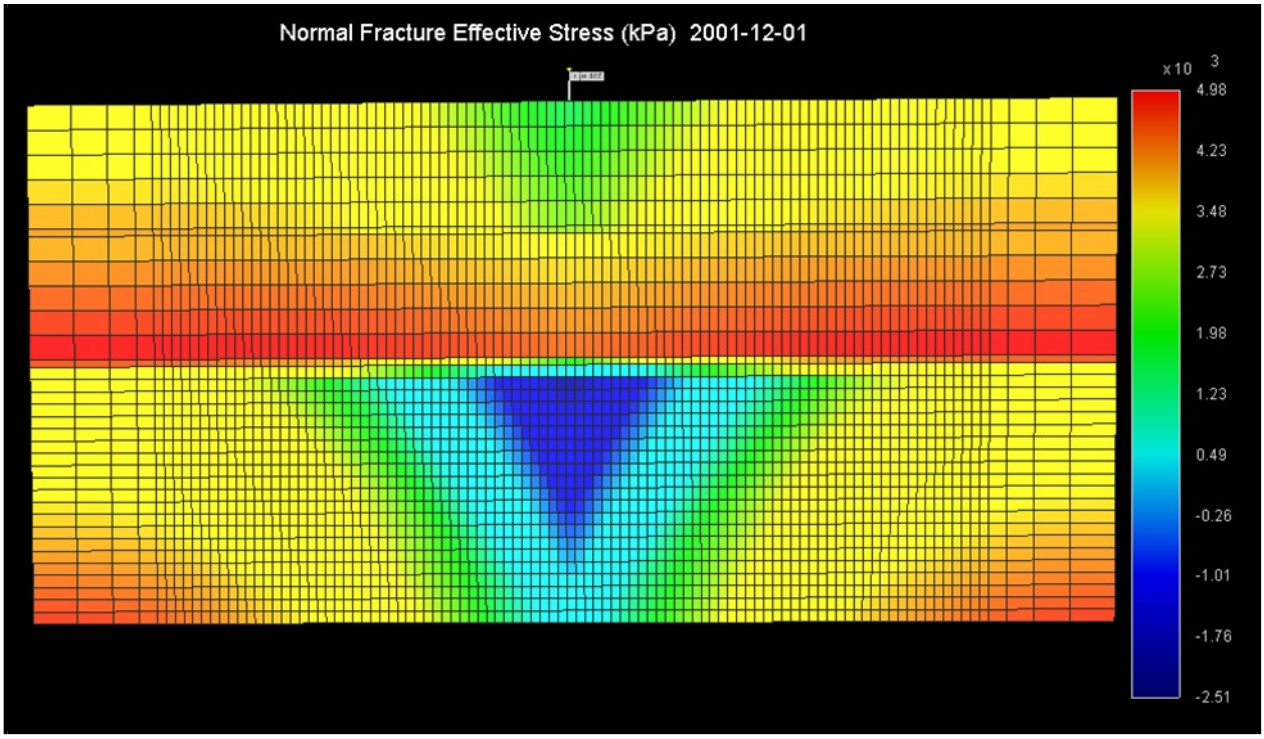

Figure 40. 2D model shows the normal fracture effective stress that is reduced with increased pressure. The blue color means this area becomes at minimum value when normal effective fracture stress reduces enough that failure occurs.

The mechanism of tensional failure is not compatible with the mineralization concept. Figures 41 and 42 show that mineralization undermines the stability of the seal. The mineralization begins after the aqueous phase of the CO_2 plume is generated and the rate of precipitation exceeds the rate of dissolution - after the injection is shutdown. For example, (Figure 42) displays the case of no tensional failure, the dissolution of carbonate acid in addition to the hydraulic pressure will try to weaken the seal stability and dissolve the carbonate ions Ca++ and Mg++ and consequently it enhances the tensional failure. The model also shows that mineralization has clearly emerged after 10 years from the tensional failure time. Thus, the mechanism of mineralization takes a longer time compared to tensional failure that occurs in the second to the fourth year of the injection time.

In Figure 41 we observe the migration of the CO_2 plume moving up through the seal zone after the tensional failure occurs and subsequently, the mineralization will enhance the area above the seal in case the CO_2 injection occurs for a long time only. However, the advantage of mineralization will not support the tensional failure in the short term since the tensional failure would occur first (Figures 41 and 42).

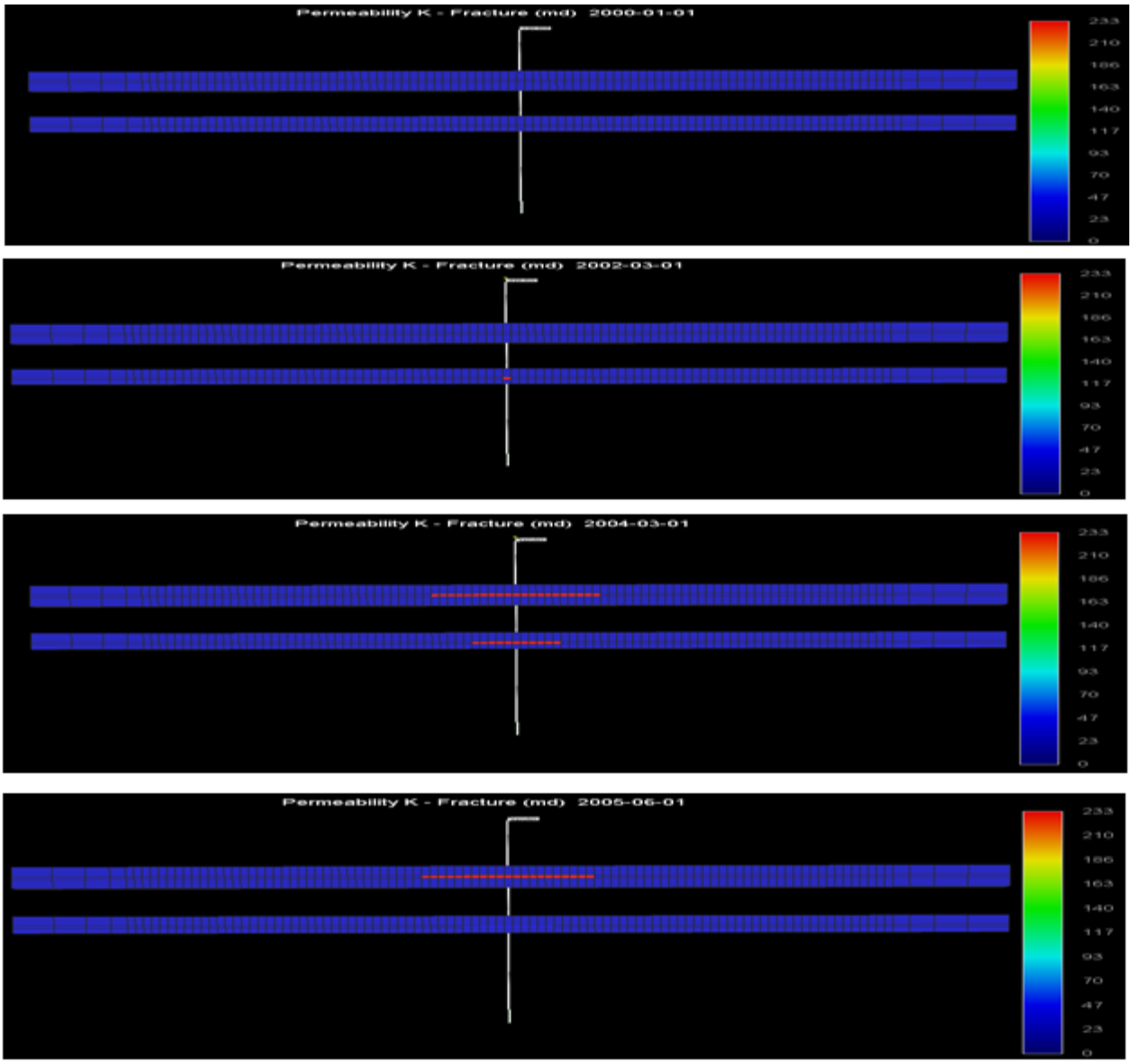

Figure 41. Permeability variation in four stages at A. The small value of permeability is 0.00000001 mD. At B, the permeability starts increasing. At C, the first seal is affected by tensional failure and that causes a fracture to allow the gas phase to pass through the deformed area. At D, the impact of permeability variation at the second seal while the first seal is reduced due to decreasing the pressure as the injection time is limited.

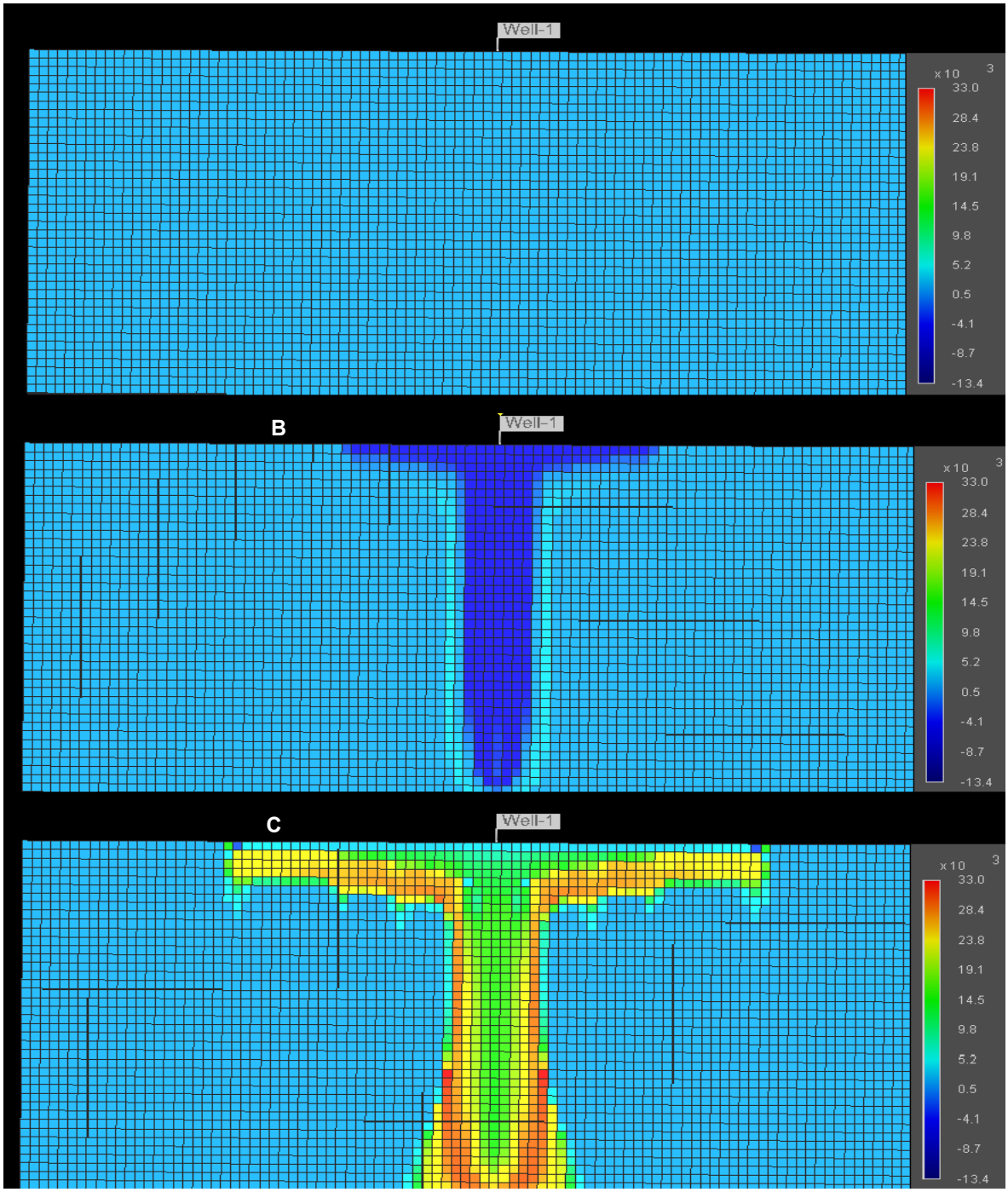

Figure 42. Carbon dioxide phases at three different times between the injection zone and the seal zone. **A** represents zero time at the beginning of the CO_2 injection. **B** is the dissolution phase showing the vertical migration of the CO_2 plume in aqueous phase after four years. **C** is the precipitation phase of calcite mineral at 2064 after injection well is shut down in 2005. The hydraulic pressure increases in the period of the first four years, the dissolution enhances the pressure factor to break through the seal. The negative values of the scale show that dissolution was dominant in the near term and positive values show the conversion to precipitation phase of calcite after long term.

Subtask 9.3 – Target Development Recommendations

The South Georgia Embayment (SGE) appears to be a good prospective target area due to an abundance of legacy 2-D seismic data. This is also the area of the only 6 exploratory wells in our entire study zone. Based on this study, the Upper/ Lower Cretaceous and Upper Jurassic strata seem to have abundant volumetric capacity for CO_2 storage.

This study builds and expands on a detailed analysis for CO_2 storage resource assessment of the Southeastern Offshore Atlantic margin by providing a comprehensive evaluation of the Upper/ Lower Cretaceous and Upper Jurassic strata with a focus on the South Georgia Embayment (SGE). The SGE appears to be a good prospective target area due to the (1) abundance of legacy 2-D seismic data, and (2) the location of legacy exploratory wells. At COST GE-1 well, old reports indicate that there are impermeable beds that could act as seals for CO_2 entrapment. The thick shales and calcareous shales between 3,600 and 5,700 ft (1,100-1,750 m), as well as thinner shales and anhydrite beds in the deeper parts, are the best estimated potential seals. In the form of shales, seals are present throughout the COST GE-1 well section. In addition, anhydrite beds, which would act as seals, are present below about 6,000 ft (1,800 m) (Scholle, 1979).

Although sandstone strata are present below 10,000 ft (3,050 m), they are tightly cemented and, in spite of some gas shows in GE-1, must be considered as non-reservoir units in offshore hydrocarbon exploration. Stratigraphic trapping through lateral facies changes are also of greater interest in this area than in other basins along the Atlantic offshore margin (Scholle, 1979).

Using legacy industry 2-D seismic reflection and well data, this assessment is the first application of innovative seismic inversion techniques to CO_2 storage. This study (1) provides a quantitative estimate of porosity and permeability regimes distributed across the prospective geologic reservoirs for CO_2 storage within the SGE; (2) demonstrates the value of using multiple seismic inversion techniques to define reservoir and seal properties; (3) delivers a reliable and repeatable workflow for Model-Based inversion which offers a better method to discriminate lithology and predict porosity; and (4) optimizes parameters for assessing geologic CO_2 storage resources. In addition, the impedance inversion workflow may be applied to future CO_2 storage resource assessments. Results of the acoustic impedance inversion indicate that the Upper Cretaceous strata at SGE contain porous intervals which have low acoustic impedance (relatively high porosity) overlain by a thick impermeable interval, mostly shale, with high impedance (low porosity) and low permeability. The seismic data were converted from time to depth using a thorough velocity analysis as shown in the Appendix.

The Model-Based inversion workflow gives an improved image to discriminate lithology, predict porosity, and calculate permeability. This workflow that proved to be most successful in this application, can be applied to future CO_2 storage resource assessment studies elsewhere. The inversion results indicate that distinct porosity and permeability regimes are present and distributed in the Upper/ Lower Cretaceous and Upper Jurassic units within the SGE. The acoustic impedance and porosity relationships show well-founded and reliable correlations. These relationships reveal several layers with low acoustic impedance that are coincident with the high porosity intervals that are subsequently proposed as potential reservoir intervals for CO_2 storage.

The results show that the Upper Cretaceous strata have two main potential reservoirs in the lower part. These are overlain by thick impermeable intervals, mostly shale that have high impedance, low porosity, and low permeability, and extend within the SGE. Since porosity distribution is estimated using multiple methods, it follows the trends of seismic signature and structures of the strata analyzed.

The extracted values of porosity, ranging from 15 to 36%, and permeability, ranging from 1 to 100 mD, are close to the measured values from the well core data at the Upper Cretaceous strata interval.

In the Upper Cretaceous strata of the SGE, two main potential reservoirs for CO_2 storage were identified as follows:

- The first potential reservoir, located at depths between 5,400 to 5,580 ft, and composed of siderite, some pyrite quartz, limestone, with high porosity (17-23%) and high permeability (3.5 to 447 mD) are encountered. It is overlain by thick seal layers, located at depths between 4,400 to 5,400 ft, composed of shale, fine bedding, and has porosity of 23.5 % and low permeability (0.1 mD).
- The second potential reservoir, which is composed of sandstone, quartzose silt, dolomite loose sand, coal, and siltsone is located at 5720 to 5950 ft depth. The estimated porosity is 19 to 30.1% and the permeability is between 3.5 to 447 mD (Scholle, 1979; Almutairi et al., 2017). However, it is capped by seal strata, composed of calcareous shale, fine-med silt, and biomicrite, and located at a depth range of 5,580 to 5,720 ft. Its average porosity is 12% and has less permeable clayey sequence.

The CO_2 storage capacity estimation of the combined units varies between ~9 to 07 GT with a varying storage efficiency factor from 10 to 90%.

The Lower Cretaceous section between depths of 5,900 ft (1,798 m) and 7,200 ft (2,195m) was divided into fourteen lithological units which are mainly composed of varying proportions of calcite, clay, shale, sandstone, limestone, and dolomite (Lizarralde et al., 1994; Poag, 1978; and Poppe et al., 1995; Table 4). This section is dominated by dolomites with porosities that vary widely and unsystematically with depth from 17 % to 32 %, and permeability between 0.3 and 550 mD. The capacity for CO_2 storage potential of the Lower Cretaceous was calculated based on the net thickness of the porous and permeable layers. The average porosities of the upper, middle, and lower reservoirs were 27.4%, 28.1% and 28.7%, respectively. The dolomite efficiency factors (E) of P_{10}, P_{50}, and P_{90} were 2.2 to 3.4% described earlier. The calculated storage capacity is 746 Gt of CO_2 at P_{50} that could be stored securely in $4.61*10^{12}$ cubic ft. The total average thickness is 1425 ft.

The Upper Jurassic sections shows three potential reservoirs separated by four seals within the Southeast Georgia Embayment. The Upper Jurassic section is bound at the bottom by the Triassic post-rift unconformity. The thicknesses of the three potential reservoirs are 392 ft, 490 ft, and 90 ft, respectively. The seal thicknesses are 468 ft, 200 ft, 920 ft, and 400 ft from top to the bottom. The reservoir porosities vary between 21 and 26 % and the storage capacity adds up to ~ 36 GT.

Geomechanical and computed tomography (CT) data collection and analyses of existing drill core data for experimental rock physics evaluation aimed to ground-truth the geophysical studies and constrain volumetric estimates are still ongoing under separate funding. Furthermore, injection simulation models were run using the Computer Modelling Group Ltd. (CMG) reservoir simulation software platform.

Conclusion

Although the capacity estimates are promising, a level of uncertainty exists within the South and Mid Atlantic study areas due to the lack of exploration data. Currently there are no active oil and gas, or research exploration leases in the Atlantic area. There is no existing infrastructure and all previously drilled wells have been abandoned. Drilling and exploration in the Atlantic would need to be authorized by the U.S. government in order for subsea bed CO_2 sequestration to progress.

However, in the Eastern Gulf of Mexico a wealth of data and information is available due to previous oil and gas industry work. Offshore geologic formations within the Gulf of Mexico contain abundant pore volume and occur at subsurface depths amenable to CO_2 storage. Additionally, the Gulf of Mexico contains ample offshore oil and gas infrastructure that can be utilized for CO_2 storage within both depleted oil fields and saline reservoirs.

List of Acronyms and Abbreviations

AAPG	American Association of Petroleum Geologists
AI	acoustic impendence
AIChE	American Institute of Chemical Engineers
AIME	American Institute of Mining, Metallurgical, and Petroleum Engineers
AMCOR	Atlantic Margin Coring
AOIs	areas of interest
ASP	Atlantic Slope Project
BCT	Baltimore Canyon Trough
BEG	Bureau of Economic Geology at The University of Texas at Austin
BHP	bottom hole pressure
BOEM	Bureau of Ocean Energy Management
BSEE	Bureau of Safety and Environmental Enforcement
CCS	carbon capture and storage
CCUS	carbon capture, utilization and storage
CMG	Computer Modeling Group Ltd.
CMP	common mid-point
CO_2-EOR	carbon dioxide enhanced oil recovery
CSE	community seismic experiment
CT	computed tomography
CEU	continuing education unit
CO2	carbon dioxide
DEMUX	Demultiplexer Digital Decoder
DFT	discreet Fourier transform
DGS	Delaware Geological Society
DOE	U.S. Department of Energy
DSDP	Deep Sea Drilling Project
E	efficiency factor
ECC	Eastern Coal Council
EEZ	Exclusive Economic Zone
EGOM	Eastern Gulf of Mexico
ENAM	Eastern North American Margin

GIS	Geographic Information System
GoM	Gulf of Mexico
GR	gamma-ray
GSA	Geological Survey of Alabama
GSI	Geophysical Services, Inc.
HILL	GERALD R HILL PHD, Inc.
IOGCC	Interstate Oil and Gas Compact Commission
KB	Kelly Bushing
LUT	thermal Look-Up Table
MBI	Model-Based Inversion
MSCL	Multi-Sensor Core Logger
MT	metric tons per year
MVA	monitoring, verification and accounting
NAMSS	National Archive of Marine Seismic Surveys
NatCARB	National Carbon Sequestration Database and Geographic Information System
NER	New England Research Group
NETL	National Energy Technology Laboratory
NGDC	National Geophysical Data Center
NOAA	National Oceanic and Atmospheric Administration
NTG	net-to-gross
O&G	oil and gas
OAG	Offshore Atlantic Group
ONR	Office of Naval Research
OCS	outer continental shelf
PDH	professional development hour
PDP	Pulse-Decay Permeameter
PI	principal investigator
PMP	Project Management Plan
R&D	research and development
RC	reflectivity coefficient
RCSP	Regional Carbon Sequestration Partnership
RECS	Research Experience in Carbon Sequestration
S/N	signal-to-noise ratio
SECARB	Southeast Regional Carbon Sequestration Partnership
SECARB-Ed	Southeast Regional CO_2 Sequestration Technology Training Program
SGE	Southeast Georgia Embayment
SIPES	Society of Independent Professional Earth Scientists
SME	Society for Mining, Metallurgy, and Exploration
SMP	Sponsorship Marketing Plan
SOPO	Statement of Project Objectives
SOSRA	Southeast Offshore Storage Resource Assessment
SSEB	Southern States Energy Board
STEP	Student Transition Engineering Program
TVD	true vertical depth
TWTT	two-way travel time
USGS	United States Geological Survey
XRF	x-ray fluorescence
VAT	Virginia Tech
VCCER	Virginia Center for Coal and Energy Research

Appendices